THERMODYNAMIC STUDY FOR APPLICATIONS OF TITANIUM AND ZIRCONIUM IN NUCLEAR ENGINEERING

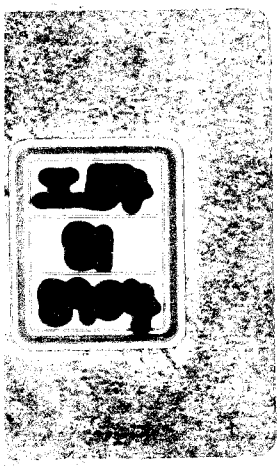

SHINSUKE YAMANAKA

1989

DISSERTATION

THERMODYNAMIC STUDY FOR APPLICATIONS OF TITANIUM AND ZIRCONIUM IN NUCLEAR ENGINEERING

（原子力材料としてのチタン、ジルコニウムに関する
熱力学的研究）

SHINSUKE YAMANAKA

Department of Nuclear Engineering

Faculty of Engineering

Osaka University

1989

TABLE OF CONTENTS

CHAPTER 1 INTRODUCTION

1. General Remarks

Titanium and zirconium both possess unique characteristics which fit them for certain vital applications. Their physico-chemical properties are closely related, as shown in Table 1[1-6]. Titanium and zirconium metals are now widely in use, mainly because of their relatively low specific weight but also thanks to their good corrosion resistance at low temperatures and their reasonably good mechanical properties. The high strength-to-weight ratio of titanium appeared useful for aerospace technology, and zirconium found important applications in nuclear engineering because of its unusually low absorption cross section for thermal neutrons. As a result, these metals were changed from laboratory curiosities to commercial articles in a few years' time.

Titanium and zirconium occur widely in the lithosphere. However, the main obstacle to their widest use has been for many years, and still is, the high price of production. One of the reasons for this is their great affinity for the gaseous elements such as oxygen, hydrogen and nitrogen. Oxygen, for example, once it is dissolved in the lattice, can hardly be reduced to a tolerably low level of concentration. The solid solutions thus formed have particularly low dissociation pressures even at a high oxygen concentration. This renders the refining of titanium and zirconium very difficult. There is no easy way around this obstacle. Therefore, use of titanium and zirconium in a particular application must be justified in terms of their unique properties.

2. Titanium and Zirconium as Nuclear Materials and Problems in Their Applications

Titanium shows increasing promise for technological uses in a nuclear fission reactor. Zirconium and its alloys have been widely adopted for fission reactor materials. The excellent properties of titanium and zirconium also make them very attractive for applications in a nuclear fusion reactor.

Oxidative attack of stainless steel cladding in liquid metal fast breeder reactors (LMFBRs) may limit the life of the fuel pins. Both intergranular and matrix attacks of the cladding by oxygen and fission products such as cesium, tellurium and iodine have been identified in post-irradiation examination of mixed oxide fuels. In light of what is presently known, the key to controlling the cladding attack is control of the oxygen potential by the insertion of oxygen getters within the fuel pin[7-9]. Titanium is a prime candidate as an oxygen

getter, because it easily reacts with oxygen and would thereby keep the oxygen potential below the threshold value considered necessary for the cladding corrosion. The titanium getter could be plated on the inner surface of the cladding or on fuel pellets as a circumferential coating. There exists a possibility of chemical interaction of titanium getter with mixed oxide fuel and aggressive fission products such as cesium and tellurium, which may affect fuel performance. Thermodynamic and kinetic arguments of interaction between titanium getter and fuel or fission products are required for successful application of titanium getter concept.

In a tritium burning fusion reactor facility, the largest inventroy of tritium will be in the fuel cycle. Titanium is one of materials being considered for use in the tritium fuel cycle of a fusion reactor[10,11]. For the tritium storage and handling system, titanium can be used as a getter which recovers tritium fuel and removes gaseous impurities such as O_2, H_2O, CO_2, CO, N_2 and NH_3. Desirable properties imposed on the material for tritium storage or collection are that it has a low equilibrium dissociation pressure for tritium and can absorb a large amount of tritium gas. From the viewpoint of safe tritium handling, it is desirable that tritium gas absorbed in the material at room temperature and the gas once collected in it cannot be easily desorbed without heating at high temperature. Titanium seems to have desirable equilibrium tritium pressure-temperature characteristics. A principal safety concern relates to hazards of the accidental exposure of the storage bed to air. Titanium may be less pyrophoric than uranium which is the most extensively investigated and widely used getter. For the practical application, knowledge of equilibrium and kinetic properties of titanium/hydrogen system should be required. Detailed information on influence of gaseous impurities on tritium absorption rate and capacity is also needed.

Zirconium, which has low thermal neutron absorption cross section, high melting point, high mechanical strength at elevated temperatures, good corrosion resistance to water and steam and reasonable cost and abundance, is widely used as cladding and structural materials in both light water reactors(LWRs) and heavy water reactors(HWRs). The zirconium alloys employed as structural or cladding material in LWRs and HWRs are the family of Zircaloy. In the family, Zircaloy 2 is employed in BWRs and HWRs, while Zircaloy 4 is employed in PWRs. However, there still remain some problems in use of Zircloy cladding under normal and accidental conditions of LWRs.

In hypothetical LWR accidents, nuclear fuel rods may be subjected to very high temperatures for periods sufficient to cause severe fuel damage. Extensive experiments[12-14] from kinetic points of view have therefore been performed under various postulated conditions to determine the extent of the UO_2/Zircaloy interaction. With regard to the UO_2/Zircaloy interaction, the previous results

explain the observed reaction by which UO_2 is reduced partially to metallic uranium as long as zirconium is not saturated with oxygen. The phase relations in the U-Zr-O ternary system are the basis for the sound understanding of the chemical interaction between LWR fuel and cladding.

The most relevant open questions combined with the release of radioactive materials during hypothetical LWR accidents refer to the chemical behavior of the highly reactive elements iodine, cesium and tellurium[15,16]. The chemical states of fission products are certain to change in response to their environment and reaction with core materials. Reviews of the chemistry and transport of fission products in LWR containment are usually confined largely to the behavior of iodine species. However, there are also interesting and important interactions of tellurium, for example, reaction of tellurium with Zircaloy cladding under various environmental conditions. The chemical form of tellurium in the containment conditions is of importance not only for an evaluation of a possible release of tellurium species, but also because tellurium is a precursor of iodine.

Hydrogen has a deleterious effect on the mechanical properties of zirconium , particularly those related to impact, creep and fatigue. Under normal operating conditions of LWRs, the embrittlement of Zircaloy cladding by hydrogen is usually attributed to the precipitation of brittle hydride plates[17]. Such precipitation would obviously be affected by any variation in the solubility of hydrogen in the α phase, and the effect of alloying and impurity elements on this solubility is therefore of great interest. There has been considerable doubt about the effect of oxygen impurity on the solubility of hydrogen in the hexagonal alpha zirconium.

One of the major problems arising from the use of nuclear energy is the disposal of the resultant radioactive wastes such as Zircaloy hull[18]. Since large amounts of tritium are present in the Zircaloy hulls (about 100 ppm hydrogen and about 0.03 - 0.10 ppm tritium), the release behavior of tritium during treatment of Zircaloy hulls must be studied. The goal is to keep the tritium release as low as possible.

Because of its high affinity for certain nonmetals, zirconium is proposed for tritium gas storage in a gas inlet system and for tritium gas collection or containment system which backs up the end stage of the pumping system of fusion reactor[19]. However, for the evaluation of zirconium, more basic data on thermodynamics and kinetics of chemical interaction between hydrogen isotope and zirconium are needed. Impurity effects on the rate of tritium uptake and on the storage capacity are especially important.

Thus, the demand for reliable thermodynamic and kinetic data concerning titanium and zirconium is growing rapidly with the increasing need for accurate information about new or improved nuclear materials for fission and fusion reactors. The present study attempts to focus on thermodynamic aspects of

problems to clarify the interaction of titanium and zirconium with fuel and fission products in LWRs and LMFBRs and to elucidate the poisoning effect on tritium solubility in these metals in fuel cycles of fusion reactors.

3. Related Binary Systems of Titanium and Zirconium

Titanium and zirconium can form binary systems with many elements, the phase diagrams of which display a variety of complex phase relations. The phase diagrams of interest are the binary systems of titanium and zirconium with oxygen, uranium, tellurium and hydrogen. The characteristics of the phase diagrams of the binary alloys containing titanium or zirconium can be classified simply. The most important question is whether a given element stabilizes the α phase or the β phase. Stabilizing the α phase means that as solute is added, the $\alpha \rightarrow \beta$ phase transition temperature is raised; β stabilization implies the converse. Oxygen and tellurium are the α stabilizers, whereas uranium and hydrogen stabilize the β phase. The features of each binary system are described briefly as follows:

Murray[5] has performed the assessment of the Ti-O binary system covering the phase equilibria and crystal structures of the condensed phases in the composition range between pure titanium and TiO_2. The assessed Ti-O phase diagram is shown in Fig. 1. Oxygen has a large solubility in hcp αTi and it stabilizes α phase, αTi(O), with respect to the high temperature bcc form βTi. Structures of the monoxides are based on the NaCl structure of the high temperature γTiO form. Additional structural modifications are identified, which are designated βTiO and αTiO. The stable condensed phase richest in oxygen is rutile TiO_2. Between the monoxides and TiO_2 is a series of discrete phases with stoichiometry Ti_nO_{2n-1} where $n \geq 2$, which are called Magneli phases such as Ti_2O_3 and Ti_3O_5. The thermodynamic properties of the titanium oxides have been studied and assessed extensively[20,21]. However, there is a little information about thermodynamics of αTi(O) solid solution phase.

Figure 2 is the phase diagram of the Zr-O binary system after Abriata et al.[22]. This phase diagram is quite similar to the Ti-O binary system, which is characterized by the hcp terminal solid solution, αZr(O), in which the maximum solubility of oxygen is 35 at% at 2065°C. The nonstoichiometric compound ZrO_{2-x}, where $0 \leq x \leq 0.44$, exists in three crystallographic forms: the low temperature monoclinic structure, denoted αZrO_2, the intermediate temperature tetragonal structure, βZrO_2, and the high temperature cubic CaF_2 type structure, γZrO_2, which melts congruently at $x = 0$ and 2710°C. The detailed critical assessments of thermochemical properties of the Zr-O system are given in the literature[20,23]. However, few thermodynamic works were made on the solid solution up to now.

The U-Ti phase diagram assessed by Murray[5] is indicated in Fig. 3. The compound U_2Ti with a hexagonal structure is stable below 898°C and has a narrow homogeneity range. The bcc forms of uranium and titanium are completely miscible as designated by (γU,βTi) in Fig. 3. Experimental measurements have not yet been performed of thermodynamic properties of the U-Ti binary system. Murray[5] has estimated the Gibbs energies of the existing phases in the U-Ti system from the qualitative features of the phase diagram.

The equilibrium phase diagram of U-Zr[24] is shown in Fig. 4. The main feature of this phase diagram is the exsitence of the bcc solid solution (γU,βZr) with complete mutual solubility above 772°C. Only one intermediate phase δUZr_2 with a composition range of about 67 - 73 at%Zr exists in this system. It is unstable above 617°C. Relatively little thermodynamic data exist for the U-Zr system. Leibowitz et al.[25] have made an analysis of the U-Zr phase diagram and estimated thermodynamic functions for all the existing phases.

The Ti-Te binary system appears to bear similarities to the Ti-S and Ti-Se systems, but has been studied less thoroughly. Several tellurides such as Ti_2Te, Ti_5Te_4, TiTe and $TiTe_2$ are found to exist. Most of the experimental work for the binary system was done by X-ray diffraction, however, thermodynamic properties of some tellurides were evaluated from vapor pressure measurements[26].

For the Zr-Te binary system, Sodeck and his coworkers[27] have performed isopiestic, thermoanalytical and X-ray studies. There appear many tellurides: Zr_5Te_4, ZrTe, $ZrTe_2$ and $ZrTe_3$. The $ZrTe_2$ is likely the most stable telluride in the binary system. Only for the $ZrTe_2$, thermodynamic measurements have been carried out by Johnson et al.[28], and the standard enthalpy of formation and the standard entropy were reported.

Numerous investigators[5,21] have published data on the phase relationships in the Ti-H binary system. The phase diagram in Fig. 5, which is of the eutectoid type, was assessed by Murray[5]. There exist two interstitial solid solution phases of hcp α and bcc β, αTi(H) and βTi(H), which are based on the allotropic forms of pure titanium. Two hydride phases are δTiH_{2-x} with a fcc structure and εTiH_2 with a tetragonally distorted fcc. The thermodynamic data of the existing phases were critically reviewed in the literature[5,21].

A considerable amount of work[23,24] has been undertaken to clarify the phase relationships in the Zr-H binary system. The phase diagram[24] is shown in Fig. 6. The eutectoid reaction occurs at 546°C between the hcp α solid solution phase, αZr(H), and fcc δ hydride phase, δZrH_{2-x}, forming a bcc β solid solution phase, βZr(H). There exists a higher hydride of εZrH_2 phase with a fct structure. Thermodynamic properties of the binary system are available in the literature[23].

4. Outline of the Present Study

The significance of phase equilibrium studies for practical applications of titanium and zirconium to nuclear engineering was stated in the preceding sections. The following research has been performed on titanium and zirconium:

For the understanding of compatibility between titanium getter and mixed oxide fuel in LMFBRs, phase equilibria in the U-Ti-O ternary system are studied, the results of which are described in chapter 2. Phase relationships in the U-Zr-O ternary system are examined to have knowledge of integrity of Zircaloy cladding under hypothetical accident conditions of LWRs. Chapter 3 contains the results of the U-Zr-O ternary equilibria. Also included is thermodynamic analysis on titanium-oxygen and zirconium-oxygen solid solutions in chapters 2 and 3.

The Ti-Te-O ternary system is studied to obtain information on chemical interaction of titanium getter with fission product tellurium in LMFBR fuel pins. Chapter 4 describes the results of the ternary equilibria and the thermodynamic stability of titanium tellurides. Phase relations of the Zr-Te-O ternary system are examined, which are of importance for an analysis of tellurium behavior at hypothetical accidents of LWRs. The experimental results and discussion are found in chapter 5.

With intention of applying titanium and zirconium to tritium storage and handling systems in fusion reactors, studies on solubilities of hydrogen isotopes are performed for titanium and zirconium contaminated by oxygen. Chapters 6 and 7 include the experimental results and the statistical thermodynamic analysis for solubility of hydrogen isotope in titanium and zirconium.

The conclusions drawn from the present study are summarized in chapter 8.

References

[1] D.M. Ma, Nuclear Reactor Materials and applications, (Van Nostrand Reinhold Company Inc., New York, 1983).

[2] R.M. Brick, A. W. Pense and R. B. Gordon, Structure and Properties of Engineering Materials, 4th Ed., (McGraw-Hill, New York, 1977).

[3] J.C. Bailar Jr., H.J. Emeleus, Sir R. Nyholm and A.F. Trotman-Dickenson, Comprehensive Inorganic Chemistry, (Pergamon Prss, Oxford, 1973).

[4] P. Villars and L.D. Calvert, Pearson's Handbook of Crystallographic Data for Intermetallic Phases, Vol 2, (ASM, Ohio, 1985).

[5] J.L. Murray, Phase Diagrams of Binary Titanium Alloys, (ASM, Ohio, 1987).

[6] C.J. Smithells, Metals Reference Book, 4th Ed., Vol 3, (Butterworth, London, 1967).

[7] M.G. Adamson, Summary Report of Technical Committee Meeting on Fuel and Cladding Interaaction, (IAEA, Vienna, 1977)p108.

[8] R.J. Jackson, R.L. Gibby, R.E. Woodley, J.W. Weber and M.G. Adamson, ibid., (IAEA, Vienna, 1977)p189.

[9] E.T. Weber, L.A. Lawrence, C.N. Wilson and R.L. Gibby, Proceedings of International Conference on Fast Breeder Reactor Fuel Performance, (ANS, Illinois, 1979).
[10] E. Willin, M. Sirch, R.D. Penzhorn and M. Devillers, Fusion Technology, 14(1988)756.
[11] F. Mannone and H. Dworschak, Fusion Engineering and Design, 5(1988)385.
[12] P. Hofmann and C. Politis, J. Nucl. Mater., 87(1979)375.
[13] P. Hofmann and D. Kerwin-Peck, KFK-3552, (1983).
[14] P. Hofmann and D. Kerwin-Peck, J. Nucl. Mater., 124(1984)80.
[15] P.E. Potter, M.H. Rand and C.B. Alcock, J. Nucl. Mater., 130(1985)139.
[16] D. Cubicciotti and B.R. Sehgal, Nucl. Technol., 65(1984)266.
[17] W.H. Erikson and D. Hardie, J. Nucl. Mater., 13(1964)254.
[18] R. Tegman and M. Burstrom, SKB Technical Report 84-14, (1984).
[19] L.S. Krochmalnek, J.P. Krasznai and M. Carney, Fusion Engineering and Design, 5(1988)337.
[20] O. Kubaschewski and C.B. Alcock, Metallurgical Thermochemistry, 5th Ed., (Pergamon Press, Oxford, 1979).
[21] K.L. Komarek, Titanium: Physico-Chemical Properties of Its Compounds and Alloys, (IAEA, Vienna, 1983).
[22] J.P. Abriata, J. Garces and R. Versaci, Bulletin of Alloy Phase Diagrams, 7(1986)116.
[23] O. Kubashewski, Zirconium: Physico-Chemical Properties of Its Compounds and Alloys, (IAEA, Vienna, 1976).
[24] T.B. Massalski, Binary Alloy Phase Diagrams, (ASM, Ohio, 1986).
[25] L. Leibowitz, R.A. Blomquist and A.D. Pelton, J. Nucl. Mater, to be published.
[26] A. Suzuki and P.G. Wahlbeck, J. Phys. Chem., 70(1966)1914.
[27] H. Sodeck, H. Mikler and K.L. Komarek, Mh. Chemie, 110(1979)1.
[28] G.K. Johnson, W.T. Murray, E.H. Van Deventer and H.E. Flotow, J. Chem. Thermodynamics, 17(1985)751.

Table 1 Physico-chemical properties of titanium and zirconium[1-6].

Property	Titanium	Zirconium
Atomic number	22	40
Atomic weight	47.90	91.22
Electronic structure	$[Ar]3d^2 4s^2$	$[Kr]4d^2 5s^2$
Crystal structure		
α form	HCP	HCP
	a=0.2951nm	a=0.3232nm
	c=0.4686nm	c=0.5147nm
β form	BCC	BCC
	a=0.332nm	a=0.362nm
	(1084°C)	(867°C)
Density, 25°C (kg/m^3)	4510	6510
Melting point (°C)	1670	1852
Heat of fusion (kJ/mol)	15.9	18.8
Heat of vaporization (kJ/mol)	473	601
Transition temperature, $\alpha \rightarrow \beta$ (°C)	882	863
Heat of transition (kJ/mol)	4.14	3.89
Heat capacity (J/mol K)	25.05	25.53
Thermal conductivity,		
50°C (W/m °C)	15.4	20.9
Thermal expansion coefficient (/°C)		
a axis	9.55×10^{-6}	5.64×10^{-6}
c axis	10.65×10^{-6}	6.39×10^{-6}
Electrical resistivity,		
25°C (Ω m)	4.20×10^{-7}	4.00×10^{-7}
Ultimate tensile strength (N/m^2)	5×10^8	2×10^8
Young modulus (N/m^2)	1.2×10^{11}	7.6×10^{10}
Thermal neutron absorption		
cross section (barn)	5.8	0.18

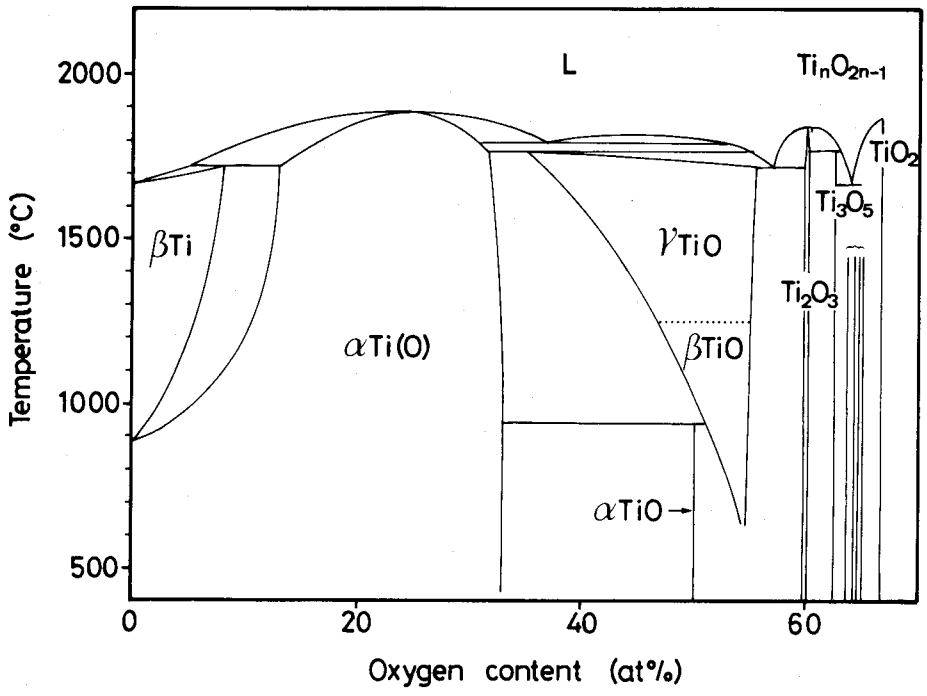

Fig. 1 Phase diagram of the Ti-O binary system[5].

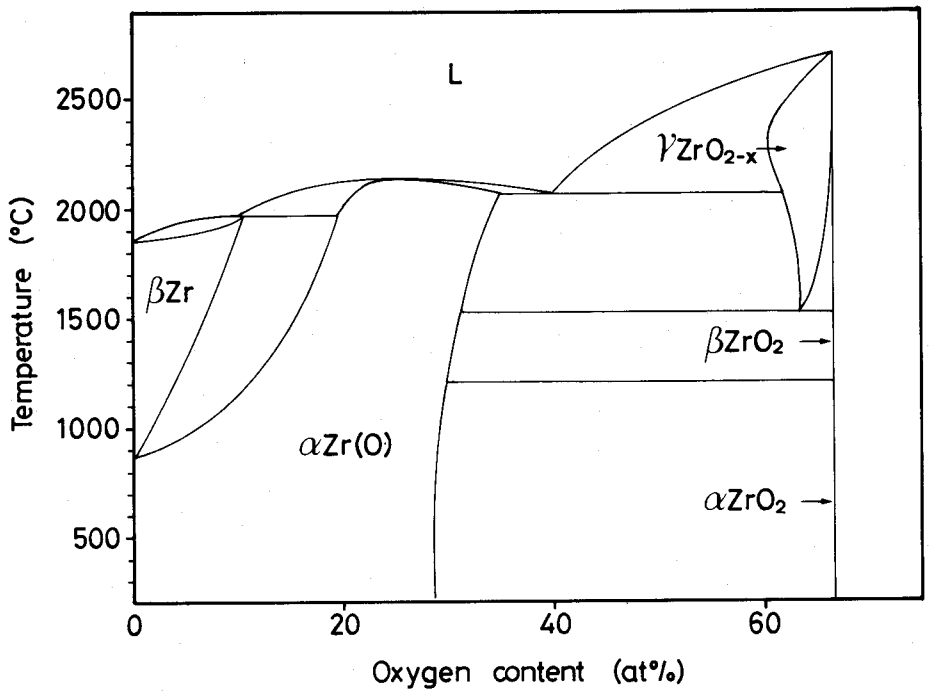

Fig. 2 Phase diagram of the Zr-O binary system[22].

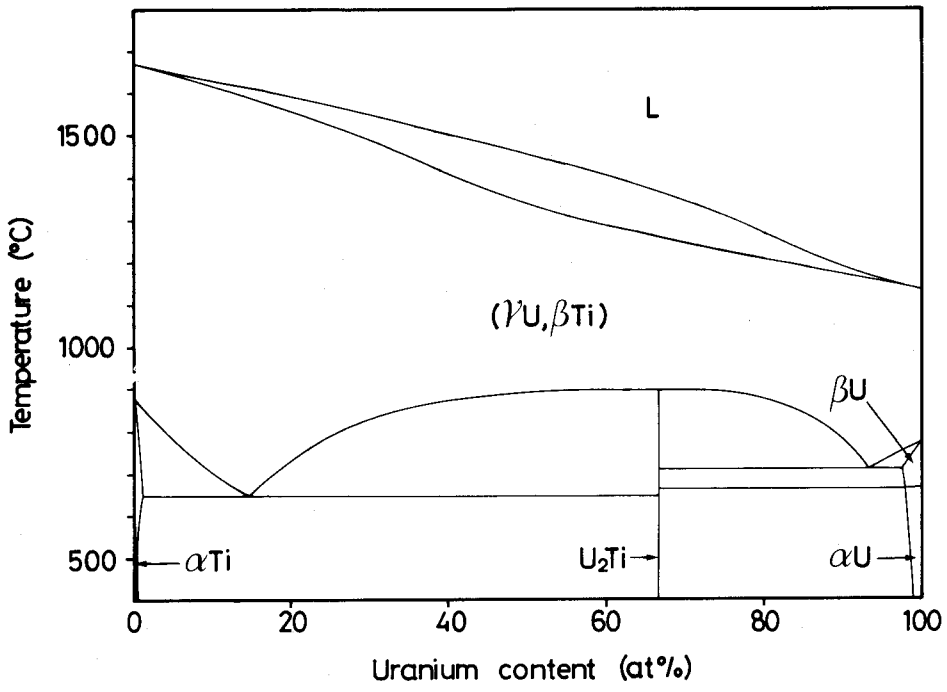

Fig. 3 Phase diagram of the U-Ti binary system[5].

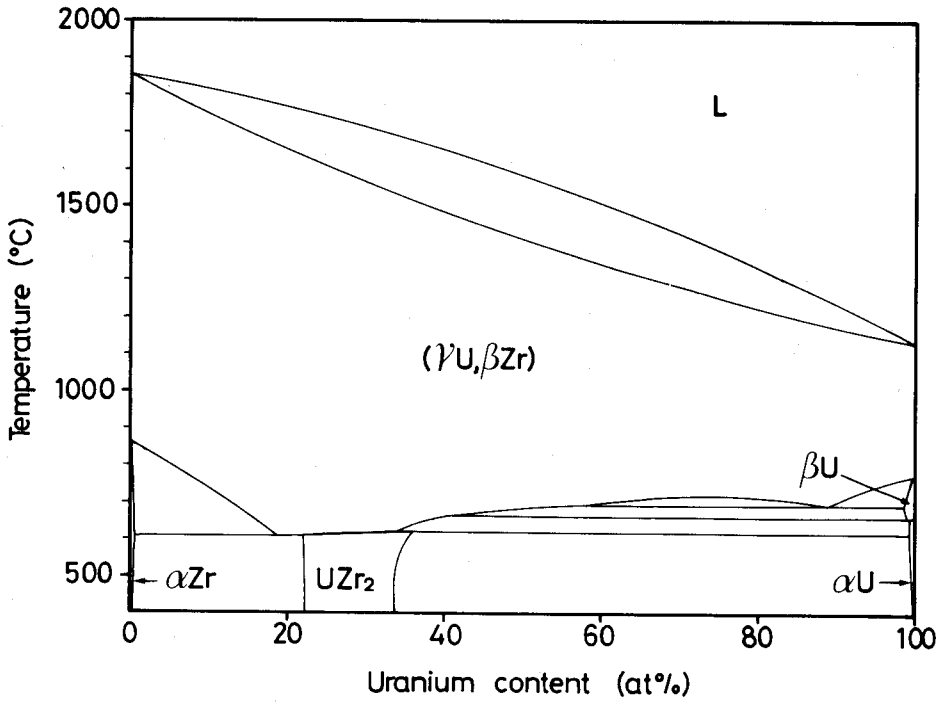

Fig. 4 Phase diagram of the U-Zr binary system[24].

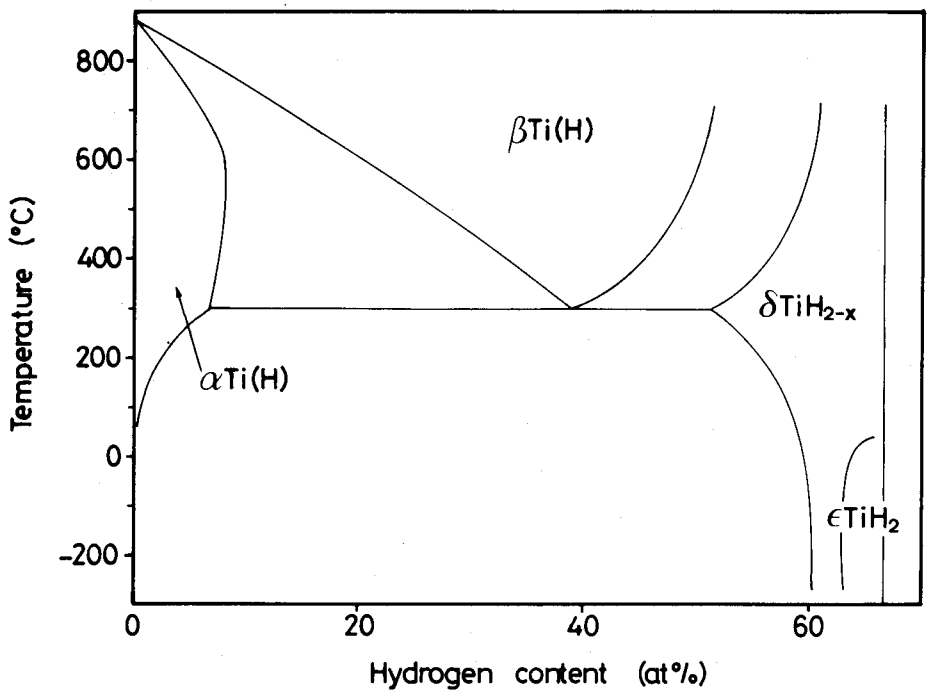

Fig. 5 Phase diagram of the Ti-H binary system[5].

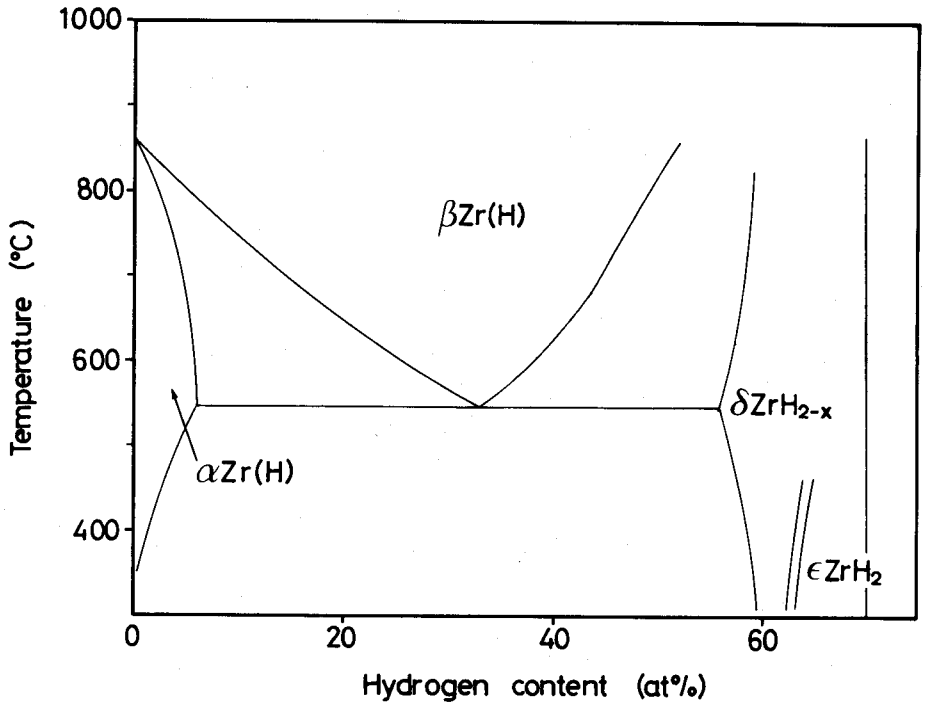

Fig. 6 Phase diagram of the Zr-H binary system[24].

CHAPTER 2 URANIUM-TITANIUM-OXYGEN TERNARY SYSTEM

1. Introduction

Inner surface corrosion of stainless steel cladding by fission products has been observed in the post-irradiation examination of several mixed oxide fuel pins of liquid metal fast breeder reactors (LMFBRs)[1-3]. Reduction or elimination of such corrosion is desirable to improve the lifetime of fuel pins. One of the major approaches to reduce the corrosion of cladding is to introduce oxygen buffer or getter materials into fuel pins[4-6].

Titanium which has a strong affinity for oxygen is considered to be one of the candidate getter materials as a cladding corrosion inhibitor. Chemical interaction of titanium with fuel is of great importance for its practical application to fuel pins. For a sound understanding of the interaction, it is required to obtain phase relationships in the U-Ti-O ternary system at elevated temperatures. Although the thermodynamic properties and the phase diagrams of U-O and Ti-O binary systems are well known, this is not the case for the U-Ti-O ternary system.

In the present study, the phase equilibria in the U-Ti-O ternary system have therefore been examined with the aid of X-ray diffraction analysis. The oxygen potential over titanium-oxygen solid solution phase was discussed in terms of results for phase equilibria in the U-Ti-O ternary system.

2. Experimental

Starting materials used in the present study were UO_2 (reactor grade, O/U ratio = 2.16), Ti (purity, 99.9 wt%), TiO (purity, 99.9 wt%), Ti_2O_3 (purity, 99.9 wt%) and TiO_2 (purity, 99.9 wt%) powders. These powders were finely ground and then mixed in desired proportions. The mixtures were pelletized and heated at 1000°C for 50 - 200 h in a vacuum lower than 10^{-4} Pa. After equilibration, the sample was rapidly cooled to room temperature.

The heated samples were powdered in a glove box filled with dry argon, and the powdered samples were embedded in glass sample holders for X-ray diffraction analysis. Diffraction patterns for the samples were obtained at room temperature with a diffractometer (Rigaku Denki, Geiger flex rad-rA) using Ni-filtered CuK_α radiation. The widths of the divergence and scatter slits were both 1° and that of the receiving slit was 0.15 mm. A step scanning width at an interval of 2θ = 0.01° and a counting time of 1.0 s were employed. Phases of the reaction products

were identified with X-ray diffraction patterns obtained. The lattice parameters of the products were evaluated from the collected reflections according to the Cohen's method[7].

3. Results and Discussion

3.1. Phase equilibria in the U-Ti-O ternary system

Figure 1 shows the results of X-ray diffraction analysis for Ti/UO_2 (samples A - V), $Ti/TiO/UO_2$ (samples a - v), $TiO/Ti_2O_3/UO_2$ (samples w - z) and $Ti_2O_3/TiO_2/UO_2$ (samples W - Y) mixtures after heating at 1000°C. It is apparent from this figure that the type and the number of phases identified are strongly influenced by the composition of the sample.

Sample A heated at 1000°C was found to consist of UO_2 and αTi. Four phases (UO_2, αTi, αU and U_2Ti) were detected in samples B - L of which titanium contents ranged from 20 to 72 at%. As an example, the X-ray diffraction pattern for sample E is indicated in Fig. 2(A). The reaction products for samples M - P were composed of αTi and U_2Ti, and UO_2 was not found, as evidenced by Fig. 2(B). The diffraction analysis for samples Q - U indicated that the reaction products contained αTi in addition to U_2Ti and βTi. Two phases (αTi and βTi) existed in sample V. The bcc βTi forms a continuous series of substitutional solid solutions with bcc γU above 898°C in the U-Ti binary system[8]. The αU, U_2Ti and βTi detected in the reaction products by X-ray diffraction analysis at room temperature are considered from the phase diagram of U-Ti system[8] to result from (γU,βTi) solid solution at 1000°C.

In samples a - e, U_2Ti coexisted with αTi, while UO_2 was not observed. The reaction products for the samples f - j were composed of UO_2, αTi, αU and U_2Ti. In the composition range for samples k - p, UO_2 and αTi were identified in the reaction products. Figure 2(C) shows the typical example of coexisting the two phases. From the results for samples q - u, it was confirmed that βTiO, of which the crystal structure is cubic, was involved with UO_2 and αTi in the reaction products. The stable form of TiO in the U-Ti-O ternary system at 1000°C was cubic, which differed from the low temperature αTiO form with a monoclinic structure. In the reaction products of samples v and w, βTiO was present together with UO_2. This means that the cubic βTiO phase has a range of homogeneity at 1000°C. Higher titanium oxides such as Ti_2O_3 (trigonal form), Ti_3O_5 (monoclinic form) and TiO_2 (Rutile) were formed in samples x - z and W - Y. However, the ternary oxide UTi_2O_6 reported in the literature[9] could not be observed in the present study.

Figure 3 represents the change in the lattice parameters a and c and the axial ratio c/a of αTi in the reaction products with gross titanium content of the Ti/UO_2 mixture pellets. The lattice parameters increased from a = 0.2951 nm and c = 0.4683 nm for the initial Ti powder to the values of a = 0.2960 - 0.2968 nm and c = 0.4745 - 0.4772 nm for samples T - C. The axial ratio c/a for the αTi was also larger than that before reaction (1.587). The extent of increase in the lattice parameters and the axial ratio varied with the composition of the sample, as shown in Fig. 3. The lattice parameters a and c for samples C - L, in which four phases UO_2, αTi, αU and U_2Ti were detected, were constant within the error in measurement. The average values of a and c were estimated to be 0.2968 nm and 0.4769 nm, respectively. The c/a ratio of 1.607 was also independent of the titanium content of the sample. Above 72 at%Ti, the lattice parameters a and c decreased with increasing titanium content, and the c/a ratio dropped from 1.607 to 1.603.

The variation in the lattice parameters a and c and the axial ratio c/a of αTi in samples a - r with the titanium content of the $Ti/TiO/UO_2$ mixture pellets is illustrated in Fig. 4. In the composition range of 84.3 to 75.0 at%Ti, the values of a, c and c/a are found from this figure to change with the titanium content. Samples f - j, in which four phases (UO_2, αTi, αU and U_2Ti) were identified, showed nearly constant a, c and c/a values, which were close to the values for Ti/UO_2 pellets having UO_2 as one of the reaction products. In the composition range where the two phases UO_2 and αTi coexisted, the values of c and c/a increased with decreasing titanium content, whereas the value of a changed in a more complicated manner. There is no marked difference in the values of a, c and c/a between samples q and r.

Heating at 1000°C resulted in a considarable elongation along the c axis and only a slight change in the a axis of αTi. The lattice parameters of pure titanium and titanium-oxygen solid solution, αTi(O), given in the literature[10-15] are shown in Fig. 5. As can be seen in this figure, dissolution of oxygen into αTi causes a marked increase in the value of c over the entire range of the solid solution. The value of a is less affected by the oxygen content but goes through a maximum at the composition of 25 at%O. The variation in the lattice spacing of αTi after heating is considered to be closely related to the dissolved oxygen amount in αTi. Assuming that the solubility of uranium in αTi(O) is quite small and that the dissolved uranium has a little effect on the lattice expansion of αTi(O), the oxygen content of αTi in the reaction products can be estimated by the value of lattice parameter c. The results of the estimation are represented in Fig. 6. In this figure, broken line, which was drawn from the literature data for the Ti-O binary system[10-15], shows the oxygen content dependence of c value for αTi(O) solid solution. It is obvious from Fig. 6 that the c values of αTi in

samples q and r containing TiO as one of reaction products are in accord with that of solubility limit about 33 at%O reported for αTi. Therefore, αTi in samples q and r appears to be saturated with oxygen. For samples p - k, the parameter c was lower than the reported value for oxygen-saturated αTi(O). The oxygen content of αTi coexisting with UO_2 may be from 24 to 33 at%. In samples C - L and f - j which consisted of UO_2, αTi, αU and U_2Ti phases, αTi showed unchanged lattice parameters and axial ratio. This fact suggests that the αTi has the same oxygen content. From the c value for the αTi, the oxygen content in the αTi for samples C - L and f - j was estimated to be about 22 at%O. In the composition range where no UO_2 was formed, the c values of αTi were smaller than those for samples C - L and f - j, as can be seen in Fig. 6. In Ti-rich samples a - e and M - T, the αTi is likely to have various oxygen contents between 13 - 22 at%.

On the other hand, the lattice parameter of UO_2 in the reaction products was slightly changed with the sample composition. In the composition range corresponding to samples B - L and f - j, which contained no titanium oxide as a reaction product, the parameter was almost constant irrespective of the sample composition. The mean value was found to be a = 0.5471 nm which is larger than the lattice parameter of UO_2 before reaction (a = 0.5467 nm). The value of 0.5471 nm is in agreement with the published data for stoichiometric UO_2[16]. The phase diagram of U-O binary system[17] shown in Fig. 7 suggests that the lowest O/U ratio of UO_2 is 2.00 at 1000°C. This fact is consistent with the X-ray results for UO_2 in the present study. Reaction at 1000°C may lead to the decrease in O/U ratio of UO_2. The values of a for UO_2 coexisting with titanium oxides such as TiO, Ti_2O_3, Ti_3O_5 and TiO_2 (samples q - z and W - Y) were from 0.5470 to 0.5469 nm, which were also larger than the lattice parameter of UO_2 before reaction. The O/U ratio of the UO_2 in these samples may be close to 2.00, but it may be slightly larger than that of UO_2 in samples B - L and f - j. It is likely that UO_2 in the reaction products possesses nearly stoichiometric composition and dissolves only a small amount of titanium.

It was verified from the results of phase identification and lattice parameter measurement that reduction of UO_2 by titanium produced uranium and that the type and the number of the phases thus formed were dependent upon the composition of the sample.

Figure 8 shows the isothermal section of the U-Ti-O ternary system at 1000°C proposed by the present results. There exists a characteristic triangle of UO_2 + αTi(O) + (γU,βTi) in the isothermal section (region X in Fig. 8). Compositions of UO_2, αTi(O) and (γU,βTi) have to be thermodynamically fixed in this three-phase region. The constancy of the lattice spacing for αTi and UO_2 phases in this region is consistent with the phase rule. The solubility of oxygen in the αTi(O) may be about 22 at%. Based on the X-ray results the αTi(O) phase is confined a

narrow region close to the Ti-O edge of the isothermal section, as shown in Fig. 8, and uranium enters little into the solution. The UO_2 may dissolve a very small amount of titanium into the solid solution at 1000°C, as can be predicted by the previous study of UO_2-TiO_2 pseudobinary system[18]. Though the composition of the (γU,βTi) solid solution coexisting with UO_2 and αTi(O) was not determined precisely, it will contain approximately 25 at%Ti. This solid solution can take a limited amount of oxygen interstitially into the lattice. The three-phase region of UO_2 + αTi(O) + (γU,βTi) may be adjacent to two-phase regions of UO_2 + αTi(O) (region Ⅱ), UO_2 + (γU,βTi) (region Ⅲ) and αTi(O) + (γU,βTi) (region Ⅳ). In the two-phase region of UO_2 + αTi(O), the αTi(O) in equilibrium with UO_2 possesses an oxygen content ranging from 22 to 33 at%. The lattice parameters of αTi within the two-phase region of αTi(O) + (γU,βTi) varied with the composition. The positions of isoparametric lines across the two-phase region can be set by evaluation of the lattice spacing of the αTi. The tentative isoparametric lines, which correspond to tie lines, are indicated in the isothermal section. In the Ti-O binary system at 1000°C, βTi with 2 at%O can be in equilibrium with αTi(O) containing 6 at%O[8]. The conjugate phases of αTi(O) with an oxygen content below 15 at% are likely to be the (γU,βTi) solid solutions having a uranium content of 0 - 15 at%. In the region of UO_2-TiO-TiO_2, the four phases stable in the Ti-O system, namely βTiO, Ti_2O_3, Ti_3O_5 and TiO_2, exist in equilibrium with UO_2 at 1000°C. The compositions with high oxygen contents are expected to correspond to three- or two-phase regions which include UO_2 and one or two titanium oxides. Strictly speaking, a number of the titanium oxides, so-called Magneli phases with formula Ti_nO_{2n-1}, exist in the concentration range between Ti_3O_5 and TiO_2[8]. Therefore, the real equilibrium state in the three-phase region of UO_2 + TiO_2 + Ti_3O_5 (region Ⅰ) may have more complex features.

3.2. Thermodynamics of the solid solution phases in the U-Ti-O ternary system

It was recognized that the Ti-UO_2 section was not pseudobinary. At 1000°C, titanium containing a small amount of oxygen is not in equilibrium with UO_2. The αTi(O) solid solution with a sufficient oxygen content equilibrates with both UO_2 and (γU,βTi). The αTi(O) with an oxygen content above 22 at%O, which is significantly lower than the solubility limit of oxygen in αTi(O), 33 at%O, can be in two-phase equilibrium with UO_2. These experimental findings indicate that oxygen potentials controlled by the αTi(O) solid solutions determine whether or not the reaction occurs between UO_2 and titanium. The key to solve compatibility problems between titanium getter and fuel is to evaluate the oxygen potential over αTi(O) solid solutions. Furthermore, the oxygen potential is a crucial factor in the gettering rate and capacity.

The oxygen potentials $\Delta\bar{G}_{O_2}(TiO_x)$ over αTi(O) solid solutions at 1000°C were reported by several investigators[19-25], as shown in Fig. 9. Unfortunately, there is a large discrepancy in the oxygen potential $\Delta\bar{G}_{O_2}(TiO_x)$ over single-phase region of αTi(O) and the oxygen potential $\Delta\bar{G}_{O_2}(TiO)$ over two-phase region of αTi(O) + βTiO among these sets of previous data[19-25]. The experimental phase diagram of the U-Ti-O ternary system provides not only information of stable phase at a given temperature and composition but also thermodynamic quantities of present phases such as oxygen potential. The author has therefore tried to estimate the oxygen potential over αTi(O) as a function of oxygen content from the isothermal section of the U-Ti-O ternary system experimentally obtained at 1000°C. The partial thermodynamic quantities of αTi(O) and (γU,βTi) such as oxygen potentials over the solution and partial molar free energies of titanium and uranium in the solution must be examined first. These properties were drawn from the data for the Ti-O and U-Ti binary systems.

For the αTi(O) solid solution phase, the Gibbs-Duhem equation offers the following relation:

$$N_{Ti}\, d(\Delta\bar{G}_{Ti}(TiO_x)) + N_O\, d(1/2\ \Delta\bar{G}_{O_2}(TiO_x)) = 0 \qquad (1)$$

where $\Delta\bar{G}_{Ti}(TiO_x)$ and $\Delta\bar{G}_{O_2}(TiO_x)$ are the partial molar excess free energy of titanium in αTi(O) and the oxygen potential. The N_{Ti} and N_O are the titanium and oxygen contents in αTi(O) in atomic fraction, and so $N_{Ti} + N_O = 1$. Integration of eq. (1) gives

$$\Delta G_f^\circ(TiO_x) = 1/2 \int \Delta\bar{G}_{O_2}(TiO_x)\, dx_O \qquad (2)$$

which is called Duhem-Margules equation. In this equation, $\Delta G_f^\circ(TiO_x)$ is the integral molar free energy of formation of the αTi(O) per one mole solution and x_O is the oxygen content in O/Ti atom ratio. The evaluation of the Duhem-Margules equation is schematicaly illustrated in Fig. 10. The area under the curve in this figure must be equal to the integral value given above. If one can obtain concentration dependence of the oxygen potential, the free energy of formation of αTi(O) can be evaluated from eq. (2).

In the present study, the $\Delta\bar{G}_{O_2}(TiO_x)$ function of x_O was chosen as a natural logarithm, as is usually the case in thermodynamics[26-28]:

$$\Delta\bar{G}_{O_2}(TiO_x) = \Delta\bar{G}_{O_2}(TiO) + 2\,A\,\ln(x_O/x_O^s) \qquad (3)$$

where $x_O^s = 0.493$ (solubility limit of oxygen in αTi(O) phase at 1000°C) and A is a constant irrespective of x_O. Consequently, integration along $\Delta\bar{G}_{O_2}(TiO_x)$ in the

single-phase region leads

$$\Delta G_f^\circ(TiO_x) = x_O/2\ \Delta\bar{G}_{O_2}(TiO) + A\ (x_O \ln (x_O/x_O^s) - x_O). \quad (4)$$

If the integration of $\Delta\bar{G}_{O_2}(TiO_x)$ is done from $x_O = 0$ to $x_O = 1$, the following equation is obtained:

$$\Delta G_f^\circ(TiO) = 1/2\ \Delta\bar{G}_{O_2}(TiO) - A\ x_O^s \quad (5)$$

where $\Delta G_f^\circ(TiO)$ is the standard free energy of formation of βTiO. As evidenced by Fig. 10, the $\Delta G_f^\circ(TiO)$ value represented by the broken line is equal to the area under the oxygen potential curve composed of two sections: single-phase region and two-phase region. When the value of $\Delta\bar{G}_{O_2}(TiO_x)$ is known at a certain x_O and reliable data of $\Delta G^\circ_f(TiO)$ are available in the literature, the oxygen potential $\Delta\bar{G}_{O_2}(TiO_x)$ can be determined as a function of x_O.

On the other hand, $\Delta G^\circ_f(TiO_x)$ is associated with $\Delta\bar{G}_{Ti}(TiO_x)$ and $\Delta\bar{G}_{O_2}(TiO_x)$ as follows:

$$\Delta G^\circ_f(TiO_x) = \Delta\bar{G}_{Ti}(TiO_x) + x_O/2\ \Delta\bar{G}_{O_2}(TiO_x). \quad (6)$$

So, the simple equation concerning the partial molar excess free energy of titanium in αTi(O) can be derived,

$$\Delta\bar{G}_{Ti}(TiO_x) = - A\ x_O. \quad (7)$$

If the value of $\Delta\bar{G}_{Ti}$ and $\Delta\bar{G}_{O_2}$ at a certain content of oxygen in αTi(O) is known, a complete relation of the oxygen potential with the oxygen content in αTi(O) can be estimated using eqs. (7) and (3).

The bcc solid solution (γU,βTi) indicates complete mutual solubility above 898°C, as mentioned before. Experimental measurements have not yet been made of thermodynamic properties of this solid solution phase. Recently, Murray[8] has estimated Gibbs energies of (γU,βTi) phase from the U-Ti binary phase diagram on the basis of a quasiregular solution model. The excess free energy of the solid solution phase ΔG^{EX}(U,Ti) in J/mol at 1000°C is represented as:

$$\Delta G^{EX}(U,Ti) = y_U\ (1 - y_U)\ \Omega,$$
$$\Omega = 18078 - 2425\ (1 - 2\ x_U) \quad (8)$$

where y_U is the uranium content in atomic fraction and Ω is so-called the interaction parameter. From eq. (8), the partial molar excess free energies of

uranium and titanium can be derived as follows:

$$\Delta\bar{G}_U\ (U,Ti) = RT\ \ln y_U + (1 - y_U)^2\ (18078 - 2425\ (1 - 4\ y_U)),$$
$$\Delta\bar{G}_{Ti}(U,Ti) = RT\ \ln (1 - y_U) + y_U{}^2\ (18078 - 2425\ (3 - 4\ y_U)). \qquad (9)$$

Figure 11 reveals the changes in $\Delta\bar{G}_U$ and $\Delta\bar{G}_{Ti}$ of (γU,βTi) phase at 1000°C with uranium content y_U. Activities of uranium and titanium in the solid solution phase are derived from the values of $\Delta\bar{G}_U$ and $\Delta\bar{G}_{Ti}$, as shown in Fig. 12. It is found from these figures that at 1000°C the solution behaves as a nearly regular solution.

Oxygen potentials $\Delta\bar{G}_{O2}(UO_2)$ over two-phase region of UO_2 + (γU,βTi) are approximately expressed by

$$\Delta\bar{G}_{O2}(UO_2) = \Delta G_f{}^\circ(UO_2) - \Delta\bar{G}_U(U,Ti). \qquad (10)$$

where $\Delta G_f{}^\circ(UO_2)$ is the standard free energy of formation of UO_2. Since $\Delta\bar{G}_U(U,Ti)$ is given as a function of uranium content y_U in eq. (9), variation in $\Delta\bar{G}_{O2}(UO_2)$ with y_U can be obtained, as shown in Fig. 13. From this figure, it is evident that $\Delta\bar{G}_{O2}(UO_2)$ over two-phase region is not affected by composition of (γU,βTi) solid solution so much.

The isothermal section of the U-Ti-O ternary system experimentally obtained at 1000°C indicates the existence of UO_2 + αTi(O) + (γU,βTi) region. The triangle of the three-phase region gives us the uranium content of (γU,βTi) y_U = 0.75 and the oxygen content of αTi(O) x_O = 0.282. Assuming that oxygen solubility of (γU,βTi) is negligibly small and αTi(O) takes a limited amount of uranium into solution, equilibria in this three-phase region can be described by the following reactions:

$$2\ O[\alpha Ti(O)] + U[(\gamma U,\beta Ti)] = UO_2$$
$$Ti[\alpha Ti(O)] = Ti[(\gamma U,\beta Ti)].$$

Since the chemical potentials of uranium, titanium and oxygen are equal at equilibrium, the relations between the partial molar quantities based on these reactions are expressed by

$$\Delta\bar{G}_{O2}(TiO_x) = \Delta G_f{}^\circ(UO_2) - \Delta\bar{G}_U(U,Ti), \text{ and}$$
$$\Delta\bar{G}_{Ti}(TiO_x) = \Delta\bar{G}_{Ti}(U,Ti). \qquad (11)$$

If eqs. (4), (5), (7), (9) - (11) and equilibrium conditions x_O = 0.282 and y_U = 0.75 are used, one would need the free energy value of either $\Delta G_f{}^\circ(UO_2)$ or

$\Delta G_f^\circ(TiO)$ to determine $\Delta\bar{G}_{O_2}(TiO_x)$ as a function of x_O. Both values of $\Delta G_f^\circ(UO_2)$ and $\Delta G_f^\circ(TiO)$ are available in the literature[29-35]. However, $\Delta G_f^\circ(UO_2)$ has been extensively assessed by several authors[29-34], and the value appears to be more reliable than that of $\Delta G_f^\circ(TiO)$[29,30,35]. The standard free energy of formation of UO_2 at 1000°C was used for estimating the oxygen potential over αTi(O), and the value chosen for calculation was -864.5 kJ/mol from Ackerman's table[32]. Because $\Delta G_f^\circ(TiO)$ value can be also estimated from eqs. (3) and (5), consistency between the obtained value and literature data was checked.

The estimated oxygen potential over αTi(O) solid solution at 1000°C, $\Delta\bar{G}_{O_2}(TiO_x)$, is shown as a function of oxygen content in Fig. 14. The value of $\Delta\bar{G}_{O_2}(TiO_x)$ decreased from -845 kJ/mol at x_O = 0.493 to -912 kJ/mol at x_O = 0.06 in the single-phase region. The estimated values of oxygen potentials in the range of 0.06 - 0.493 O/Ti ratio fell into the scatter of literature data[19-25]. The oxygen potential in the two-phase region of αTi(O) + βTiO agreed with the experimental value reported by Suzuki et al.[22] and the IAEA recommended value[19]. The standard free energy of formation of βTiO at 1000°C was estimated to be -430.4 kJ/mol, which was close to the reported values[29,30,35].

It should be noted that all the estimated values of $\Delta\bar{G}_{O_2}(TiO_x)$, $\Delta\bar{G}_{O_2}(TiO)$ and $\Delta G_f^\circ(TiO)$ were consistent with the previous results. The concentration dependence of estimated oxygen potential over αTi(O) solid solution therefore seems to be reliable. Thus, the author demonstrated that the partial thermodynamic quantity can be evaluated from the ternary phase diagram. Reduction of UO_2 caused by low oxygen potentials over αTi(O) forms a metallic uranium alloy. In like manner, $(U,Pu)O_2$ mixed oxide fuel may not be compatible with αTi(O) at an elevated temperature, and a (U,Pu,Ti) ternary solution appears to result from the reaction between them.

Even though the lowest oxygen potential of titanium among candidate getter/buffer materials such as chromium, vanadium and niobium is attractive for its practical use in LMFBR fuel pins, the existence of potential compatibility problems between titanium getter and LMFBR fuel was indicated by the results for the phase equilibria in the U-Ti-O ternary system at 1000°C corresponding to a typical surface temperature of the fuel. At the initial stage, drastic reduction of fuel by titanium getter may bring about metallic uranium alloy because of the extremely low oxygen potential over αTi(O) solid solution. The occurrence of a large amount of uranium alloy at the interface between getter and fuel may provide an adverse effect on fuel performance. From the standpoint of the compatibility, there will be a great risk in mixing of titanium getter with fuel. If titanium were employed as a getter material, thin coating on fuel pellets or on cladding rather than bulk metal would be favorable. However, for accurate knowledge of reaction of mixed oxide fuel $(U,Pu)O_2$ with titanium getter, more detailed

information is required on the quaternary system of U-Pu-Ti-O.

4. Conclusions

In order to elucidate interaction of titanium getter with fuel, equilibrium phase relations in the U-Ti-O ternary system have been studied by X-ray diffraction technique. The isothermal section at 1000°C was constructed for the U-Ti-O system. Phase regions including (γU,βTi) solid solution occurred between UO_2 and titanium at 1000°C. It should be noted that nearly stoichiometric UO_2 can be in equilibrium with αTi(O) solid solutions at an oxygen content between 22 and 33 at% and with the titanium oxides βTiO, Ti_2O_3, Ti_3O_5 and TiO_2. Titanium can reduce UO_2 and may produce (γU,βTi) alloy until the oxygen content of titanium reaches about 22 at%.

The oxygen potentials over αTi(O) at 1000°C were derived from experimental data of the isothermal section of the U-Ti-O ternary system. The estimated thermodynamic quantities such as oxygen potentials over αTi(O) and standard free energy of formation of βTiO were in reasonable agreement with the reported values.

It was concluded from the present equilibrium study that there exist potential problems for compatibility of titanium getter with the fuel. If titanium were adopted as a corrosion inhibitor, special attention should be paid to the geometry and placement of the titanium getter in LMFBR fuel pins.

References

[1] O. Gotzmann and Ph. Dunner, Summary Report of Technical Committee Meeting on Fuel and Cladding Interaction, (IAEA, Vienna, 1977)p43.

[2] L.A. Lawrence, J.W. Weber and J.L. Devary, Proceedings of International Conference on Fast Breeder Reactor Fuel Performance, (ANS, Illinois, 1979)p432.

[3] W.E. Roake, R.F. Hilbert, M.G. Adamson, S. Langer, J.W. Weber, R.L. Gibby, E.T. Weber and R.E. Woodley, Summary Report of Technical Committee Meeting on Fuel and Cladding Interaction, (IAEA, Vienna, 1977)p137.

[4] M.G. Adamson, ibid., (IAEA, Vienna, 1977)p108.

[5] R.J. Jackson, R.L. Gibby, R.E. Woodley, J.W. Weber and M.G. Adamson, ibid., (IAEA, Vienna, 1977)p189.

[6] E.T. Weber, L.A. Lawrence, C.N. Wilson and R.L. Gibby, Proceedings of International Conference on Fast Breeder Reactor Fuel Performance, (ANS, Illinois, 1979)p445.

[7] M.U. Cohen, Rev. Sci. Inst., 6(1935)68.

[8] J.L. Murray, Phase Diagram of Binary Titanium Alloys, (AMS, Ohio, 1987).

[9] C. Keller, Gmelin Handbuch der Anorganichen Chemie Uran C3, (Springer-Verlag, 1975)p273.

[10] S. Yamaguchi, J. Phys. Soc. Japan, 27(1969)155.

[11] D. Gupta and S. Weinig, Trans. Metall. AIME, 215(1959)209.
[12] E.S. Makarov and L.M. Kuzneov, Zh. Strukt Khim, 1(1960)170.
[13] R.J. Wasilewski, Trans. Metall. AIME, 221(1961)1231.
[14] A. Jostons and R. McDougall, Sci. Technol. Appl. Titanium, (1970)745.
[15] E.A. Garcia, J. Com-Nougue, X. Lucas, G. Beranger and P. Lacombe, C. R. Hebd. Seanes Acad. Sci., 277(1973)1291.
[16] K. Suzuki, K. Maruya and M. Kubota, J. Atomic Energy Soc. Japan, 5(1963)587.
[17] T.B. Massalski, Binary Alloy Phase Diagrams, (ASM, Ohio, 1986).
[18] J.B. Ainscough, F. Rigby and S.C. Osborn, J. Nucl. Mater., 52(1974)191.
[19] K.L. Komarek, Titanium: Physico-Chemical Properties of Its Compounds and Alloys, (IAEA, Vienna, 1983).
[20] O. Kubaschewski and W.A. Dench, J. Inst. Metals, 82(1954)87.
[21] idem.,ibid.,84(1956)440.
[22] K. Suzuki and K. Sambongi, Tesu To Hagane, 58(1972)1579.
[23] G. Boureau and P. Gerdanian, Acta Metall., 24(1976)717.
[24] R. Tetot, C. Picard, G. Boureau and P. Gerdanian, J. Chem. Phys., 69(1978)326.
[25] K. Komarek and M. Silver, Thermodynamics of Nuclear Materials, (IAEA, Vienna, 1962)p749.
[26] O. Gotzmann, J. Nucl. Mater., to be published.
[27] T.B. Lindemer and T.M. Besmann, J. Nucl. Mater., 130(1985)473.
[28] T.M. Besmann and T.B. Lindemer, J. Nucl. Mater., 130(1985)489.
[29] I. Barin, O. Knacke and O. Kubaschewski, Thermochemical Properties of Inorganic Substances, (Springer Verlag, Berlin, 1973).
[30] O. Kubaschewski and C.B. Alcock, Metallurgical Thermochemistry, 5th Ed., (Pergamon Press, Oxford, 1979).
[31] L.B. Pankratz, Thermodynamic Properties of the Elements and Oxides, U.S. Dept. Interior Bureau of Mines, Bulletin 672, (U.S. Gov't. Printing Office, Washington D.C., 1982).
[32] R.J. Ackermann, Thermodynamics of Nuclear Materials, (IAEA, Vienna, 1980)p18.
[33] CORDA Task Group, J. Chem. Thermodynamics., 10(1978)903.
[34] G.H. Winslow, High Temp. Sci., 7(1975)81.
[35] M.W. Chase Jr., C.A. Davies, J.R. Downey Jr., D.J. Frurip, R.A. McDonald and A.N. Syverud, JANAF Thermochemical Tables, 3rd Ed., (American Institute of Physics, Inc., New York, 1985).

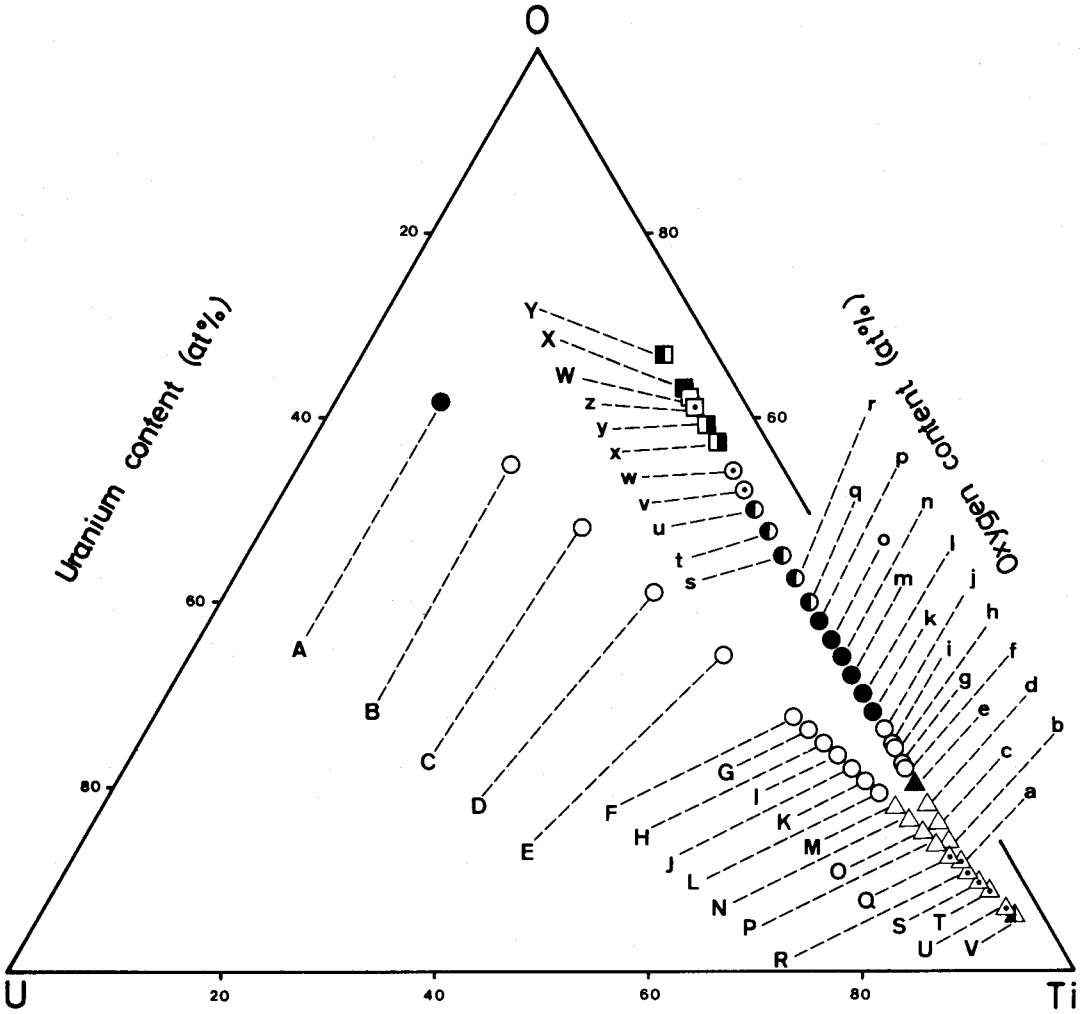

Fig. 1 Reaction products of the mixture pellets after heating at 1000°C.

- $UO_2 + TiO_2$,
- $UO_2 + Ti_3O_5 + Ti_2O_3$,
- $UO_2 + Ti_2O_3 + \beta TiO$,
- $UO_2 + \beta TiO + \alpha Ti$,
- $UO_2 + \alpha Ti + \alpha U + U_2Ti$,
- $\alpha Ti + U_2Ti$,
- $\alpha Ti + \beta Ti$.
- $UO_2 + Ti_3O_5$,
- $UO_2 + Ti_2O_3$,
- $UO_2 + \beta TiO$,
- $UO_2 + \alpha Ti$,
- $\alpha Ti + \alpha U + U_2Ti$,
- $\alpha Ti + U_2Ti + \beta Ti$,

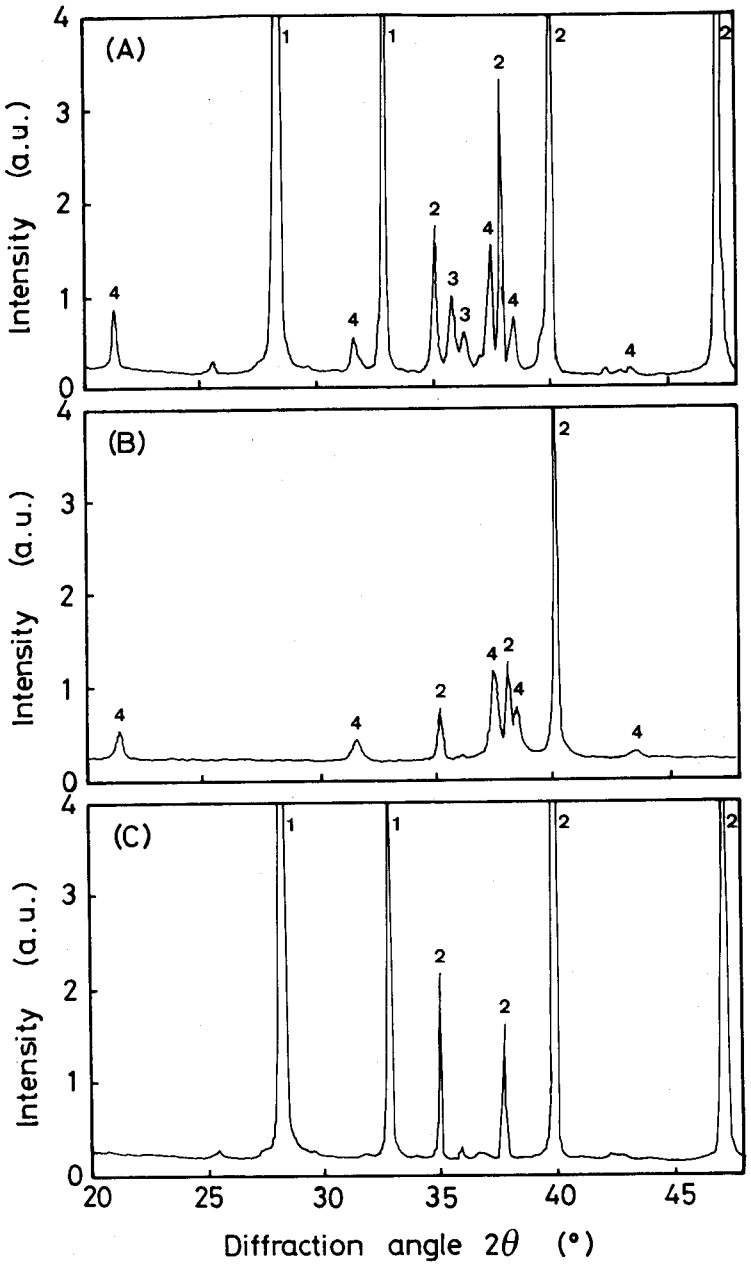

Fig. 2 X-ray diffraction patterns of the reaction products.
(A) sample E, (B) sample P, (C) sample I.
1: UO_2, 2: αTi, 3: αU, 4: U_2Ti.

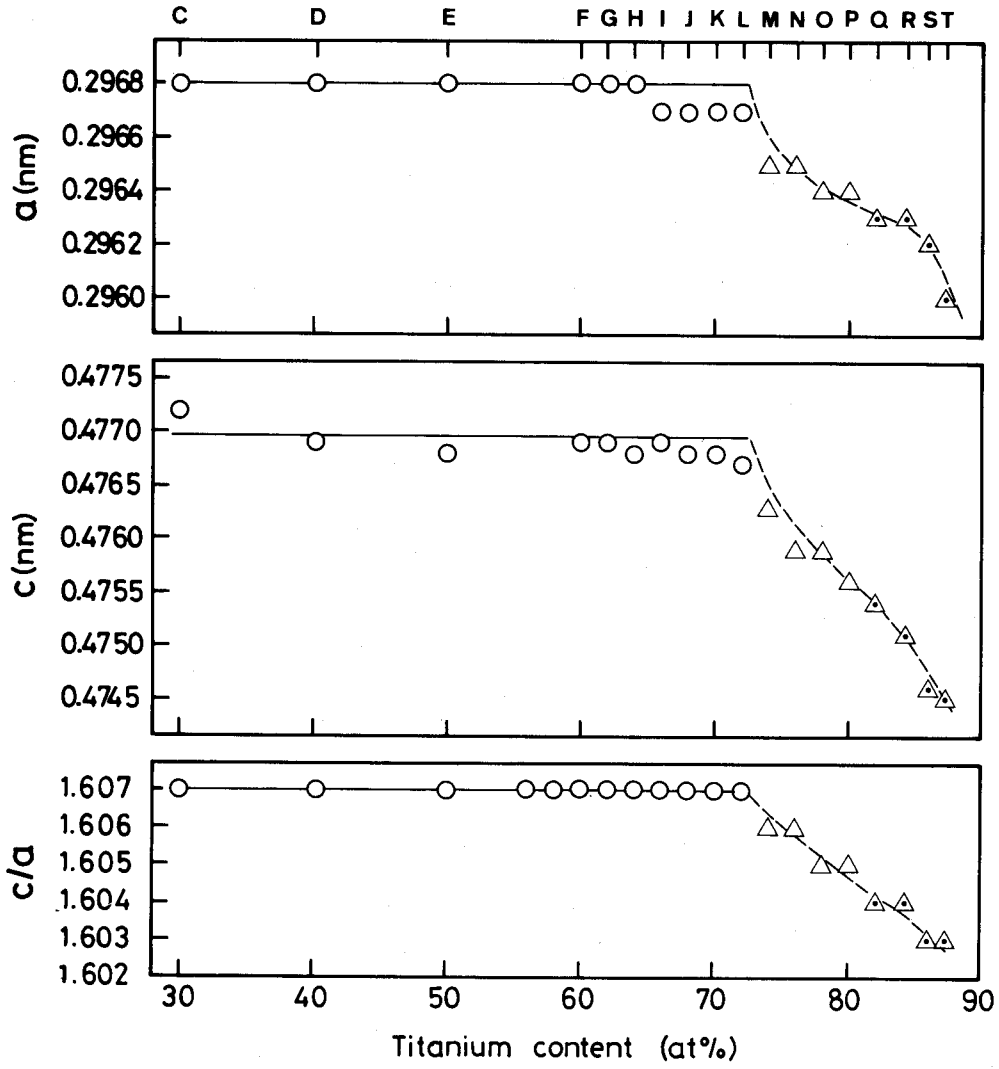

Fig. 3 Change in the lattice parameters a and c and the axial ratio c/a of αTi in the reaction products of samples C - T with titanium content.

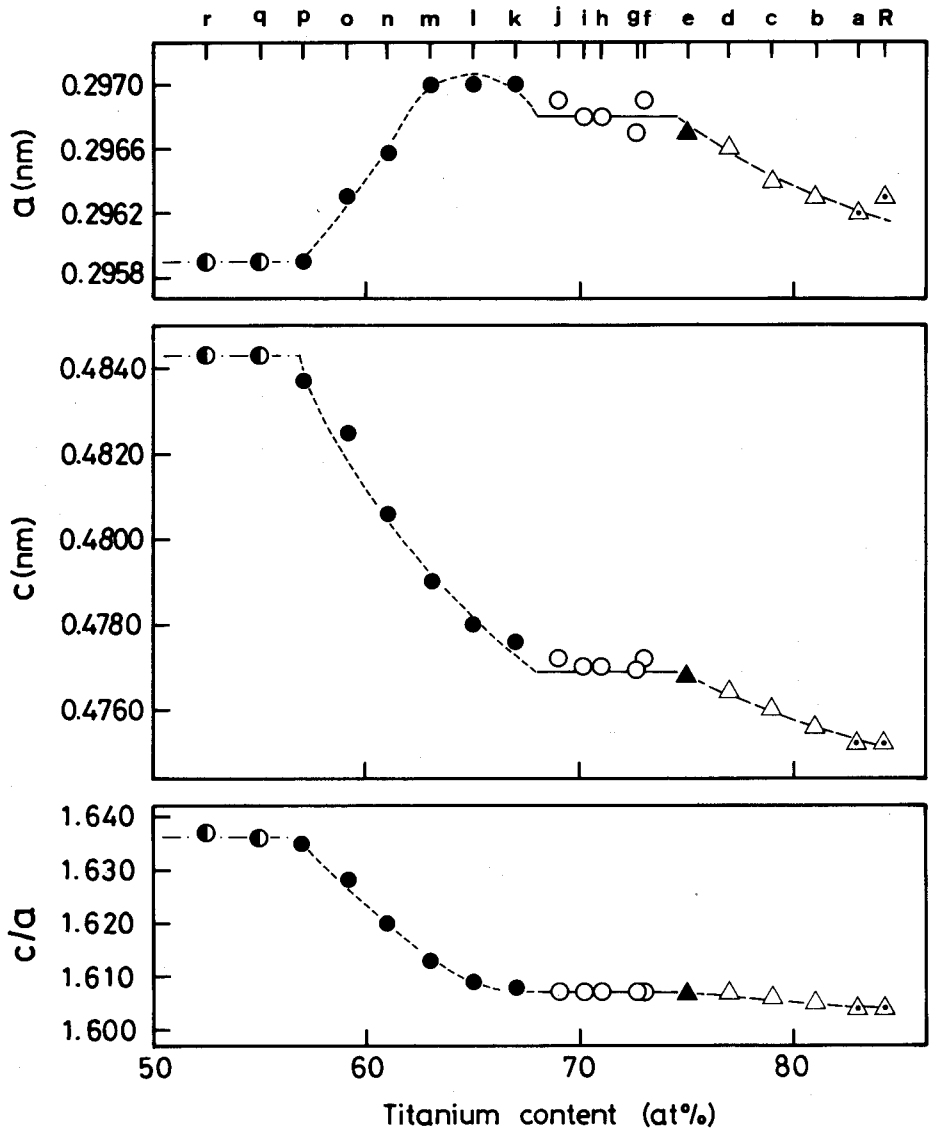

Fig. 4 Change in the lattice parameters a and c and the axial ratio c/a of αTi in the reaction products of samples a - r and R with titanium content.

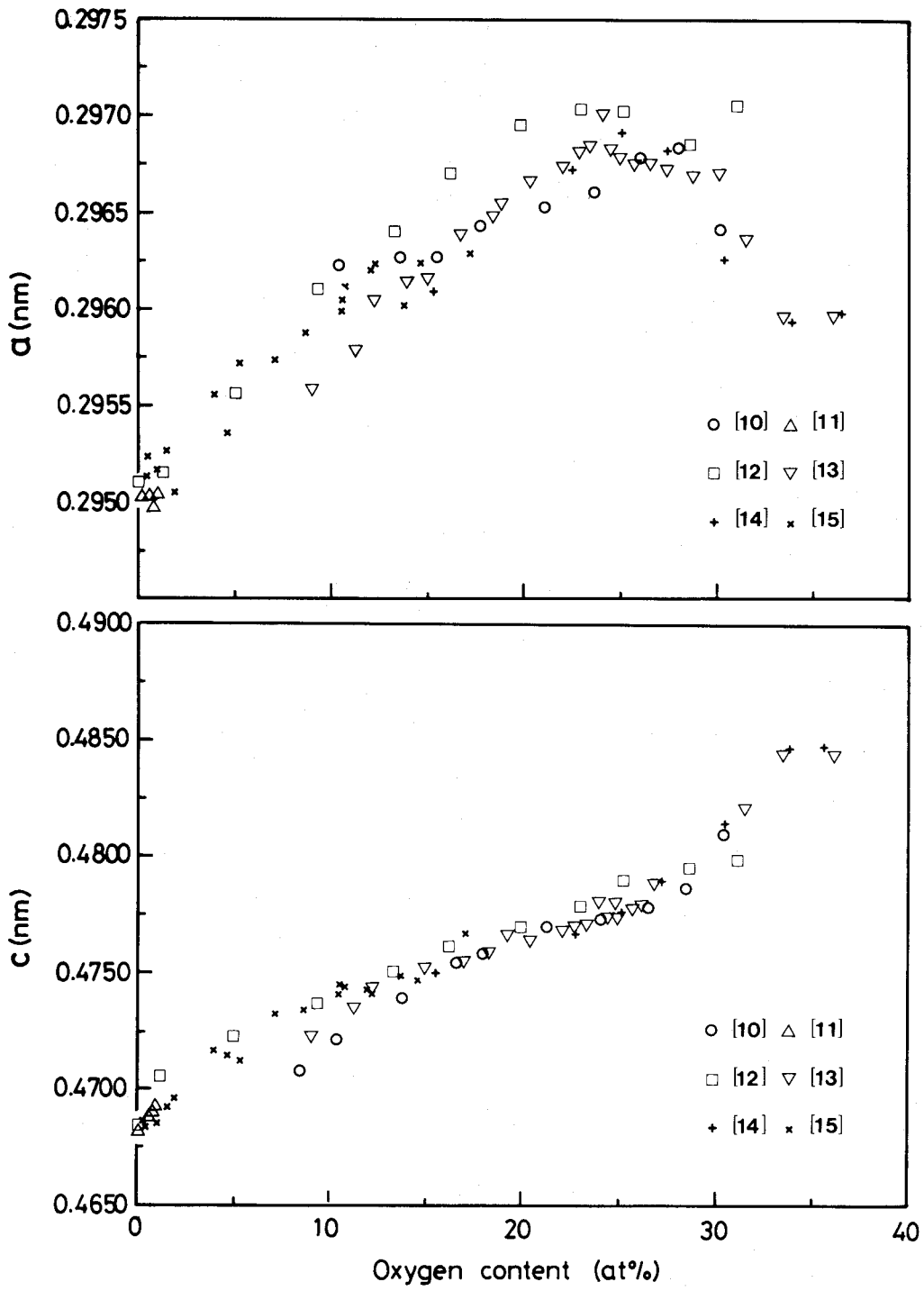

Fig. 5 Change in the lattice parameters a and c of αTi with oxygen content reported in the literature[10-15].

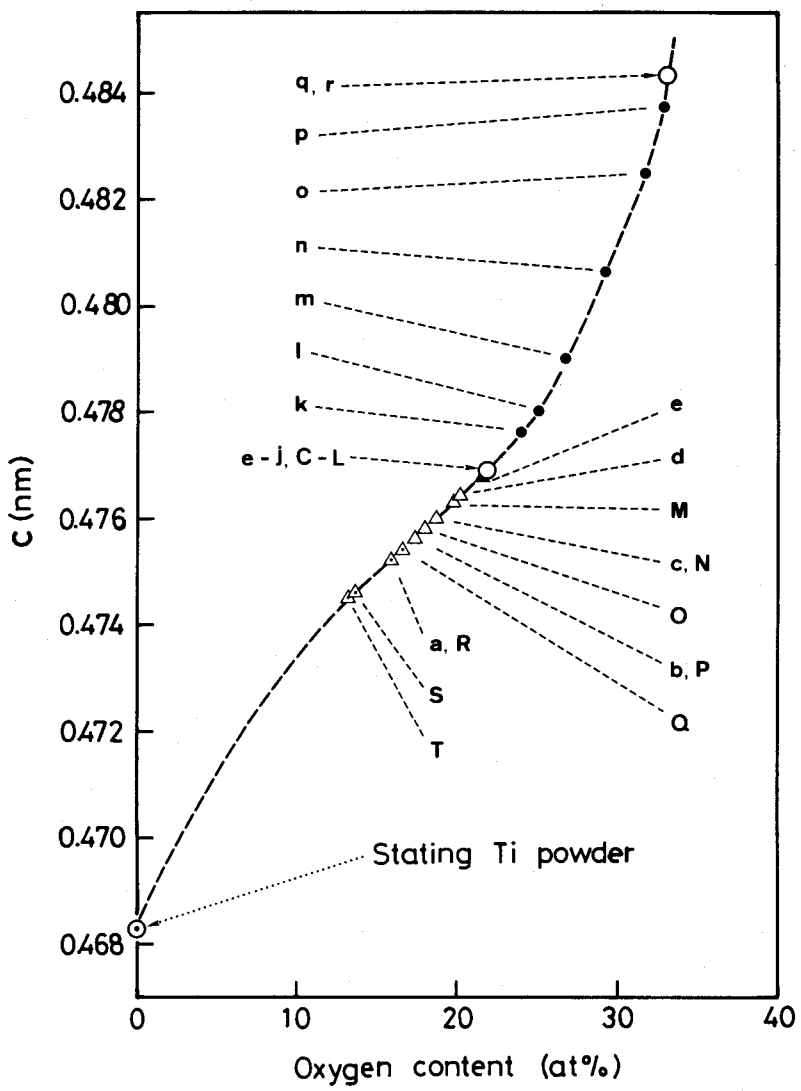

Fig. 6 Estimation of oxygen content of αTi in the reaction products of samples C - T and a - r.

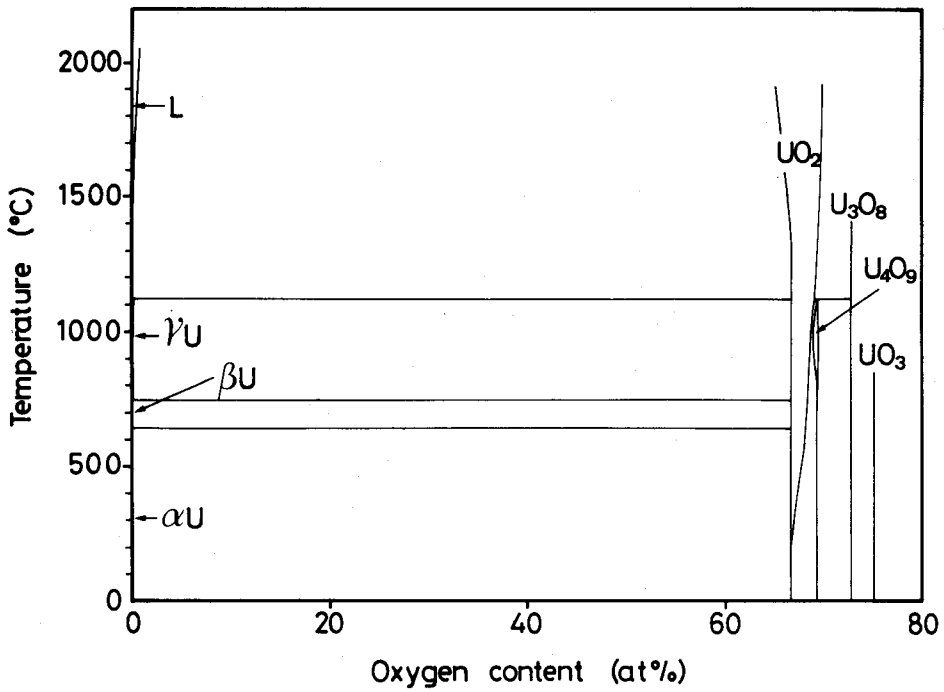

Fig. 7 Phase diagram of the U-O binary system[17].

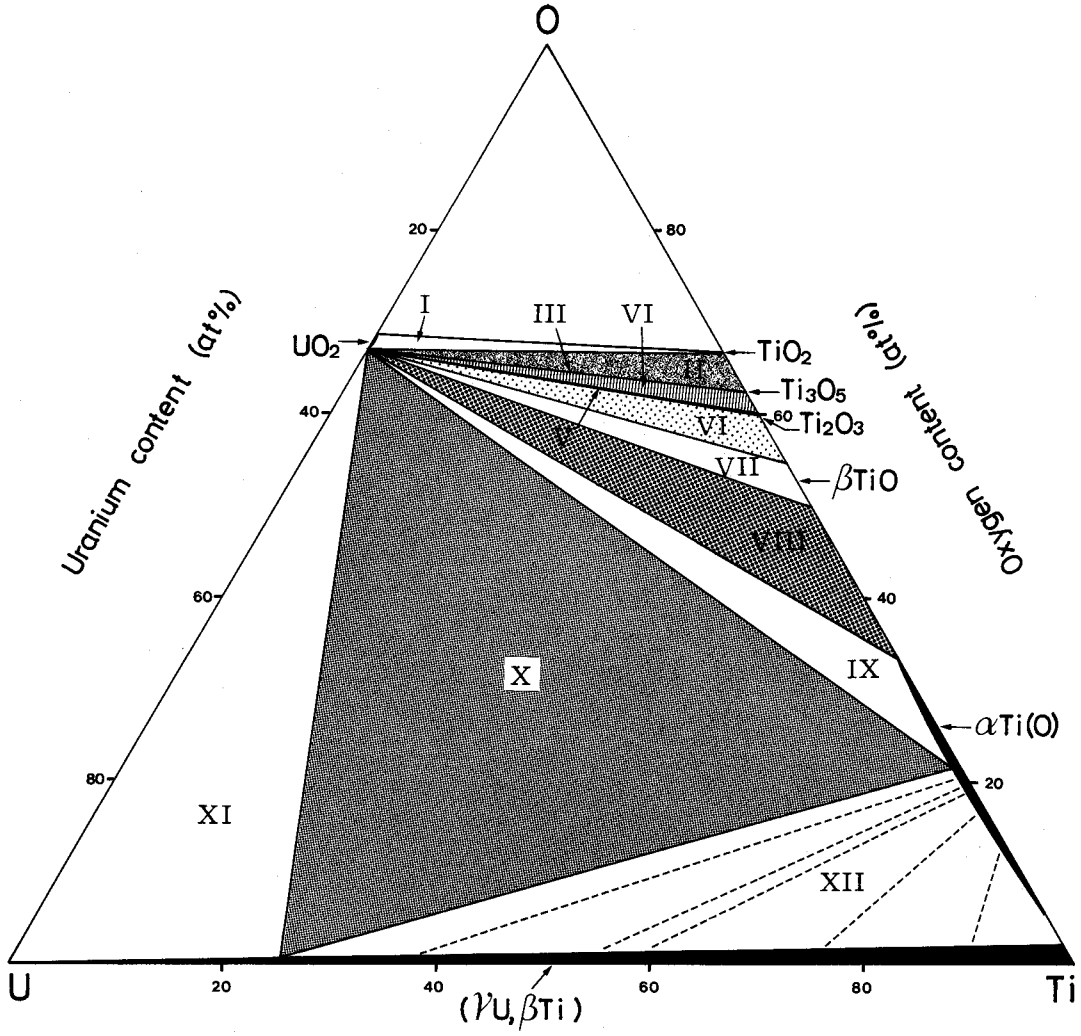

Fig. 8 Isothermal section of the U-Ti-O ternary system at 1000°C.

I UO_2 + TiO_2,
II UO_2 + TiO_2 + Ti_3O_5,
III UO_2 + Ti_3O_5,
IV UO_2 + Ti_3O_5 + Ti_2O_3,
V UO_2 + Ti_2O_3,
VI UO_2 + Ti_2O_3 + βTiO,
VII UO_2 + βTiO,
VIII UO_2 + βTiO + αTi(O),
IX UO_2 + αTi(O),
X UO_2 + αTi(O) + (γU,βTi),
XI UO_2 + (γU,βTi),
XII αTi(O) + (γU,βTi).

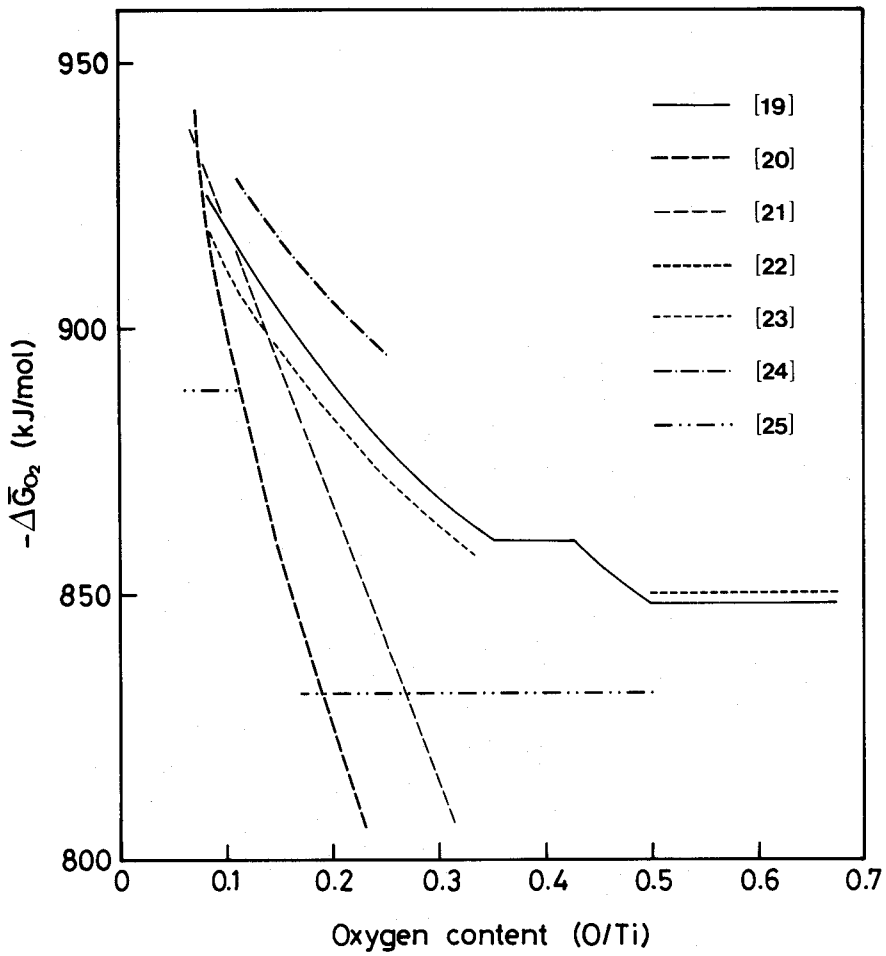

Fig. 9 Oxygen potential over αTi(O) solid solution, $\Delta\bar{G}_{O_2}(TiO_x)$, at 1000°C reported in the literature[19-25].

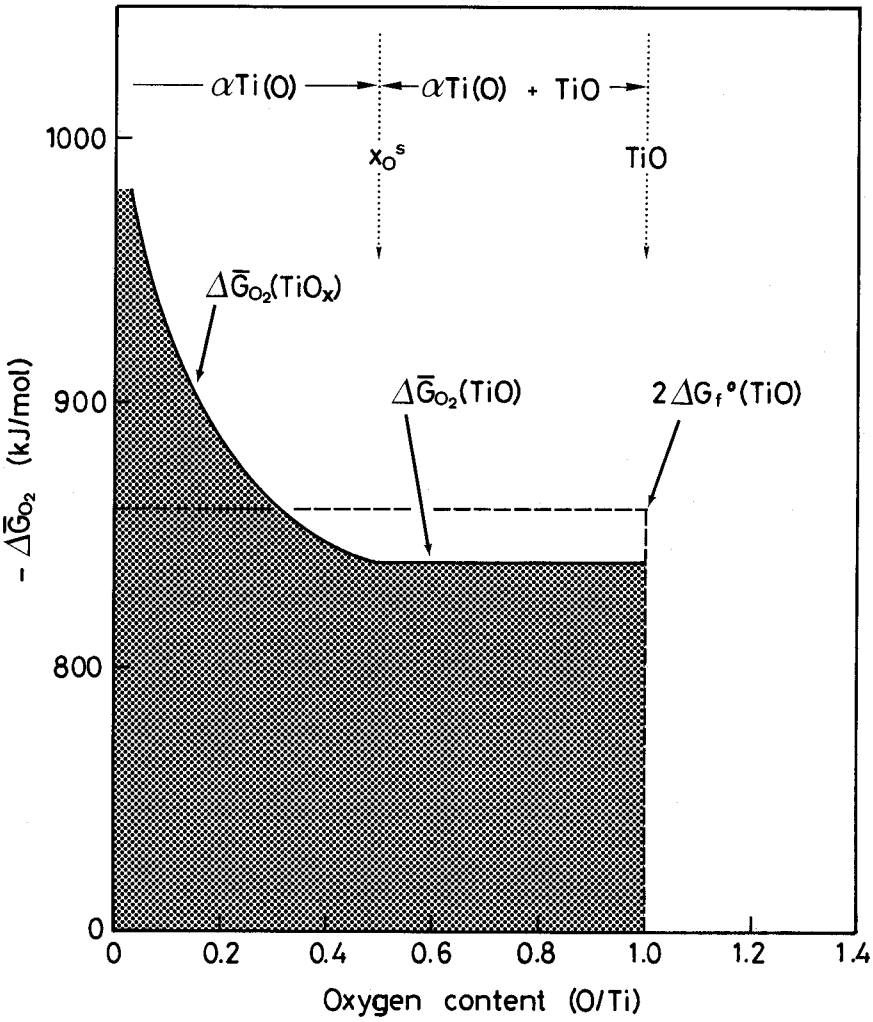

Fig. 10 Schematic representation of relation between oxygen potential over αTi(O) solid solution, $\Delta\bar{G}_{O_2}(TiO_x)$, and standard free energy of formation of TiO, $\Delta G_f°(TiO)$.

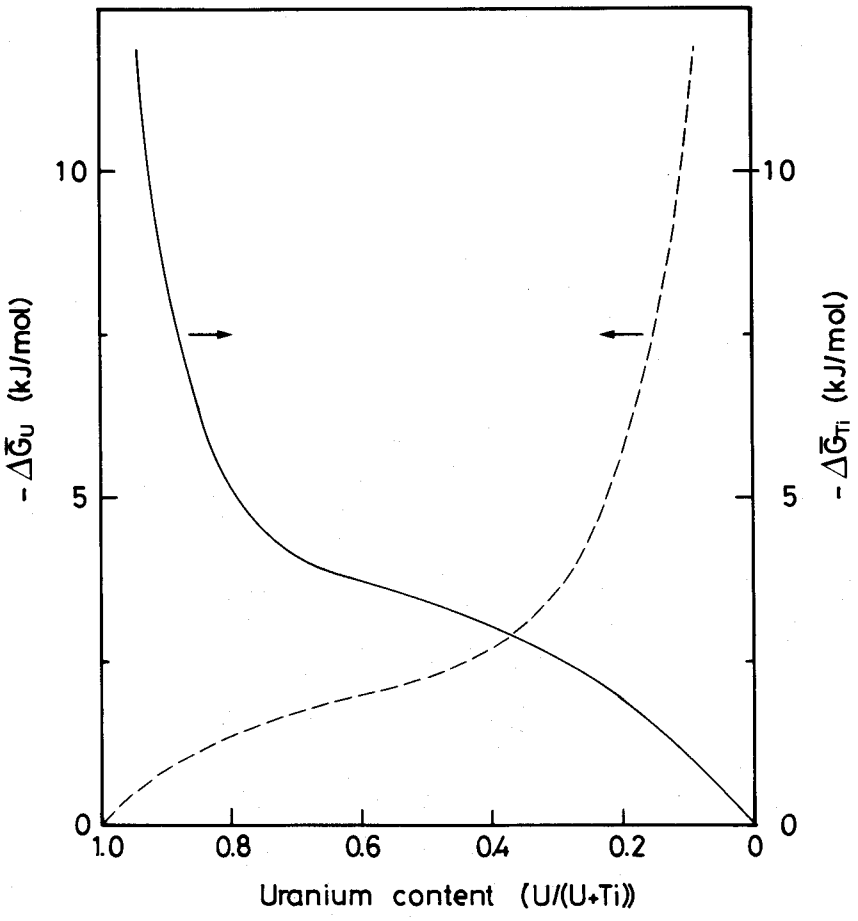

Fig. 11 Change in the partial molar excess free energies of uranium and titanium in (γU,βTi) solid solution, $\Delta\bar{G}_U$ and $\Delta\bar{G}_{Ti}$, with uranium content at 1000°C.

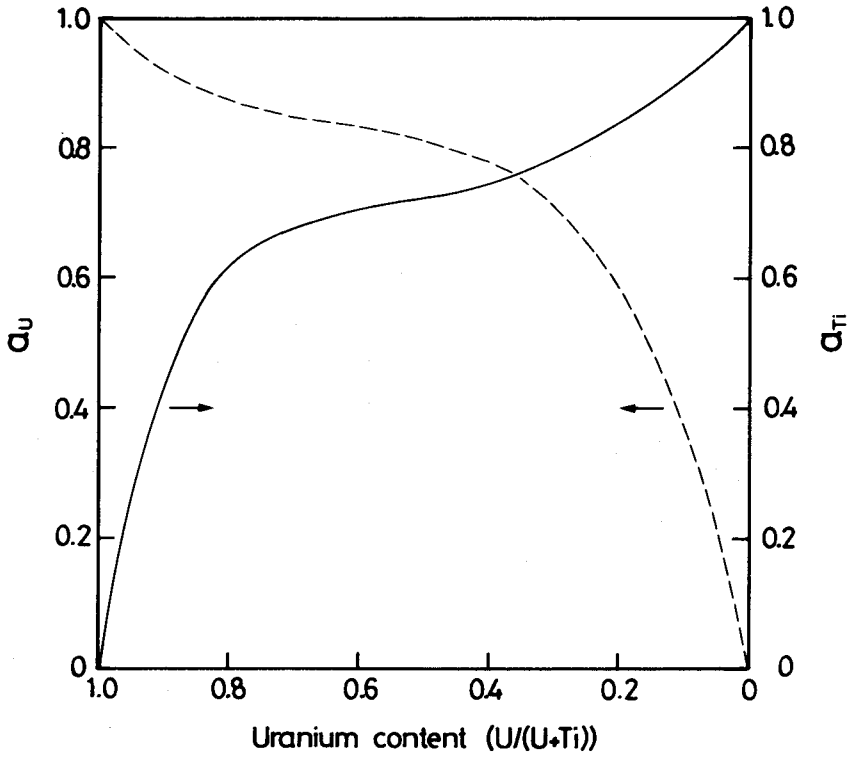

Fig. 12 Change in the thermodynamic activities of uranium and titanium in (γU,βTi) solid solution, a_U and a_{Ti}, with uranium content at 1000°C.

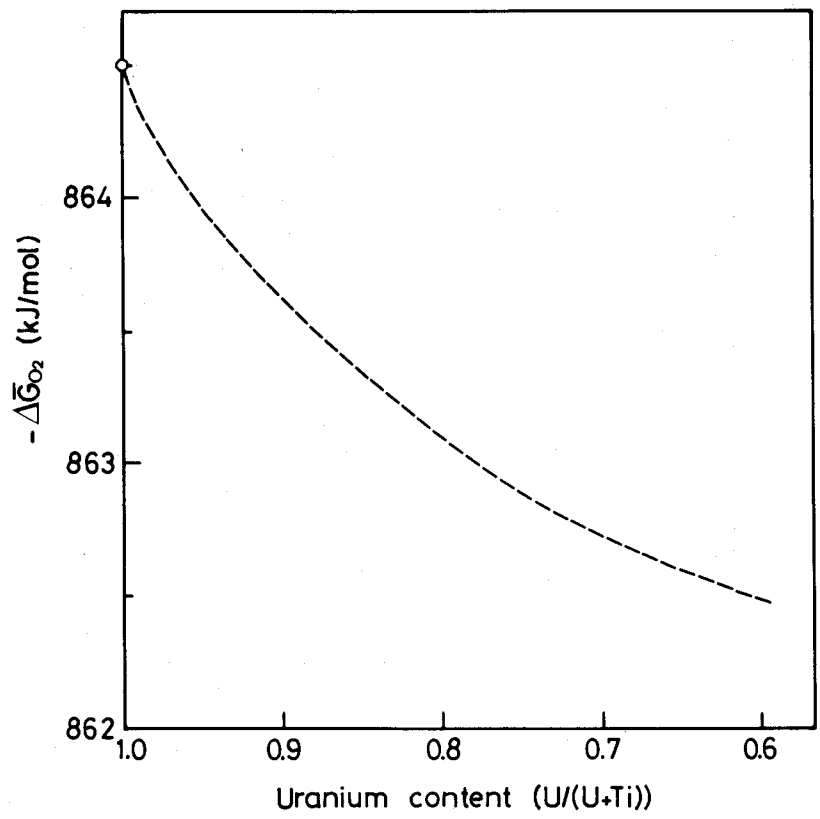

Fig. 13 Change in the oxygen potential over (γU,βTi) solid solution in two-phase equilibrium with UO_2, $\Delta\bar{G}_{O_2}(UO_2)$, with uranium content at 1000°C.

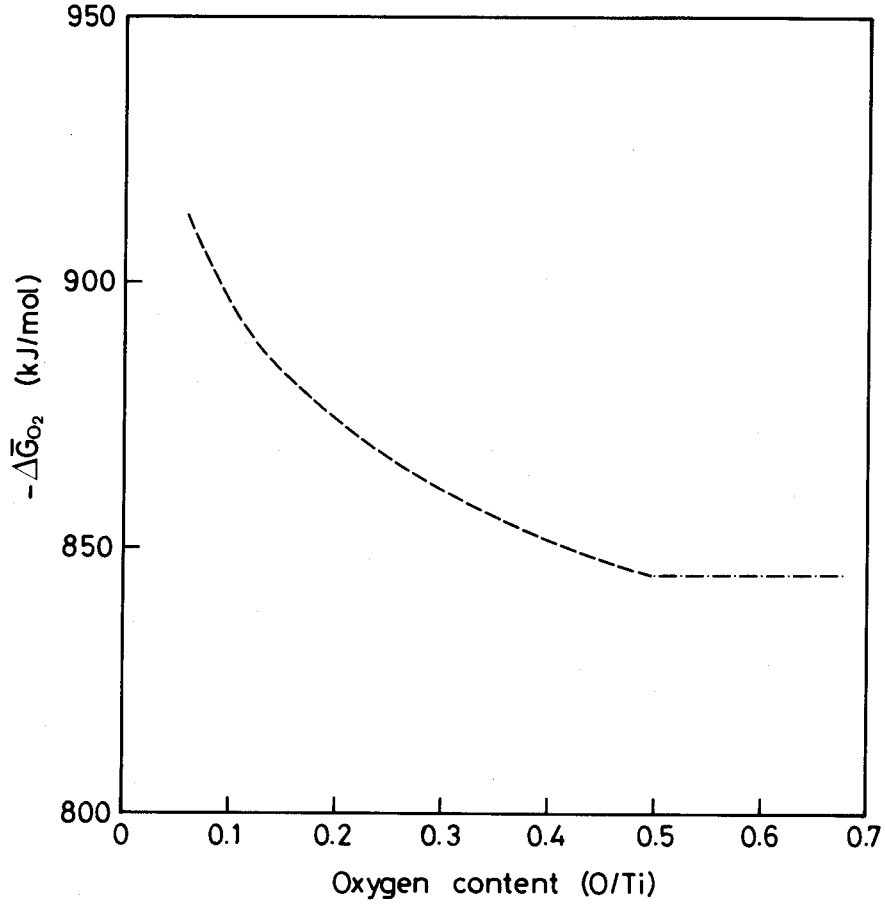

Fig. 14 Estimated oxygen potential $\Delta\bar{G}_{O_2}$ over α Ti(O) solid solution at 1000°C.

CHAPTER 3 URANIUM-ZIRCONIUM-OXYGEN TERNARY SYSTEM

1. Introduction

In recent years, high temperature interaction between UO_2 fuel and Zircaloy cladding has been studied to elucidate the fuel rod behavior under hypothetical accident conditions of light water reactors (LWRs). Interfacial reaction of UO_2 with Zircaloy has been extensively investigated from kinetic points of view[1-3], and several analytical models have been proposed for the reaction[4-6].

For the understanding of the UO_2/Zircaloy chemical interaction, it is required to obtain information both on the reaction kinetics and on phase equilibria in the U-Zr-O ternary system. The UO_2/Zircaloy interaction cannot be explained in terms of a pseudobinary UO_2-Zr system, but should be treated as a ternary reaction in the U-Zr-O system.

Recently, the U-Zr metallic fuel for a liquid metal fast breeder reactor is being watched with keen notice from the economic viewpoint of fuel recycling process. Renewed interest in metallic fuel promoted reassessment of thermodynamics of U-Pu-Zr ternary system[7-10]. Oxygen impurity was found from the recent research[8] to affect the microstructure of the U-Pu-Zr metallic fuel. Information on phase equilibria in the U-Zr-O ternary system also help in evaluating the influence of oxygen impurity on the integrity of the U-Zr metallic fuel.

The first study of phase relations in the U-Zr-O system has been made by Saller et al.[11], and Politis[12] has proposed the isothermal sections of this system at 1000, 1500 and 2000°C. Skokan and his coworkers[13] have performed thermal analysis on the quasibinary section between UO_2 and oxygen-saturated αZr(O).

In order to interpret the chemical composition of the phases and the sequence of the reaction zone in the UO_2/Zircaloy chemical interaction, further investigation of phase equilibria is considered to be needed. The purpose of the present study is to clarify whether or not formation of (γU,βZr) phase can be produced by the reaction of zirconium with UO_2 at high temperatures and to examine phase regions and boundaries in the U-Zr-O ternary system.

Quantitative knowledge of thermodynamics of αZr(O) solid solution is scant indeed. This information will lay out interaction patterns of zirconium with oxide fuels. The author attempted to estimate the partial molar quantities of the αZr(O) solid solution from experimental findings of the U-Zr-O ternary system.

2. Experimental

Powders of UO_2 (reactor grade, O/U ratio = 2.16), Zr (purity, 99.9 wt%) and ZrO_2 (purity, 99.9 wt%) were used as starting materials. These powders were well ground and then mixed in desired proportions. The mixtures with various compositions were pelletized. An equilibrium heat treatment of the compact was made at temperatures of 1000 and 1400°C for periods ranging from 10 to 200 h in a vacuum below 10^{-4} Pa. After the heat treatment, the sample was rapidly cooled to room temperature

The heated sample was powdered in a dry argon filled glove box, and phase identification for the powdered sample was performed by a computer controlled X-ray diffractometer. The detailed procedure was described in the preceding chapter. Lattice parameters of the reaction products were evaluated from reflections according to Cohen's method[14].

Metallographic examination was also made for some of the samples with the aid of a scanning electron microscope (SEM) and an optical microscope. Compositions of reaction products were analyzed by means of an energy dispersive X-ray analyser(EDXA).

3. Results and Discussion

3.1. Phase equilibria in the U-Zr-O ternary system

Figure 1 indicates the phases identified in the X-ray diffraction patterns for the reaction products in samples A - Y and a - x after heating at 1000°C. It is obvious from this figure that the number and the type of phases in the reaction products vary according to the composition of the sample.

Sample A consisted of UO_2, αZrO_2 and αZr, though the starting pellet was a mixture of Zr and UO_2. There existed two phases of UO_2 + αZr in sample B. The X-ray diffraction pattern exhibited that αU coexisted with UO_2 and αZr in samples C - J whose zirconium contents ranged from 20 to 66 at%. The typical example of X-ray diffraction pattern for the samples in which the three phases were detected is shown in Fig. 2(A). In samples K - U, αZr existed with αU and/or UZr_2 but no UO_2 was involved, as indicated in Fig. 2(B). Samples V - Y were composed of both α and βZr. The αU, βZr and UZr_2 were considered to be the phases produced during the time interval of cooling process from 1000°C to room temperature. The stable phase at 1000°C appears to be a (γU,βZr) solid solution, which may be transformed to αU and/or UZr_2.

The reaction products in samples a - f ($Zr/ZrO_2/UO_2$ mixture) are quite

similar to those of sampes K - L (Zr/UO_2 mixture), the diffraction patterns of which showed no evidence for existence of UO_2. There existed three phases (UO_2 + αU + αZr) in samples g - j. Neither uranium or uranium intermetallic compound was detected in samples k and l, as can be seen in Fig. 2(C). Monoclinic αZrO_2 was contained in the composition range for samples m - x. αZrO_2 coexisted with only UO_2 in sample x.

Figure 3 shows the change in the lattice parameters a and c and the axial ratio c/a of hexagonal αZr in the Zr/UO_2 mixture pellets (samples A - W) with sample composition in at%Zr. The values of a and c and c/a were larger for αZr in the heated samples than a = 0.3233 nm and c = 0.5149 nm for the starting Zr powder. The lattice parameters strongly depended upon sample composition. The values of a and c are found from Fig. 3 to vary from A to C (2.5 - 20 at%Zr). However, the lengths of a and c axes scarcely changed with sample composition in the range of 20 to 66 at%Zr (sample C - J), corresponding to the composition range where three phases of UO_2, αZr and αU were detected. The mean values were found to be a = 0.3246 nm and c = 0.5195 nm for αZr in samples C - J. For the samples K - W above a zirconium content of 68 at%, the a and c values differed from those for samples C - J. As the zirconium content increased, the value of c monotonically decreased, while the value of a once increased and went through a maximum at 75 at%Zr.

The variation in the lattice parameters and the axial ratio of αZr in the $Zr/ZrO_2/UO_2$ mixture pellets (samples a - u) with zirconium content of sample is shown in Fig. 4. The values of a, c and c/a varied with zirconium content for the samples a - f with 84 - 72 at%Zr. In the composition range 70 - 64 at%, a, c and c/a were independent of sample composition and similar to those for samples C - J. As can be seen in Fig. 4, the lattice parameters for αZr coexisting with only UO_2 (samples k and l) is likely to be influenced by the zirconium content. For αZr in samples m - u containing αZrO_2, nearly constant values of a = 0.3244 nm and c = 0.5199 nm were obtained.

Reaction at 1000°C resulted in a considerable expansion in the direction of the c axis and only a slight change in the a axis in αZr. The lattice parameters of pure zirconium and zirconium-oxygen binary solid solution, $\alpha Zr(O)$, are provided in the literature [15-19]. As evidenced by Fig. 5, the incorporation of oxygen atoms into the αZr lattice causes a marked increase in the value of c over the entire range of solid solubility. The value of a is less affected by the oxygen content but passes through a pronounced maximum at the composition of 20 at%O. The change in the lattice spacing after heating is considered to be closely related to oxygen dissolution in αZr. The change in the lattice dimension of αZr offers indication for amount of oxygen dissolved in αZr. On the assumption that the solubility of uranium in αZr is quite small, the author evaluated the oxygen

content in αZr for various samples from the c value of αZr. The results for the estimation are shown in Fig. 6. In this figure, the broken line drawn from the literature data[15-19] for Zr-O binary system indicates the dependence of c value of αZr on the oxygen content. The c values for samples m - u containing αZrO_2 agreed with that of oxygen-saturated αZr. The αZr in these samples is inferred to dissolve about 29 at%O. The samples k and l showed the lower c value, and hence αZr in sample k and l contains slightly smaller oxygen content than the solubility limit. The αZr in samples C - J and g - j consisting of UO_2, αZr and αU possesed almost constant lattice parameters, implying the same oxygen content of αZr. It is evident from Fig. 6 that the oxygen content in αZr in these samples is about 25 at%. For the samples K - W and a - f in which UO_2 was not detected, the c values of αZr were smaller than those for the samples C - J and g - j. The αZr in the samples K - W and a - f appears to have various oxygen contents below 25 at%.

The lattice parameter of UO_2 in the reaction products slightly increased from a = 0.5467 nm for the starting material to a = 0.5470 nm. No marked change in the a value was observed with sample composition. The value of 0.5470 nm was in accord with the reported data for stoichiometric UO_2[20]. Reaction of UO_2 with zirconium appears to cause reduction in O/U ratio of UO_2.

The Zr/UO_2 samples F, G, L, Q, U, X and Y heated at 1000°C were examined by SEM and optical microscope. Figure 7 indicates typical results for SEM observations. The existence of three phases, UO_2, αZr and metallic uranium was confirmed in samples F and G by metallography, as shown in Fig. 7(A). This is consistent with the results obtained by X-ray diffraction method. The metallic region in samples F and G was analyzed by EDXA and found to contain mainly uranium, > 0.95 U/(U+Zr) atomic fraction. The uranium content in αZr phase in samples F and G was less than 0.01 U/(U+Zr). Microstructures of samples L and Q are indicated in Figs. 7(B) and (C). The αZr particles were surrounded by a metallic phase. The metallic region in sample L had a uranium content of 0.90 U/(U+Zr), which was slightly lower than that of samples F and G. The microstructure of sample Q was similar to that of sample L, but the uranium content of metallic region in sample Q (0.36 U/(U+Zr)) was quite different from sample L. General features in the structure of sample U were almost the same as sample Q, whereas the needlelike α' precipitates were observed in the metallic region of sample U whose uranium content was 0.09 U/(U+Zr). The U-rich metallic region for these sample appears to exist as a (γU,βZr) solid solution phase at 1000°C. The EDXA analysis revealed that αZr can exist with (γU,βZr) having various uranium contents in the range of composition where X-ray analysis showed no presence of UO_2 in samples. Figure 7(D) shows a characteristic structure for Zr-rich samples X and Y. The platelike α' precipitates which may be generated in the course of cooling were found to be formed in prior-βZr matrix. Although αZr

islands were observed in samples L, Q, U and X, they were not detected in sample Y. Therefore, sample Y seems to comprise a single βZr phase at 1000°C.

The isothermal section of the U-Zr-O ternary system at 1000°C was reconstructed, based on the present results for Zr/UO_2 and $Zr/ZrO_2/UO_2$ reaction experiments, as shown in Fig. 8. The phase relationships essentially agree with the results of Saller et al.[11] and Politis[12] indicated in Fig. 9. The existence of three-phase region of UO_2 + αZr(O) + (γU,βZr) (region Ⅳ in Fig. 8) characterizes the isothermal section at 1000°C. The solubility of zirconium in UO_2 may be negligible according to the pseudobinary phase diagram of UO_2-ZrO_2 system[21]. The solid solution (γU,βZr) with zirconium content of < 3 at%Zr can equilibrate with UO_2 and αZr(O). In the two-phase region of UO_2 + αZr(O) (region Ⅲ), the αZr(O) phase has oxygen contents between 25 and 29 at%. The oxygen-saturated αZr(O) can be in three-phase equilibrium with monoclinic αZrO_2 and UO_2 (region Ⅱ). The lattice parameter evaluation of αZr permits an isoparametric line to be drawn in the two-phase region of αZr(O) + (γU,βZr) (region Ⅵ). The tentative isoparametric lines, tie lines, are shown in the isothermal section . In the Zr-O binary system at 1000°C, βZr phase of 1.6 at%O can be in equilibrium with αZr(O) phase of 6 at%O[22]. The conjugate phase of (γU,βZr) solid solution over a wide zirconium concentration range from 50 to 95 at% appears to be αZr(O) with an oxygen content of 20 - 25 at%. The compositions of (γU,βZr) in equilibrium with αZr(O), which were estimated from the isoparametric lines, agreed with the results obtained by EDXA analysis of Zr/UO_2 pellets.

The results for X-ray diffraction analysis of mixture pellets of Zr/UO_2 (samples A' - Y') and $Zr/ZrO_2/UO_2$ (samples a' - x') heated at 1400°C are given in Fig. 10. It is apparent from this figure that the type and the number of phases are strongly dependent upon the composition of sample.

For the Zr/UO_2 mixture pellets after heating at 1400°C, only the sample A' was found to contain ZrO_2 in the reaction products. The X-ray diffraction pattern for sample B' revealed that two phases of UO_2 and αZr existed in the reaction products. The three phases of UO_2, αZr and αU were detected in the samples C' - J' with the zirconium content of the samples from 20 to 66 at%, as can be seen in a X-ray diffraction pattern shown in Fig. 11 (A). The reaction products for the samples K' - T' were composed of αU and/or UZr_2 in addition to αZr, but UO_2 was not detected. Figure 11(B) indicates the mixture of αU, UZr_2 and αZr. The diffraction analysis for the samples U' - Y' provided that the reaction products consisted of αZr and βZr. The αU, βZr and UZr_2 detected in the reaction products by X-ray diffraction analysis at room temperature are inferred to result from (γU,βZr) liquid or solid solution at 1400°C.

No formation of UO_2 was observed for the samples a' - f', while in the samples g', h' and i', UO_2, αZr and αU were detected. The UO_2 and αZr were

present in the reaction products of samples j' - n', as shown in Fig. 11(C). In the composition range for samples o' - w', UO_2, αZr and ZrO_2 were identified in the reaction products. The X-ray diffraction patterns of samples t' - x' indicated that tetragonal βZrO_2 phase was involved in addition to monoclinic αZrO_2. The reaction products for sample x' were composed of UO_2, α and βZrO_2. The monoclinic αZrO_2 is presumed from the literature of UO_2-ZrO_2[21] and Zr-O[22] binary systems to be a transformed phase, and the stable form of ZrO_2 at 1400°C seems to be tetragonal.

The dependence of the lattice parameters a and c and the axial ratio c/a of αZr in the reaction products on the zirconium content of the Zr/UO_2 mixture pellet (samples C' - V') is illustrated in Fig. 12. The lattice parameters of αZr in the reaction products increased from a = 0.3233 nm and c = 0.5149 nm for the starting Zr powder to the values of a = 0.3252 - 0.3246 nm and c = 0.5176 - 0.5195 nm for samples C'- V'. The axial ratio c/a of αZr was also larger than that before reaction, 1.593. The extent of increase in the lattice parameters and the axial ratio is found from this figure to vary with the composition of sample. The samples C' - J' in which three phases of UO_2, αZr and αU were detected showed nearly constant values of a = 0.3247 nm and c = 0.5194 nm. In this composition range, the c/a ratio of 1.600 was also independent of the sample composition. Above 68 at%Zr, the lattice parameter c decreased with increasing zirconium content, whereas a more complicated change in the a value was observed as the zirconium content increased. The c/a ratio rapidly decreased from 1.600 to 1.593.

Figure 13 represents the variation in the lattice parameters a and c and the axial ratio c/a of αZr with the zirconium content of the $Zr/ZrO_2/UO_2$ mixture pellet (samples a' - v'). The lattice parameters and the axial ratio changed with zirconium content in the range of 82 - 72 at% (samples a' - f'). The samples g' - i' in which three phases of UO_2, αZr and αU were detected revealed nearly constant a, c and c/a values, which were close to the data for the Zr/UO_2 pellets having UO_2 as one of the reaction products. In the composition range where two phases of UO_2 and αZr coexisted (samples j' - n'), the lattice parameter c and the c/a ratio increased with decreasing zirconium content, but a value decreased. There is no marked difference in values of a, c and c/a among the samples of o - v with lower zirconium contents. The mean values of the lattice parameters and axial ratio were a = 0.3245 nm, c = 0.5200 nm and c/a = 1.602.

A considerable expansion in the direction of c axis and only a slight change in the a axis in αZr was caused by reaction at 1400°C. This is the same as the results obtained at 1000°C. Assuming that solubility of uranium in αZr is quite small and dissolved uranium does not affect the lattice expansion of αZr, estimation of oxygen content in zirconium was made from the literature data[15-19] for relationship between lattice parameters of αZr and oxygen content. Figure 14

reveals the estimation of oxygen content in αZr from the c value. The lattice parameter c of αZr in the samples o' - v' containing ZrO_2 as one of the reaction products indicated a constant value irrespective of the sample composition and was in accord with that reported for αZr at the solubility limit of about 30 at%O. Therefore, it can be concluded that in the samples o' - v' αZr with UO_2 and ZrO_2 may be saturated with oxygen. For the samples C' - J' and g' - i' which consisted of UO_2, αZr and αU, the αZr showed nearly constant values, which were lower than the reported value for oxygen-saturated αZr. This suggests that αZr coexisting with UO_2 and αU has a constant oxygen content and may be unsaturated with oxygen. From Fig. 14, αZr in the reaction products for samples C' - J' and g' - i' can be estimated to contain about 25 at%O. However, in the composition range where no UO_2 was identified in the reaction products, the c value of αZr changed with the zirconium content of sample and were lower than those for the samples C' - J' and g' - i'. The αZr in samples K' - V' and a' - f' appears to have various oxygen contents below 25 at%O.

Metallographic examination was carried out for the Zr/UO_2 samples of F', G', L', Q', U', X' and Y' after heating at 1400°C by means of SEM and optical microscope. Typical results for SEM observation are shown in Fig. 15. The samples F' and G' in which three phases of UO_2, αZr and αU were detected by X-ray diffraction method were metallographically found to contain UO_2, αZr and metallic uranium. As evidenced by Fig. 15(A), there exist large αZr particles, and UO_2 region locates around αZr particles. The EDXA analysis of the metallic region exhibited that the U/(U+Zr) ratio of this region was 0.95 - 0.90. From the morphology of this U-rich phase, it was difficult to know whether at 1400°C this phase was liquid or not. However, the result for EDXA analysis established that on the basis of the binary phase diagram of U-Zr system[8,22] the U-rich phase should be liquid rich in uranium at 1400°C. The uranium content in the αZr particle was evident from EDXA analysis to be very low and can be estimated to be below 2 at%. The samples in this composition range seem to contain three phases of UO_2, αZr and liquid at 1400°C. Microstructures of samples L' and Q' are shown in Figs. 15(B) and (C). In sample L', large αZr particles were surrounded by U-rich region possessing U/(U+Zr) ratio = 0.53. The micrograph of sample Q' (Fig. 15(C)) indicates that the U-rich region involves needlelike α' precipitates. The U-rich region in sample Q' had a U/(U+Zr) ratio of 0.27. The structure of sample U' was almost similar to that of sample Q'. The value of U/(U+Zr) for the U-rich region was 0.08. For these samples, the U-rich region may exist as a (γU,βZr) solid solution at 1400°C. In the composition range where no UO_2 was detected in the reaction products by X-ray analysis, αZr appears to coexist with (γU,βZr) solid solutions with various uranium contents. As can be seen in Fig. 15(D), a number of platelike α' precipitates are formed in prior-βZr matrix. This was a

characteristic structure for Zr-rich samples of X' and Y'. The α' precipitates were introduced during cooling. Since the αZr islands as observed in the samples L', Q' and U' were not formed, the samples X' and Y' are considered to consist of βZr single-phase at 1400°C.

Figure 16 exhibits the isothermal section of the U-Zr-O ternary system at 1400°C proposed from the present results for Zr/UO_2 and $Zr/ZrO_2/UO_2$ reaction experiments. The phase relationships which are different from obtained at lower temperatures[11,12] are essentially consistent with the results of Politis at 1500°C[12] and Skokan et al. at 1600°C[13] shown in Fig. 17. In the isothermal section at 1400°C, there exists a characteristic triangle of UO_2 + αZr(O) + L, (L = liquid) (region Ⅳ in Fig. 16). Compositions of UO_2, αZr(O) and liquid have to be thermodynamically fixed in this three-phase region. Actually, the experimental results of lattice spacing of αZr in this phase region were in agreement with the phase rule. The solubility of oxygen and uranium in αZr(O) are 25 at%O and < 2 at%U, respectively. The UO_2 takes little amount of zirconium into solution at 1400°C, as can be predicted by the UO_2-ZrO_2 pseudobinary phase diagram[21]. Although the composition of liquid phase in equilibrium with αZr(O) and UO_2 was not determined precisely, it will contain about 10 at%Zr. This three-phase region may be adjacent to two-phase regions of UO_2 + L (region Ⅴ), αZr(O) + L (region Ⅵ), and UO_2 + αZr(O) (region Ⅲ). In the two-phase region of UO_2 + αZr(O), the αZr(O) in equilibrium with UO_2 possesses the oxygen content ranging from 25 to 30 at%. Compositions for samples with higher oxygen contents are expected to come into the three-phase region of UO_2, tetragonal βZrO_2 and αZr(O). In the two-phase region of αZr(O) and (γU,βZr) (region Ⅶ), the lattice parameters of αZr varied with composition. The results for X-ray diffraction analysis of αZr in this region allow us to draw isoparametric lines. The tentative isoparametric lines which correspond to tie lines are shown in the isothermal section. In the Zr-O binary system at 1400°C, βZr with 6 at%O can equilibrate with 14 at%O αZr(O)[22]. The conjugate phase of αZr(O) with an oxygen content around 15 at% is likely to be a (γU,βZr) solid solution with a limited zirconium concentration range of 0 - 10 at%. The compositions of (γU,βZr) in equilibrium with αZr(O) estimated from the isoparametric lines agreed with the results obtained by EDXA analysis of Zr/UO_2 mixture pellets.

The isothermal section at 1400°C differs from that at 1000°C in that two additional phase regions, namely the regions designated as Ⅴ, Ⅵ in Fig. 16, appear in the former.

Hofmann and Politis[1] have attempted to explain the formation of the observed sequence resulting from the reaction between UO_2 and Zircaloy 4 using the isothermal section at 1500°C, which is essentially similar to that at 1400°C (Fig. 16). They assumed that the diffusion path was the straight line connecting UO_2

with Zr. In contrast to this model, a rather complicated diffusion path was adopted in the theoretical model proposed by Olander[5] and he could explain the experimental results of Hofmann and Politis[1] at 1500°C. However, Olander's analysis is restricted to 1500°C. The isothermal section at 1500°C is different from that at 1000°C, and the line between UO_2 and Zr crosses two additional phase regions at 1500°C. Therefore, the models of Hofmann and Politis[1] and Olander[5] are no longer valid without taking the existence of these two regions into consideration. However, the reaction zone consisting of three different layers does develop in the reaction between UO_2 and Zircaloy 4 at 1000°C where the above mentioned two regions do not appear, as can be seen in Fig. 8. Furthermore, the previous results for the U-Zr-O ternary system seem not to be valid in the locations of phase boundaries and compositions of existing phases. Therefore, the UO_2/Zircaloy reaction should be analyzed in terms of a model applicable to the experimental results over a wide range of temperatures, and accurate information on the phase relationships in the U-Zr-O system at the relevant temperatures is required.

3.2. Thermodynamics of the solid and liquid solution phases in the U-Zr-O ternary system

It is of particular interest to note that at both 1000 and 1400°C UO_2 cannot equilibrate with a αZr(O) solid solution with an oxygen content below 25 at%. In other words, zirconium can reduce UO_2 and may produce solid or liquid uranium as long as the oxygen content of zirconium is less than 25 at%. The hexagonal αZr(O) phase may play an important role in interaction between zirconium and UO_2. The oxygen potential over a αZr(O) solid solution is a dominant factor governing whether the interaction occurs or not. Thermodynamics concerning the αZr(O) solid solution may help in evaluating not only the Zr/UO_2 interaction but also the reactivity of U-Zr metallic fuel towards oxygen gas.

The phase diagram of Zr-O binary system was well established and the phase boundary between αZr(O) and ZrO_2 was precisely determined. However, a small number of thermodynamic studies have been performed on the αZr(O) solid solution. Kubaschewski et al.[23] using a transfer method of oxygen in solid state have measured the composition of αZr(O) solution in equilibrium with Ca/CaO, Mg/MgO and Ba/BaO only at 1000°C. The oxygen potential over αZr(O) has been determined by Komarek et al.[24] using the same method in the range of 800 - 1000°C. The data sets of oxygen potentials previously reported for αZr(O)[23-25] are shown in Fig. 18. The author's interest has been sparked by a large discrepancy in the oxygen potential of αZr(O) between the literature data sets[23-25], as indicated in Fig. 18. In the preceding chapter, the author demonstrated the possibility of deducing

the oxygen potential over αTi(O) from the experimental phase diagram. This method is also applicable to the analysis of oxygen potential over αZr(O).

In order to evaluate the oxygen potential, it is necessary to know the relationship between oxygen potential and oxygen content in zirconium. The following expression is presumed to hold between oxygen potential $\Delta\bar{G}_{O_2}(ZrO_x)$ and oxygen content x_O in αZr(O):

$$\Delta\bar{G}_{O_2}(ZrO_x) = \Delta\bar{G}_{O_2}(ZrO_2) + 2\,A\,\ln(x_O/x_O^s) \tag{1}$$

where $\Delta\bar{G}_{O_2}(ZrO_2)$ is the oxygen potential in the two-phase region of αZr(O) + ZrO_2 and x_O^s is the solubility limit of oxygen in αZr(O) (x_O^s = 0.410 O/Zr at 1000°C and x_O^s = 0.439 O/Zr at 1400°C). In this equation, A is a temperature dependent constant, but independent of x_O. The graphical method which was the same manner as αTi(O) was employed to determine integral values from partial quantities. Figure 19 represents the development of the oxygen potential as a function of the oxygen content in zirconium. As shown in this figure, the $\Delta\bar{G}_{O_2}$ curve has two portions. In the single-phase region of αZr(O), $\Delta\bar{G}_{O_2}$ varies with x_O up to the solubility limit, however, $\Delta\bar{G}_{O_2}$ is constant in the two-phase region. Integrating of $\Delta\bar{G}_{O_2}(ZrO_x)$ in the single-phase region,

$$\Delta G_f^\circ(ZrO_x) = x_O/2\;\Delta\bar{G}_{O_2}(ZrO_2) + A\,(x_O\,\ln(x_O/x_O^s) - x_O) \tag{2}$$

is obtained, where $\Delta G_f^\circ(ZrO_x)$ is the standard free energy of formation of αZr(O). By integration up to x_O = 2, equation (1) becomes

$$\Delta G_f^\circ(ZrO_2) = \Delta\bar{G}_{O_2}(ZrO_2) - A\,x_O^s. \tag{3}$$

In this equation, $\Delta G_f^\circ(ZrO_2)$ is the standard free energy of formation of ZrO_2.

The $\Delta G_f^\circ(ZrO_x)$ is expressed as the other form:

$$\Delta G_f^\circ(ZrO_x) = \Delta\bar{G}_{Zr}(ZrO_x) + x_O/2\;\Delta\bar{G}_{O_2}(ZrO_x) \tag{4}$$

where $\Delta\bar{G}_{Zr}(ZrO_x)$ is the partial molar excess free energy of zirconium in αZr(O). Substitution of eqs. (1) and (2) into (4) gives

$$\Delta\bar{G}_{Zr}(ZrO_x) = -A\,x_O. \tag{5}$$

There are several methods to determine the $\Delta\bar{G}_{O_2}(ZrO_x)$ as a function of x_O using the above equations. If $\Delta\bar{G}_{Zr}(ZrO_x)$ and $\Delta\bar{G}_{O_2}(ZrO_x)$ are known at a specific value of x_O, we can determine the values of A and $\Delta\bar{G}_{O_2}(ZrO_2)$ in eq. (1). This method

also allows us to estimate $\Delta G_f^\circ(ZrO_2)$. In the case that reliable $\Delta G_f^\circ(ZrO_2)$ value is available, we would need the oxygen potential at a certain x_O to evaluate A value.

Little thermodynamic data exist for high temperature phases in the U-Zr binary system such as (γU,βZr) solid solution and liquid. Fedorov et al.[26,27] have reported EMF data for (γU,βZr) solution at temperatures of 760 - 911°C, and thermodynamic properties were obtained by high temperature mass spectrometry in the temperature range of 1427 - 1787°C[9]. However, Leibowitz et al.[10] pointed out serious discrepancies in these data and the reliability of these data was doubted in their paper. Assessment of the U-Zr binary phase diagram was also performed by Leibowitz et al.[10], and thermodynamic functions for all the existing phases were derived. They obtained the following excess free energies of the (γU,βZr) solid solution and liquid in J/mol:

$$\Delta G^{EX}(U,Zr) = y_U(1 - y_U)\,\Omega_S$$
$$\Omega_S = [43810 - 22.0\,T - 22090\,(1 - y_U) + 12880\,(1 - y_U)^2] \quad (6)$$

$$\Delta G^{EX}(L) = y_U(1 - y_U)\,\Omega_L$$
$$\Omega_L = [41150 - 22.0\,T - 16550\,(1 - y_U) + 12880\,(1 - y_U)^2] \quad (7)$$

where y_U is the uranium content of solution in atomic fraction and T is the temperature in K. From eqs. (6) and (7), the partial molar excess free energies of uranium and zirconium are found to be expressed as

$$\Delta\bar{G}_U(U,Zr) = RT \ln y_U + (1 - y_U)^2\,[65890 - 22.0\,T - 69930\,(1 - y_U) + 38640\,(1 - y_U)^2]$$
$$\Delta\bar{G}_{Zr}(U,Zr) = RT \ln (1 - y_U) + y_U^2\,[43810 - 22.0\,T - 44170\,(1 - y_U) + 38640\,(1 - y_U)^2] \quad (8)$$

for (γU,βZr) solid solution phase, and

$$\Delta\bar{G}_U(L) = RT \ln y_U + (1 - y_U)^2\,[57700 - 22.0\,T - 58860\,(1 - y_U) + 38640\,(1 - y_U)^2]$$
$$\Delta\bar{G}_{Zr}(L) = RT \ln (1 - y_U) + y_U^2\,[41150 - 22.0\,T - 33100\,(1 - y_U) + 38640\,(1 - y_U)^2] \quad (9)$$

for liquid phase. The standard states of $\Delta\bar{G}_U(U,Zr)$ and $\Delta\bar{G}_{Zr}(U,Zr)$ for solid solution are pure γU and βZr. However, pure liquid uranium and pure liquid zirconium are chosen as standard states in $\Delta\bar{G}_U(L)$ and $\Delta\bar{G}_{Zr}(L)$. If a different standard state is selected for the liquid solution, the standard free energies of

transition should be taken into account:

$$\Delta G^{\circ}(U,\gamma\rightarrow L) = -5435 + 79.073\ T - 10.4\ T \ln T \qquad (10)$$

for the melting of γU, and

$$\Delta G^{\circ}(Zr,\beta\rightarrow L) = 9657 + 68.927\ T - 2.32\times10^{-3}\ T^{2} - 10.23\ T \ln T \qquad (11)$$

for the melting of βZr.

Figure 20 indicates the variations of the partial molar excess free energies of uranium and zirconium for solid and liquid solutions at 1000 and 1400°C with the uranium content, which were calculated from eqs. (8) and (9). For the solution at 1400°C, pure liquid uranium and pure solid β zirconium are the standard states. As can be seen in Fig. 20, at 1000°C, $\Delta\bar{G}_U$ and $\Delta\bar{G}_{Zr}$ change smoothly with y_U, while at 1400°C a flat region is found in each curve, indicating the existence of heterogeneous region of liquid and solid solutions. Similar tendency is observed for activity curves of uranium and zirconium, as shown in Fig. 21.

Oxygen potentials $\Delta\bar{G}_{O_2}(UO_2)$ over (γU,βZr) solid and liquid solutions in two-phase equilibrium with UO_2 can be roughly estimated from eqs. (8) and (9) using the standard free energy of formation of UO_2, $\Delta G_f^{\circ}(UO_2)$ as follows:

$$\Delta\bar{G}_{O_2}(UO_2) = \Delta G_f^{\circ}(UO_2) - \Delta\bar{G}_U(U,Zr) \qquad (12)$$

and

$$\Delta\bar{G}_{O_2}(UO_2) = \Delta G_f^{\circ}(UO_2) - \Delta\bar{G}_U(L). \qquad (13)$$

The estimated $\Delta\bar{G}_{O_2}(UO_2)$ at 1000 and 1400°C is shown in Fig. 22. Both at temperatures of 1000 and 1400°C, $\Delta\bar{G}_{O_2}(UO_2)$ slightly increases with decreasing uranium content. In a three-phase region of UO_2 + (γU,βZr) + L, which is not however an equilibrium phase region at 1400°C, $\Delta\bar{G}_{O_2}(UO_2)$ shows a constant value of -791kJ/mol, as can be seen in Fig. 22.

The isothermal section of the U-Zr-O ternary system at 1000°C indicated the existence of three-phase region of UO_2 + αZr(O) + (γU,βZr). Uranium-rich liquid equilibrated with UO_2 and αZr(O) in a different three-phase region at 1400°C. These data in the isothermal sections can be used for estimating the oxygen potential over αZr(O). The uranium contents of (γU,βZr) and liquid in the three-phase regions are y_U = 0.975 at 1000°C and y_U = 0.900 at 1400°C. The αZr(O) has the same oxygen content of x_O = 0.333 in the three-phase regions at 1000 and

1400°C. On the assumption that (γU,βZr), liquid and αZr(O) solutions are binary, the equilibrium reactions can be simplified as

$$2\ O[\alpha Zr(O)] + U[(\gamma U,\beta Zr)] = UO_2$$
$$Zr[\alpha Zr(O)] = Zr[(\gamma U,\beta Zr)]$$

at 1000°C, and

$$2\ O[\alpha Zr(O)] + U[L] = UO_2$$
$$Zr[\alpha Zr(O)] = Zr[L]$$

at 1400°C. At equilibrium, the partial molar quantities can be therefore correlated with each other,

$$\Delta\bar{G}_{O2}(ZrO_x) = \Delta G_f^\circ(UO_2) - \Delta\bar{G}_U(U,Zr)$$
$$\Delta\bar{G}_{Zr}(ZrO_x) = \Delta\bar{G}_{Zr}(U,Zr) \qquad (14)$$

at 1000°C, and

$$\Delta\bar{G}_{O2}(ZrO_x) = \Delta G_f^\circ(UO_2) - \Delta\bar{G}_U(L)$$
$$\Delta\bar{G}_{Zr}(ZrO_x) = \Delta\bar{G}_{Zr}(L) \qquad (15)$$

at 1400°C.

The standard free energies of UO_2 at 1000 and 1400°C, which are known and reliable, and equilibrium conditions (y_U = 0.975 at 1000°C and y_U = 0.900 at 1400°C) offer the $\Delta\bar{G}_{O2}$ and $\Delta\bar{G}_{Zr}$ for αZr(O) at x_O = 0.333 by use of eqs. (8) - (15). Consequently, $\Delta\bar{G}_{O2}(ZrO_x)$-$x_O$ relationships can be obtained using eqs. (1) and (5).

In Fig. 23, the estimated oxygen potential over αZr(O) solid solution $\Delta\bar{G}_{O2}(ZrO_x)$ at 1000 and 1400°C is illustrated as a function of oxygen content. As shown in this figure, the value of $\Delta\bar{G}_{O2}$ at 1000°C decreases from -833 kJ/mol at x_O^s = 0.410 to -1099 kJ/mol at x_O = 0.07. The $\Delta\bar{G}_{O2}(ZrO_2)$ in the two-phase region was found to be -833 kJ/mol, which was close to -826 kJ/mol reported by Kubaschewski et al.[23]. The general trend in $\Delta\bar{G}_{O2}$-x_O relation at 1000°C was in accord with the reported results shown in Fig. 18. The $\Delta\bar{G}_{O2}(ZrO_2)$ was -750 kJ/mol at 1400°C. The standard free energies of formation of ZrO_2 were estimated to be -863.8 kJ/mol at 1000°C and -784.6 kJ/mol at 1400°C, in excellent agreement with the values in the JANAF table[28] (-857.9 kJ/mol at 1000°C and -786.0 kJ/mol at 1400°C).

It is interesting to compare the partial molar enthalpy and entropy $\Delta\bar{H}_{O2}$ and

$\Delta\bar{S}_{O_2}$ derived from the estimated $\Delta\bar{G}_{O_2}$ with the reported values. Assuming that $\Delta\bar{H}_{O_2}$ and $\Delta\bar{S}_{O_2}$ are independent of temperature, these values were estimated by the following equation:

$$\Delta\bar{G}_{O_2} = \Delta\bar{H}_{O_2} - T\,\Delta\bar{S}_{O_2}. \tag{16}$$

The $\Delta\bar{H}_{O_2}$ and $\Delta\bar{S}_{O_2}$ thus obtained are given in Fig. 24.

As the oxygen content in αZr(O) increases, the $\Delta\bar{H}_{O_2}$ value increases from -1172 kJ/mol at x_O = 0.17 to -1063 kJ/mol at x_O = 0.41, as indicated in Fig. 24. Recently, Boureau et al.[29] have applied Tian-Calvet microcalorimetric method to determination at 1050°C the partial molar enthalpy of oxygen in zirconium and reported that the $\Delta\bar{H}_{O_2}$ value for αZr(O) increases from -1190 to -1080 kJ/mol in the range of 0.1 - 0.4 O/Zr. The agreement between the estimated and reported $\Delta\bar{H}_{O_2}$ values may be considered as satisfying. The increase in the partial molar enthalpy with oxygen content is consistent with the presence of ordered structures in αZr(O) at low temperatures[22]. And, this may suggest strong repulsive interaction between oxygen atoms in hexagonal αZr.

No experimental data on partial molar entropy of oxygen are available. Kubaschewski[25] has recommended $\Delta\bar{S}_{O_2}$ values for αZr(O) in the IAEA text book. In the composition of 0.18 - 0.42 O/Zr, the recommended $\Delta\bar{S}_{O_2}$ values distribute from -190 to -140 J/mol K, which agree with the estimated values. Strong repulsive interaction between oxygen atoms in αZr influences the configurational entropy of oxygen in αZr. An oxygen atom in an octahedral interstitial site excludes two surrounding sites from being occupied by other oxygen atoms. The configurational entropy of oxygen $\bar{S}_O{}^c$ is written by

$$\bar{S}_O{}^c = R\,\ln((1 - 2\,x_O)^2/(1 - x_O)). \tag{17}$$

The non-configurational part of $\Delta\bar{S}_{O_2}$ can be calculated from

$$\Delta\bar{S}_{O_2}{}^{non-c} = \Delta\bar{S}_{O_2} - 2\,\bar{S}_O{}^c. \tag{18}$$

Figure 24 also reveals an increase in the calculated non-configurational $\Delta\bar{S}_{O_2}{}^{non-c}$ with oxygen content in αZr(O). The partial excess entropy of oxygen in αZr(O), $\bar{S}_O$, (standard state: oxygen gas at 0 K) can be represented as

$$\Delta\bar{S}_{O_2}{}^{non-c} = - S_{O_2}{}^\circ + 2\,\bar{S}_O. \tag{19}$$

At 1200°C (the average temperature of 1000 and 1400°C), $S_{O_2}{}^\circ$ = 230.5 J/mol K according to JANAF[28]. Substituting $S_{O_2}{}^\circ$ value into eq. (19), the author

obtained $\bar{S}_O$ values from 25 J/mol K at x_O = 0.17 to 42 J/mol K at x_O = 0.41. These values are the same order of magnitude as those reported for oxygen in Ti(O)[30], Nb(O)[31] and V(O)[32] solid solutions. The partial molar excess entropy $\bar{S}_O$ may consist of vibrational, dilatometric (volume expansion) and electronic contributions. Though it is not easy to predict absolute values of $\bar{S}_O$ from each contribution precisely, dilatometric and electronic terms mainly contribute to the change in $\bar{S}_O$ with oxygen content in αZr(O).

The fairly good agreement between the estimated and reported partial molar quantities is noteworthy. This suggests that the estimated oxygen potential over αZr(O) have reasonable precision. The estimated oxygen potential over αZr(O) was quite low even at 1400°C, and at x_O = 0.17 it was close to that over Th + ThO_2. When zirconium is used in contact with oxide nuclear fuel or other oxide ceramics, a compatibility problem due to a low oxygen potential over αZr(O) will inevitably occur. Therefore, special precautions should be taken in applying zirconium to such an environment.

4. Conclusions

The isothermal sections for the U-Zr-O system were constructed at 1000 and 1400°C. The section at 1400°C differed from that at 1000°C in that the two additional phase regions containing liquid rich in uranium occur at 1400°C. It should be noted that at 1000 and 1400°C UO_2 can equilibrate with αZr(O) of oxygen content above 25 at%. Zirconium can reduce UO_2 and may produce solid or liquid uranium as long as oxygen content of zirconium is less than about an oxygen content of 25 at%. However, above 25 at%O zirconium can no longer take up oxygen from UO_2. The tentative tie lines were determined in the two-phase region of αZr(O) and (γU,βZr) at 1000 and 1400°C.

The composition dependence of oxygen potential over αZr(O) at 1000 and 1400°C was derived from the experimental data on the U-Zr-O ternary system. The obtained thermodynamic quantities for αZr(O) solid solution were consitent with the previous data.

Under hypothetical LWR accidents, oxidation of Zircaloy cladding due to chemical reaction with UO_2 fuel (internal oxidation) will cause cladding embrittlement and rupture in addition to external oxidation with steam. This internal oxidation also generates extremely low oxygen potential environments within a LWR fuel rod: $\Delta\bar{G}_{O_2} < -800$ kJ/mol, which may result in a drastic change of chemical forms of fission products such as cesium, iodine and tellurium and of their release behavior from a failed fuel rod.

References

[1] P. Hofmann and C. Politis, J. Nucl. Mater., 87(1979)375.
[2] P. Hofmann and D. Kerwin-Peck, KFK-3552, (1983).
[3] P. Hofmann and D. Kerwin-Peck, J. Nucl. Mater., 124(1984)80.
[4] A. W. Cronenberg and M. S. El-Genk, J. Nucl. Mater., 78(1978)390.
[5] D. R. Olander, J. Nucl. Mater., 115(1983)271.
[6] A. Denis and E. A. Garcia, J. Nucl. Mater., 116(1983)44.
[7] Y. Takahashi, M. Yamawaki and K. Yamamoto, J. Nicl. Mater., 154(1988)141.
[8] L. Leibowitz, E. Veleckis and R.A. Blomquist, ibid., 154(1988)145.
[9] M. Kanno, M. Yamawaki, T. Koyama and M. Morioka, ibid., 154(1988)154.
[10] L. Leibowitz, R.A. Blomquist and A.D. Pelton, ibid., to be published.
[11] H. A. Saller, F. A. Rough, J. M. Fackelmann, A. A. Bauer and J. R. Doig, BMI-1023, (1955).
[12] C. Politis, KFK-2167, (1975).
[13] A. Skokan, K. Biemuller, G. Reiser and G. Schlickeiser, KFK-3350, (1983).
[14] M.U. Cohen, Rev. Sci. Inst., 6(1935)68.
[15] R. F. Dommagala and D. J. McPherson, U.S.A.E.C. Publ. COO-181, (1954).
[16] B. Holmberg and T. Dagerhamn, Acta Chemica Scand., 15(1961)919.
[17] P. Boisot and G. Beranger, Compt. Rend., C269(1969)587.
[18] S. Yamaguchi, J. Phys. Soc. Japan, 24(1968)855.
[19] B.D. Litcher, Trans. Metall. Soc. AIME, 218(1960)1015.
[20] K. Suzuki, K. Maruya and M. Kubota, J. Atomic Energy Soc. Japan, 5(1963)587.
[21] K. A. Romberger, C. F. Baes,Jr. and H. H. Stone, J. Inorg. Nucl. Chem., 29(1967)1619.
[22] T.B. Massalski, Binary Alloy Phase Diagrams, (ASM, Ohio, 1986).
[23] O. Kubaschewski and W.A. Dench, J. Inst. Metals, 84(1956)440.
[24] K.L. Komarek and M. Silver, Thermodynamics of Nuclear Materials, (IAEA, Vienna, 1962)p749.
[25] O. Kubaschewski, Zirconium: Physico-Chemical Properties of Its Compounds and Alloys, (IAEA, Vienna, 1983).
[26] G.B. Fedrov and E.A. Smirnov, Sov. J. At. Energ., 25(1966)837.
[27] idem., ibid., 25(1968)795.
[28] M.W. Chase Jr., C.A. Davies, J.R. Downey Jr., D.J. Frurip, R.A. McDonald and A.N. Syverud, JANAF Thermochemical Tables, 3rd Ed., (American Institute of Physics, Inc., New York, 1985).
[29] G. Boureau and P. Gerdanian, J. Phys. Chem. Solids, 45(1984)141.
[30] idem., Acta Metall., 24(1976)717.
[31] T. Matsui and K. Naito, J. Nucl. Mater., 115(1983)178.
[32] W. Banchorndhevankul, T. Matsui and K. Naito, J. Nucl. Sci. Technol., 23(1986)873.

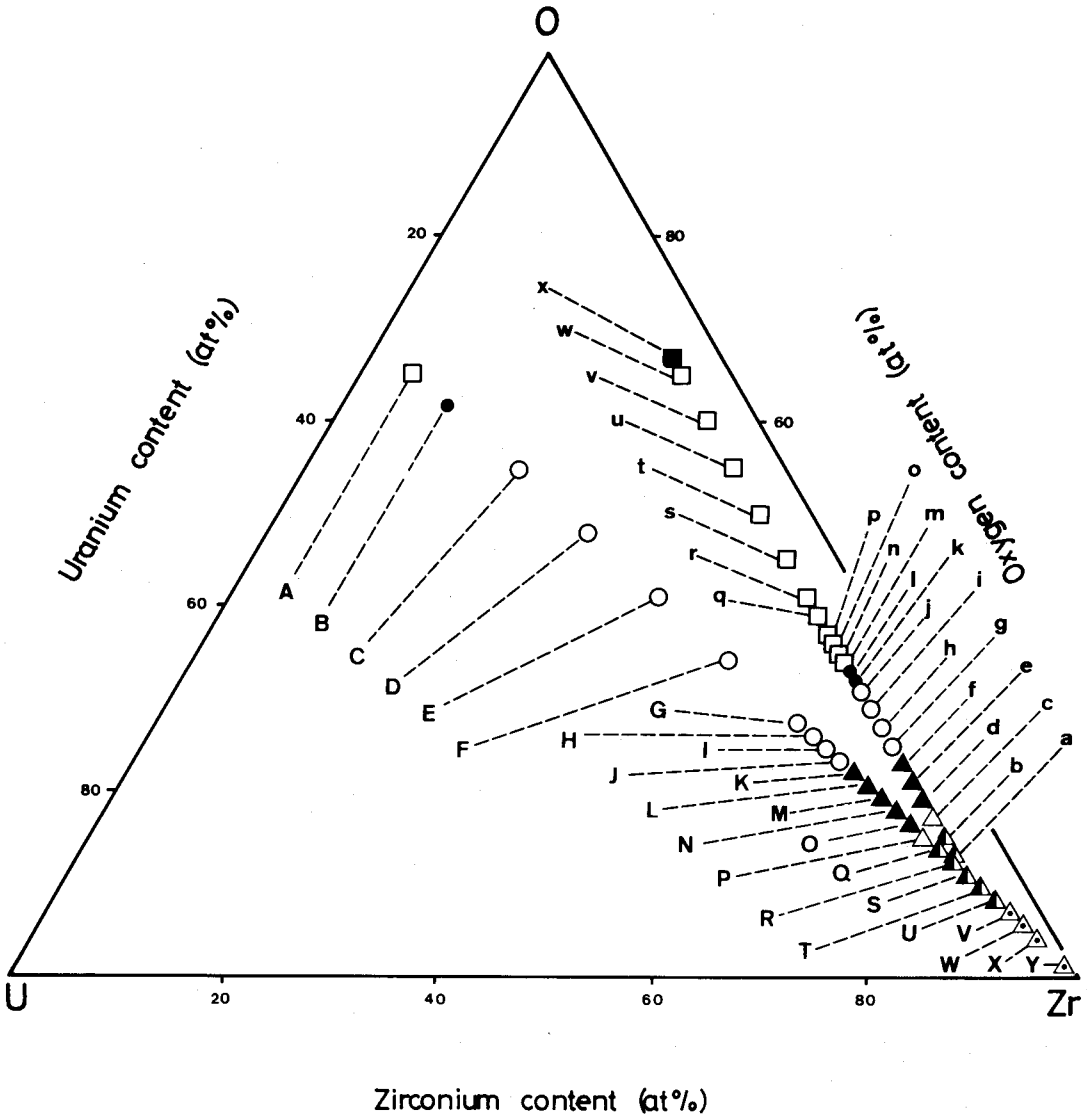

Fig. 1 Reaction products of the mixture pellets after heating at 1000°C.

- ■ UO_2 + αZrO_2,
- ● UO_2 + αZr,
- ▲ αZr + αU,
- ◭ αZr + UZr_2,
- □ UO_2 + αZrO_2 + αZr,
- ○ UO_2 + αZr + αU,
- △ αZr + αU + UZr_2,
- ◬ αZr + βZr.

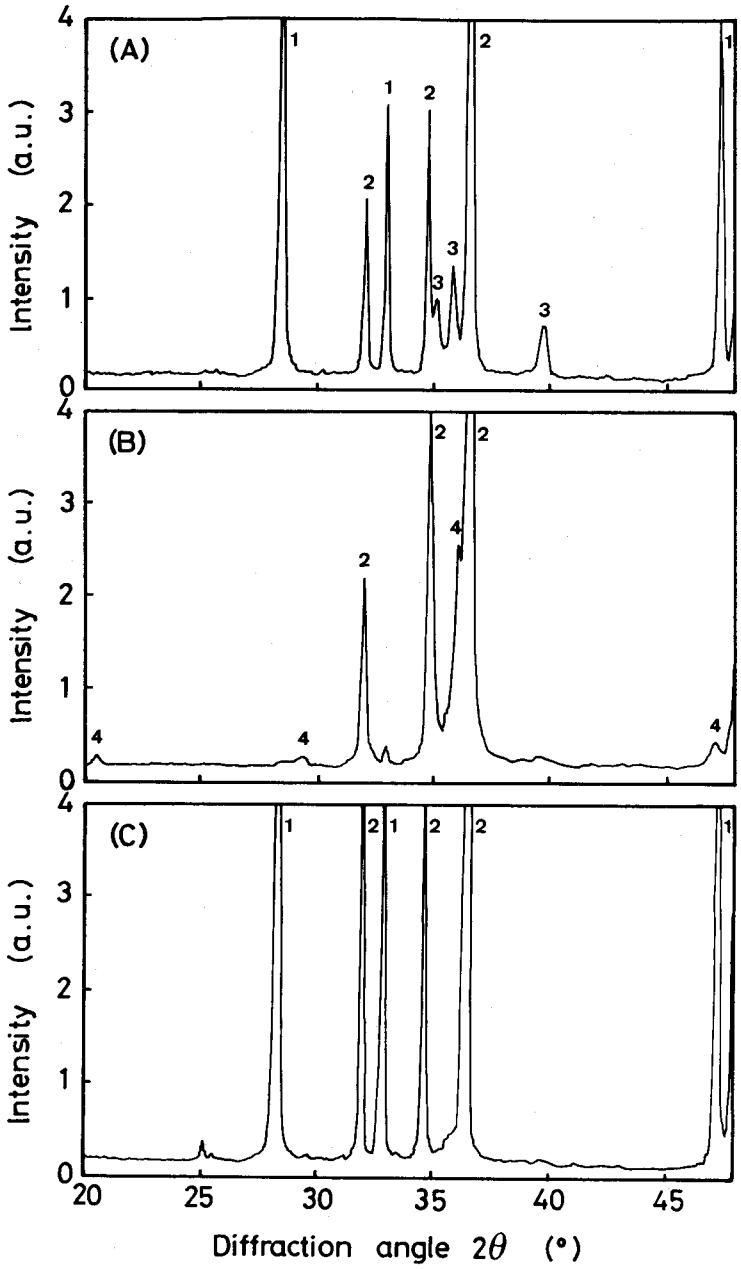

Fig. 2 X-ray diffraction patterns of the reaction products after heating at 1000°C.

(A) sample F, (B) sample Q, (C) sample k.

1: UO_2, 2: αZr, 3: αU, 4: UZr_2.

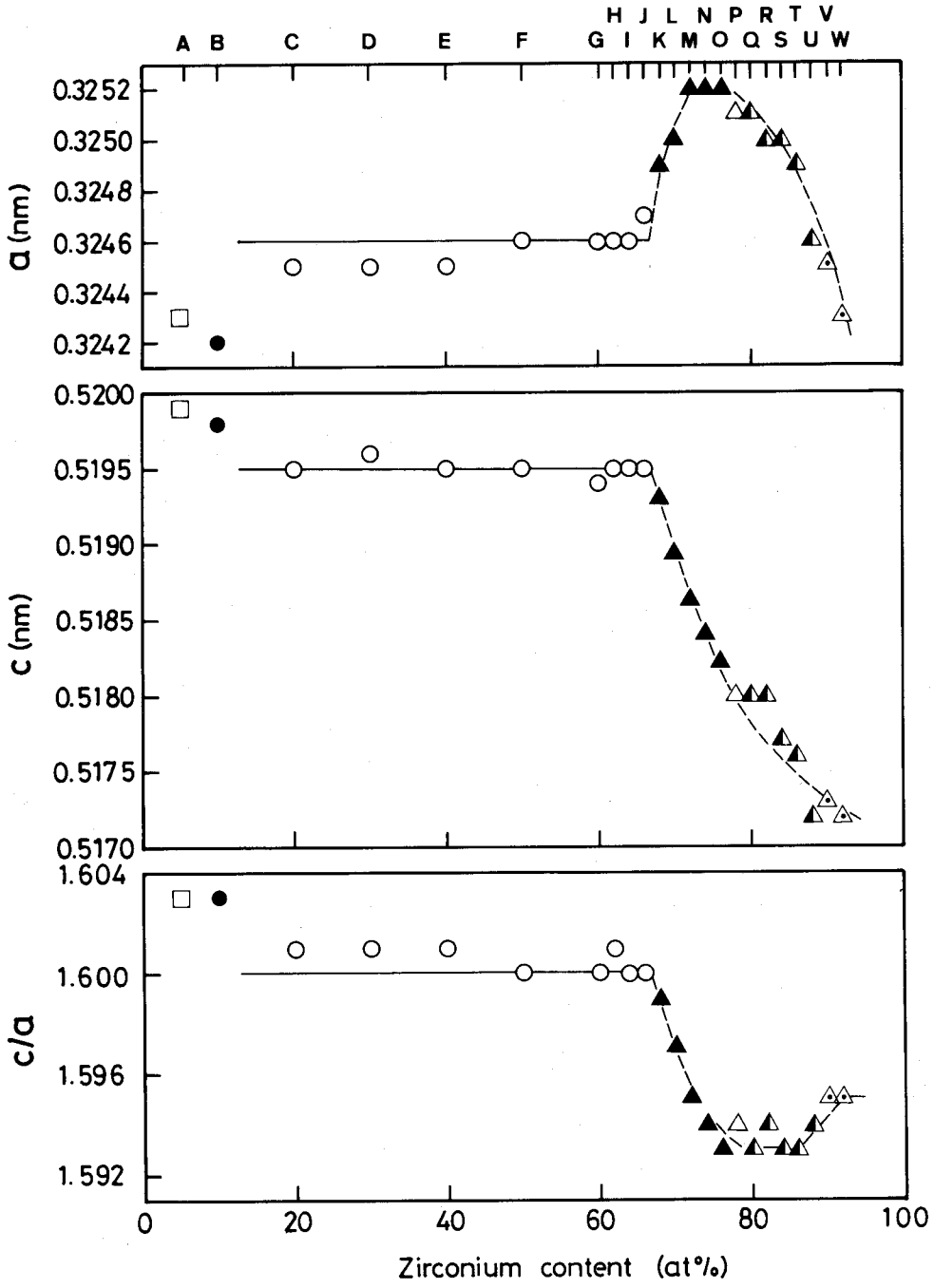

Fig. 3 Change in the lattice parameters a and c and the axial ratio c/a of αZr in the reaction products of samples A - W with zirconium content.

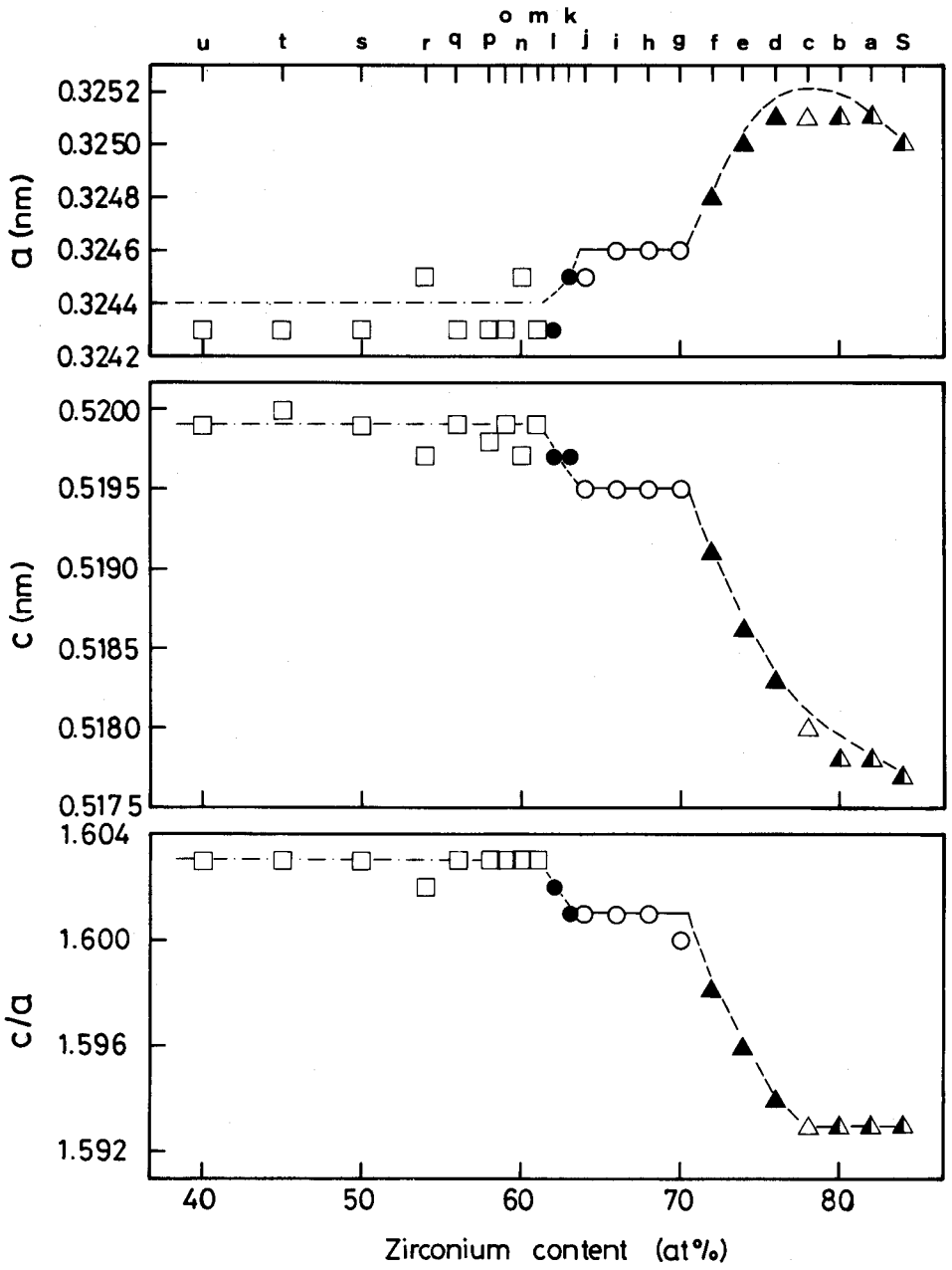

Fig. 4 Change in the lattice parameters a and c and the axial ratio c/a of αZr in the reaction products of samples a - u and S with zirconium content.

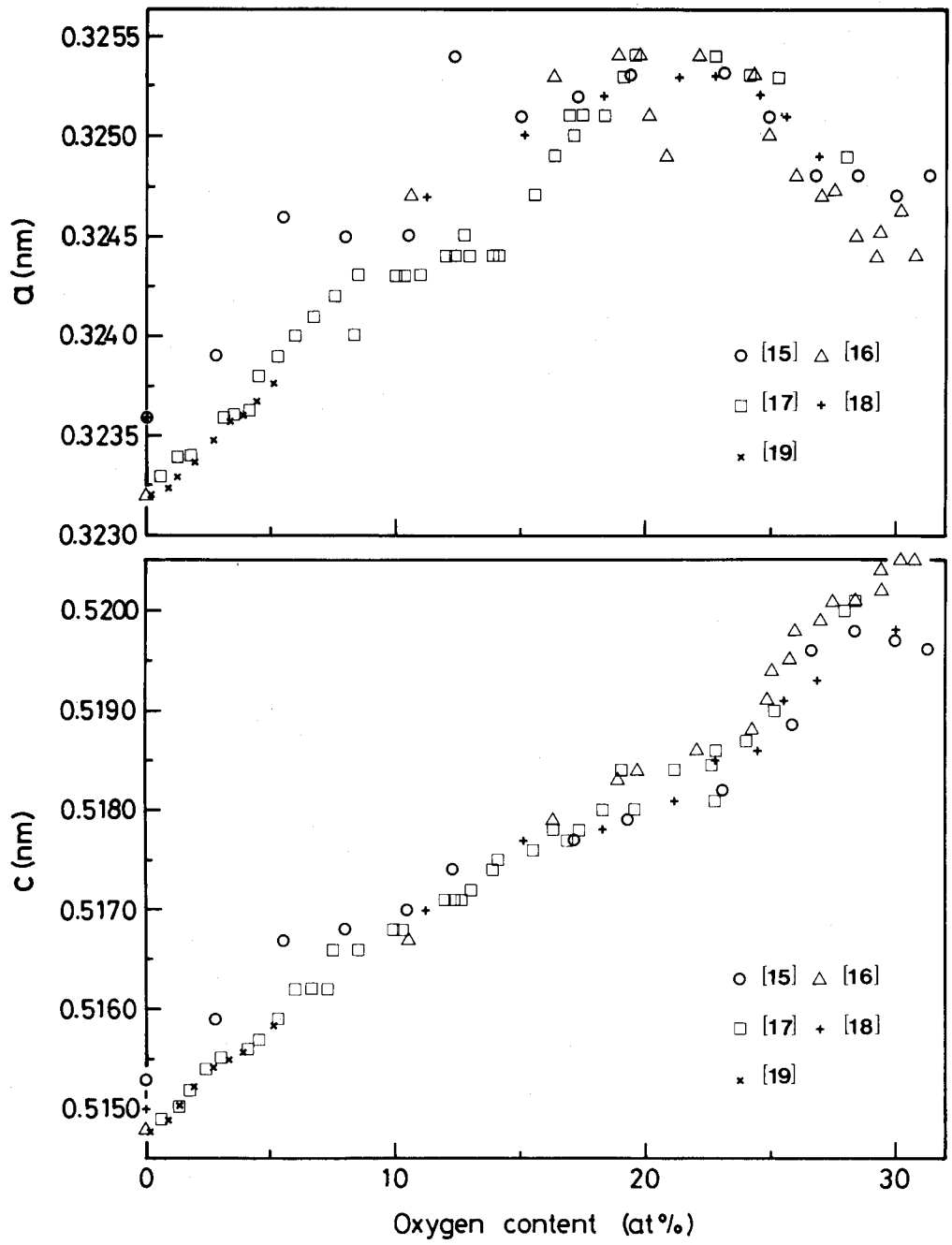

Fig. 5 Change in the lattice parameters a and c of αZr with oxygen content reported in the literature[15-19].

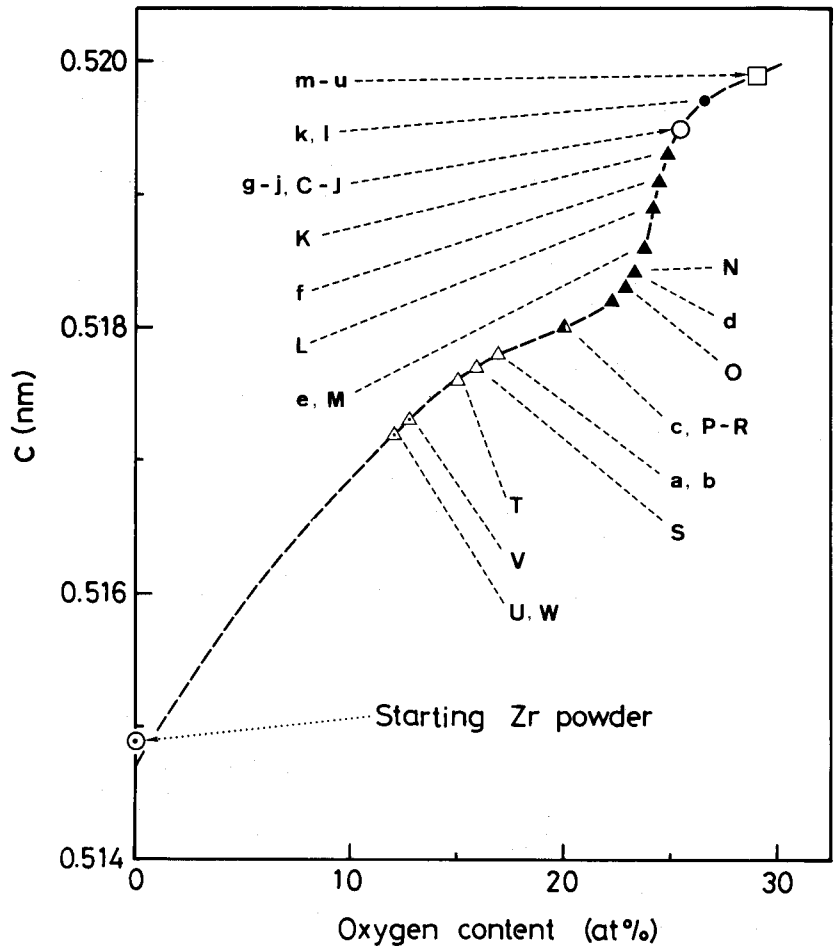

Fig. 6 Estimation of oxygen content of αZr in the reaction products of samples A - W and a - u.

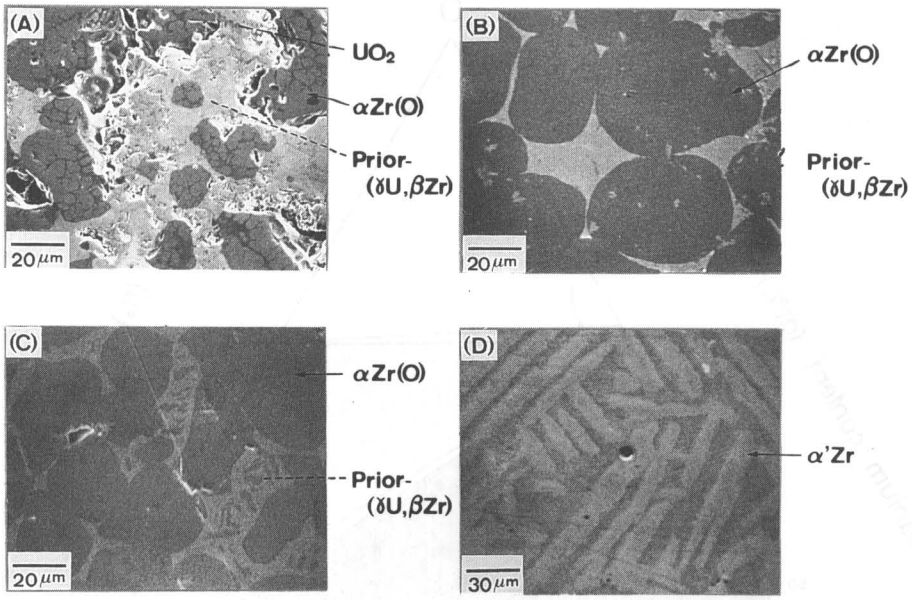

Fig. 7 Microstructures of the mixture pellets after heating at 1000°C. (A) sample F, (B) sample L, (C) sample Q, (D) sample Y.

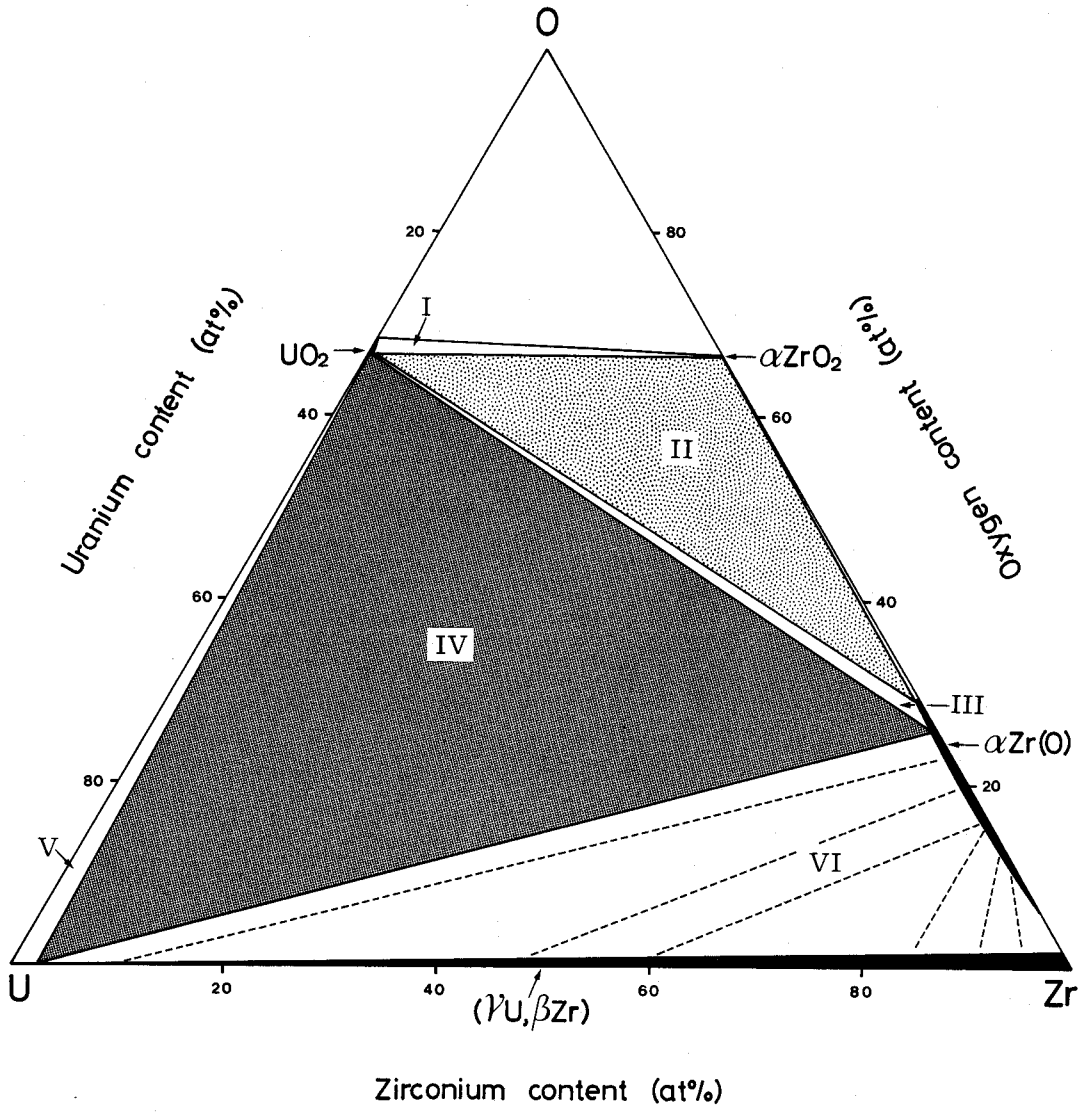

Fig. 8 Isothermal section of the U-Zr-O ternary system at 1000°C.

Ⅰ UO_2 + αZrO_2,
Ⅱ UO_2 + αZrO_2 + $\alpha Zr(O)$,
Ⅲ UO_2 + $\alpha Zr(O)$,
Ⅳ UO_2 + $\alpha Zr(O)$ + (γU,βZr),
Ⅴ UO_2 + (γU,βZr),
Ⅵ $\alpha Zr(O)$ + (γU,βZr).

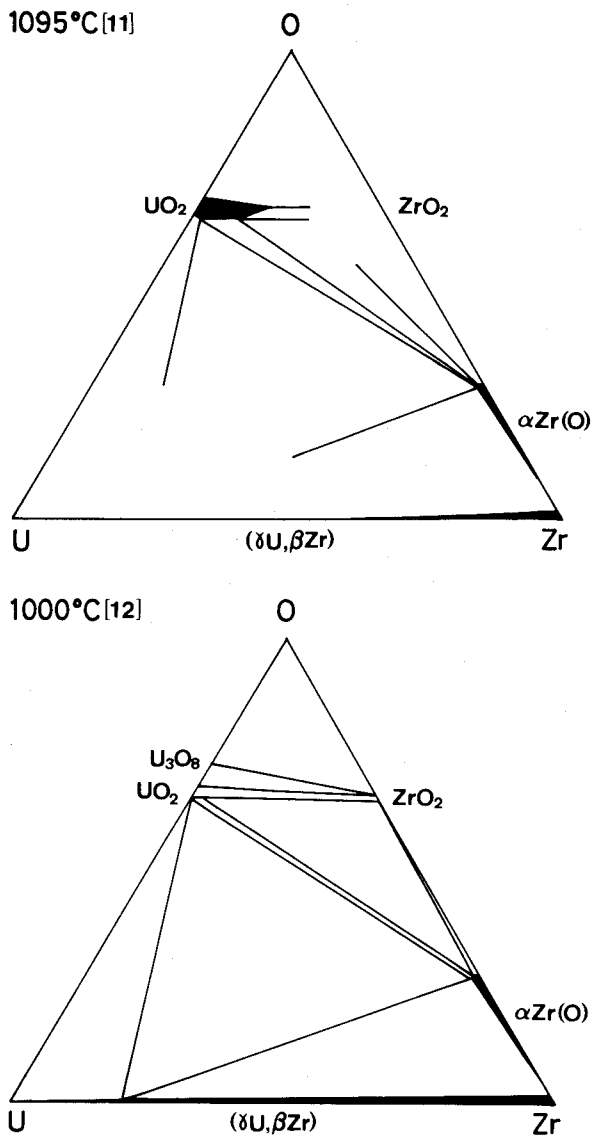

Fig. 9 Isothermal sections of the U-Zr-O ternary system at 1095[11] and 1000°C[12].

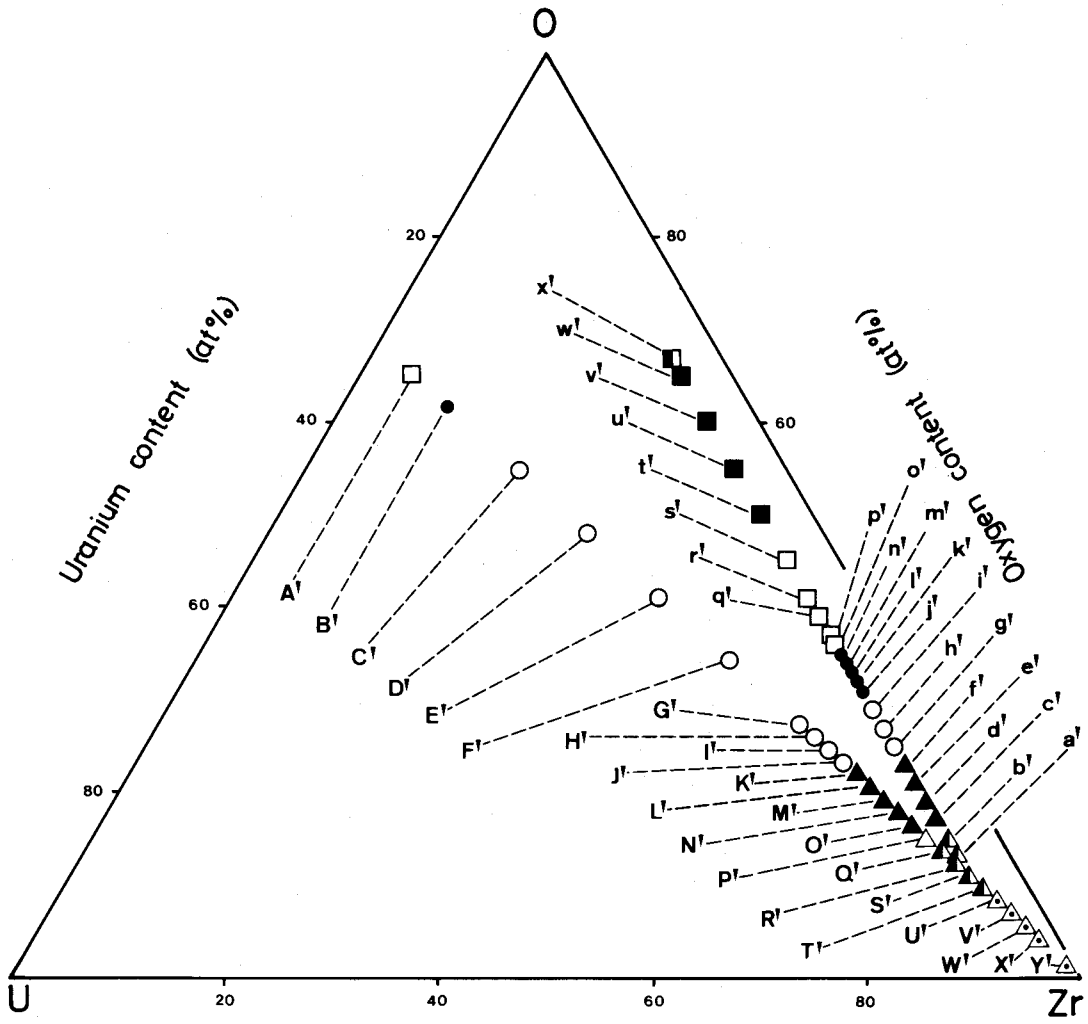

Fig. 10 Reaction products of the mixture pellets after heating at 1400°C.

- $UO_2 + \alpha ZrO_2 + \beta ZrO_2$,
- $UO_2 + \alpha ZrO_2 + \beta ZrO_2 + \alpha Zr$,
- $UO_2 + \alpha ZrO_2 + \alpha Zr$,
- $UO_2 + \alpha Zr$,
- $UO_2 + \alpha Zr + \alpha U$,
- $\alpha Zr + \alpha U$,
- $\alpha Zr + \alpha U + UZr_2$,
- $\alpha Zr + UZr_2$,
- $\alpha Zr + \beta Zr$.

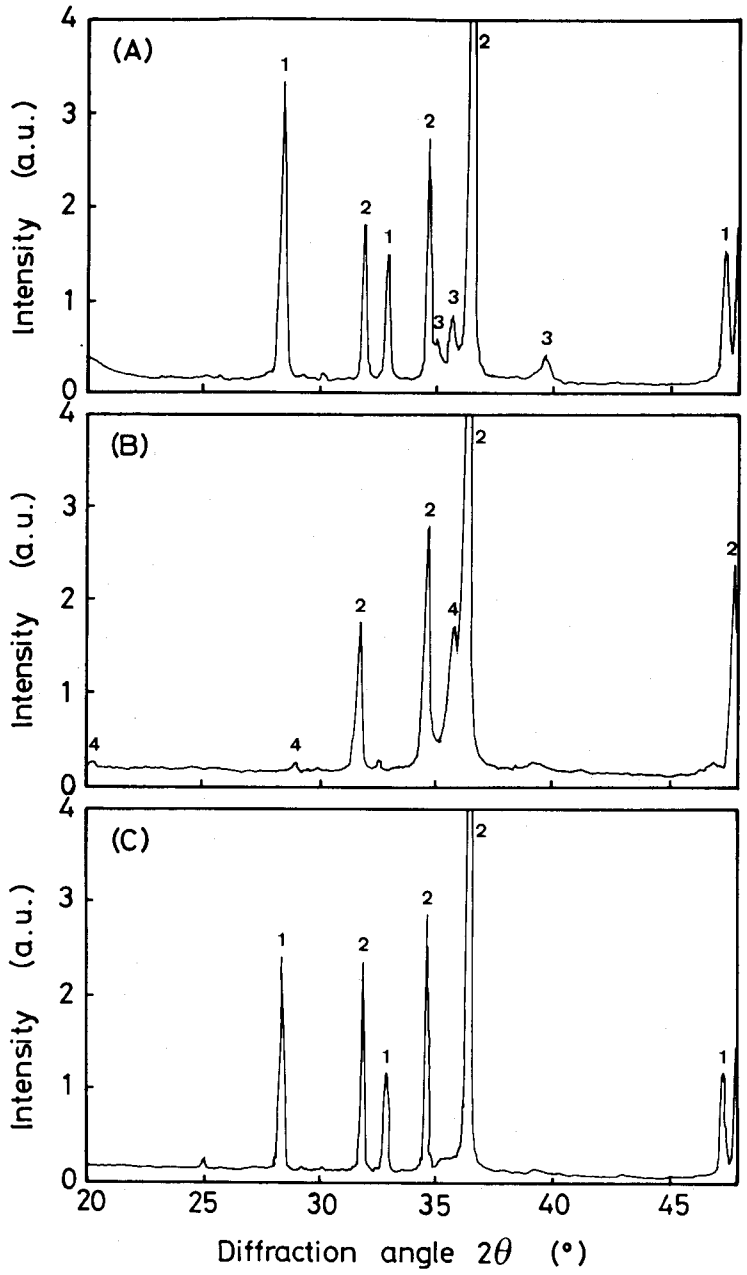

Fig. 11 X-ray diffraction patterns of the reaction products after heating at 1400°C.

(A) sample F', (B) sample Q', (C) sample k'.

1: UO_2, 2: αZr, 3: αU, 4: UZr_2.

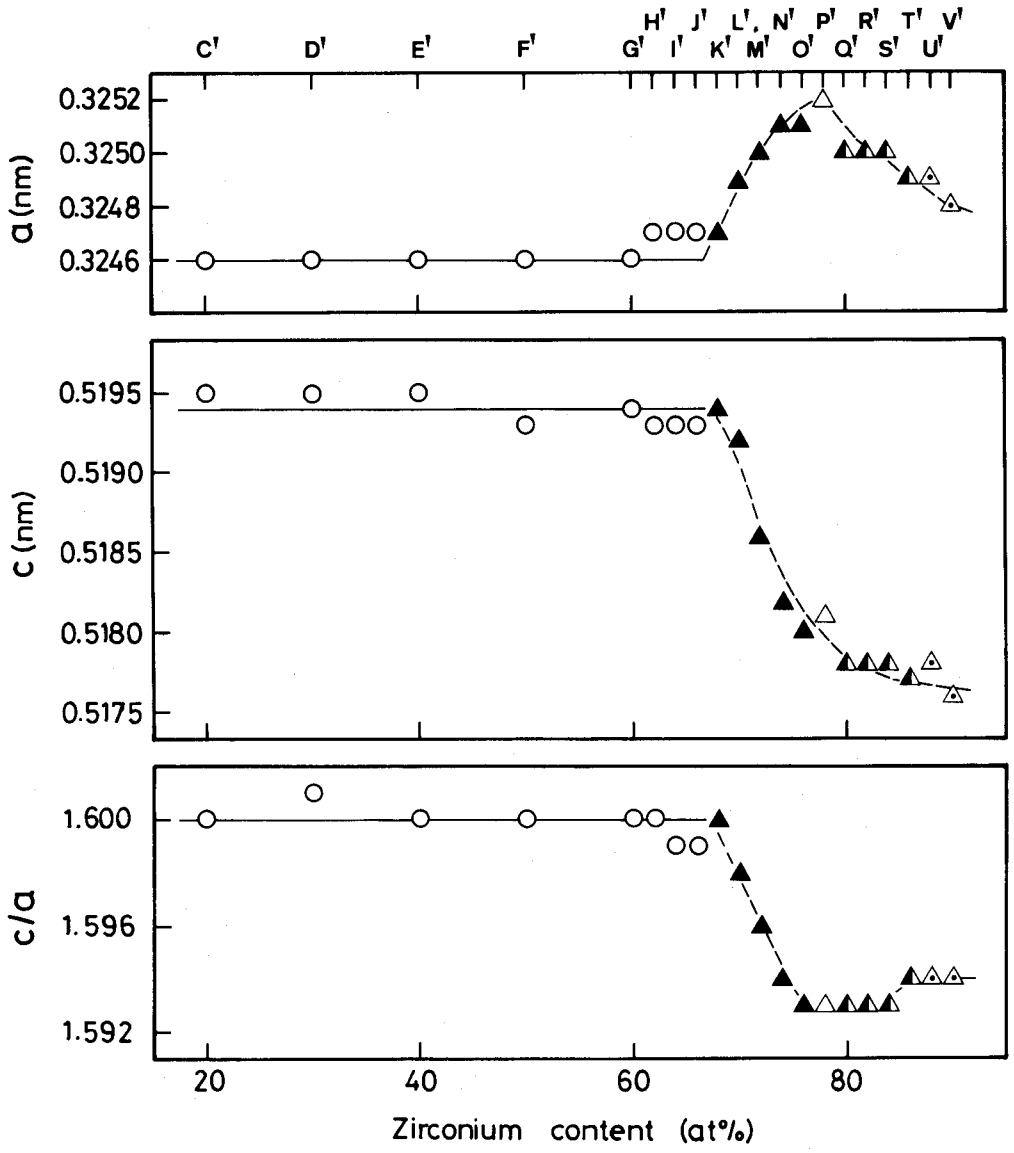

Fig. 12 Change in the lattice parameters a and c and the axial ratio c/a of αZr in the reaction products of samples C' - V' with zirconium content.

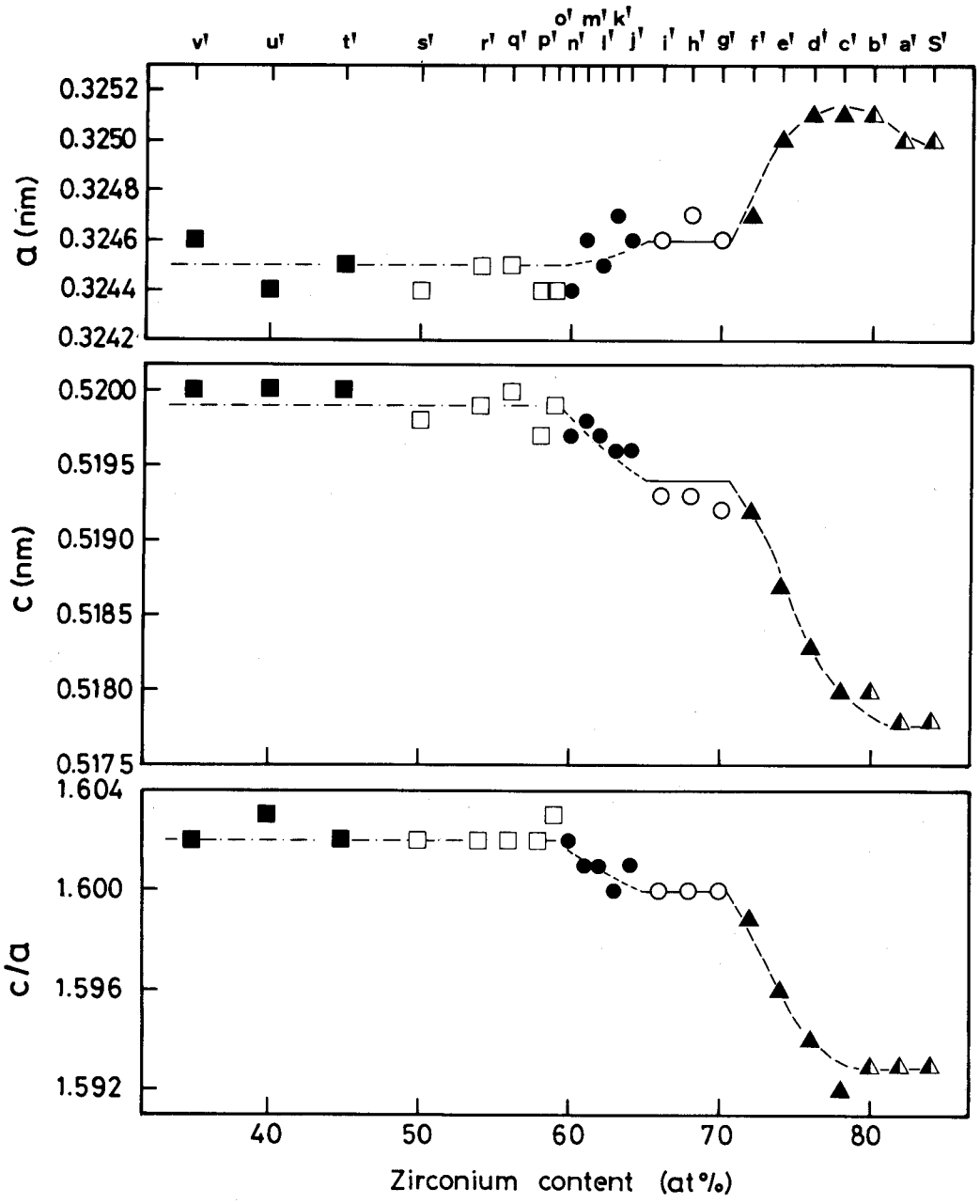

Fig. 13 Change in the lattice parameters a and c and the axial ratio c/a of αZr in the reaction products of samples a' - v' and S' with zirconium content.

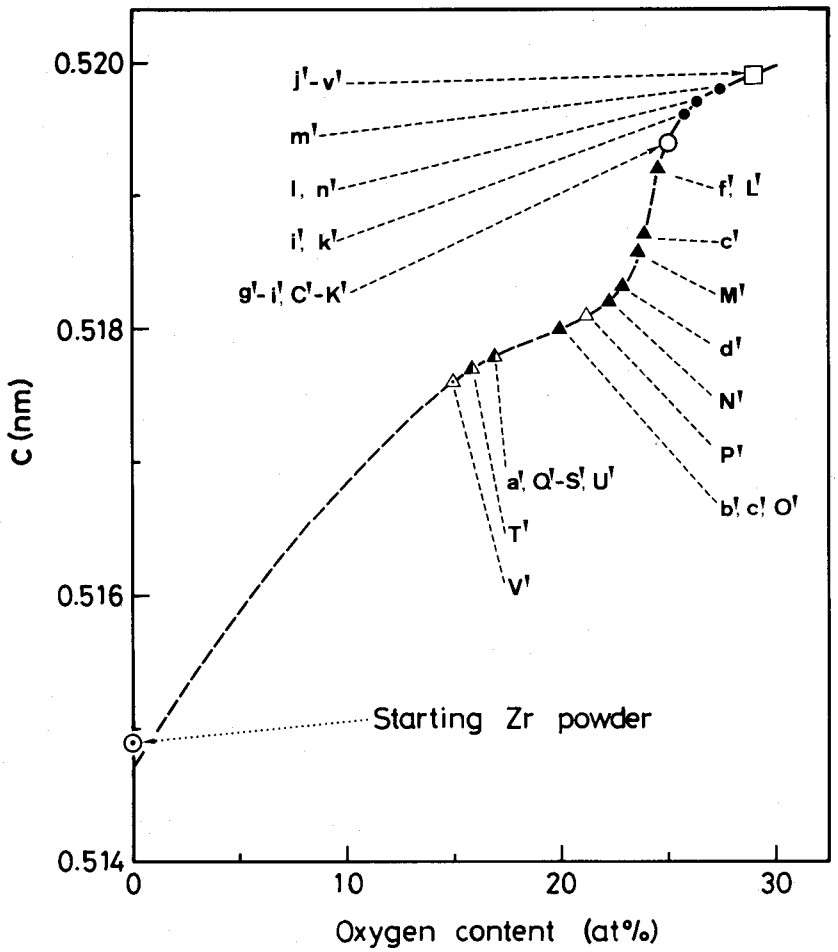

Fig. 14 Estimation of oxygen content of αZr in the reaction products of samples C' - V' and a' - v'.

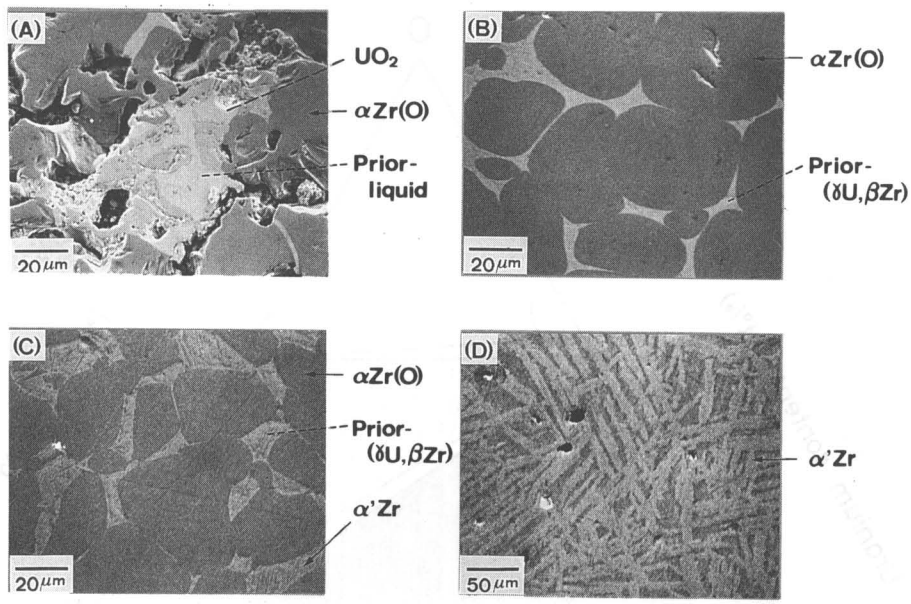

Fig. 15 Microstructures of the mixture pellets after heating at 1400°C. (A) sample F', (B) sample L', (C) sample Q', (D) sample Y'.

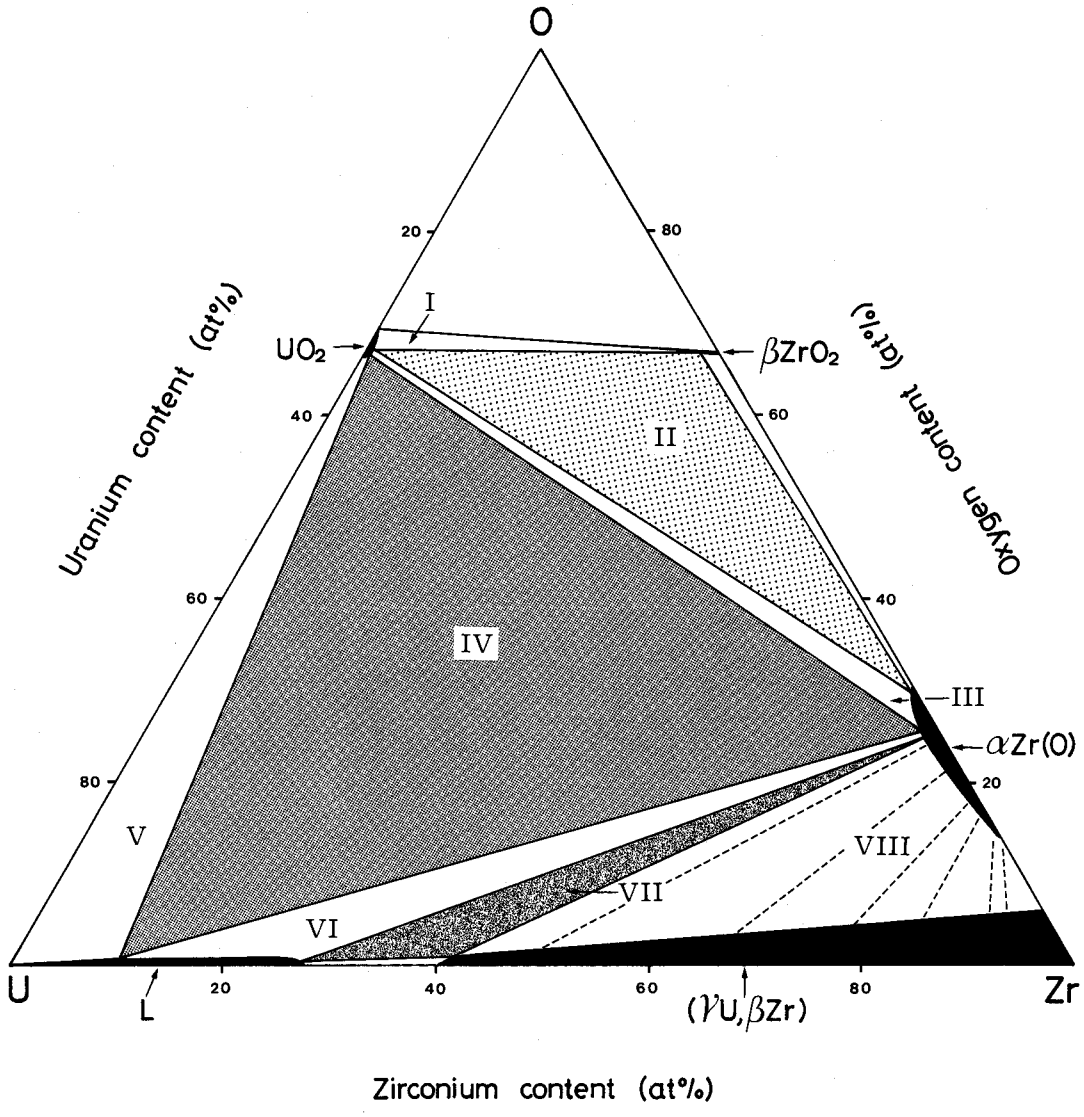

Fig. 16 Isothermal section of the U-Zr-O ternary system at 1400°C.

Ⅰ UO_2 + βZrO_2, Ⅱ UO_2 + βZrO_2 + $\alpha Zr(O)$,

Ⅲ UO_2 + $\alpha Zr(O)$, Ⅳ UO_2 + $\alpha Zr(O)$ + L,

Ⅴ UO_2 + L, Ⅵ $\alpha Zr(O)$ + L,

Ⅶ $\alpha Zr(O)$ + L + (γU,βZr), Ⅷ $\alpha Zr(O)$ + (γU,βZr).

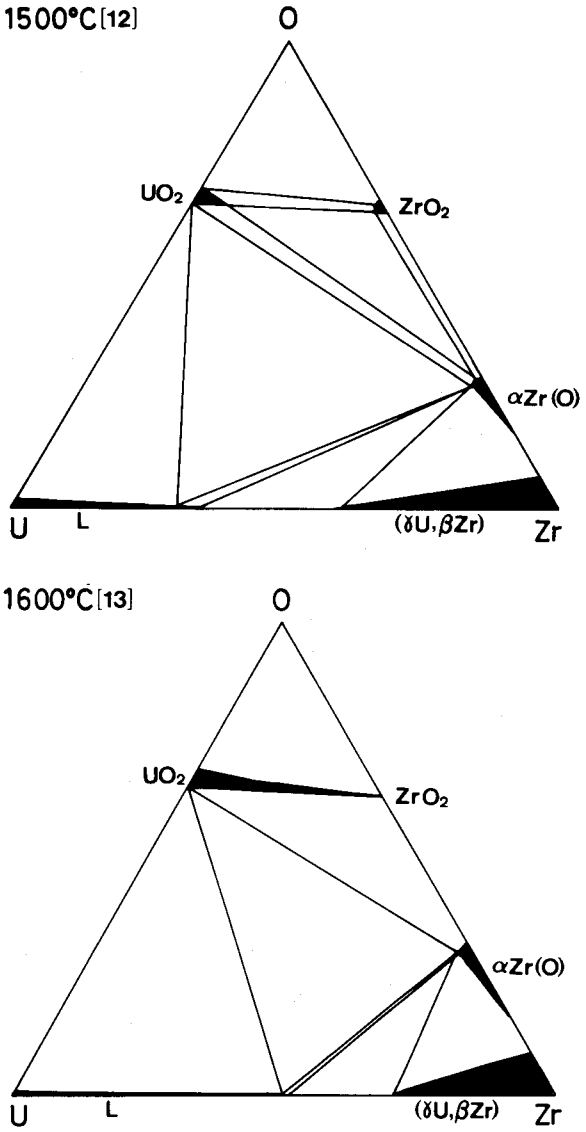

Fig. 17 Isothermal sections of the U-Zr-O ternary system at 1500[12] and 1600°C[13].

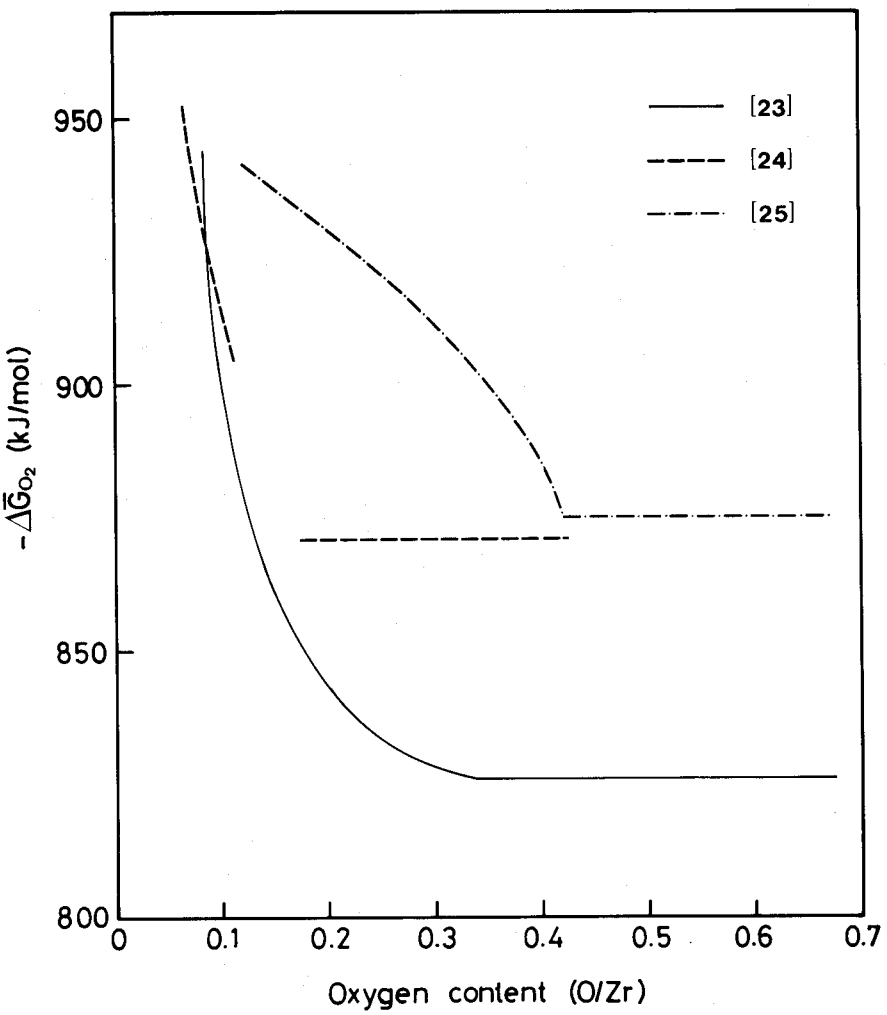

Fig. 18 Oxygen potential over αZr(O) solid solution, $\Delta\bar{G}_{O_2}(ZrO_x)$, at 1000°C reported in the literature[23-25].

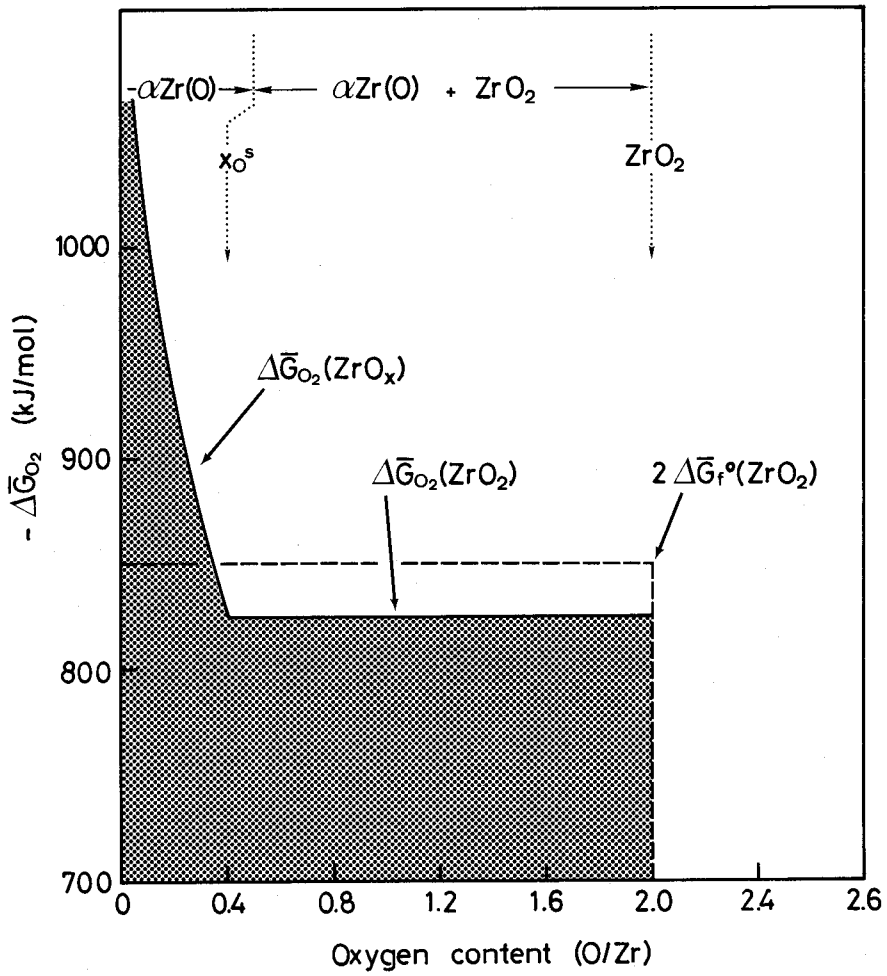

Fig. 19 Schematic representation of relation between oxygen potential over αZr(O) solid solution, $\Delta\bar{G}_{O_2}(ZrO_x)$, and standard free energy of formation of ZrO_2, $\Delta G_f^\circ(ZrO_2)$.

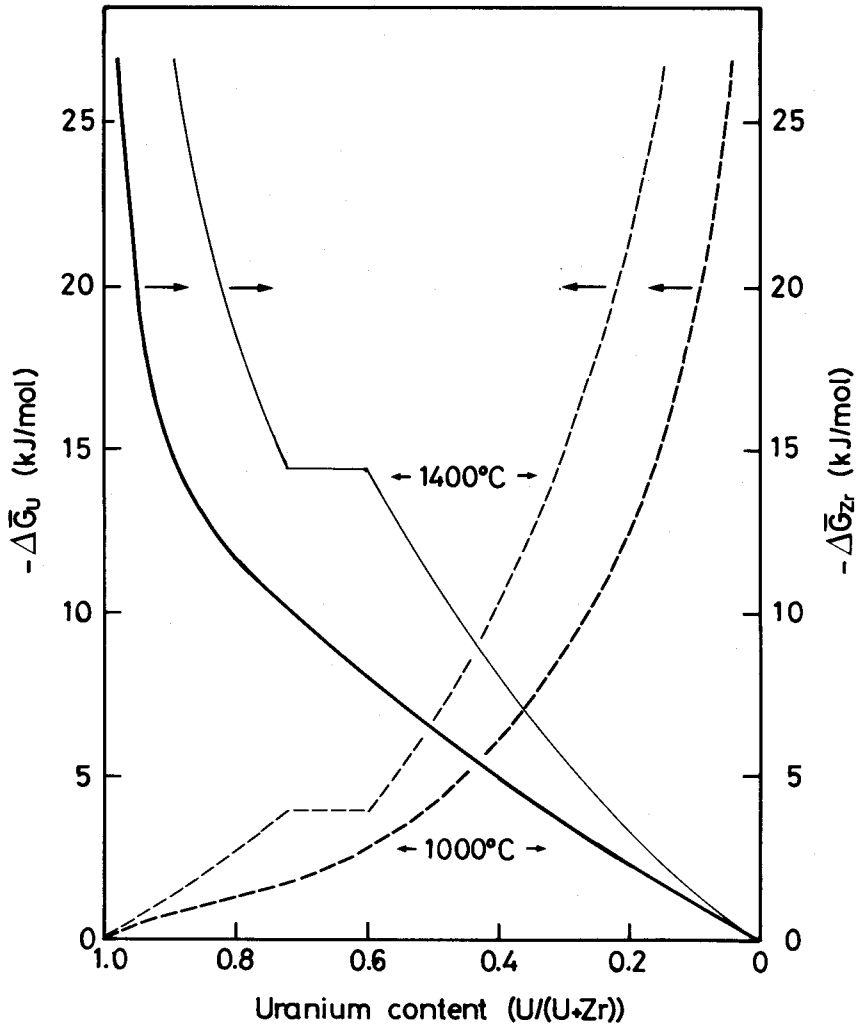

Fig. 20 Change in the partial molar excess free energies of uranium and zirconium in (γU,βZr) solid and liquid solutions, $\Delta\bar{G}_U$ and $\Delta\bar{G}_{Zr}$, with uranium content at 1000 and 1400°C.

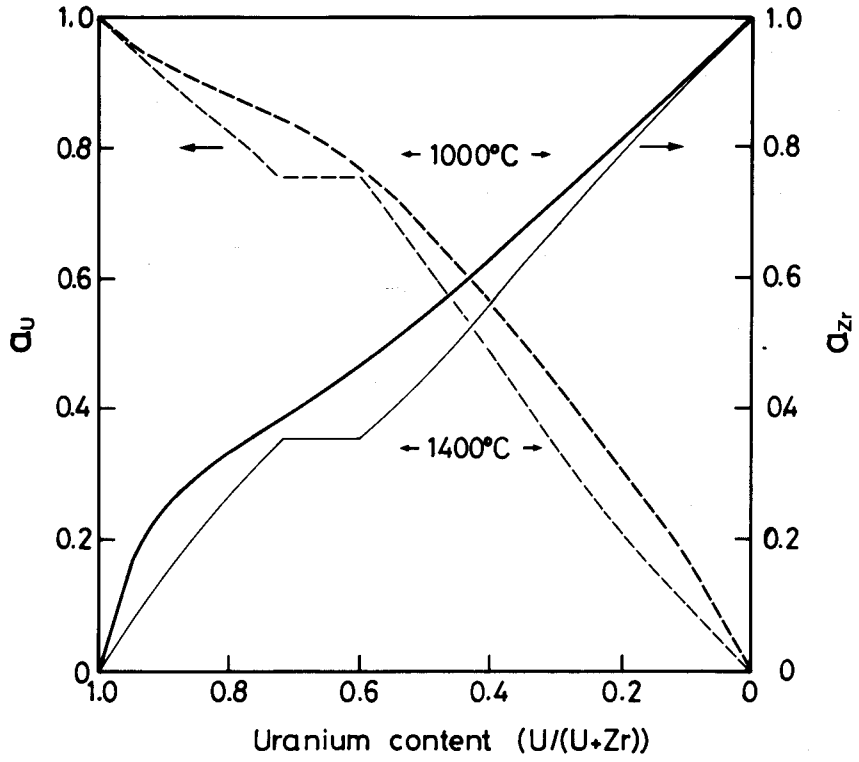

Fig. 21 Change in the thermodynamic activities of uranium and zirconium in (γU,βZr) solid and liquid solutions, a_U and a_{Zr}, with uranium content at 1000 and 1400°C.

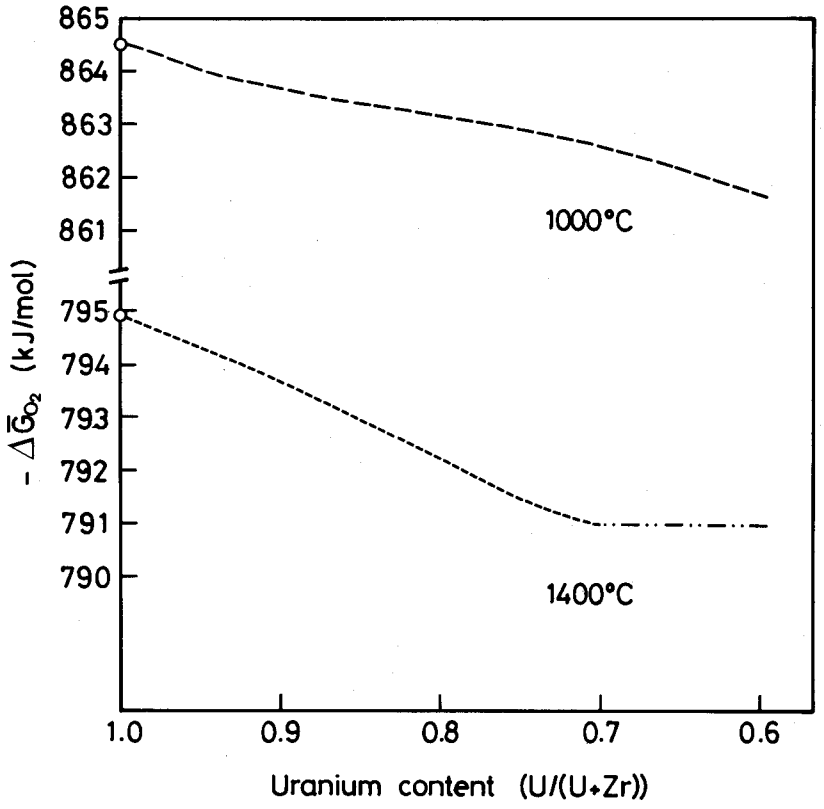

Fig. 22 Change in the oxygen potential over (γU,βZr) solid and liquid solutions in two-phase equilibrium with UO_2, $\Delta\bar{G}_{O_2}(UO_2)$, with uranium content at 1000 and 1400°C.

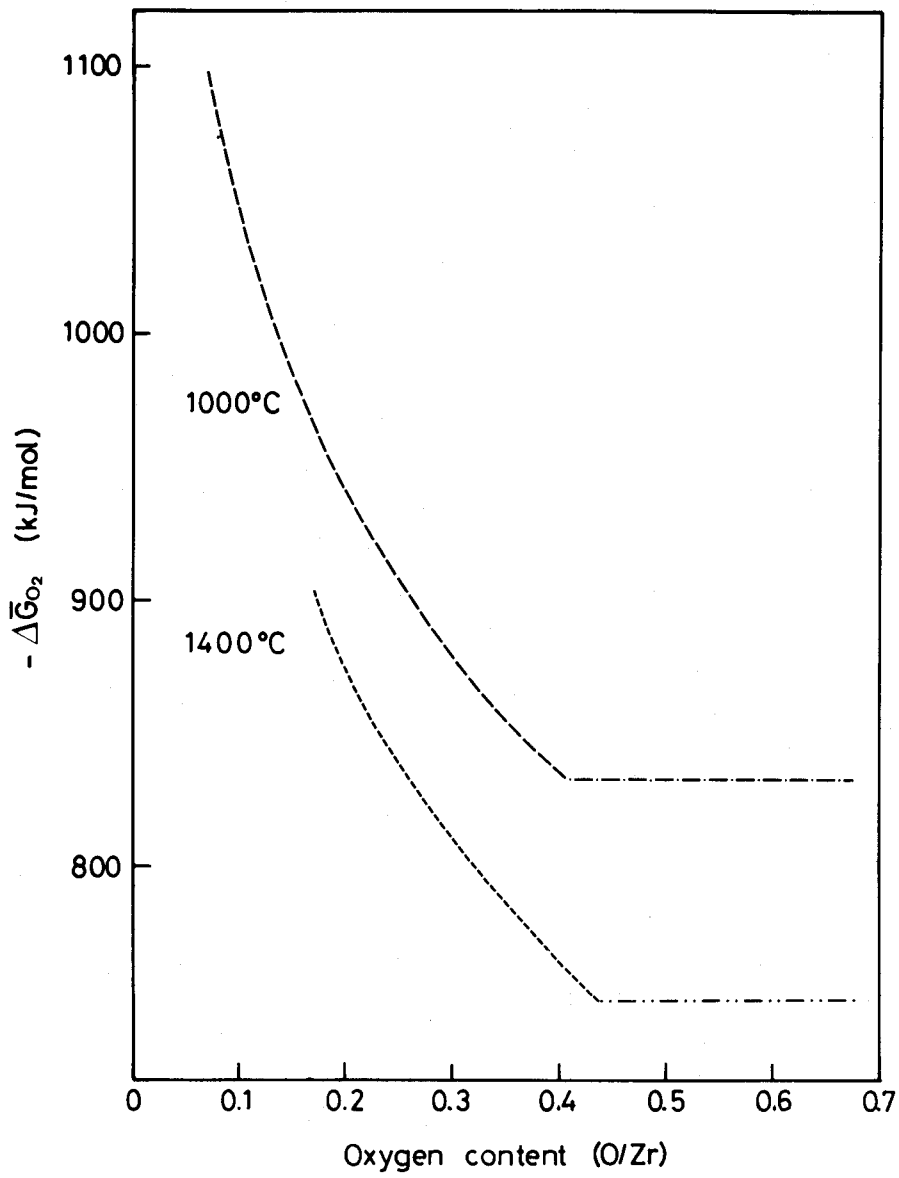

Fig. 23 Estimated oxygen potential $\Delta\bar{G}_{O_2}$ over αZr(O) solid solution at 1000 and 1400°C.

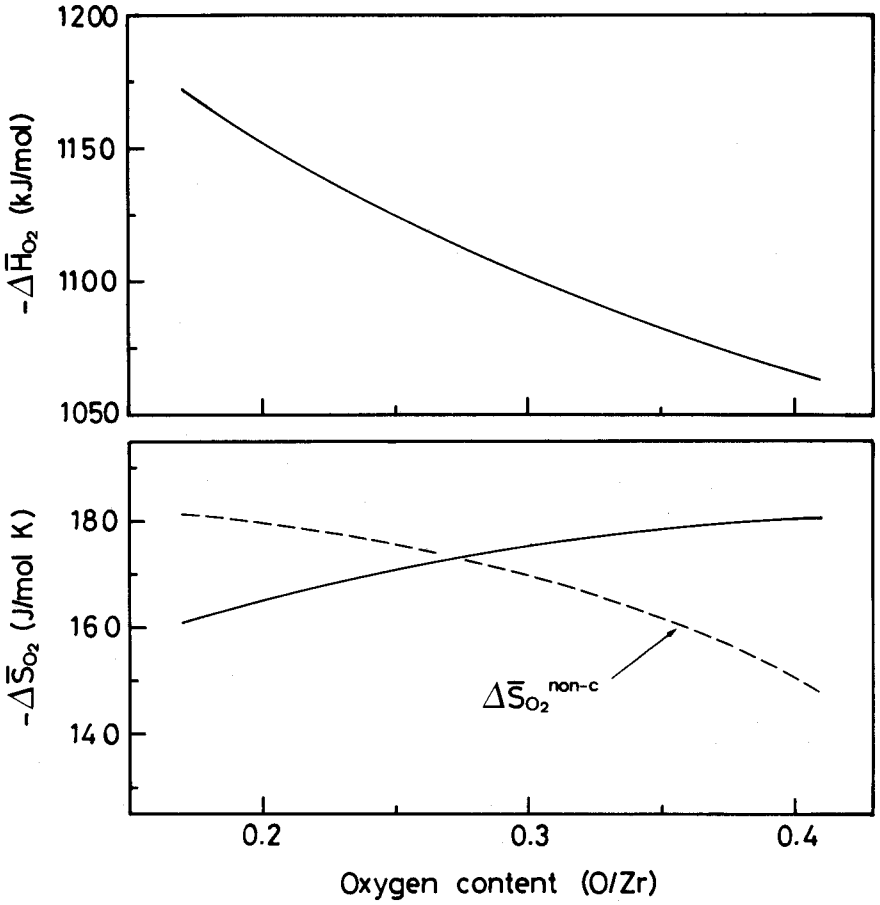

Fig. 24 Changes in the $\Delta\bar{H}_{O_2}$ and $\Delta\bar{S}_{O_2}$ values with oxygen content.

CHAPTER 4 TITANIUM-TELLURIUM-OXYGEN TERNARY SYSTEM

1. Introduction

Severe corrosion of stainless steel cladding induced by fission products is known to occur in irradiated mixed oxide fuel pins of liquid metal fast breeder reactors (LMFBRs)[1-3]. The oxygen potential is recognized as a crucial factor determining the cladding corrosion. One of the major approaches for inhibiting the corrosion is placement of materials into fuel pins which maintain the oxygen potential below the threshold for the corrosion reaction. Titanium has a great affinity for oxygen and is proposed as an oxygen-getter material in oxide fuel pins[4-6].

Chemical interaction of the titanium getter with the fission products is important for its practical application to fuel pins. As tellurium is one of the most aggresive fission products, the chemical reactions in the multicomponent system including titanium, oxygen and tellurium are therefore of particular interest. Knowledge of phase equilibria in the Ti-Te-O ternary system will contribute towards the prediction and the understanding of the interaction between the titanium getter and the fission product tellurium in LMFBR fuel pins.

Several investigators have synthesized various tellurides of titanium and studied their crystal structure[7-16]. The existence of at least seven compounds; Ti_2Te, Ti_5Te_4, TiTe, Ti_3Te_4, Ti_5Te_8 and $TiTe_2$ was reported. There appear discrepancies concerning existing phases in the binary system and their ranges of homogeneity. Thermochemical properties of titanium tellurides have been evaluated by vapor pressure measurements[16], and the partial phase diagram of Ti-Te binary system involving additional subtellurides, Ti_2Te_3, Ti_4Te_7 and $Te_{10}Te_{19}$, was constructed from the results. The binary phase diagrams of Ti-O and Te-O systems have been assessed in the handbooks of Murray[17] and Samsonov[18], and the thermodynamic properties of stable condensed phases were also reviewed[19,20]. The only information pertaining to the Ti-Te-O ternary system is a report on the crystal structure of the $TiTe_3O_8$ double oxide[21].

The present study has therefore been directed mainly to phase equilibria in the Ti-Te-O ternary system at 700°C with the aid of X-ray diffraction technique. The Ti-Te binary system at 700°C was also reexamined to clarify the types of tellurides and their range of homogeneity. The results experimentally obtained were interpreted in terms of a calculated stability diagram for the Ti-Te-O ternary system.

2. Experimental

Materials used in the present study were powders of Ti (purity, 99.9 wt%), Te (purity, 99.99 wt%), TiO (purity, 99.9 wt%), Ti_2O_3 (purity, 99.9 wt%), TiO_2 (purity, 99.9 wt%) and TeO_2 (purity, 99.99 wt%). A titanium-oxygen solid solution (αTi(O)) powder with 20 at%O, which was prepared by vacuum annealing of Ti and TiO mixtures, was also employed as a starting material. These powders were mixed in desired compositions and then pelletized. The pellets were sealed into silica tubes evacuated at a pressure less than 10^{-3} Pa. An equilibrium heat treatment was carried out at 700°C for 40 - 150 h, and subsequently the tube was quenched in ice water.

After the heat treatment, the tube was opened in a glove box filled with dry argon, and the pellet was powdered for phase identification. All the powdered samples were examined by X-ray diffractometry with monochromated Cu Kα radiation. Details of the measurements were described in the preceding chapter. Lattice parameters of some identified phases were evaluated by applying Cohen's method[22] to the diffraction intensity data.

3. Results and Discussion

3.1. Phase equilibria in the Ti-Te binary system

The results of phase identification for reaction products in binary samples a - o (75 - 5 at%Te) are shown in a compositional triangle, as can be seen in Fig. 1. The tellurides found in the present study were hexagonal $\alpha Ti_{2-x}Te_2$, monoclinic $\beta Ti_{2-x}Te_2$ and tetragonal Ti_5Te_4.

The hexagonal $\alpha Ti_{2-x}Te_2$ coexisted with Te in sample a. The lattice parameters of Te together with $\alpha Ti_{2-x}Te_2$ were evaluated to be a = 0.446 nm and c = 0.593 nm; in agreement with the literature data of a = 0.44572 nm and c = 0.59290 nm for pure Te powder[23]. This suggests that tellurium liquid at 700°C may dissolve a small amount of titanium into the solution. The lattice parameters of $Ti_{2-x}Te_2$ in sample a were found to be a = 0.3772 nm and c = 0.6499 nm, which agreed with the reported values for a titanium ditelluride[7-9,12,14,15]. Between 60 and 66.7 at%Te (samples e - b), a single-phase of $\alpha Ti_{2-x}Te_2$ was observed. The typical X-ray diffraction pattern of $\alpha Ti_{2-x}Te_2$ (sample c) is indicated in Fig. 2(A). Figure 3 reveals the variation in a and c values with tellurium content of sample. In this figure, $\sqrt{3}a$ and 2c are indicated instead of a and c values in order to be able to compare the hexagonal unit cell dimensions with the monoclinic ones; a, b, c and β. The a and c values of $\alpha Ti_{2-x}Te_2$ in the sample b were close

to those for sample a. The a value increased with decreasing tellurium content, while c and c/a values markedly decreased.

In samples f - j, there existed a $\beta Ti_{2-x}Te_2$ with a monoclinic structure. Figure 2(B) (sample f) is the representative of monoclinic diffraction pattern, rather complicated than hexagonal one. The single-phase monoclinic $\beta Ti_{2-x}Te_2$ was formed in a range of composition from 50 - 57.5 at%Te (samples i - f). The change in the lattice parameters a, b, c and β and the axial ratio c/2b is shown in Fig. 3. As seen in this figure, the values of a, b, c and β decrease as the tellurium content increases. X-ray diffraction pattern of sample j supported the evidence for coexistence of $\beta Ti_{2-x}Te_2$ with Ti_5Te_4, of which the reflections were idexed as tetragonal. The lattice parameters of $\beta Ti_{2-x}Te_2$ in this sample could not be evaluated because of difficulties due to the weak intensity of the lines and the similarity of the structures.

The tetragonal Ti_5Te_4 whose diffraction pattern is given in Fig. 2(C) was contained in samples j - o. At 44.4 at%Te (sample k), a single-phase of Ti_5Te_4 was found to be formed. The lattice parameters of the Ti_5Te_4 were estimated to be a = 1.017 nm and c = 0.377 nm, which were in good agreement with those reported by Raaum et al.[10]. A mixture of Ti_5Te_4 and αTi was observed in samples l - o rich in titanium. The a and c values of Ti_5Te_4 were nearly independent of sample composition, implying that Ti_5Te_4 may have a narrow composition range. The lattice parameters of αTi coexisting with Ti_5Te_4 were a = 0.2950 nm and c = 0.4684 nm, which were almost the same as those for the starting Ti powder (a = 0.2951 nm and c = 0.4683 nm). Based on the lattice parameters of αTi, the solubility of tellurium in αTi is inferred to be quite low at 700°C. This is consistent with the estimate of Goldhoff et al.[24] derived from their metallographic study of Ti-Te alloys at 790°C.

The author verified from the X-ray diffraction study that the stable phase in the binary system at 700°C are Te, hexagonal $\alpha Ti_{2-x}Te_2$, monoclinic $\beta Ti_{2-x}Te_2$, tetragonal Ti_5Te_4 and αTi. Raaum et al.[12] have concluded that from about 55 to 60 at%Te the phase has a monoclinic structure related to the NiAs type and the phase has a hexagonal NiAs-CdI_2 type structure between 60 and 67 at%Te. The results of the present study appear to be similar to those of Raaum et al.[12], but the monoclinic $Ti_{2-x}Te_2$ phase may have a wider homogeneity range expanding from 60 to 50 at%Te at 700°C. The existence of a two-phase region of hexagonal and monoclinic tellurides could not be confirmed. Suzuki et al.[16] have proposed on the basis of a vaporization study that the composition range of 46.8 to 66.7 at%Te contains several distinct phases such as TiTe, Ti_2Te_3, Ti_4Te_7, $Ti_{10}Te_{19}$ and $TiTe_2$. The group of Chevreton[11,13] have also presented evidence for subtellurides in this composition range of 50 - 67 at%Te: monoclinic Ti_3Te_4 and hexagonal Ti_5Te_8. The monoclinic $\beta Ti_{2-x}Te_2$ phase region found in the present

study is identical with the TiTe region (46.8 - 57.6 at%Te) reported by Suzuki et al.[16]. The composition of monoclinic Ti_3Te_4 reported by Chevreton et al.[11] also falls into this region. The hexagonal $\alpha Ti_{2-x}Te_2$ phase region may consist of subtellurides with the same crystal structure such as Ti_2Te_3, Ti_4Te_7, $Ti_{10}Te_{19}$ and $TiTe_2$. Though there is a difference in chemical formula, the Ti_5Te_8 with a homogeneity range of 60 - 63 at%Te as reported by Brunie and Chevreton[13] appears to correspond to Ti_2Te_3 (58.7 - 60.8 at%Te) as reported by Suzuki and Wahlbeck[16]. Vaporization measurements at 1250°C[16] exhibited the existence of Ti_2Te and Ti_5Te_4 in the Ti-rich region, and a tetragonal structure was assigned to Ti_2Te and Ti_5Te_4[9,10,12,16]. The present results differ from the previous results[9,16] in showing that at the composition corresponding to a stoichiometric Ti_2Te only a two-phase mixture of αTi and Ti_5Te_4 is present. The Ti_2Te phase may disproportionate at a lower temperature of 700°C, as expected by Suzuki et al.[16]. Further examination is required for precise determination of existing phases and boundaries in the composition range from TiTe to $TiTe_2$.

3.2. Phase equilibria in the Ti-Te-O ternary system

Figure 1 also represents the results of phase identification for ternary samples: TeO_2/TiO_2 mixtures (samples A - C), $Ti_2O_3/TeO_2/Te$ mixtures (samples D - G), TiO/Te mixtures (samples H - K) and $\alpha Ti(O)/TeO_2/Te$ mixtures (samples L - T). A double oxide $TiTe_3O_8$ was the only ternary compound appearing in the Ti-Te-O ternary system. The X-ray diffraction pattern of $TiTe_3O_8$ (Fig. 4(A)) was indexed as a cubic with a distorted CaF_2 structure. Sample A - E contained $TiTe_3O_8$ as one of the reaction products. Sample B (mole ratio of TeO_2 to TiO_2 = 3/1) was composed of only $TiTe_3O_8$, whereas for samples A and C, TiO_2 or TeO_2 in addition to $TiTe_3O_8$ was detected. The presence of this ternary compound does not allow TiO_2 to be compatible with TeO_2 at 700°C. Three phases including $TiTe_3O_8$ and Te existed in Samples E and D. In the TiO_2-TeO_2-Te region, the double oxide $TiTe_3O_8$ can coexist with Te, TeO_2 or TiO_2. The X-ray diffraction data obtained for $TiTe_3O_8$ in the samples A - E were indexed as a cubic with a = 1.095 nm, irrespective of the type of the coexisting phase. The a value obtained was close to a = 1.0956 nm reported by Meunier and Galy[19]. This means that $TiTe_3O_8$ is a stoichiometric compound.

Titanium oxides observed in the ternary samples A - S and W - Y were TiO_2, Ti_3O_5, Ti_2O_3 and αTiO, except for $TiTe_3O_8$. For samples F and G, only simple oxides of titanium were found together with Te. Magneli phases Ti_nO_{2n-1} seem to be involved in sample F, but the chemical forms could not be determined. According to the assessment of Murray et al.[17], $\alpha Ti_{1-x}O$ and Ti_3O_2 are stable at 700°C. The presence of $\alpha Ti_{1-x}O$ and Ti_3O_2 in the ternary samples was not confirmed

by the present study. There still remains some question as to whether or not the low temperature phases, $\alpha Ti_{1-x}O$ and Ti_3O_2, exist in the Ti-O binary system at 700°C.

It is obvious from Fig. 1 that titanium telluride phases were identified over a wide range of composition (samples H - Y). Hexagonal $\alpha Ti_{2-x}Te_2$ coexisted with both Te and Ti_2O_3 in samples J - N. The two phases Ti_2O_3 and $\alpha Ti_{2-x}Te_2$ were found in sample I. The phase $\alpha Ti_{2-x}Te_2$ coexisted with Ti_2O_3 and αTiO in samples H and O. Monoclinic $\beta Ti_{2-x}Te_2$ phase coexisted with αTiO in samples P, Q and Y. Figure 4(B) is a typical example of X-ray diffraction pattern indicating the coexistence of the $Ti_{2-x}Te_2$ with Titanium oxides.

The variation in the lattice parameters is indicative of the extent of the range of composition in the $Ti_{2-x}Te_2$ phase. In Fig. 5, the lattice parameters of $Ti_{2-x}Te_2$ are given as a function of tellurium content in the ternary sample. There is no marked difference in the a and c values of hexagonal $\alpha Ti_{2-x}Te_2$ for the samples J - N containing three phases, and the values were close to those for the binary samples a and b. The a and c values for sample I hardly differ from those for the samples J - N. The $\alpha Ti_{2-x}Te_2$ in the samples H and O showed almost the same lattice parameters, which were quite different from those for the samples J - N. Assuming that oxygen solubility in $Ti_{2-x}Te_2$ is small and the dissolved oxygen scarcely influences the lattice expansion of $Ti_{2-x}Te_2$, one can estimate the tellurium content of $Ti_{2-x}Te_2$ in the ternary samples from the lattice parameters. The values of a and c shown in Fig. 5 suggest that the tellurium content in $\alpha Ti_{2-x}Te_2$ are about 67 at%Te for the samples I - N and about 60 at%Te for the samples H and O. The lattice parameters of monoclinic $\beta Ti_{2-x}Te_2$ for samples P and Q are also shown in Fig. 5. Judging from the values of a, b, c and β, the tellurium contents of monoclinic $Ti_{2-x}Te_2$ in samples P and Q are close to those for the binary samples f and i.

The X-ray diffraction analysis revealed that Ti_5Te_4 coexisted with both αTiO and αTi in samples R, S, W and X, as indicated in Fig. 4(C). For samples T - V, the reaction products were αTi and Ti_5Te_4, but no titanium oxide was detected. The lattice parameters of Ti_5Te_4 in the ternary samples R - X were almost similar to those for the single-phase Ti_5Te_4 (sample k). Therefore, the homogeneity range of Ti_5Te_4 is presumed to be very narrow. Since only a limited amount of tellurium is anticipated to be soluble in a hexagonal αTi, the oxygen content of αTi coexisting with Ti_5Te_4 can be estimated from the hexagonal unit cell dimension. The lattice parameters of αTi in the samples containing αTiO and Ti_5Te_4 were in accord with the reported value of αTi at the solubility limit of oxygen, about 33 at%O[17]. Hence, αTi in samples R, S, W and X appears to be saturated with oxygen. For samples T - V, the a and c values for αTi varied with composition of sample. The estimated oxygen contents of αTi were 22, 26 and 31 at% for samples

T, U and V, respectively. It can be concluded that the nearly stoichiometric Ti_5Te_4 is the only telluride which can coexist with αTi having various oxygen contents from 0 to 33 at%.

The existence of Te was recognized in the ternary samples D - G and J - N, as indicated in Fig. 1. The lattice parameters of Te in these samples were the same unaffected by the composition of samples, and agreed with the literature data[23] for pure Te. Tellurium, which is liquid at 700°C, is expected to dissolve little oxygen and titanium into the solution.

The tentative isothermal section of the Ti-Te-O ternary system at 700°C was constructed from the results of phase identification and lattice parameter determination, as illustrated in Fig. 6. Only tellurium appears to comprise a liquid phase designated as L in this figure. The composition field bounded by TiO_2, TeO_2 and Te was characterized by a ternary compound of $TiTe_3O_8$. The stoichiometric $TiTe_3O_8$ is in equilibrium with TeO_2, TiO_2 or Te and forms two three-phase triangles (regions Ⅰ and Ⅱ in Fig. 6). At 700°C, titanium oxides of TiO_2, Ti_3O_5 and Ti_2O_3 are compatible with liquid tellurium. The phase region Ⅱ (TiO_2 + Ti_3O_5 + L) may become more complex, since between Ti_3O_5 and TiO_2 there exists a series of discrete phases with Ti_nO_{2n-1} which are called Magneli phases[17]. Hexagonal $\alpha Ti_{2-x}Te_2$ with a range of homogeneity can equilibrate with Ti_2O_3. According to Suzuki and Wahlbeck[16] and Chevreton and his coworkers[11,13], this hexagonal phase is considered to be composed of several distinct subtellurides such as Ti_2Te_3, Ti_4Te_7, $Ti_{10}Te_{19}$ and $TiTe_2$. αTiO forms a two-phase equilibrium with at least three kinds of tellurides: hexagonal $\alpha Ti_{2-x}Te_2$, monoclinic $\beta Ti_{2-x}Te_2$ and Ti_5Te_4. The isothermal section indicates that αTiO is the only oxide which cannot equilibrate with liquid tellurium at 700°C. Mutual solubility of titanium tellurides and αTiO is likely to be small. Tie lines in the region Ⅱ may originate from αTiO on the Ti-O binary edge. The lowest telluride Ti_5Te_4 may have no appreciable homogeneity range. Among the two-phase regions belonging to the isothermal section, the region indicated as Ⅲ (Ti_5Te_4 + αTi(O)) is one with a wide composition range. In this two-phase region, tie lines can be drawn from the nearly stoichiometric Ti_5Te_4 to the αTi(O) solid solutions with oxygen contents of 0 - 33 at%.

3.3. Thermodynamic stability of titanium tellurides

Thermodynamic stability of titanium tellurides in the Ti-Te-O ternary system was assessed mainly on the basis of equilibrium tellurium and oxygen pressures, which can be calculated from the standard Gibbs free energy change at a temperature for the corresponding chemical equilibria, ΔG°_T. If the relationship of ΔG°_T vs temperature for a given reaction is not available in the literature,

the value of ΔG°_T is derived from a sufficiently accurate approximation,

$$\Delta G^\circ_T = \Delta H^\circ_{298} - T\,\Delta S^\circ_{298} \quad (1)$$

where ΔH°_{298} and ΔS°_{298} are the differences in the enthalpies and entropies of formation of the products and reactants at 298 K, and T is the temperature in K. The estimated and reported thermodynamic data were used to evaluate ΔG°_T. Chemical species chosen for calculation are listed in Table 1. Condensed phases chosen for the calculation are twelve solids; titanium oxides and tellurides and elemental titanium, and one liquid; elemental tellurium. Tellurides considered in the calculation were Ti_5Te_4, TiTe, Ti_2Te_3, Ti_4Te_7, $Ti_{10}Te_{19}$ and $TiTe_2$. TiO_2, Ti_3O_5, Ti_2O_3 and TiO were taken as titanium oxides. It was assumed that all the chemical species are stoichiometric and pure. That is to say, their activities are equal to unity. For vapor species, two diatomic gases Te_2 and O_2 were taken into account. Monatomic Te gas was neglected, because of its low partial pressure at 700°C.

Relative stability of titanium tellurides among metal-tellurium binary systems was examined by decomposition vapor pressure of Te_2. The tellurium pressures over Ti_5Te_4, TiTe, Ti_2Te_3, Ti_4Te_7, $Ti_{10}Te_{19}$ and $TiTe_2$ are determined according to the reactions,

$5\ Ti(s) + 2\ Te_2(g) = Ti_5Te_4(s)$,

$2\ Ti_5Te_4(s) + Te_2(g) = 10\ TiTe(s)$, and so on.

The equilibrium tellurium pressure P_{Te2} was evaluated from

$$\Delta G^\circ_T = RT\ \ln(P_{Te2}/P_{Te2}^\circ) \quad (2)$$

where P_{Te2}° = tellurium pressure in the standard state (1.0132×10^5 Pa) and R = gas constant (8.314 J/mol K). The ΔG°_T in eq. (2) is the standard free energy change of reaction per one mole gas of Te_2. The reported data[16,20] of $\Delta H_f^\circ{}_{298}$ and S°_{298} were employed for titanium tellurides, as shown in Table 2. The ΔG°_T equations for relevant reactions evaluated from eq. (1) are given in Table 3. Figure 7 illustrates the decomposition pressures obtained for titanium tellurides. At a temperature of 700°C, Ti_5Te_4, TiTe and Ti_2Te_3 show Te_2 pressures of 9.3×10^{-10}, 2.3×10^{-8} and 7.5×10^{-8} Pa, respectively. This suggests that these compounds are stable even at a high temperature. However, Te-rich tellurides have relatively higher Te_2 pressures: 7.4 Pa for $Ti_{10}Te_{19}$ and 164 Pa for $TiTe_2$.

The equilibrium partial pressures of Te_2 over tellurides were also calculated for fission products (La, Ce, Nd, Cs, Ba, Sr, Mo and Pd) and cladding constituents

(Fe, Ni and Cr) to clarify the relative stability of titanium telluride in the LMFBR system. For each metal, the tellurides stable at 700°C were surveyed in the literature[25,26], and the metal-richest telluride in the binary system was selected for the calculation (for instance, LaTe among four lanthanum tellurides of LaTe, La_3Te_4, $LaTe_2$ and $LaTe_3$). Thermodynamic properties of Pd_4Te and CrTe estimated by the author were used for calculating P_{Te_2}. As shown in Table 3, linear equations for the free energy changes for the tellurides were organized by the author using the literature data[25,27,28-30]. The equilibrium pressures of Te_2 over the tellurides are shown in Fig. 7. Among the constituents of stainless steel cladding, the most stable telluride is considered to be CrTe. Titanium tellurides such as Ti_5Te_4, TiTe and Ti_2Te_3 indicate lower tellurium pressures than cladding components. The tellurides for lanthanide (La, Ce and Nd) and alkali and alkaline earth metals (Cs, Ba and Sr) may be more stable, with respect to titanium. The remaining elements form less stable tellurides rather than the titanium tellurides. These lanthanides form much stable oxides under normal conditions within LMFBR fuel pins. Alkali metals may be in the gas phase instead of condensed phases, and this brings about less stability of their tellurides. Titanium tellurides may therefore become to be comparatively stable in LMFBR fuel pins under a certain condition. For an oxidizing situation, noble metals such as Pd might tie up much of tellurium.

The stability diagram at 700°C was calculated for the Ti-Te-O ternary system to estimate the chemical stability of titanium telluride as a function of oxygen and tellurium partial pressures and to ascertain the thermodynamic validity of the isothermal section experimentally obtained. Thermodynamic stabilities of the phases present in the Ti-Te-O ternary system can be evaluated from the standard Gibbs free energy changes at 700°C for possible reaction equilibria. From the phase rule there is one degree of freedom in the three-phase region (for example, TiO(s) + TiTe(s) + Ti_2O_3(s)), and setting the temperature fixes the oxygen and tellurium partial pressures. The oxygen pressure in the three-phase region of TiO(s) + TiTe(s) + Ti_2O_3(s) is established by

$$6\ TiTe(s) + O_2(g) = 2\ Ti_2O_3(s) + 2\ TiO(s)$$

and can be calculated from the free energy change of the reaction. The phase rule also offers two degrees of freedom in the two-phase region (e.g., TiO(s) + TiTe(s)). Consequently, the tellurium pressure changes with the oxygen pressure at a given temperature. The dependence of tellurium pressure on oxygen pressure in the TiO(s) + TiTe(s) region can be evaluated from the free energy change of the following reaction:

$$2\ TiTe(s) + O_2(g) = 2\ TiO(s) + Te_2(g).$$

The thermodynamic data in the literature[16,19,20,24] were used to derive the free energy changes for the corresponding equilibria. As no thermodynamic information for $TiTe_3O_8$ was available, the standard enthalpy and entropy of formation were estimated by the author for the calculation. In Table 2, the values of $\Delta H_f^\circ{}_{298}$ and $S^\circ{}_{298}$ are yielded for the relevant compounds and elements.

The stability diagram at 700°C thus obtained is shown in Fig. 8, the coordinates of which are the natural logarithm of the oxygen and tellurium partial pressures, $\ln P_{O_2}$ and $\ln P_{Te_2}$. In this figure, single-phase areas indicate that chemical species are stable under the given conditions. Two phases can coexist along the lines drawn in the diagram and three phases only at the triple points. The line is the allowed variation in oxygen and tellurium pressures required for each equilibrium. At low oxygen pressures, titanium tellurides can be stable. If the oxygen pressure slightly increases, Ti-rich tellurides such as Ti_5Te_4 and TiTe are oxidized to TiO. Ti_2Te_3 can equilibrate with TiO and Ti_2O_3. The Te-rich tellurides such as $Ti_{10}Te_{19}$ and $TiTe_2$ occupy a wider range of partial pressures. Under more oxidizing atmospheres, titanium oxides become stable relative to the tellurides. The double oxide $TiTe_3O_8$ phase field lies between the TiO_2 and TeO_2 regions. The stability diagram indicates the existence of eight three-phase regions including titanium tellurides. The $TiTe_3O_8$ forms two three-phase regions. It should be noted that the phase relationships experimentally obtained in the present study satisfy the thermodynamic restrictions.

These results vividly demonstrate that oxygen reduces the chemical stability of the titanium tellurides. In the fuel-cladding gap of normal operating LMFBR fuel pins, the oxygen potential is controlled by $(U,Pu)O_2$ fuel to be around -400 kJ/mol or more less. This value is not low enough to allow the formation of titanium tellurides even at a Te_2 pressure of 1 Pa. If the titanium getter itself decreases the oxygen potential in fuel pins, once oxidized, the titanium may pick up tellurium to form titanium tellurides. At extremely high oxygen potentials, $TiTe_3O_8$ becomes the predominant tellurium containing species. Although the present conclusion might not strictly be applied to a complete chemical behavior of titanium in LMFBR fuel pins, knowledge of the Ti-Te-O phase relationships can provide a foundation for the understanding of the complex chemistry of interaction between the titanium getter and the fission products.

4. Conclusions

The phase relations in the Ti-Te-O ternary system have been studied at 700°C,

and the isothermal section of the Ti-Te-O system was proposed. The three kinds of tellurides, Ti_5Te_4, monoclinic $\beta Ti_{2-x}Te_2$ and hexagonal $\alpha Ti_{2-x}Te_2$ were confirmed to be stable at 700°C in the Ti-Te binary system. These compounds formed equilibrium phase regions with αTiO and Ti_2O_3. Solubility of oxygen in these tellurides may be quite low. The ternary compound $TiTe_3O_8$ was found to exist on the TiO_2-TeO_2 join in the isothermal section.

Titanium tellurides were expected from the dissociation vapor pressure of Te_2 to be relatively stable compounds themselves in comparison with other tellurides of fission products and cladding constituents.

The stability diagram for the Ti-Te-O system at 700°C was constructed using $\ln P_{O_2}$ and $\ln P_{Te_2}$ as variables. It was verified from the calculated diagram that at low oxygen partial pressures tellurides exist in the ternary system but that the stable compound changes from tellurides to oxides under a more oxidizing atmosphere. In the range of high oxygen potentials, the tellurium pressure may be lowered by consumption in forming $TiTe_3O_8$ instead of the simple oxides. Phase relations predicted from the stability diagram were almost identical with the experimental isothermal section of the Ti-Te-O ternary system.

In LMFBR fuel pins under normal operating conditions, the titanium getter is unlikely to react with the fission product tellurium. If the titanium getter itself reduces an oxygen potential in a LMFBR fuel pin by absorption of oxygen, tellurium will be entrapped in the getter. In a case that the oxygen potential is sufficiently increased, the ternary compound $TiTe_3O_8$ would be important tellurium-containing species.

References

[1] O. Gotzmann and Ph. Dunner, Summary Report of Technical Committee Meeting on Fuel and Cladding Interaction, (IAEA, Vienna, 1977)p43.
[2] L.A. Lawrence, J.W. Weber and J.L Devary, Proc. Int. Conf. on Fast Breeder Reactor Fuel Performance, (ANS, Illinois, 1979)p432.
[3] W.E. Roake, R.F. Hilbert, M.G. Adamson, S. Lnger, J.W. Weber, R.L. Gibby, E.T. Weber and R.E. Woodley, Summary Report of Technical Committee Meeting on Fuel and Cladding Interaction, (IAEA, Vienna, 1977)p137.
[4] M.G. Adamson, ibid., p108.
[5] R.J. Jackson, R.L. Gibby, R.E. Woodley, J.W. Weber and M.G. Adamson, ibid., p189.
[6] E.T. Weber, L.A. Lawrence, C.N. Wilson and R.L. Gibby, Proc. Int. Conf. on Fast Breeder Reactor Fuel Performance, (ANS, Illinois, 1979)p445.
[7] P. Ehrlich, Z. Anorg. Chem., 260(1949)13.
[8] F.K. McTarget and A.D. Wadsley, Aust. J. Chem., 11(1958)445.
[9] H. Hahn and P. Ness, Z. Anorg. Chem., 302(1959)17.
[10] F. Gronvold, A. Kjekshus and F. Raaum, Acta Crystall., 14(1961)930.
[11] M. Chevreton and F. Bertaut, Compt. Rend., 225(1962)1275.
[12] F. Raaum, F. Gronvold, A. Kjekshus and H. Haraldsen, Z. Anorg. Chem.,

317(1962)91.
[13] S. Brunie and M. Chevreton, Mat. Res. Bull., 3(1968)309.
[14] H.P.B. Rimmington and A.A. Balchin, J. Crystal Growth, 21(1974)171.
[15] Y. Arnaud and M. Chevreton, J. Solid State Chem., 39(1981)230.
[16] A. Suzuki and P.G. Wahlbeck, J. Phys. Chem., 70(1966)1914.
[17] J.L. Murray, Phase Diagrams of Binary Titanium Alloys, (ASM, Ohio, 1987).
[18] G.V. Samsonov, The Oxide Handbook, 2nd Ed., (Plenum Press, New York, 1981).
[19] O. Kubaschewski and C.B. Alcock, Metallurgical Thermochemistry, 5th Ed., (Pergamon Press, New York, 1979).
[20] K.L. Komarek, Titanium: Physico-Chemical Properties of Its Compounds and Alloys, (IAEA, Vienna, 1983).
[21] P.G. Meunier and J. Galy, Acta Crystall., 27(1971)602.
[22] M.U. Cohen, Rev. Sci. Instr., 6(1935)68.
[23] P. Cherin and P. Unger, Acta Crystall., 23 (1967)679.
[24] R.M. Goldhoff, H.L. Shaw, C.M. Craighead and R.I. Jaffee, Trans. ASM, 45(1953)941.
[25] K.C. Mills, Thermodynamic Data for Inorganic Sulphide, Selenides, and Tellurides, (Butterworth, London, 1971).
[26] T.B. Massalski, Binary Alloy Phase Diagrams, (ASM, Ohio, 1986).
[27] P.E. Blackburn and C.E. Johnson, ANL-82-42, (1982).
[28] P.A.G. O'Hare, J. Chem. Thermodynamics., 19(1987)675.
[29] E.H.P. Cordfunke, W. Ouweltjes, J.C. Van Miltenburg and A. Schuijff, ibid., 19(1987)293.
[30] E.H.P. Cordfunke and W. Ouweltjes, ibid., 19(1987)377.

Table 1 Chemical species chosen for the calculation.

Ⅰ)	Condensed Phases	
	Solid:	Ti_5Te_4, TiTe, Ti_2Te_3, Ti_4Te_7, $Ti_{10}Te_{19}$, $TiTe_2$
		TiO, Ti_2O_3, Ti_3O_5, TiO_2, TeO_2, $TiTe_3O_8$
		Ti
	Liquid:	Te
Ⅱ)	Vapor Species	
	Diatomic gas:	O_2, Te_2

Table 2 Thermodynamic properties of chemical species related to the Ti-Te-O ternary system[16,19,20].

Chemical Species	$\Delta H_f^\circ{}_{298}$(kJ/mol)	$S^\circ{}_{298}$(J/mol K)
Ti_5Te_4	-481	379
TiTe	-121	83.7
Ti_2Te_3	-355	207
Ti_4Te_7	-802	440
$Ti_{10}Te_{19}$	-2090	1140
$TiTe_2$	-213	117
TiO	-542.7	34.7
Ti_2O_3	-1521	77.24
Ti_3O_5	-2459	129.4
TiO_2	-944.7	50.33
TeO_2	-323	74.17
$TiTe_3O_8$	-2000*	243*
Ti	--	30.6
Te	--	49.50
O_2	--	205

* Estimated value

Table 3 Linear equation for standard free energy change of telluride formation[25,27,28-30]: ΔG°_{T}(J/mol of Te_2 gas) = A + B T.

Telluride	- A x 10^{-3}	B
Ti_5Te_4	396.7	138.9
TiTe	403.0	172.2
Ti_2Te_3	382.1	160.7
Ti_4Te_7	340.3	222.7
$Ti_{10}Te_{19}$	273.3	201.4
$TiTe_2$	231.5	184.7
$FeTe_{0.9}$	207.7	134.3
$NiTe_{1.1}$	260.3	153.1
CrTe	302.2	123.1
Cs_2Te	887.3	249.7
BaTe	702.6	198.0
SrTe	783.8	180.5
LaTe	758.6	188.9
CeTe	767.5	194.6
NdTe	761.1	205.4
Mo_3Te_4	189.2	106.5
Pd_4Te	230.8	160.2

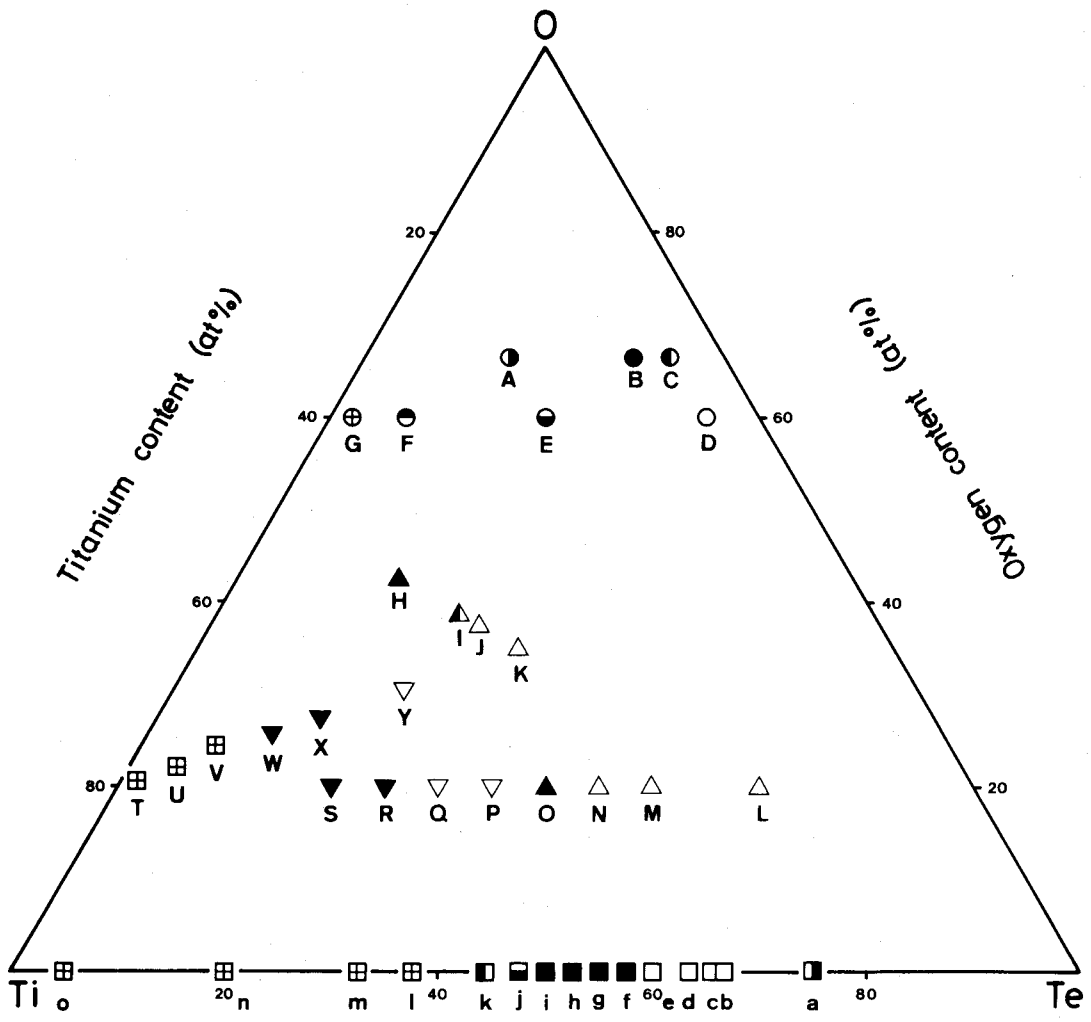

Fig. 1 Phases identified in the samples a - o and A - Y.

- Te + $\alpha Ti_{2-x}Te_2$,
- $\alpha Ti_{2-x}Te_2$,
- $\beta Ti_{2-x}Te_2$,
- $\beta Ti_{2-x}Te_2$ + Ti_5Te_4,
- Ti_5Te_4,
- Ti_5Te_4 + αTi,
- $TiTe_3O_8$ + TiO_2,
- $TiTe_3O_8$,
- $TiTe_3O_8$ + TeO_2,
- $TiTe_3O_8$ + TeO_2 + Te,
- $TiTe_3O_8$ + TiO_2 + Te,
- Ti_nO_{2n-1}? + Te,
- Ti_3O_5 + Ti_2O_3 + Te,
- Ti_2O_3 + Te + $\alpha Ti_{2-x}Te_2$,
- Ti_2O_3 + $\alpha Ti_{2-x}Te_2$,
- Ti_2O_3 + $\alpha Ti_{2-x}Te_2$ + αTiO,
- αTiO + $\beta Ti_{2-x}Te_2$,
- αTiO + Ti_5Te_4 + αTi.

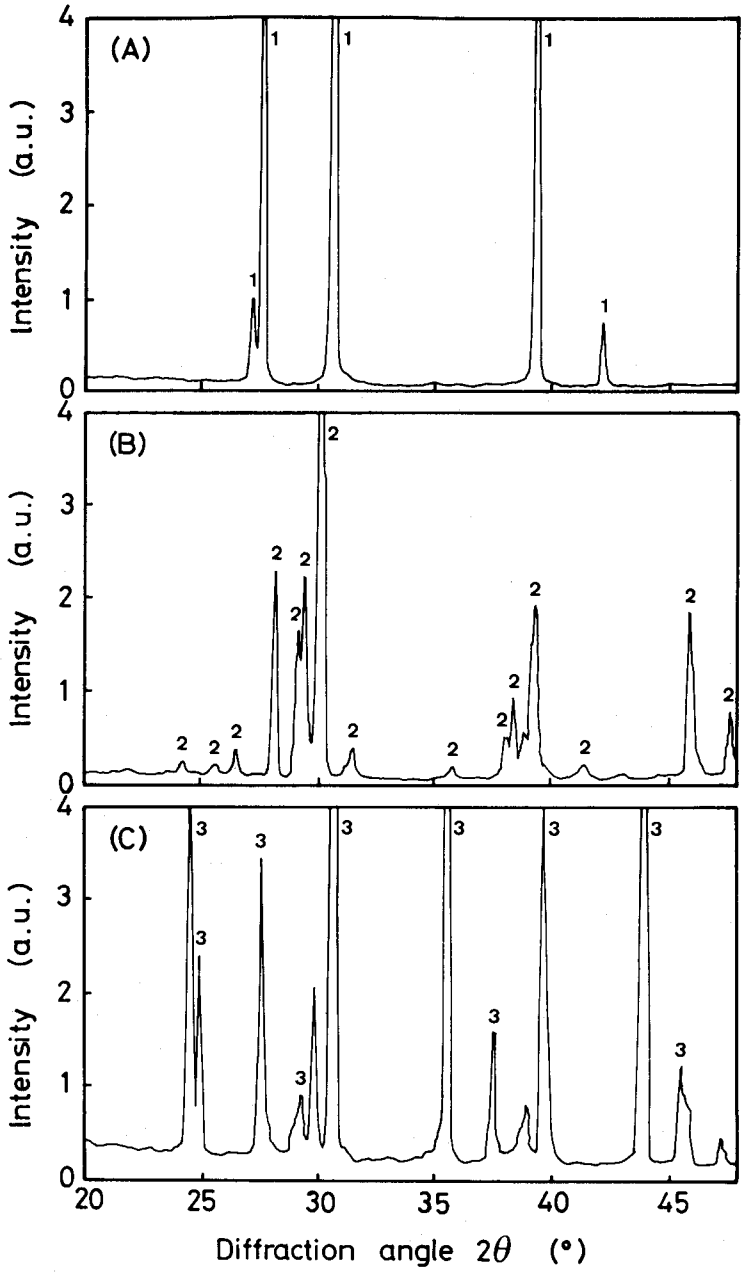

Fig. 2 X-ray diffraction patterns of the reaction products.
(A) sample c, (B) sample f, (C) sample k.
1: $\alpha Ti_{2-x}Te_2$, 2: $\beta Ti_{2-x}Te_2$, 3: Ti_5Te_4.

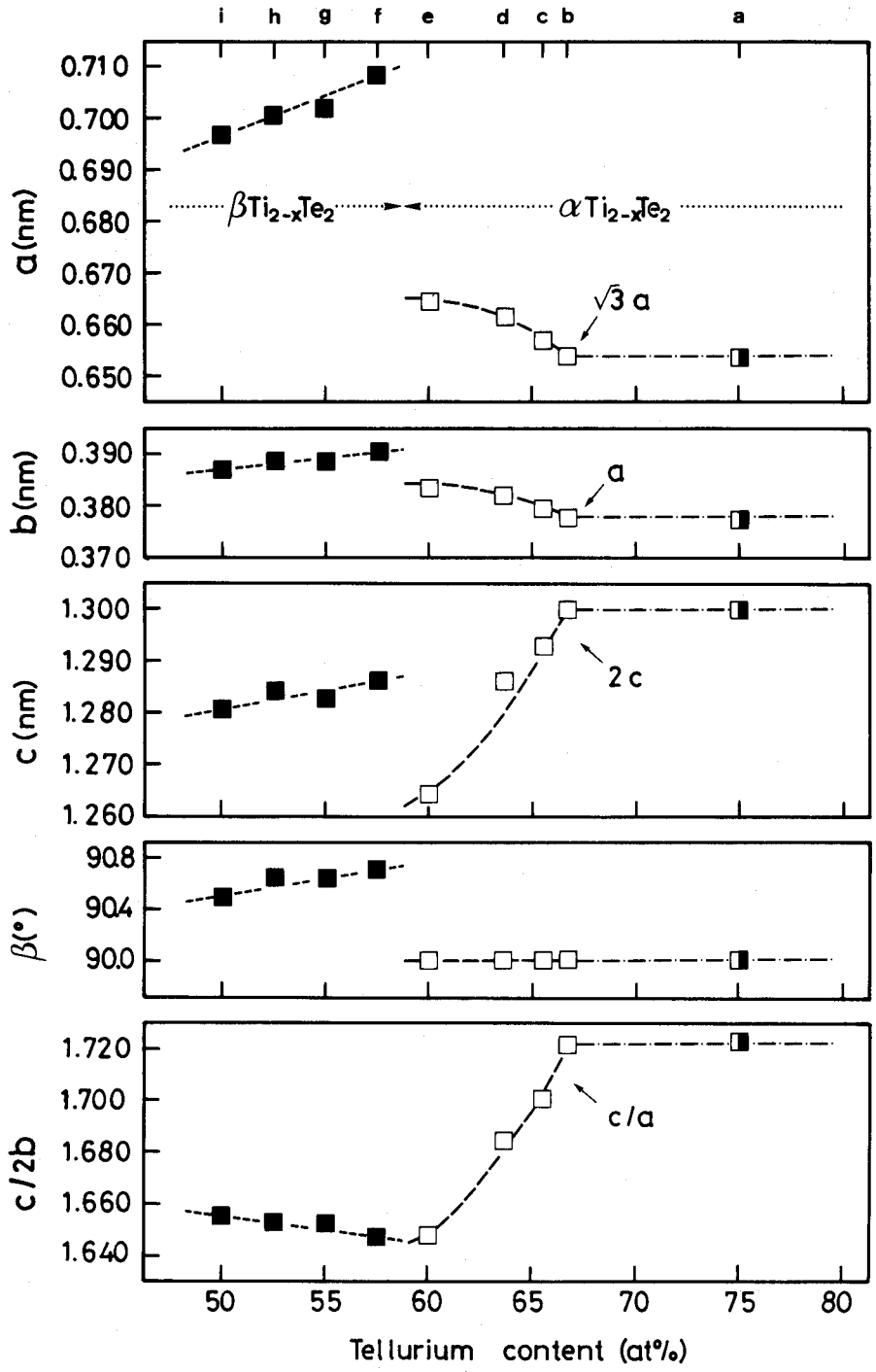

Fig. 3 Change in the lattice parameters and the axial ratio of monoclinic and hexagonal $Ti_{2-x}Te_2$ with tellurium content.

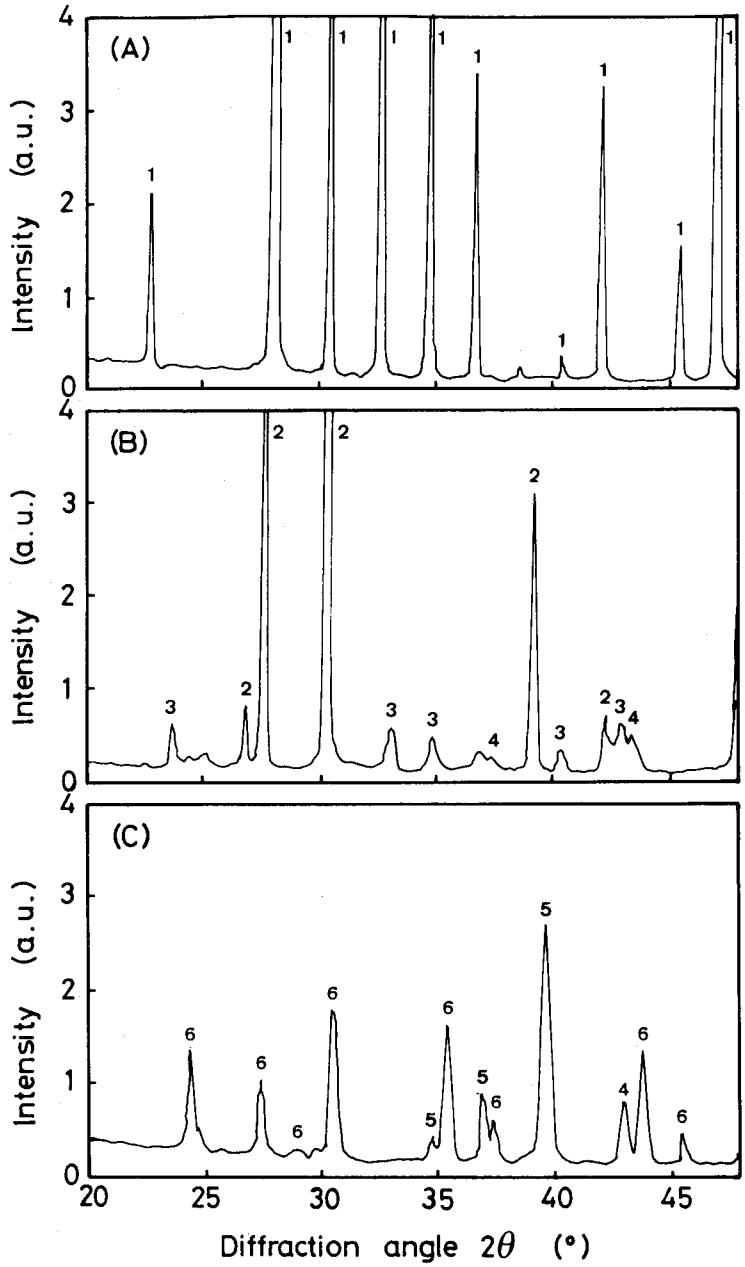

Fig. 4 X-ray diffraction patterns of the reaction products.
(A) sample B, (B) sample H, (C) sample W.
1: $TiTe_3O_8$, 2: $\alpha Ti_{2-x}Te_2$, 3: Ti_2O_3, 4: αTiO, 5: αTi, 6: Ti_5Te_4.

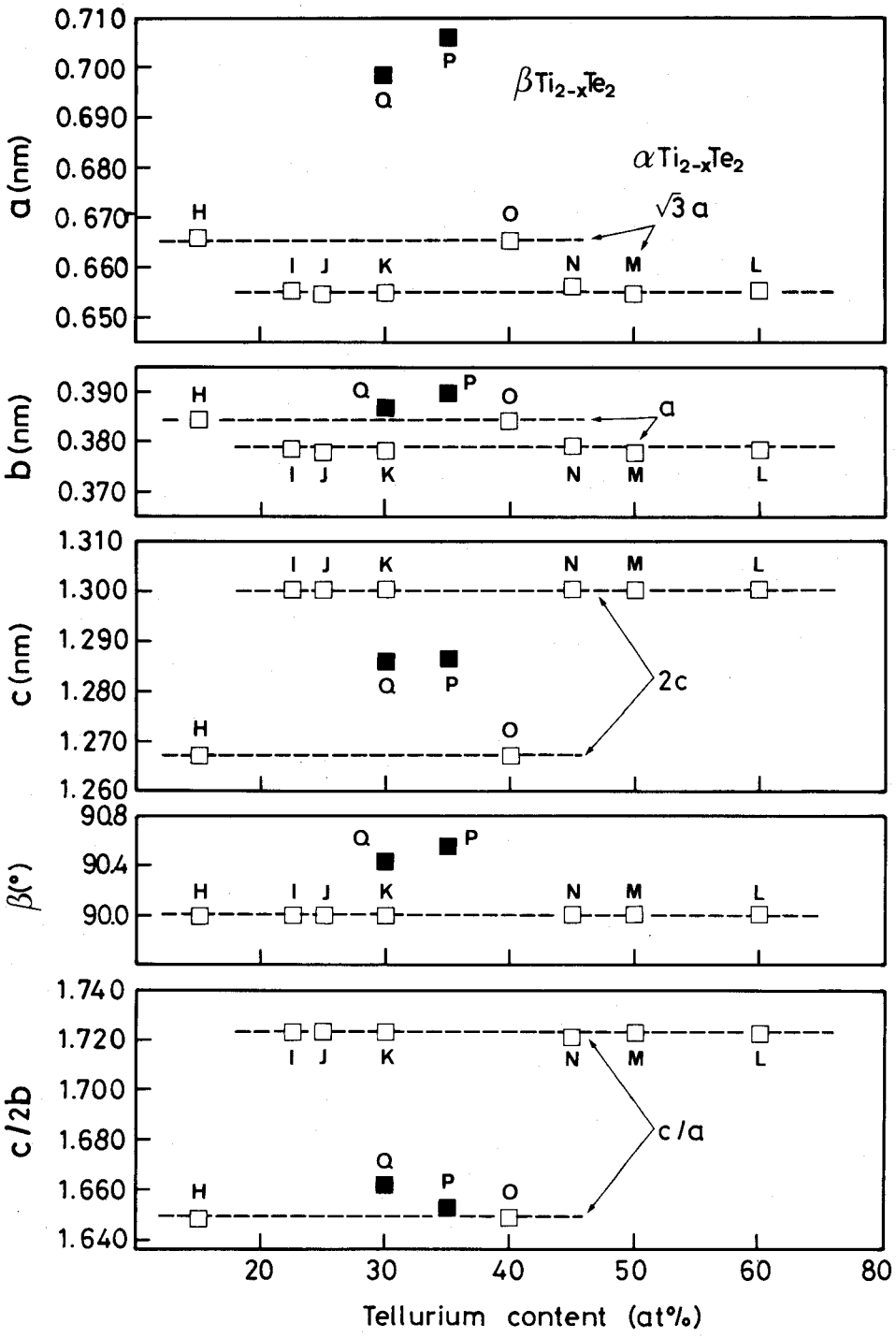

Fig. 5 Change in the lattice parameters and the axial ratio of monoclinic and hexagonal $Ti_{2-x}Te_2$ coexisting with titanium oxide with tellurium content.

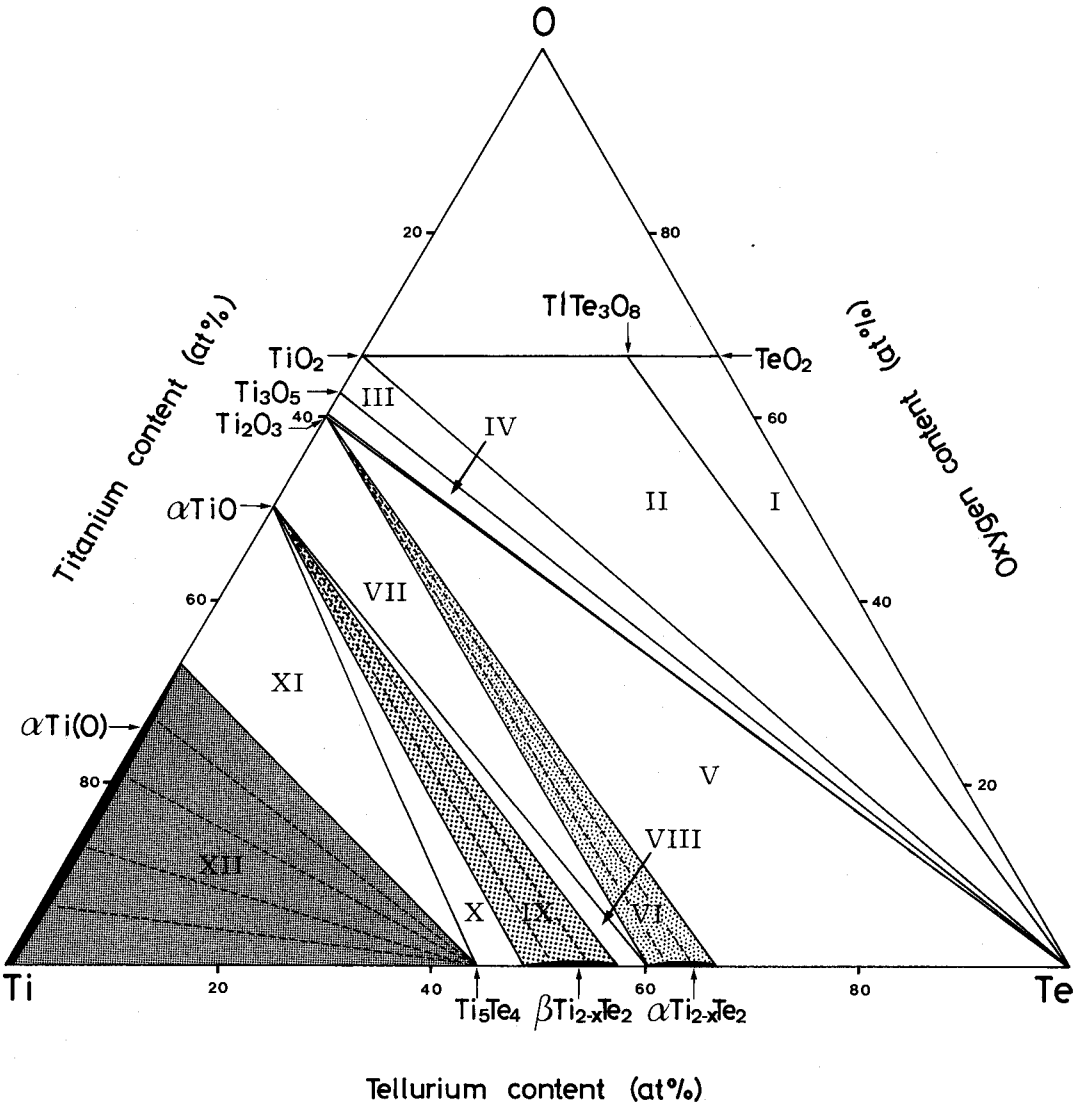

Fig. 6 Isothermal section of the Ti-Te-O ternary system at 700°C.

I $TiTe_3O_8 + TeO_2 + L$,
II $TiTe_3O_8 + TiO_2 + L$,
III $TiO_2 + Ti_3O_5 + L$,
IV $Ti_3O_5 + Ti_2O_3 + L$,
V $Ti_2O_3 + L + \alpha Ti_{2-x}Te_2$,
VI $Ti_2O_3 + \alpha Ti_{2-x}Te_2$,
VII $Ti_2O_3 + \alpha Ti_{2-x}Te_2 + \alpha TiO$,
VIII $\alpha Ti_{2-x}Te_2 + \alpha TiO + \beta Ti_{2-x}Te_2$,
IX $\alpha TiO + \beta Ti_{2-x}Te_2$,
X $\alpha TiO + \beta Ti_{2-x}Te_2 + Ti_5Te_4$,
XI $\alpha TiO + Ti_5Te_4 + \alpha Ti(O)$,
XII $Ti_5Te_4 + \alpha Ti(O)$.

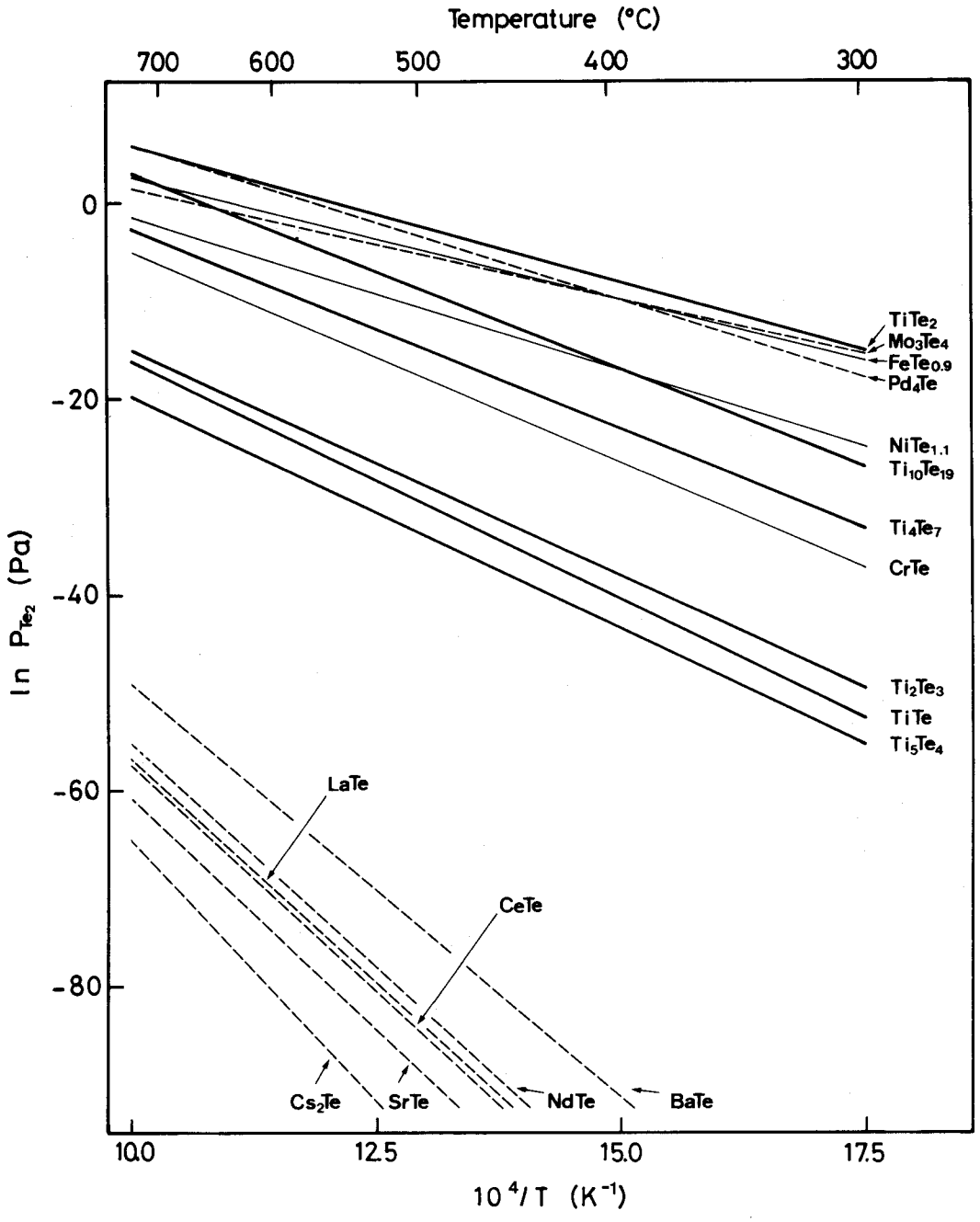

Fig. 7 Decomposition vapor pressures of tellurium in metal-tellurium binary systems.

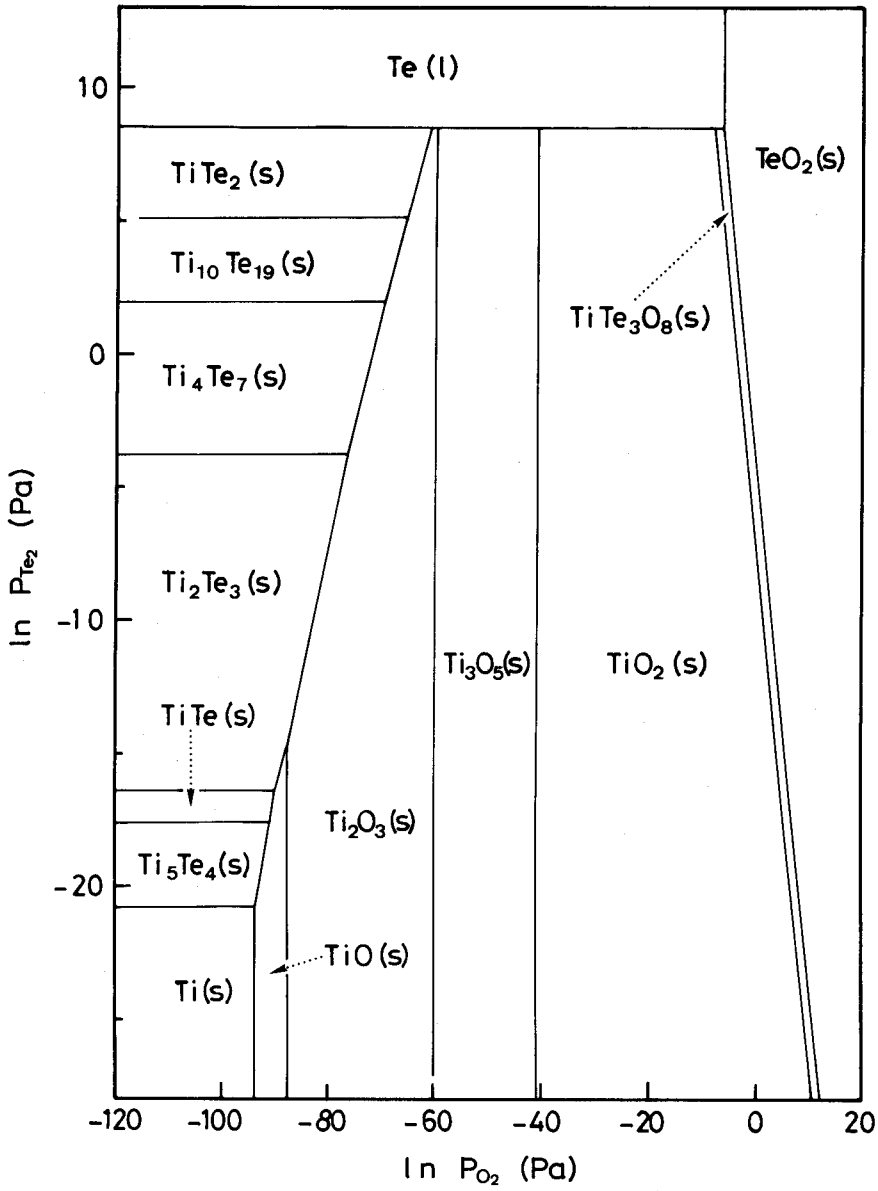

Fig. 8 Stability diagram for the Ti-Te-O ternary system at 700°C.

CHAPTER 5 ZIRCONIUM-TELLURIUM-OXYGEN TERNARY SYSTEM

1. Introduction

The fission product tellurium has a possibility of radiological hazards in a hypothetical accident of light water reactors (LWRs) because of its high volatility. In normally operating fuel rods, the chemical form of tellurium is likely to be tellurides such as Cs_2Te[1-3]. The amount of tellurium released from a failed fuel rod into mixtures of steam and hydrogen depends upon the state of the degraded core, but the dominant volatile species will be elemental tellurium and hydrogen telluride[1,2,4]. It has recently been suggested that oxidation of Zircaloy cladding might play a crucial role in the tellurium release[5]. Interaction of tellurium with zirconium in the cladding to form zirconium tellurides is important for predicting the release of the tellurium species.

The structural studies for zirconium tellurides have been carried out by several investigators[6-12]. There exist five different compounds, Zr_5Te_4, ZrTe, $ZrTe_2$, $ZrTe_3$ and $ZrTe_5$, in the partial phase diagram of Zr-Te binary system[13]. Thermodynamic properties have been measured only for $ZrTe_2$[14]. The data on the phase diagrams of Zr-O and Te-O binary systems have been collected and assessed in the handbooks of Masalski[15] and Samsonov[16]. However, only insufficient information is available from them for the phase relations in Zr-Te-O ternary system, except for the existence of a double oxide $ZrTe_3O_8$, which can be thought as being composed of ZrO_2 and TeO_2[17].

Knowledge of phase equilibria in the multicomponent system including tellurium, zirconium and oxygen is required to elucidate tellurium behavior under an oxidizing atmosphere. The phase relations in the Zr-Te-O ternary system are of great importance as a basis for the prediction of tellurium behavior under hypothetical LWR accident conditions. The present study has therefore been performed on the ternary system at 700°C with the aid of X-ray diffraction technique. Thermodynamic properties such as standard enthalpy of formation and standard entropy were estimated for some compounds related to the Zr-Te-O ternary system. On the basis of the known and estimated thermodynamic data, phase stability diagrams and temperature dependence of oxygen potential were examined to assess the thermodynamic stability of zirconium tellurides.

2. Experimental

Starting materials were powders of Zr (purity, 99.9 wt%), ZrO_2 (purity, 99.9

wt%), Te (purity, 99.99 wt%) and TeO_2 (purity, 99.99 wt%). Zirconium-oxygen solid solution (αZr(O)) powders of 10 - 29 at%O were also used, which were prepared by vacuum annealing of Zr and ZrO_2 mixtures. These powders were mixed in desired proportions and then pelletized. The compacts were sealed into silica tubes evacuated to lower than 10^{-3} Pa. An equilibrium heat treatment was made at 700°C for 20 - 240 h, and subsequently the tube was quenched in ice water.

After the heat treatment, the tube was opened in a glove box filled with dry argon, and the sample was powdered immediately before X-ray diffraction analysis for phase identification. Some of the samples were embedded in aluminum holders with epoxy resin in order to avoid oxidation or hydration of zirconium tellurides during the X-ray diffraction measurement. Glass holders were used for the other samples. X-ray powder patterns for all the samples were taken on a diffractometer using Ni-filtered Cu K_α radiation. More detailed conditions for diffraction analysis were the same as given in the preceding chapter. The lattice parameters of identified phases were obtained by applying the Cohen's method[18] to the diffraction intensity data.

3. Results and Discussion

3.1. Phase equilibria in the Zr-Te binary system

The Zr-Te binary system was studied at 700°C to clarify the types of tellurides and their range of homogeneity. The results of phase identification by X-ray diffraction technique are shown in a compositional triangle, as can be seen in Fig. 1. Binary mixtures with tellurium contents ranging from 80 - 20 at% are designated as samples a - m. The tellurides found in the present study were $ZrTe_3$, $Zr_{1+x}Te_2$ and Zr_5Te_4.

The monoclinic $ZrTe_3$ coexisted with Te in sample a and with $Zr_{1+x}Te_2$ in samples c and d. At 75 at%Te (sample b), a single-phase of $ZrTe_3$ was observed in a diffraction pattern (Fig. 2(A)). The lattice parameters of $ZrTe_3$ were found to be a = 0.588 nm, b = 0.393 nm, c = 1.01 nm and β = 97.9° , which were in agreement with the reported value[7,12,13]. Since the values of a, b, c, and β did not vary with composition, $ZrTe_3$ seems to have a narrow composition range. The lattice parameters of hexagonal Te coexisting with $ZrTe_3$ were determined to be a = 0.446 nm and c = 0.593 nm; in agreement with the published data of a = 0.44572 nm and c = 0.59290 nm for pure Te powder[19]. This means that tellurium liquid at 700°C may take a small amount of zirconium into the solution.

In samples c - j, there existed $Zr_{1+x}Te_2$ with hexagonal NiAs like structure. The single-phase $Zr_{1+x}Te_2$ was formed in a wide range of composition from 65 - 54

at%Te (samples e - h). Figure 2(B) is a representative of X-ray diffraction patterns indicating a hexagonal $Zr_{1+x}Te_2$. The change in the lattice parameters a and c and the axial ratio c/a of the $Zr_{1+x}Te_2$ with tellurium content is shown in Fig. 3. As seen in this figure, the values of a, c and c/a decrease with increasing tellurium content. For the samples in which two phases coexisted, the lattice parameters a and c of $Zr_{1+x}Te_2$ were nearly constant. Although the homogeneity region of $Zr_{1+x}Te_2$ between 52 and 66 at%Te slightly differs from those in the literature[9-11], there is a good agreement between the a and c values previously reported and those obtained in the present study.

In Zr-rich samples i - m, Zr_5Te_4 of which the X-ray diffraction pattern(e.g., Fig. 2(C)) can be indexed as a tetragonal structure was contained. This telluride appears to be a stoichiometric compound. Samples l and m consisted of a mixture of Zr_5Te_4 and αZr, indicating that Zr_5Te_4 is the lowest zirconium telluride stable at 700°C.

It was verified that the stable phases in the binary system at 700°C were Te, $ZrTe_3$, $Zr_{1+x}Te_2$, Zr_5Te_4 and αZr. The presence of $ZrTe_3$ at 700°C was confirmed in the present study, though Sodeck et al.[13] had reported that $ZrTe_3$ decomposes peritectically at 630°C to solid $Zr_{1+x}Te_2$ and liquid Te. A series of reaction experiments with various compositions and reaction periods was performed at 700°C where the two phases of $Zr_{1+x}Te_2$ solid and Te liquid would be produced on the basis of the partial phase diagram of Zr-Te binary system[13], but no evidence was found that $Zr_{1+x}Te_2$ coexists with Te at 700°C. At a tellurium content of 75 at%, the product was the single-phase $ZrTe_3$ with no trace of the formation of $Zr_{1+x}Te_2$ or Te, and it can hardly be considered that the $ZrTe_3$ was synthesized from $Zr_{1+x}Te_2$ + Te during the quenching process. Therefore, $ZrTe_3$ appears to be stable up to a higher temperature than 630°C. In the composition range where a stoichiometric ZrTe with WC type structure would comprise a stable phase according to the phase diagram proposed by Sodeck et al.[13], equilibrium assemblage was $Zr_{1+x}Te_2$ + Zr_5Te_4; i.e. this ZrTe phase was not confirmed by the present study. Owing to the similar crystal structures, there were some difficulties in distinguishing NiAs type from WC type crystals. Further examination is needed to make it clear that WC type ZrTe phase is present or not at 700°C.

3.2. Phase equilibria in the Zr-Te-O ternary system

Figure 1 also represents the results of the X-ray diffraction analysis for ternary samples: TeO_2/ZrO_2 mixtures (samples A - C), TeO_2/Zr mixtures (samples L - Q, X), Te/αZr(O)/ZrO_2 mixtures (samples U - W), Te/TeO_2/αZr(O)/ZrO_2 mixtures (samples D - K, R - T) and Te/αZr(O) mixtures (samples n - x).

A double oxide $ZrTe_3O_8$ with a distorted fluorite type structure was the only

one ternary compound occurring in the Zr-Te-O system. X-ray diffraction pattern of $ZrTe_3O_8$ is shown in Fig. 4(A). Samples A - G contained the $ZrTe_3O_8$ as one of the reaction products. For samples A and C whose starting materials were TeO_2/ZrO_2 mixtures, monoclinic αZrO_2 or TeO_2 in addition to $ZrTe_3O_8$ was detected, but sample B (mole ratio of TeO_2 to ZrO_2 = 3/1) was composed of only $ZrTe_3O_8$. Thus, αZrO_2 was not compatible with TeO_2 at 700°C. The X-ray diffraction patterns of samples D - G exhibited the existence of two or three phases including $ZrTe_3O_8$ and Te. It is obvious from the results for ZrO_2-TeO_2-Te region that the double oxide $ZrTe_3O_8$ is able to coexist with Te, TeO_2 or αZrO_2. The lattice parameter of a = 1.133 nm for $ZrTe_3O_8$ in the samples A - G was independent of composition. The value obtained was close to a= 1.1308 nm evaluated by Meunier and Galy[17]. This may imply that $ZrTe_3O_8$ is stoichiometric.

It is seen from Fig. 1 that monoclinic αZrO_2 is identified over a wide range of composition (samples H - W and n - x). In addition to Te and αZr, zirconium tellurides such as $ZrTe_3$, $Zr_{1+x}Te_2$ and Zr_5Te_4 were found together with αZrO_2. The lattice parameters of αZrO_2 in these samples were almost the same and close to the literature values of baddeleyite ZrO_2[20], irrespective of the type of the coexisting phases. Therefore, the homogeneity range of αZrO_2 is presumed to be very small. Sample H was found to contain αZrO_2 and Te. In samples I, L, V, W, o and n, both αZrO_2 and $ZrTe_3$ existed with Te or $Zr_{1+x}Te_2$, as can be seen in the diffraction pattern (Fig. 4(B)). There was no marked difference in the lattice parameters of $ZrTe_3$ for these samples, and the values were almost the same as those for the single-phase $ZrTe_3$. Presumably only a small amount of oxygen can be incorporated into the $ZrTe_3$ lattice. Two phases (αZrO_2 and $Zr_{1+x}Te_2$) were observed in samples M, T, U and p - w.

In Fig. 5, the lattice parameters of $Zr_{1+x}Te_2$ coexisting with αZrO_2 are indicated as a function of gross tellurium content of ternary sample. The values of a and c for $Zr_{1+x}Te_2$ were larger for one group of samples t - w than for another group of samples p - s. In each group, a and c axes gradually decreased as the tellurium content of the sample increased. The variation in lattice parameters with sample composition is indicative of the range of composition in the $Zr_{1+x}Te_2$. On the assumption that oxygen solubility in $Zr_{1+x}Te_2$ is quite small and that the dissolved oxygen does not influence the lattice expansion of $Zr_{1+x}Te_2$, the tellurium content in $Zr_{1+x}Te_2$ for the ternary samples can be estimated from the lattice parameters a and c using the relationship between tellurium content and lattice parameters for the binary samples (Fig. 3). The values of a and c shown in Fig. 5 indicate that the tellurium contents are about 65 at% for the samples p - s and 56 - 60 at% for the samples t - w.

The X-ray diffraction analysis indicated that Zr_5Te_4 was found together with αZrO_2 and $Zr_{1+x}Te_2$ in samples J, N and x and together with αZrO_2 and αZr in

samples K and O - S. The typical result is given in Fig. 4(C). For sample X, the reaction products were αZr and Zr_5Te_4, whereas no formation of ZrO_2 was observed. It can be concluded that Zr_5Te_4 is the only one telluride which can coexist with αZr(O) solid solutions with various oxygen contents. As tellurium is soluble in hexagonal αZr to an amount less than 1 at% [8], low solubility of tellurium might be anticipated for the αZr(O) solid solution.

The existence of Te was confirmed in tenary samples D - I, W and n, as indicated in Fig. 1. The lattice parameters of Te in these samples are the same unaffected by the composition of the sample and in accord with the literature data[19] for pure Te. Tellurium, which is liquid at 700℃, is expected to dissolve little oxygen and zirconium into the solution. This prediction conforms to the binary phase diagrams of Te-TeO_2[16] and Zr-Te[13].

Figure 6 illustrates the isothermal section of the Zr-Te-O ternary system at 700°C, which was constructed on the basis of phase identification and lattice parameter determination. At 700°C, a liquid phase, L in Fig. 6, is consisted mainly of tellurium. The Zr-Te-O system is characterized by the formation of a ternary compound $ZrTe_3O_8$ with a stoichiometric composition. In the ZrO_2-TeO_2-Te region, $ZrTe_3O_8$ forms one of the apices of two three-phase triangles (regions Ⅰ and Ⅱ in Fig. 6). Another feature of the isothermal section is that αZrO_2 can be in two-phase equilibrium with all the existing phases other than TeO_2. The three tellurides stable in the Zr-Te binary system, namely $ZrTe_3$, $Zr_{1+x}Te_2$ and Zr_5Te_4, coexisted with αZrO_2. The $ZrTe_3$ and Zr_5Te_4 phases may have no appreciable range of homogeneity, whilst the $Zr_{1+x}Te_2$ phase in equilibrium with αZrO_2 may have a tellurium content from 52 to 66 at%. Among two-phase regions belonging to the isothermal section, regions Ⅴ (αZrO_2 + $Zr_{1+x}Te_2$) and Ⅶ (Zr_5Te_4 + αZr(O)) showed a wide composition range. As demonstrated in Fig. 6, conjugate phases are fixed by a tie line in these two-phase regions. It is recognized from the constancy of αZrO_2 unit cell dimensions amongst various samples that tie lines originate from ZrO_2 on the binary Zr-O edge. The compositions of $Zr_{1+x}Te_2$ in samples p - w estimated from these tie lines are consistent with the results obtained by comparing Fig. 5 with Fig. 3. Tie lines can be drawn between nearly stoichiometric Zr_5Te_4 and αZr(O) having an oxygen content of 0 - 29 at%. The mutual solubility of αZrO_2 and zirconium tellurides is likely to be negligibly small.

3.3. Thermodynamic stability of zirconium tellurides

A particular attention has been paid to the chemical stability of zirconium telluride under various partial pressures of oxygen and tellurium. A phase stability diagram was calculated for the Zr-Te-O ternary system to ascertain the

thermodynamic validity of the isothermal section of the ternary system experimentally obtained.

The Zr-Te binary system is complex, and there are five different compounds, Zr_5Te_4, ZrTe, $ZrTe_2$, $ZrTe_3$ and $ZrTe_5$, in the phase diagram[13]. In the present study, three of them were observed at 700°C. Experimental measurements of thermodynamic properties have been made only for $ZrTe_2$[14]. In the Zr-Te-O ternary system, there are three oxides. Thermodynamic information is available for ZrO_2 and TeO_2[20]. A double oxide $ZrTe_3O_8$ has been previously characterized by X-ray diffraction[17], and the author also found the existence of the double oxide at 700°C. Thermodynamic data for the $ZrTe_3O_8$ double oxide have not yet been reported.

In the present study, Zr_5Te_4, $ZrTe_2$ and $ZrTe_3$ were selected as zirconium tellurides, and their chemical stability and phase equilibria in the Zr-Te-O ternary system were examined. The double oxide $ZrTe_3O_8$ is also expected to be a likely compound formed under oxidizing conditions, and it was employed as a relevant oxide in addition to ZrO_2 and TeO_2. Chemical species chosen for estimation of thermodynamic stability are listed in Table 1. Condensed phases consist of eight solids and one liquid. It is assumed that the condensed species are pure and the activities are equal to unity. For vapor species, two diatomic gases, Te_2 and O_2, were taken into account. Monatomic Te was neglected, because the partial pressure of monatomic Te is much lower than that of Te_2 in the temperature range for the present study.

To determine the equilibria in the Zr-Te-O system, the value of standard free energy change ΔG°_T for each equilibrium is needed, as described in the preceding chapter. Values such as free energy, enthalpy and entropy for the relevant species were obtained from the literature[14,20,21,22,23]. However, the measured values for evaluating ΔG°_T were not available for some of oxides and tellurides considered here. Therefore, the author first has to estimate the standard enthalpy of formation at 298 K, $\Delta H_f^\circ{}_{298}$ and the standard entropy at 298 K, S°_{298} for the compounds. The following methods of estimating $\Delta H_f^\circ{}_{298}$ and S°_{298} have been used for Zr_5Te_4, $ZrTe_2$, $ZrTe_3$ and $ZrTe_3O_8$.

Kubaschewski[20] has described several methods for estimating unknown enthalpy of formation, $\Delta H_f^\circ{}_{298}$ and suggested that a graphical method is one of useful techniques. A relationship generally holds between $\Delta H_f^\circ{}_{298}$ values for two groups of compounds having chemical similarities each other. The resulting correlation between the two allows to estimate the unknown $\Delta H_f^\circ{}_{298}$ value. Mills[23] has correlated known $\Delta H_f^\circ{}_{298}$ for metal tellurides versus those for metal sulphides. In the present study, the relation of $\Delta H_f^\circ{}_{298}$ for tellurides with those for sulphides was reexamined using the values available in the past 15 years, and the values for $ZrTe_2$ and $ZrTe_3$ were estimated from the literature data

of zirconium sulphides.

Figure 7 shows the relationship between standard enthalpies of formation $\Delta H_f^\circ{}_{298}(M_xTe_y)$ and $\Delta H_f^\circ{}_{298}(M_xS_y)$ for metal tellurides and sulphides. The number of compounds shown in this figure was 37 for 28 elements. Plots in Fig. 7 are distinguished by the differences between electronegativity for metal, ε_M, and that for tellurium, $\varepsilon_{Te} = 2.1$: $\Delta\varepsilon = \varepsilon_{Te} - \varepsilon_M$. From Fig. 7, it is apparent that there exists a correlation between $\Delta H_f^\circ{}_{298}(M_xS_y)$ and $\Delta H_f^\circ{}_{298}(M_xTe_y)$, except for the data set of alkali and alkaline earth metals, whose $\Delta\varepsilon$ are larger than 0.9. Tellurides and sulphides for alkali and alkaline earth metals are ionic commpounds and their chemical properties are different from those for other metals. The strong ionic nature of the compounds may result in the deviations from the correlation. For the group of metals such as Ni and Cu whose electronegativities are close to the value of tellurium ($\Delta\varepsilon \leq 0.3$), both $\Delta H_f^\circ{}_{298}(M_xS_y)$ and $\Delta H_f^\circ{}_{298}(M_xTe_y)$ are rather small, but there seems to be a good correlation between $\Delta H_f^\circ{}_{298}(M_xS_y)$ and $\Delta H_f^\circ{}_{298}(M_xTe_y)$ for metals with $\Delta\varepsilon \leq 0.8$. The linear relationship between standard enthalpies of formation for sulphides and tellurides was obtained as follows:

$$\Delta H_f^\circ{}_{298}(M_xTe_y) = 0.540 \times \Delta H_f^\circ{}_{298}(M_xS_y). \quad (1)$$

$\Delta H_f^\circ{}_{298}(ZrTe_2) = -312$ kJ/mol and $\Delta H_f^\circ{}_{298}(ZrTe_3) = -339$ kJ/mol were estimated by comparison with the values for ZrS_2 and ZrS_3 and the above relation.

As no information on the enthalpy of formation was available for Zr_5S_4 type sulphide, $\Delta H_f^\circ{}_{298}(Zr_5Te_4)$ could not be estimated by the same manner. If two elements form several compounds of different compositions, certain fairly general relationships between their enthalpies of formation are known to exist[20]. Figure 8 shows the same regularities between the enthalpy of formation and the composition in chalcogen/metal atom ratio (A/M) for the chalcogenides of the elements in the fourth group of the periodic table. The enthalpy of formation for Zr_5Te_4 can be estimated from this figure to be -732 kJ/mole.

The enthalpy of formation for double oxide $ZrTe_3O_8$ cannot be determined by the analogous approach. Double oxides containing titanium, zirconium or hafnium possess small and negative enthalpies of formation from the constituent oxides, $\Delta H_f^\circ{}_{298,ox}$[20,21,24,25]. The values of $\Delta H_f^\circ{}_{298,ox}$ fell within the limits from -20 to -150 kJ/mol, if alkali and alkaline earth double oxides were excluded. The standard enthalpy of formation from the elements, $\Delta H_f^\circ{}_{298}(ZrTe_3O_8)$, may be -2090 to -2220 kJ/mol.

Consequently, these procedures led to estimation of $\Delta H_f^\circ{}_{298}$ values given in Table 2. The estimated value for $ZrTe_2$ was reasonably consistent with $\Delta H_f^\circ{}_{298}(ZrTe_2)$ of -294.1 kJ/mol reported by Johnson et al.[14]. This suggests

that the estimated $\Delta H_f^\circ{}_{298}$ values for zirconium tellurides may be close to the real values.

For estimation of standard entropies of ionic compounds, $S^\circ{}_{298}$, Latimer has developed a method[20]. The value of $S^\circ{}_{298}$ can be yielded additively from the data found empirically for the cationic and anionic constituents. However, it is also known for compounds with less ionic nature the Latimer additive method provides larger entropy than the real value. In the present case zirconium tellurides may have less ionic nature, and hence the Latimer method was not adopted for Zr_5Te_4, $ZrTe_2$ and $ZrTe_3$. Whereas, $ZrTe_3O_8$ is inferred to be an ionic compound and its value of $S^\circ{}_{298}$ was found from the Latimer method to be 252 J/mol K. In the calculation, entropy contribution due to ion mixing was neglected.

Another common method for evaluating entropy is based on the calculation of the average entropy of formation from the elements, $\Delta S^\circ{}_{298}$, of compounds possessing chemical similarities to the compounds of interest[20,26]. The average value can be used to predict the unknown $S^\circ{}_{298}$ value. An analysis of the entropy change has been performed for reactions involving one gaseous species such as oxygen and sulphur[26]. A similar analysis was applied to telluride formation to obtain the standard entropy, $S^\circ{}_{298}$, of Zr_5Te_4, $ZrTe_2$ and $ZrTe_3$. The entropy changes of the following reaction, $\Delta S^\circ{}_{298}$, were calculated for 47 tellurides of 33 elements,

$$2x/y\ M(c) + Te_2(g) = 2/y\ M_xTe_y(c),$$

where M(c) and $M_xTe_y(c)$ are the condensed phases of metal and telluride, and $Te_2(g)$ diatomic tellurium gas. If the average $\Delta S^\circ{}_{298}$ is obtained, the standard entropy for tellurides, $S^\circ{}_{298}(M_xTe_y)$ would be derived from the equation,

$$S^\circ{}_{298}(M_xTe_y) = y/2\ \Delta S^\circ{}_{298} + y/2\ S^\circ{}_{298}(Te_2) + x\ S^\circ{}_{298}(M), \qquad (2)$$

where $S^\circ{}_{298}(Te_2)$ and $S^\circ{}_{298}(M)$ are the standard entropies of Te_2 gas and metal, respectively. The $\Delta S^\circ{}_{298}$ values of telluride formation for various metals are plotted in Fig. 9. The average value is

$$\Delta S^\circ{}_{298} = -167 \pm 28 \text{ J/mol of } Te_2 \text{ gas K}. \qquad (3)$$

The values of $\Delta S^\circ{}_{298}$ for formation of chalcogenides such as oxide, sulphide, selenide and telluride will be nearly the same, because $\Delta S^\circ{}_{298}$ is governed by contribution of the entropy for the chalcogen gas quite larger than those for the condensed phases. To identify the validity of the average value of $\Delta S^\circ{}_{298}$ for telluride formation, comparison with those for other chalcogenides was made. A

reaction between metal, M, and diatomic chalcogen gas, A_2, to form a chalcogenide, M_xA_y, is written as

$$2x/y\ M(c) + A_2(g) = 2/y\ M_xA_y(c),$$

and the entropy change of the reaction is given by

$$\Delta S^\circ_{298} = 2/y\ S^\circ_{298}(M_xA_y) - S^\circ_{298}(A_2) - 2x/y\ S^\circ_{298}(M), \quad (4)$$

where $S^\circ_{298}(M_xA_y)$ and $S^\circ_{298}(A_2)$ denote the standard entropies of chalcogenide and chalcogen gas, respectively. The average value of ΔS°_{298} for selenide formation was calculated by the author using the S°_{298} values in the literature[20,23], and the avarage values of ΔS°_{298} for oxide and sulphide formation shown in Fig. 10 were the data reported by Swalin[26]. In Fig. 10, the values of ΔS°_{298} are all negative, and there is no marked difference in the magnitude among chalcogens as expected. Though the average ΔS°_{298} value thus obtained for telluride formation shows slightly greater deviation than those for O_2 and S_2, it is considered to enable us to estimate the unknown S°_{298} value. For ΔS°_{298} value of -167 J/mol of Te_2 gas K, the standard entropies are 378 J/mol K for Zr_5Te_4, 130 J/mol K for $ZrTe_2$ and 172 J/mol K for $ZrTe_3$.

The estimated entropy data are summarized in Table 2. The value of S°_{298} obtained for $ZrTe_2$ agrees with the reported value of 124.24 J/mol K. Judging from this consistency, the estimated S°_{298} values for Zr_5Te_4 and $ZrTe_3$ are presumed not to be far from the real values.

The thermodynamic stability of the phase present in the Zr-Te-O ternary system was assessed mainly on the basis of equilibrium tellurium and oxygen pressures, which can be calculated from the standard Gibbs free energy change at a temperature for the corresponding chemical equilibrium, ΔG°_T. The estimated and reported thermodynamic data were used to evaluate ΔG°_T. The oxygen potential, $\Delta \bar{G}_{O_2}$, was also used as one of the fundamental parameters defining chemical stability of compounds, and expressed by

$$\Delta \bar{G}_{O_2} = RT\ \ln(P_{O_2}/P_{O_2}{}^\circ), \quad (5)$$

where R = gas constant (8.314 J/mol K), P_{O_2} = oxygen partial pressure (Pa), and $P_{O_2}{}^\circ$ = oxygen pressure in the standard state (1.0132×10^5 Pa). Calculation for the thermodynamic stability was made at temperatures from 300 to 700°C.

Relative stability of zirconium tellurides among metal-tellurium binary systems was examined by decomposition vapor pressure of Te_2, as indicated in Fig. 11. The tellurium pressure over Zr_5Te_4, $ZrTe_2$ and $ZrTe_3$ are determined according

to the reactions,

$$5\ Zr(s) + 2\ Te_2(g) = Zr_5Te_4(s),$$
$$Zr_5Te_4(s) + 3\ Te_2(g) = 5\ ZrTe_2(s) \text{ and}$$
$$2\ ZrTe_2(s) + Te_2(g) = 2\ ZrTe_3(s).$$

The $\Delta H_f^\circ{}_{298}$ and $S^\circ{}_{298}$ values for Zr_5Te_4 and $ZrTe_3$ estimated in the present study were used to calculate the tellurium pressure, but the reported data were employed for $ZrTe_2$[14]. At a temperature of 700°C, Zr_5Te_4 and $ZrTe_2$ show Te_2 pressures of 2.1×10^{-15} and 2.1×10^{-8} Pa, respectively. This suggests that these compounds are stable even at a high temperature.

The equilibrium partial pressures of Te_2 over tellurides were also calculated for fission products (La, Ce, Nd, Cs, Ba, Sr, Mo, Pd and Ru), cladding constituents (Fe and Sn) and control rod materials (In, Ag and Cd) to clarify the relative stability of zirconium telluride in the LWR system. The results are shown in Fig. 11. Linear equations for the free energy changes were organized for the tellurides, as shown in Table 3. Among the constituents of Zircaloy cladding, the most stable telluride is considered to be Zr_5Te_4. The tellurides for lanthanides such as La, Ce, Nd and alkali and alkali earth metals such as Cs, Ba and Sr may be more stable. The remaining elements form less stable tellurides rather than Zr_5Te_4. If these lanthanides and alkali metals form much stable oxides under normal and accident conditions of LWRs, zirconium tellurides become to be comparatively stable. For an extreme oxidizing situation, much of tellurium and noble metals such as Pd and Ru might be bound together.

The phase stability diagram at 700°C was constructed for the Zr-Te-O ternary system, as shown in Fig. 12. The standard enthalpy of formation for $ZrTe_3O_8$ was taken as -2150 kJ/mol. It is seen from Fig. 12 that at low oxygen partial pressures zirconium tellurides of Zr_5Te_4, $ZrTe_2$ and $ZrTe_3$ can exist, but that these tellurides are oxidized to ZrO_2 if the pressure slightly increases. The ZrO_2 phase is stable in a wide range of oxygen and tellurium partial pressures. Under a more oxidizing atmosphere, the double oxide $ZrTe_3O_8$ may become stable. The $ZrTe_3O_8$ appears in the case of $\Delta H_f^\circ{}_{298} = -2150$ kJ/mol, however if $\Delta H_f^\circ{}_{298} \geq -2100$ kJ/mol, it would be unstable at 700°C and may decompose to ZrO_2 and TeO_2. The calculated stability diagram suggests that there exist three-phase regions of [ZrO_2 + Zr_5Te_4 + αZr], [ZrO_2 + $ZrTe_2$ + Zr_5Te_4], [ZrO_2 + $ZrTe_2$ + $ZrTe_3$], [ZrO_2 + L + $ZrTe_3$], [$ZrTe_3O_8$ + ZrO_2 + L] and [$ZrTe_3O_8$ + TeO_2 + L], L = liquid Te. All the species other than TeO_2 are expected to coexist with ZrO_2. Phase stability trends are virtually consistent with the isothermal section of the Zr-Te-O ternary system (Fig. 6). It should be noted that the phase relationships experimetally obtained in the present study satisfy the thermodynamic constraints.

At a lower temperature of 300°C, almost similar phases appear in the stability diagram shown in Fig. 13, but tellurium is in the solid phase. The ZrO_2 is stable again. Even if more positive $\Delta H_f^\circ{}_{298}$ values for $ZrTe_3O_8$ were used to construct the stability diagram, the double oxide will appear at 300°C. The equilibrium phase relationships at 300°C seem to be almost the same as at higher temperatures.

Although the zirconium tellurides are relatively stable compounds among metal-tellurium binary systems, the chemical stabilities of zirconiuum tellurides were found from these stability diagrams to be quite sensitive to oxygen pressure, irrespective of temperature. The temperature of cladding inner surface under normal operating condition of LWR may be slightly higher than the temperature of 300°C employed here, but there may be no marked change in the phase stability for the Zr-Te-O system between the two temperatures. On the assumption that the oxygen potential in the fuel-cladding gap is controlled by the UO_2 fuel, the $\Delta\bar{G}_{O_2}$ is around -400 kJ/mol or more less, which is not low enough to allow the formation of zirconium tellurides even at a Te_2 pressure of 0.1 Pa. At a high oxygen pressure and high temperature like reactor accidents, formation of $ZrTe_3O_8$ becomes to be important rather than zirconium tellurides.

The temperature dependence of the oxygen potential $\Delta\bar{G}_{O_2}$ in the Zr-Te-O ternary system is illustrated in Fig. 14, which is often called the Ellingham diagram. From the phase rule there is one degree of freedom in the three-phase region (for instance, ZrO_2 + $ZrTe_2$ + $ZrTe_3$), and setting the temperature fixes the oxygen potential and the tellurium partial pressure. The oxygen potential in the three-phase region of ZrO_2+ $ZrTe_2$+ $ZrTe_3$ is established by

$$3\ ZrTe_2(s) + O_2(g) = 2\ ZrTe_3(s) + ZrO_2(s),$$

and can be calculated from $\Delta G^\circ{}_T$ for the above reaction. The temperature dependence of oxygen potential in a three-phase region is shown by a solid line in Fig. 14. On the other hand, the phase rule offers two degrees of freedom in the two-phase region (e.g., ZrO_2 + $ZrTe_2$). Consequently, the tellurium pressure depends upon the oxygen potential at a given temperature. The tellurium pressure in the ZrO_2 + $ZrTe_2$ two-phase region can be evaluated from the tellurium pressure-oxygen potential relation associated with the reaction,

$$ZrTe_2(s) + O_2(g) = ZrO_2(s) + Te_2(g).$$

Dashed lines in Fig. 14 represent Te_2 isobars in two-phase regions. Figure 14 suggests that in a temperature range from 300 to 700°C Zr_5Te_4, $ZrTe_2$ and $ZrTe_3$ are stable only at a quite low oxygen potential. The equilibrium tellurium pressure

at a given temperature is smaller in the ZrO_2 + Zr_4Te_5 two-phase region than in the ZrO_2 + $ZrTe_2$ region. At the normal temperature of cladding inner surface in LWRs, the tellurium pressure much greater than 0.1 Pa is required to form $ZrTe_3$ at $\Delta\bar{G}_{O2}$ = -650 kJ/mol. No change in tellurium pressure is observed with the oxygen potential in the Te + ZrO_2 region. The region of ZrO_2 + Te + $ZrTe_3O_8$ shows a higher oxygen potential than other three-phase regions. The tellurium pressure in ZrO_2 + $ZrTe_3O_8$ region is found to be strongly affected by temperature and to be smaller than that in Te + ZrO_2 region. At higher oxygen potentials encountered in a failed fuel rod, zirconium tellurides are not likely to be formed at any temperatures. However, the tellurium pressure is lowered by the consumption of tellurium in forming the ternary compound of $ZrTe_3O_8$.

From the stability diagrams and the $\Delta\bar{G}_{O2}$-T relationship thus obtained, it can be concluded that oxygen reduces strongly the chemical stability of zirconium telluride. The oxygen potential may not be enough low to form zirconium tellurides in the fuel-cladding gap of normally operating LWR. However, sufficiently low oxygen potentials are supposed to be attained by UO_2/Zircaloy cladding interaction at the initial stage of reactor accident, and in such a situation Zircaloy cladding will pick tellurium up. At high oxygen potentials encountered after failure of fuel rod in reactor accidents, the zirconium tellurides are unlikely to be formed on Zircaloy cladding. Collins and his coworkers[5] have observed that a considerably large amount of tellurium is retained by metallic Zircaloy cladding up to 2000°C, but that tellurium once gettered is rapidly released after Zircaloy oxidation by steam. Higher stability of ZrO_2 than zirconium tellurides over a wide range of oxygen potentials explains the tellurium behavior in the recent test by Collins et al.[5]. Under a certain condition, however, the oxidized Zircaloy may tie up tellurium to form the ternary compound of $ZrTe_3O_8$.

As the present study was directed toward the Zr-Te-O ternary system, the present conclusion might not strictly be applied to the phenomena which would take place in the multicomponent system involving the other fission products and core materials. Although the Zr-Te-O phase relationships only are insufficient to represent complete chemical behavior of many fission products in hypothetical LWR accidents, such knowledge can provide a useful basis for an analysis of the complex chemistry of fission products' release from failed fuels.

4. Conclusions

The phase relationships in the Zr-Te-O ternary system have been studied at 700°C. The isothermal section of the Zr-Te-O system at 700°C was proposed using

the results of X-ray diffraction analysis. The ternary compound $ZrTe_3O_8$ was confirmed to exist along the ZrO_2-TeO_2 join in the isothermal section. The three tellurides, Zr_5Te_4, $Zr_{1+x}Te_2$ and $ZrTe_3$ were found to be stable at 700°C in the Zr-Te binary system, and these compounds formed equilibrium phase regions with αZrO_2. A limited amount of oxygen can be dissolved in these tellurides.

The thermodynamic properties such as $\Delta H_f^\circ{}_{298}$ and $S^\circ{}_{298}$ were estimated for Zr_5Te_4, $ZrTe_2$, $ZrTe_3$ and $ZrTe_3O_8$ to serve as a basis for calculation of the phase stability and the Ellingham diagrams for the Zr-Te-O ternary system.

On the basis of evaluation of the equilibrium pressure of Te_2, Zr_5Te_4 and $ZrTe_2$ were found to be relatively stable compounds themselves, compared with other tellurides of fission products, cladding constituents and control rod materials.

The stability diagrams for the Zr-Te-O system were constructed at 700 and 300°C using $\ln P_{O_2}$ and $\ln P_{Te_2}$ as variables, and the temperature dependence of the oxygen potential in the Zr-Te-O system was obtained. It was verified from the stability diagrams and the $\Delta\bar{G}_{O_2}$ vs temperature relationship that at extremely low oxygen potentials there exist zirconium tellurides in the ternary system and that ZrO_2 is quite stable over a wide range of oxygen and tellurium partial pressures. In the range of higher oxygen potentials, tellurium pressure may be lowered in forming $ZrTe_3O_8$ instead of ZrO_2. The phase relations expected from the calculated diagram were almost identical with the experimental isothermal section of the Zr-Te-O ternary system.

A scenario of LWR accident determines whether or not zirconium tellurides are stable with respect to ZrO_2. The $ZrTe_3O_8$ would become an important tellurium-containing species if the oxygen potential is increased sufficiently.

References

[1] P.E. Potter and M.H. Rand, CALPHAD, 7(1983)165.
[2] P.E. Potter M.H. Rand and C.B. Alcock, J. Nucl. Mater., 130(1985)139.
[3] S. Imoto, J. Nucl. Mater., 140(1986)19.
[4] D. Cubicciotti and B.R. Sehgal, Nucl. Technol., 65(1984)266.
[5] J.L. Collins, M.F. Osborne and R.A. Lorenz, Proceedings of International ANS/ENS Topical Meeting on Thermal Reactor Safety, (ANS, 1986)445.
[6] F.K. McTaggart and A.D. Wadsley, Aust. J. Chem., 11(1958)445.
[7] V.H. Hahn and P. Ness, Z. anorg. allg. Chem., 302(1959)136.
[8] L. Brattas and A. Kjekshus, Acta Chem. Scand., 25(1971)2350.
[9] A. Gleizes and Y. Jeannin, J. Solid State Chem., 5(1972)42.
[10] F.D. Jenkins, Thesis, Univ. of Missouri, Rolla, USA, (1972).
[11] L. Brattas and A. Kjekshus, Acta Chem, Scand., 27(1973)1290.
[12] S. Furuseth, L. Brattas and A. Kjekshus, ibid., 29(1975)623.
[13] H. Sodeck, H. Mikler and K.L. Komarek, Mh. Chem., 110(1979)1.
[14] G.K. Johnson, W.T. Murray, E.H. Van Deventer and H.E. Flotow, J. Chem. Thermodynamics, 17(1985)751.
[15] T.B. Masalski, Binary Alloy Phase Diagrams, (ASM, Ohio, 1986).

[16] G.V. Samsonov, The Oxide Handbook, 2nd Ed., (Plenum Press, New York, 1981).
[17] P.G. Meunier and J. Galy, Acta Cryst., 27(1971)602.
[18] M.U. Cohen, Rev. Sci. Inst., 6(1935)68.
[19] P. Cherin and P. Unger, Acta Cryst., 23(1967)670.
[20] O. Kubaschewski and C.B. Alcock, Metallurgical Thermochemistry, 5th Ed., (Pergamon Press, Oxford, 1979).
[21] O. Kubaschewski, Zirconium: Physico-Chemical Properties of Its Compounds and Alloys, (IAEA, Vienna, 1976).
[22] P.E. Blackburn and C.E. Johnson, ANL-82-42, (1982).
[23] K.C. Mills, Thermodynamic Data for Inorganic Sulphide, Selenides, and Tellurides, (Butterworth, London, 1971).
[24] K.L. Komarek, Hafnium: Physico-Chemical Properties of Its Compounds and Alloys, (IAEA, Vienna, 1981).
[25] K.L. Komarek, Titanium: Physico-Chemical Properties of Its Compounds and Alloys, (IAEA, Vienna, 1983).
[26] R.A. Swalin, Thermodynamics of Solid, 2nd Ed., (John Wiley&Sons, New York, 1972).

Table 1 Chemical species chosen for the calculation.

Ⅰ) Condensed Phases	
Solid:	Zr_5Te_4, $ZrTe_2$, $ZrTe_3$, ZrO_2, TeO_2, $ZrTe_3O_8$, Zr, Te
Liquid:	Te
Ⅱ) Vapor Species	
Diatomic gas:	O_2, Te_2

Table 2 Thermodynamic properties of chemical species related to the Zr-Te-O ternary system[14,20].

Chemical Species	$\Delta H_f^\circ{}_{298}$(kJ/mol)	$S^\circ{}_{298}$(J/mol K)
Zr_5Te_4	-732*	378*
$ZrTe_2$	-312*	130*
	-294.1	124.24
$ZrTe_3$	-339*	172*
ZrO_2	-1101	50.71
TeO_2	-323	74.17
$ZrTe_3O_8$	-2150*	252*
Zr	--	39.0
Te	--	49.50
O_2	--	205

* Estimated value

Table 3 Linear equation for standard free energy change of telluride formation[14,22,23]: ΔG°_{T}(J/mol of Te_2 gas) = A + B T.

Telluride	- A x 10^{-3}	B
Zr_5Te_4	522.3	160.2
$ZrTe_2$	402.3	170.6
$ZrTe_3$	245.8	156.2
SnTe	287.2	179.7
$FeTe_{0.9}$	207.7	134.3
CrTe	302.2	123.1
Cs_2Te	887.3	249.7
BaTe	702.6	198.0
SrTe	783.8	180.5
LaTe	758.6	188.9
CeTe	767.5	194.6
NdTe	761.1	205.4
Mo_3Te_4	189.2	106.5
Pd_4Te	230.8	160.2
$RuTe_2$	265.0	158.1
InTe	298.0	163.4
CdTe	435.3	180.0
Ag_2Te	228.2	115.2

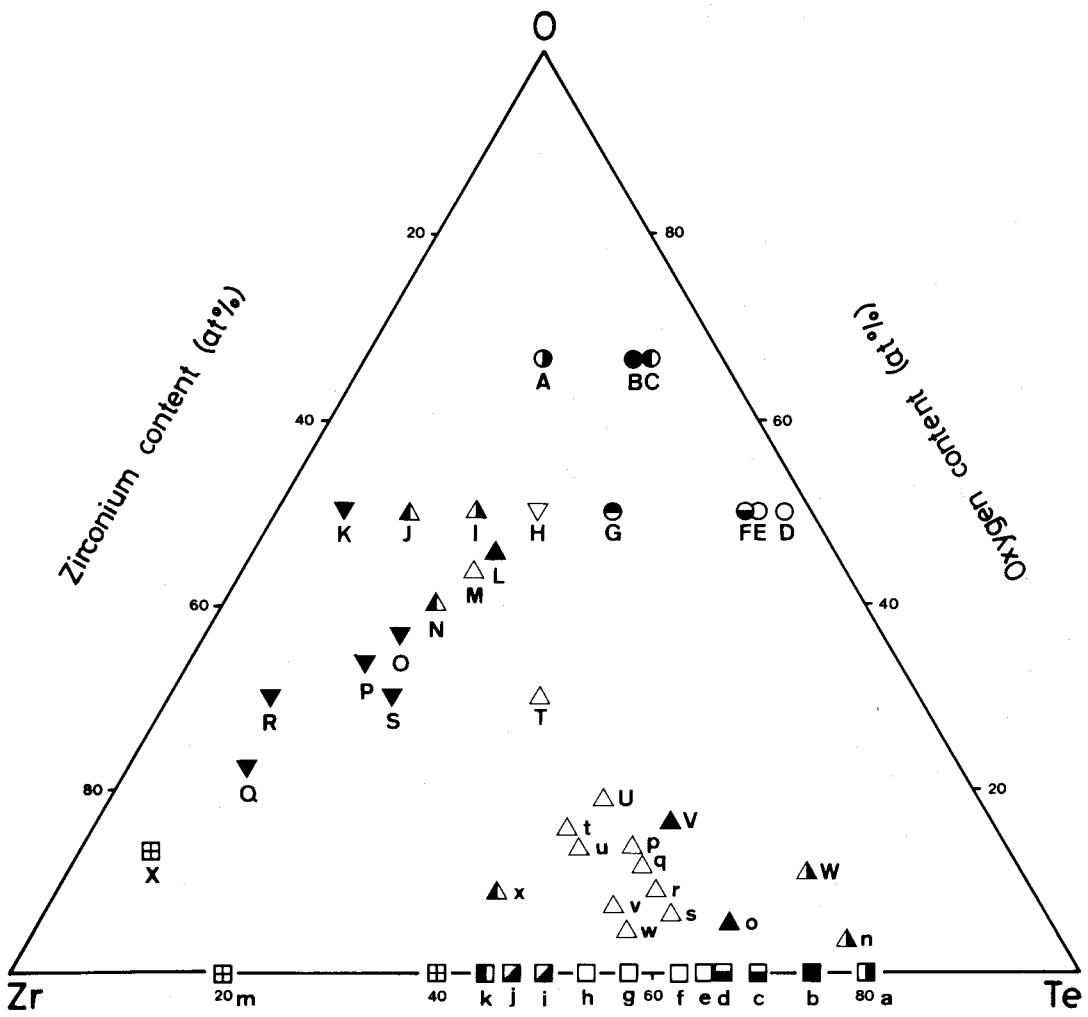

Fig. 1 Phases identified in the samples a - x and A - X.

- $ZrTe_3$ + Te,
- $ZrTe_3$ + $Zr_{1+x}Te_2$,
- $Zr_{1+x}Te_2$ + Zr_5Te_4,
- Zr_5Te_4 + αZr,
- $ZrTe_3O_8$ + αZrO_2,
- $ZrTe_3O_8$ + Te,
- $ZrTe_3O_8$ + αZrO_2 + Te,
- αZrO_2 + Te + $ZrTe_3$,
- αZrO_2 + $Zr_{1+x}Te_2$,
- αZrO_2 + Zr_5Te_4 + αZr.
- $ZrTe_3$,
- $Zr_{1+x}Te_2$,
- Zr_5Te_4,
- $ZrTe_3O_8$,
- $ZrTe_3O_8$ + TeO_2,
- $ZrTe_3O_8$ + Te + TeO_2,
- αZrO_2 + Te,
- αZrO_2 + $ZrTe_3$ + $Zr_{1+x}Te_2$,
- αZrO_2 + $Zr_{1+x}Te_2$ + Zr_5Te_4,

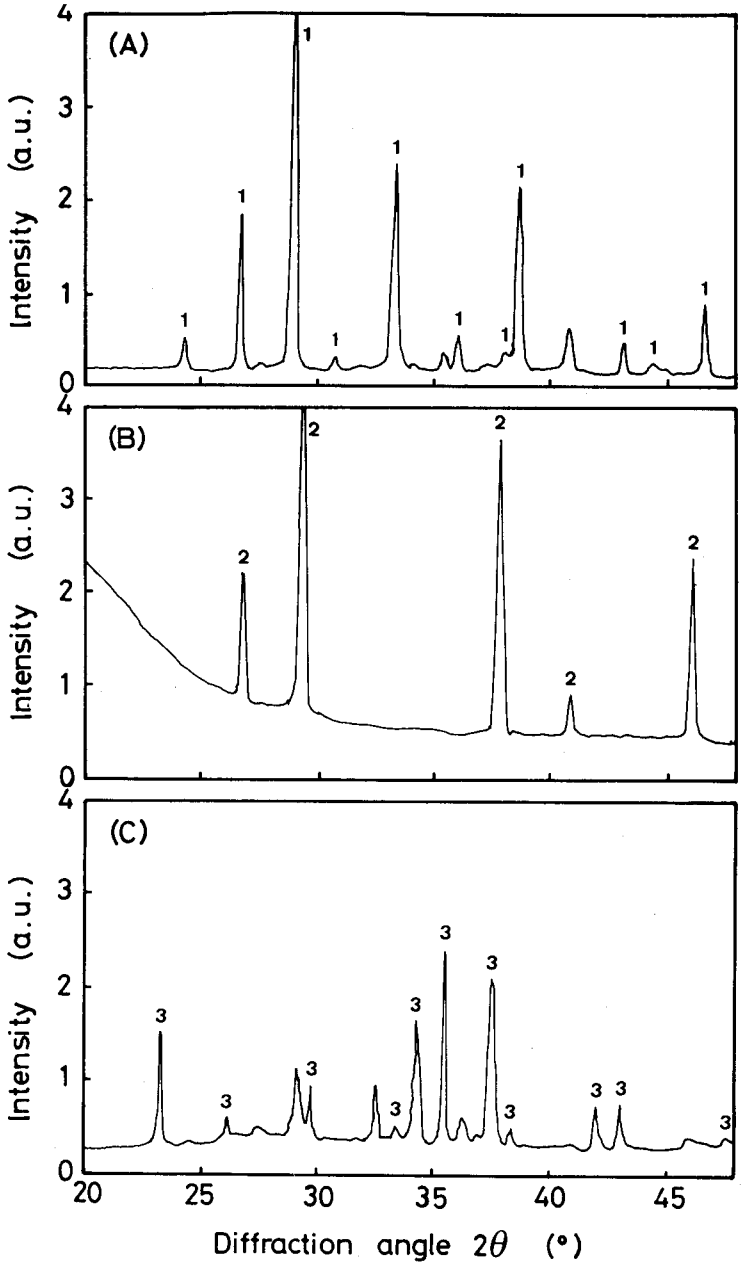

Fig. 2 X-ray diffraction patterns of the reaction products.
(A) sample b, (B) sample e, (C) sample k.
1: $ZrTe_3$, 2: $Zr_{1+x}Te_2$, 3: Zr_5Te_4.

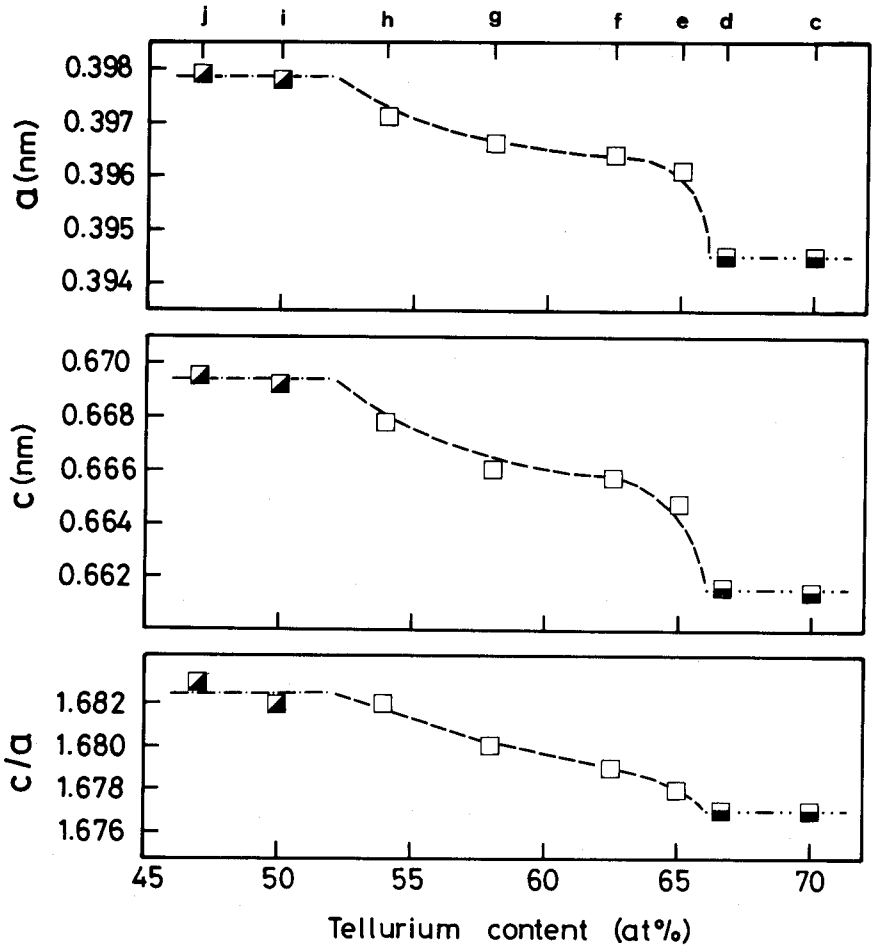

Fig. 3 Change in the lattice parameters a and c and the axial ratio c/a of $Zr_{1+x}Te_2$ with tellurium content.

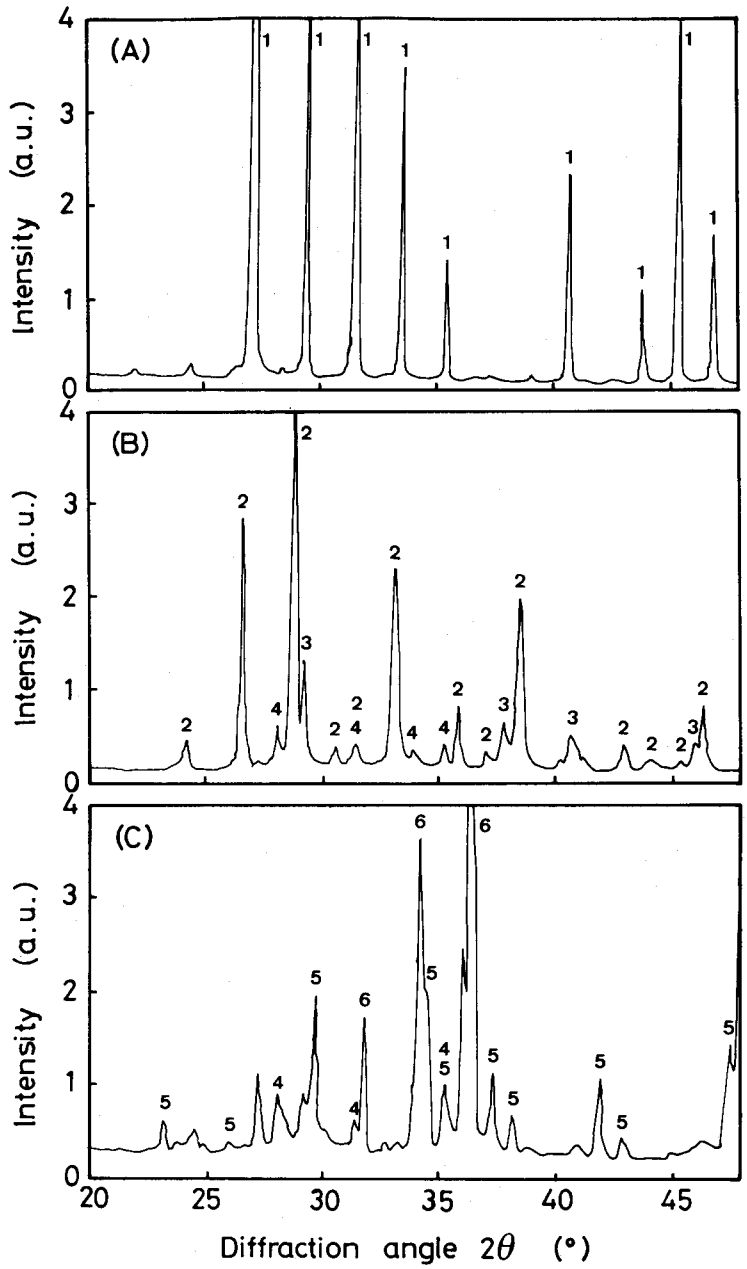

Fig. 4 X-ray diffraction patterns of the reaction products.
(A) sample B, (B) sample V, (C) sample R.
1: $ZrTe_3O_8$, 2: $ZrTe_3$, 3: $Zr_{1+x}Te_2$, 4: αZrO_2, 5: Zr_5Te_4, 6: αZr.

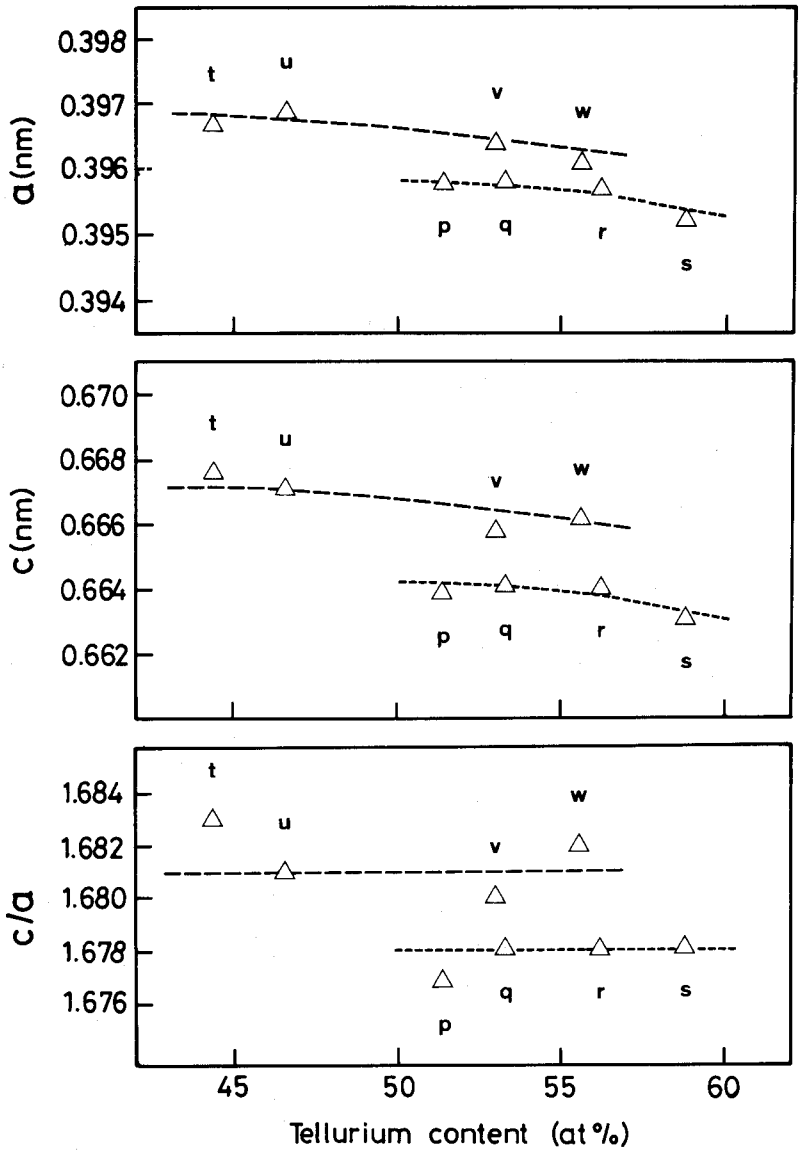

Fig. 5 Change in the lattice parameters a and c and the axial ratio c/a of $Zr_{1+x}Te_2$ coexisting with αZrO_2 with tellurium content.

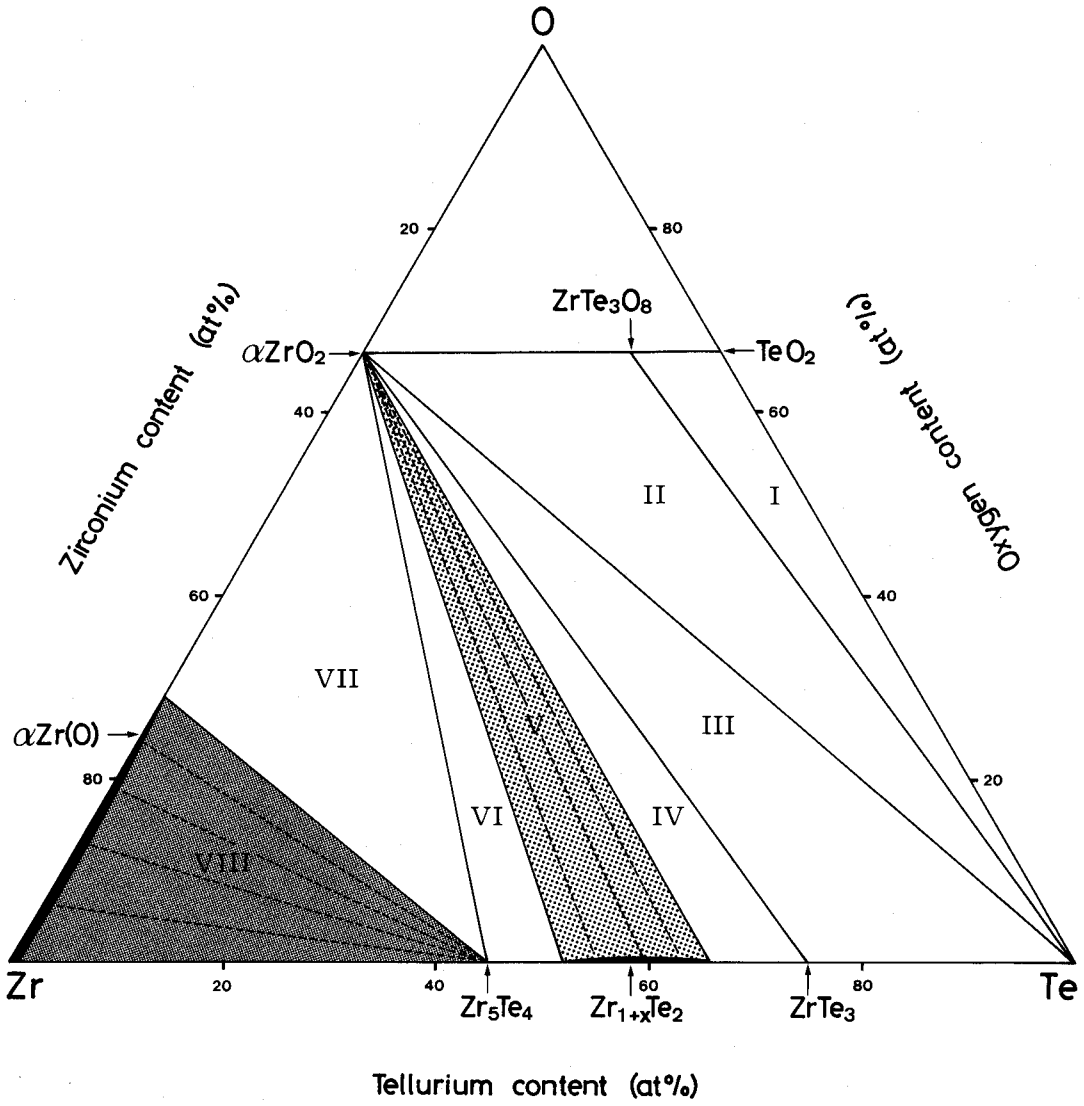

Fig. 6 Isothermal section of the Zr-Te-O ternary system at 700°C.

Ⅰ $ZrTe_3O_8 + TeO_2 + L$,
Ⅱ $ZrTe_3O_8 + \alpha ZrO_2 + L$,
Ⅲ $\alpha ZrO_2 + L + ZrTe_3$,
Ⅳ $\alpha ZrO_2 + ZrTe_3 + Zr_{1+x}Te_2$,
Ⅴ $\alpha ZrO_2 + Zr_{1+x}Te_2$,
Ⅵ $\alpha ZrO_2 + Zr_{1+x}Te_2 + Zr_5Te_4$,
Ⅶ $\alpha ZrO_2 + Zr_5Te_4 + \alpha Zr(O)$,
Ⅷ $Zr_5Te_4 + \alpha Zr(O)$.

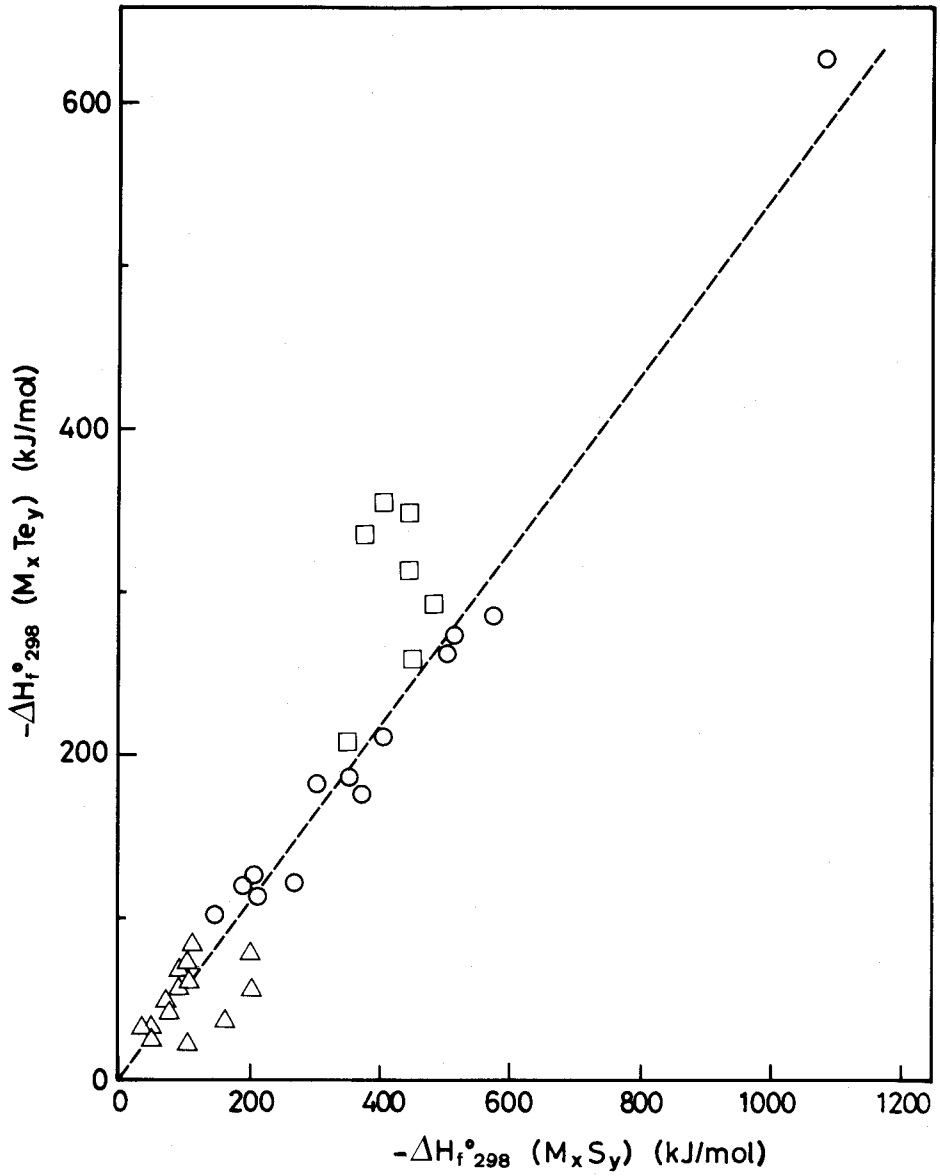

Fig. 7 Relationship between the standard enthalpies of formation for sulphides $\Delta H_f°_{298}(M_xS_y)$ and tellurides $\Delta H_f°_{298}(M_xTe_y)$.
○ $0.4 \leq \varepsilon \leq 0.8$, △ $\varepsilon \leq 0.3$, □ $\varepsilon \geq 0.9$

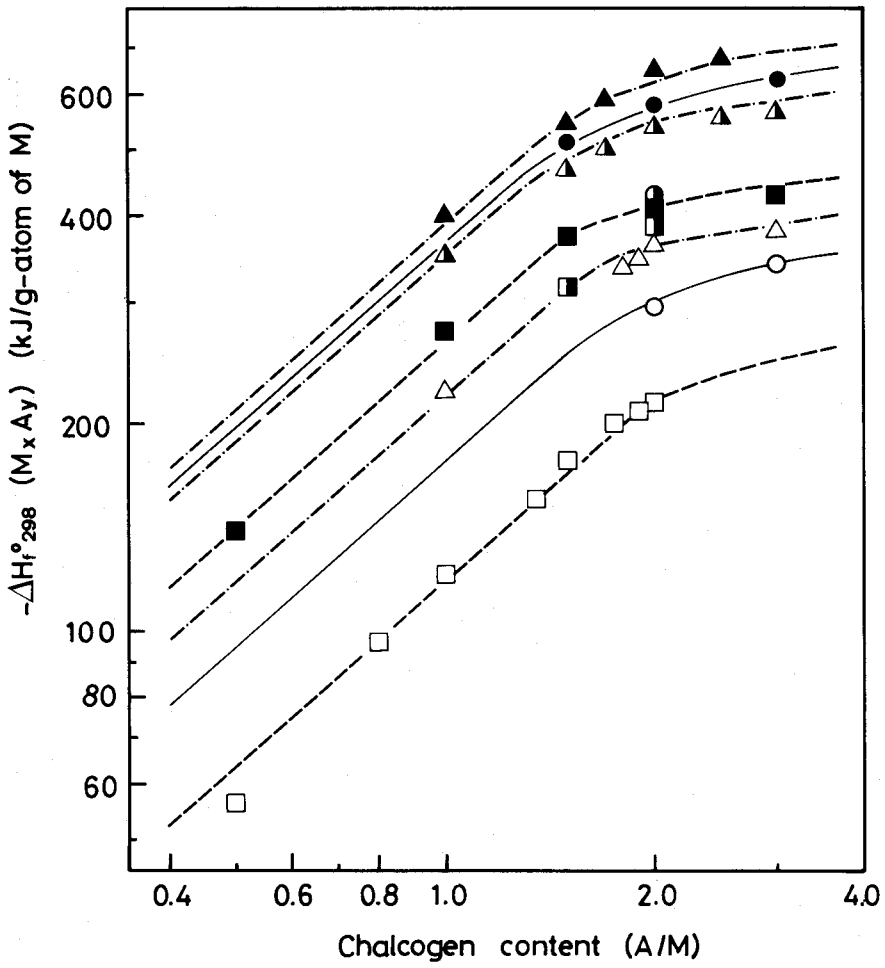

Fig. 8 Relationship between the standard enthalpies of formation of chalcogenides $\Delta H_f^\circ{}_{298}$ and the chalcogen content for the elements in the Ⅳ group of periodic table.

- ■ Ti sulphides, ◨ Ti selenides, ⬚ Ti tellurides,
- ● Zr sulphides, ◑ Zr selenides, ○ Zr tellurides,
- ▲ Th sulphides, ◭ Th selenides, △ Th tellurides.

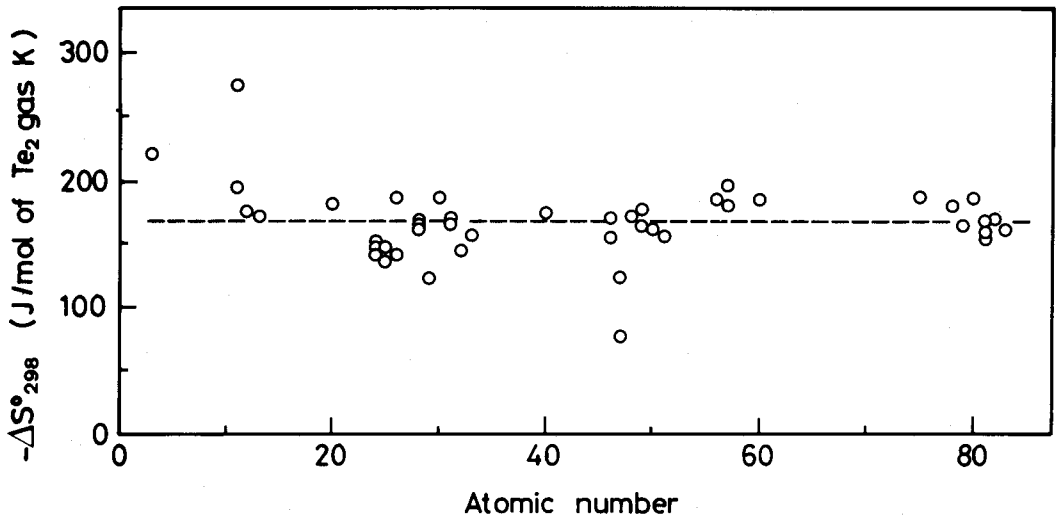

Fig. 9 Standard entropy change of telluride formation, ΔS°_{298}.

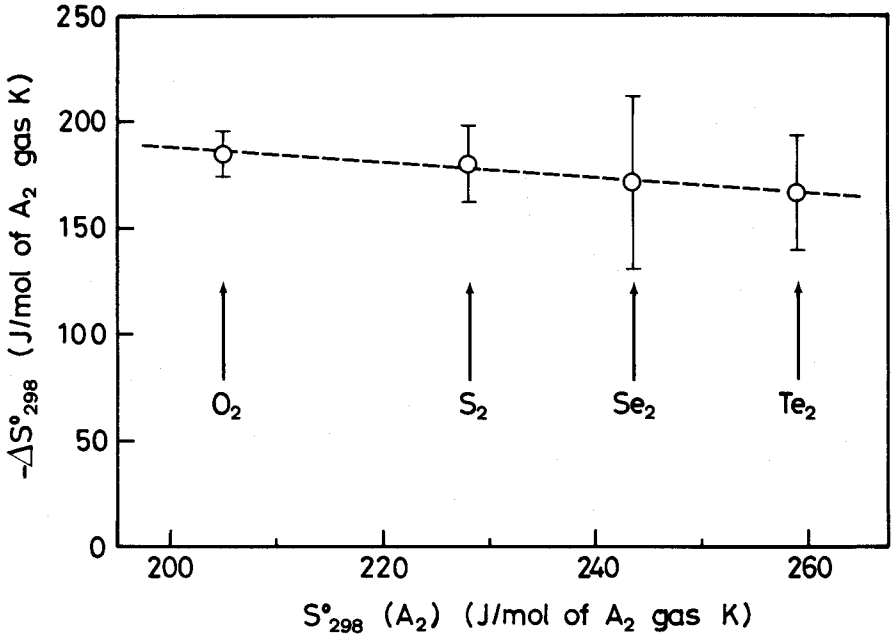

Fig. 10 Average standard entropy change of chalcogenide formation, ΔS°_{298}.

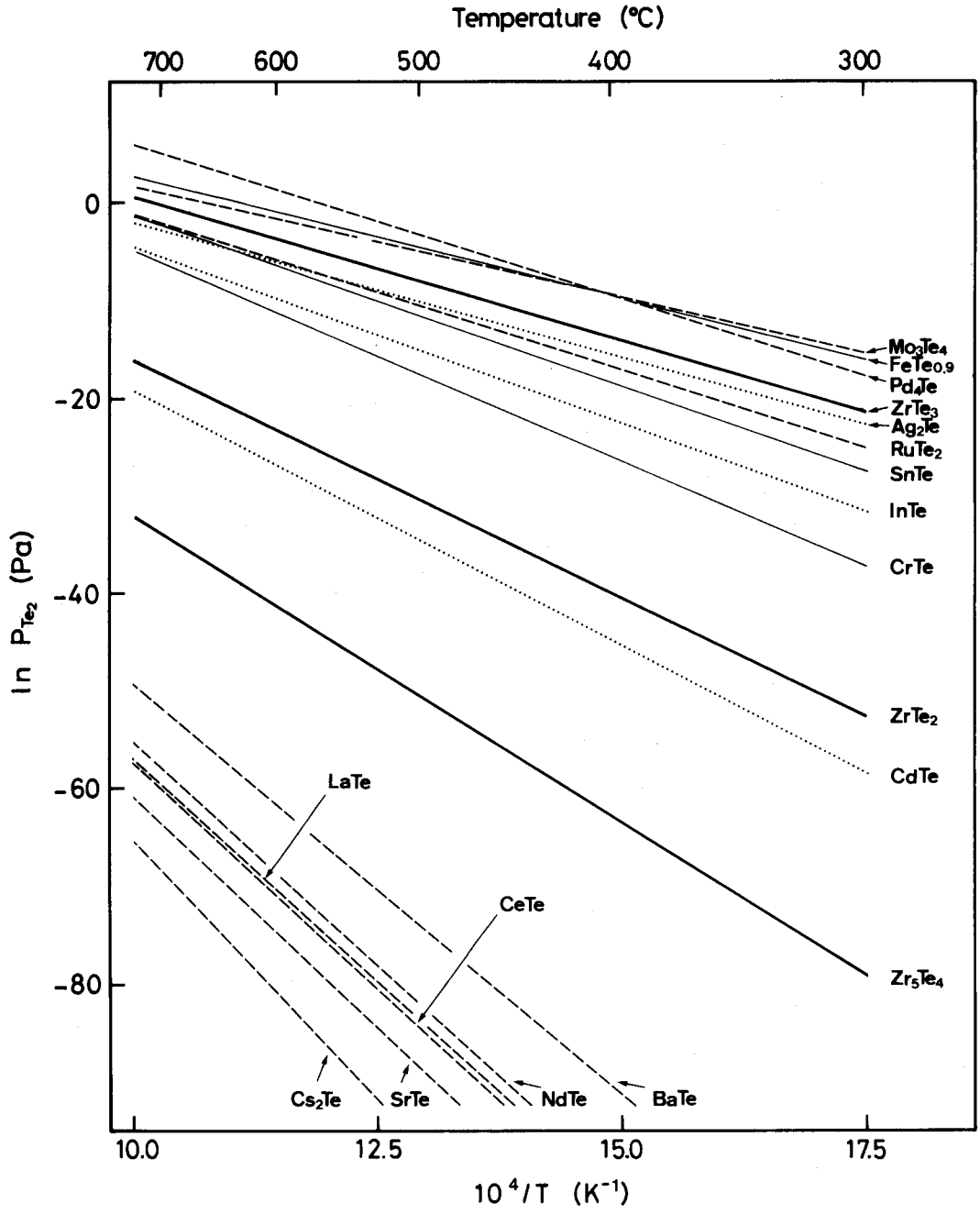

Fig. 11 Decomposition vapor pressures of tellurium in the metal-tellurium binary systems.

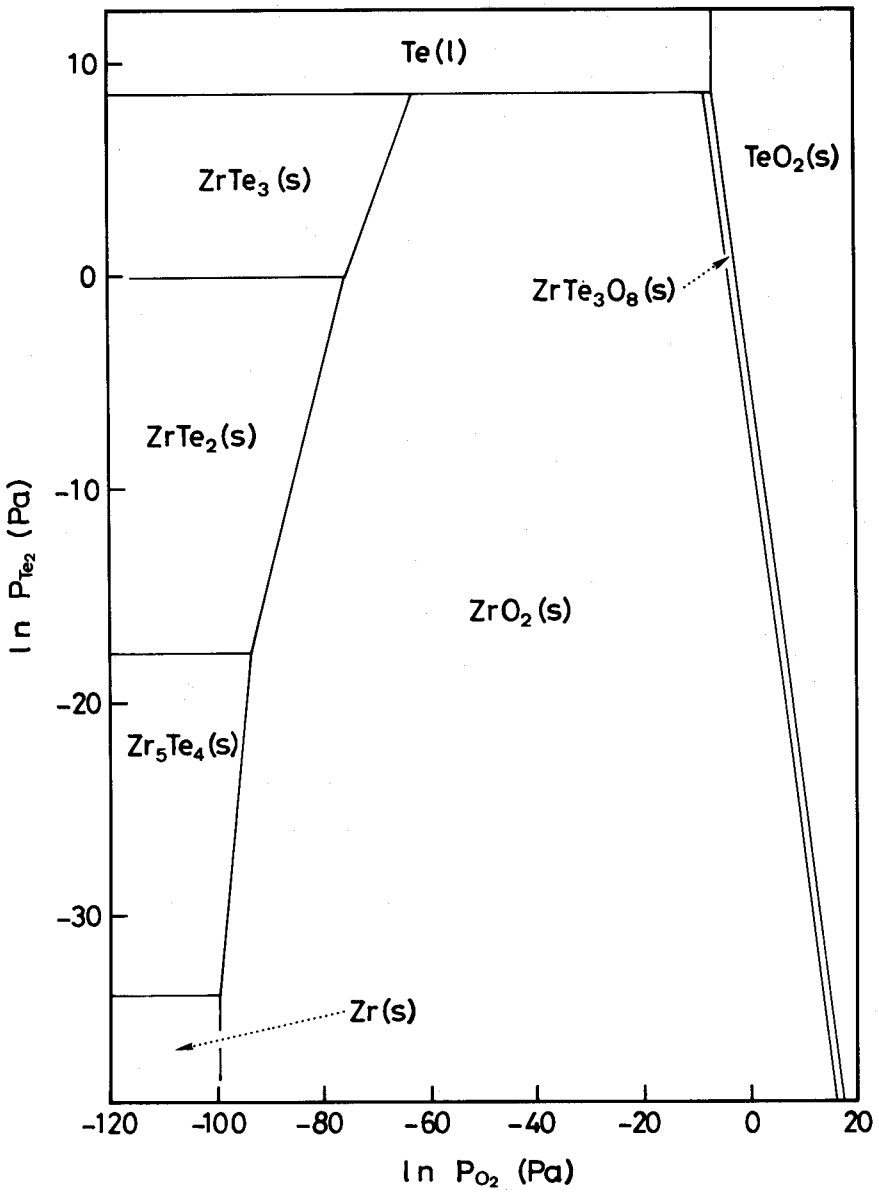

Fig. 12 Stability diagram for the Zr-Te-O ternary system at 700°C.

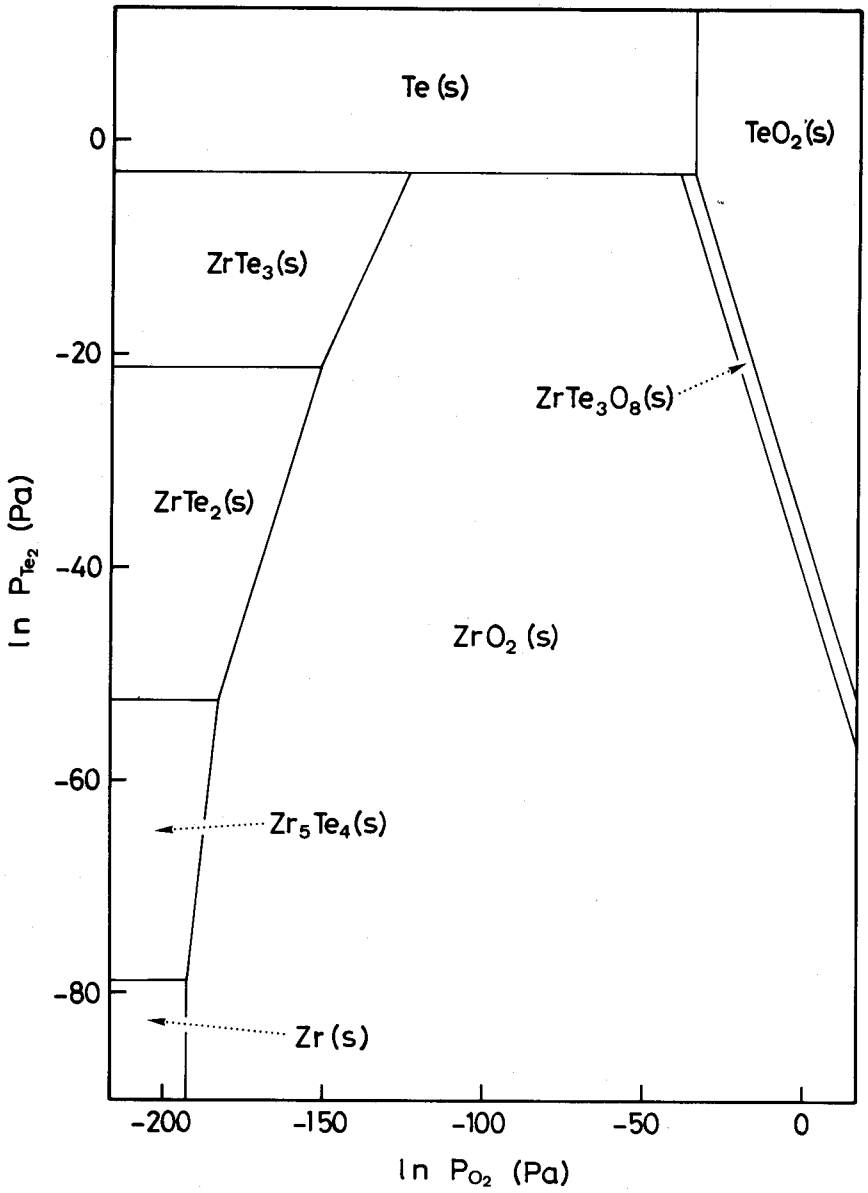

Fig. 13 Stability diagram for the Zr-Te-O ternary system at 300°C.

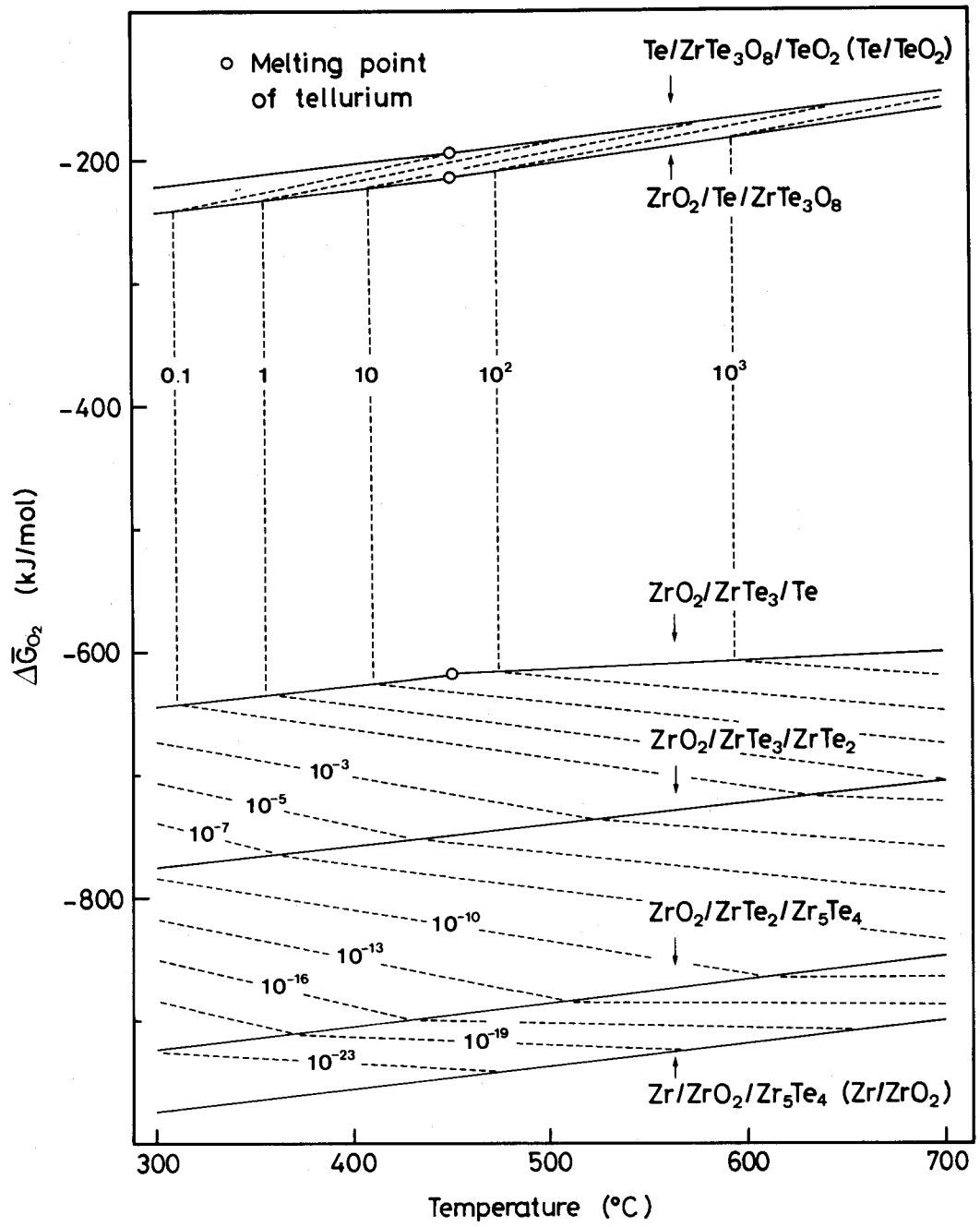

Fig. 14 Temperature dependence of oxygen potential $\Delta\bar{G}_{O_2}$ in the Zr-Te-O ternary system from 300 to 700°C.

Dashed lines: Tellurium isobars (in Pa).

CHAPTER 6 SOLUBILITY OF HYDROGEN ISOTOPE IN TITANIUM-OXYGEN SOLID SOLUTION

1. Introduction

Titanium is now widely used as a gettering material in vacuum technology because of its great sorption ability for chemically active gases. In fusion technology it was of primary interest as a getter to reduce impurity levels of plasma in tokamaks[1-3]. A gas handling system with titanium bed has recently been proposed for tritium fixation and disposal[4-6]. The titanium getter appears to be one of the most likely candidates for scavenging tritium and other impurity gases from the helium coolant of a high temperature gas cooled reactor[7]. For practical applications of titanium and its alloys to tritium handling systems in fission and fusion reactors, it is of importance to obtain the sorption rate and capacity for hydrogen isotopes.

Hydrogen behavior in titanium and its alloys is also important for metallurgical reasons. Mechanical performance and corrosion resistance of structural parts containing titanium-base alloys are strongly influenced by absorbed hydrogen. Much effort has been spent to clarify the effect on hydrogen on the metallurgical properties of titanium[8,9].

The sorption rates of hydrogen isotopes by titanium have been reported in the literature[10,11]. The solubilities and the phase diagrams are well known for the Ti-H and Ti-D binary systems[12-16]. Irreversible sorption of other active gases such as H_2O, CO_2 and CO appears to affect the behavior of hydrogen isotopes in titanium. Oxygen is likely to be the most important element among the impurities dissolved in titanium. However, only limited information is available for hydrogen solubility in titanium-oxygen solid solution[17-19].

The present study has therefore been performed on the Ti-O-H and Ti-O-D ternary systems to elucidate the effects of solute oxygen on the equilibrium phase relationships and on the solubilities of hydrogen isotopes in titanium. The isotope effect of hydrogen and deuterium on the solubility was discussed, and tritium solubility in titanium-oxygen solid solution was estimated from experimental results for hydrogen and deuterium.

2. Experimental

Pure titanium and titanium-oxygen solid solution, αTi(O), were employed in the present study. The pure titanium specimen was in the form of sheet (1 mm x 10

mm x 12 mm), the principal impurities of which were 320 wtppm Fe, 360 wtppm O, 31 wtppm N and 21 wtppm H. Prior to solubility measurements, the specimen was mechanically polished and ultrasonically cleaned. Pellets of αTi(O) solid solutions (8 mmϕ x 2 - 3 mmh) were prepared by vacuum annealing of Ti (purity, 99.9 wt%) and TiO (purity, 99.9 wt%) mixture powders. The oxygen content of αTi(O) ranged from 0.111 to 0.429 O/Ti atom ratio. Phase identification by X-ray diffraction technique indicated that the pellets thus prepared were α solid solutions with a hexagonal structure. The homogeneity of the αTi(O) solutions was also checked by a microhardness tester and a microscope. The compositions were chemically analyzed before and after solubility measurements. Hydrogen (purity, 99.999 vol%) and deuterium (purity, 99.5 vol%) gases were used with purification by passing over hot titanium sponges.

Solubilities of hydrogen and deuterium in the pure titanium and the αTi(O) solid solutions were measured by a modified Sieverts apparatus shown schematically in Fig. 1. The apparatus was constructed mainly of stainless steel and capable of being evacuated less than 10^{-6} Pa with an oil diffusion pump having a liquid nitrogen trap. Pressures of hydrogen and deuterium were recorded by three capacitance manometers which covered the pressure range of 1.33×10^{-1} to 1.33×10^{5} Pa. The specimen temperature was measured by a CA thermocouple and controlled within ± 1°C.

The specimen of approximately 0.5 g in a molybdenum crucible was placed inside a silica tube and outgassed at 900°C for several hours in a vacuum of 10^{-6} Pa before hydrogen addition. An appropriate amount of hydrogen or deuterium gas was adimitted from the calibrated volume to the specimen tube kept at a constant temperature. After equilibrium was established, the pressure was measured. The procedure was repeated up to a predetermined pressure. The solubility of hydrogen isotope was evaluated from change in pressure on dissolution of gas into the specimen at constant volume. The solubility measurements were carried out in the temperature range of 600 to 850°C at pressures ranging from 1 to 10^{2} Pa. Only at 600°C, hydrogen solubility was measured up to 10^{5} Pa to gain information on phase equilibria in the Ti-O-H ternary system.

3. Results and Discussion

3.1. Phase equilibria in the Ti-O-H ternary system

At 600°C, equilibrium pressures of hydrogen in pure titanium and αTi(O) solid solutions with oxygen contents of 0.111, 0.176, 0.250, 0.333 and 0.429 O/Ti atom ratios were measured up to 10^{5} Pa. Isothermal equilibrium hydrogen pressure-

equilibrium hydrogen content (P-C) curves are shown in Fig. 2.

At low hydrogen contents, linearity of the P-C curves for pure titanium and αTi(O) solid solutions reveals that Sieverts' law is obeyed for all the domain of the dilute α solution. As hydrogen content is increased, each curve (except for pure titanium) exhibits some curvature. Discontinuities in slope appear on the P-C curves at higher hydrogen contents, which are indicated by open circles in Fig. 2. These points on the P-C curves indicate the presence of phase boundaries.

Five distinct portions of the P-C curves can be seen for the Ti-H binary system, corresponding to equilibrium conditions between hydrogen gas and dissolved hydrogen in three single-phase regions of αTi(H) (hcp solid solution), βTi(H) (bcc solid solution) and δTiH_{2-x} (fcc hydride) and in two two-phase regions of αTi(H) + βTi(H) and βTi(H) + δTiH_{2-x}. There exist two plateau pressure regions in the P-C curve for the Ti-H binary system. The two solid phases αTi(H) and βTi(H) equilibrate each other in the plateau region at a lower pressure, and βTi(H) and δTiH_{2-x} in another plateau region. The phase boundaries obtained in the Ti-H binary system are in good agreement with those in the literature[20].

For the P-C curves of αTi(O) solutions with 0.111 - 0.250 O/Ti, the regions adjacent to αTi(O,H) phase are inferred to be αTi(O,H) + βTi(H). The plateau pressure region is observed, where three phases of αTi(O,H), βTi(H) and δTiH_{2-x} coexist in the solid phase. Since at the discontinuities in slope on the P-C curves the equilibrium pressures for αTi(O) of 0.333 and 0.429 O/Ti are larger than the plateau pressure, this change in slope marks the appearance of δTiH_{2-x} phase. That is to say, two phases αTi(O,H) and δTiH_{2-x} are in equilibrium in the portion of the curve above the discontinuity.

Figure 3 indicates the tentative isothermal section of the Ti-O-H ternary system at 600°C, proposed from the results of P-C curves for pure titanium and αTi(O) solid solutions. The existence of αTi(O,H) + βTi(H) + δTiH_{2-x} (region Ⅱ in Fig. 3) characterizes the isothermal section of the Ti-O-H system. This three-phase region is adjacent to two-phase regions of αTi(O,H) + βTi(H), βTi(H) + δTiH_{2-x} and αTi(O,H) + δTiH_{2-x}. On the basis of the P-C curves, isoactivity lines, which are called tie lines, are drawn in the two-phase regions.

From the results obtained in the present study, the α phase is found to be stabilized by oxygen dissolution. On the other hand, the area of the β phase region is likely to be relatively small. The phase boundary between αTi(O,H) and αTi(O,H) + βTi(H) shown in Fig. 3 agrees with the results for αTi(O) with an oxygen content below 0.156 O/Ti previously reported by Jostsons and Jenkins[18]. The three-phase region including αTiO (region Ⅲ) seems to exist in a higher oxygen content region, though it could not be evidenced by the P-C curve measurements in the present study.

3.2. Hydrogen solubility in the Ti-O solid solution

Below a hydrogen pressure of 10^2 Pa, all the solubility data for hydrogen in pure titanium and αTi(O) solid solutions with oxygen contents from 0.111 to 0.429 O/Ti closely followed Sieverts' law, which states that the solubility of a diatomic gas in a metal is proportional to the square root of the pressure:

$$C_H = K_H P_{H_2}^{1/2}. \quad (1)$$

In this equation, K_H is the Sieverts' constant, C_H the solubility of hydrogen in atom ratio (H/Ti), and P_{H_2} the equilibrium pressure of hydrogen gas in Pa. Figure 4 indicates a representative of the linear relation between the square root of the equilibrium pressure and hydrogen content. Since Sieverts' law applied in all the αTi(O) solid solutions, hydrogen-hydrogen pair interaction in the solution seems to be negligible.

Figure 5 shows the change in the Sieverts' constant K_H for hydrogen with temperature. It is seen from this figure that temperature dependence of Sieverts' constant can be represented by

$$\ln K_H = A + B/T \quad (2)$$

where A and B are constants and T is the specimen temperature in K. In Table 1, the parameters A and B are listed together with the enthalpies of solution of hydrogen into pure titanium and αTi(O) solutions ΔH (kJ/g-atom) derived from the value of B.

Different workers[12-16] have studied hydrogen solubility in pure titanium and reported the A values ranging from -11.6 to -13.1 and the B values from 5300 to 6400, as given in Table 2. The solubility data for pure titanium obtained in the present study are in reasonable agreement with these sets of data.

The hydrogen solubility at a constant pressure is found from Fig. 5 to decrease with increasing oxygen content in titanium. It is obvious from Table 1 that the enthalpy of solution is slightly reduced by oxygen addition.

The reduction in the solubility of hydrogen by dissolved oxygen is attributable to a repulsive interaction between hydrogen and oxygen within titanium. Site occupations of hydrogen and oxygen are indicated in Fig. 6. Oxygen atoms in a hexagonal lattice of titanium are located on octahedral sites[21], whereas tetrahedral sites in titanium are highly favored to receive hydrogen atoms[22,23]. The presence of oxygen atom in an octahedral site is inferred to cause changes in the state and configuration of hydrogen atoms in adjacent tetrahedral sites. This is presumed to influence the solubility of

hydrogen in titanium.

Taking into consideration the site occupation of interstitial atoms, the effect of oxygen on hydrogen solubility was analyzed by a dilute solution model[24,25].

The chemical potential of hydrogen in the solid solution is expressed by,

$$\mu_H{}^s = \bar{H}_H - T\,\bar{S}_H + kT\,\ln(C_H/(2-C_H)). \quad (3)$$

In this equation, $\bar{H}_H$ and $\bar{S}_H$ are the partial molar enthalpy and the partial molar excess entropy of hydrogen which are referred to the standard state of hydrogen atoms at rest in a vacuum, and k is Boltzmann constant. The last term on the right hand side of eq. (3) is related to the configurational entropy of hydrogen, derived on the assumption that the hydrogen atoms have access to two tetrahedral interstitial sites per titanium atom.

The chemical potential of atomic hydrogen in the gas phase is represented as,

$$\mu_H{}^g = kT\,\ln P_{H_2}{}^{1/2} + kT\,\ln(A_{H_2}\,T^{-7/4}) + E^d{}_{H_2} \quad (4)$$

where $-E^d{}_{H_2}$ is one half of the dissociation energy of the hydrogen molecule at 0 K. The A_{H_2} refers to the partition functions of hydrogen gas[24]:

$$A_{H_2} = [(h^3/(2\pi 2m_H kT)^{3/2})(\sigma h^2/8\pi^2 I_{H_2} kT)(1/Z^v)(1/Z^e)]^{1/2} \times (1/kT)^{1/2} \times T^{7/4}. \quad (5)$$

The first term in the bracket is for the translational degrees of freedom, the second for the rotational degrees of freedom. In these terms, m_H is the atomic weight of hydrogen, σ the symmetry number of hydrogen molecule, I_{H_2} its moment of inertia, and h the Planck constant. The σ is 2 for the hydrogen molecule. The values of $E^d{}_{H_2}$ and I_{H_2} can be evaluated from the literature data[26,27]. The remaining Z^v and Z^e are the vibrational and electronic partition functions of hydrogen molecule. The Z^v is represented by

$$Z^v = (1 - \exp(-h\nu_{H_2}/kT))^{-1}. \quad (6)$$

In this equation the ν_{H_2} is the vibrational frequency of the hydrogen molecule, the value of which can be obtained from the spectroscopic data[26]. The electronic partition function Z^e can be replaced by the degeneracy of the ground state for the hydrogen molecule: $Z^e = 1$ corresponding to a $^1\Sigma$ ground state.

At equilibrium, $\mu_H{}^s = \mu_H{}^g$. Hence, the following solubility equation was obtained for a dilute solution ($C_H \ll 1$),

$$\ln (C_H T^{7/4}/2 P_{H_2}{}^{1/2} A_{H_2}) = - (\bar{H}_H - E^d{}_{H_2})/kT + \bar{S}_H/k. \quad (7)$$

The equation (7) was applied to the solubility data. Plots of $\ln(C_H T^{7/4}/2 P_{H_2}{}^{1/2} A_{H_2})$ vs 1/T are shown in Fig. 7, indicating good straight lines for pure titanium and αTi(O) solid solutions. The values of the slope and the intercept give the $-(\bar{H}_H - E^d{}_{H_2})/k$ and the $\bar{S}_H/k$. For pure titanium, the enthalpy term of $\bar{H}_H - E^d{}_{H_2}$ and the entropy term of $\bar{S}_H$ were estimated to be -31.0 kJ/mol and 28.4 J/mol K, respectively. The values of the enthalpy term for αTi(O) solid solutions were slightly smaller than that for pure titanium. The entropy term markedly decreased with oxygen content in αTi(O).

The changes in the hydrogen solubility and the enthalpy of solution by insertion of oxygen atoms into the titanium lattice were analyzed on the basis of differences in the partial molar thermodynamic functions between pure titanium and αTi(O) solid solutions. The differences in the partial molar enthalpy and the partial molar excess entropy are defined as,

$$\partial\bar{H}_H = \bar{H}_H - \bar{H}_H^\circ \text{ and } \partial\bar{S}_H = \bar{S}_H - \bar{S}_H^\circ \quad (8)$$

where $\bar{H}_H^\circ$ and $\bar{S}_H^\circ$ are the values for pure titanium.

In Fig. 8, the change in the $\partial\bar{H}_H$ value with oxygen content C_O (O/Ti) is shown. The $\partial\bar{H}_H$ is found from this figure to be slightly reduced by the presence of oxygen in titanium. For the αTi(O) with an oxygen content of 0.111 O/Ti, $\partial\bar{H}_H$ = -1.6 kJ/mol. No marked change in $\partial\bar{H}_H$ was observed for the solid solutions with oxygen contents above 0.111 O/Ti.

In general, a decrease in the enthalpy requires an increase in the hydrogen solubility. The tendency in the partial molar enthalpy as can be seen in Fig. 8 seems to be in conflict with the reduction in hydrogen solubility by solute oxygen. One of the physical effects which result in decrease in partial molar enthalpy is the lattice expansion due to insertion of impurity atoms into titanium. Oxygen in titanium brings about considerable expansion of the hexagonal lattice[20]. The lattice strain resulting from solute oxygen affects the $\partial\bar{H}_H$ value. In the region of low oxygen content, $\bar{H}_H$ for a αTi(O) solid solution is approximately:

$$\bar{H}_H = \tilde{E}_H - (\bar{V}_H\bar{V}_O/V_{Ti}K_{Ti}) \times C_O$$
$$\tilde{E}_H = (\partial E/\partial n)_{V,T} \quad (9)$$

where $\tilde{E}_H$ is the partial molar energy of hydrogen at constant volume. Wagner[28] and Lupis[29] have given detailed explanations for the volume contribution to thermodynamic functions. The $\bar{V}_H$ and $\bar{V}_O$ are the partial molar volumes of hydrogen

and oxygen in titanium, and V_{Ti} (1.06×10^{-5} m^3/mol) and K_{Ti} (9.51×10^{-12} m^2/N) are the molar volume and the compressibility for pure titanium. If $\bar{E}_H$ is independent of oxygen content in titanium, the value of $\partial\bar{H}_H$ can be estimated in terms of

$$\partial\bar{H}_H = -(\bar{V}_H\bar{V}_O/V_{Ti}K_{Ti}) \times C_O. \quad (10)$$

The partial molar volume of oxygen in titanium was evaluated from the reported values of lattice parameters of αTi(O) solid solution[20] to be $1.5 - 2.5\times10^{-6}$ m^3/mol. Assuming $\bar{V}_H = 2\times10^{-6}$ m^3/mol and setting $\bar{V}_O = 2.5\times10^{-6}$ m^3/mol, the author calculated the volume contribution to $\partial\bar{H}_H$, as indicated by the dashed line in Fig. 8. It should be noted that at a low oxygen content there is no marked difference between the calculated and experimental $\partial\bar{H}_H$ values. At higher oxygen contents, the calculated values are in wide disagreement with the experimental findings. Other physical effects such as a repulsive interaction of oxygen with hydrogen and an electronic contribution of oxygen may cause the discrepancy. These effects positively contribute to the partial molar enthalpy, as the oxygen content increases.

Figure 9 shows the change in the $\partial\bar{S}_H$ value with oxygen content in αTi(O). In contrast to $\partial\bar{H}_H$, the value of $\partial\bar{S}_H$ continuously decreases with oxygen content. If non-configurational contributions to the partial molar excess entropy $\bar{S}_H$ (e.g., electronic) do not change with oxygen content, $\partial\bar{S}_H$ arises from deviation from complete randomness in the distribution of hydrogen. The strong repulsive interaction between oxygen and hydrogen in titanium lattice reduces the configurational entropy, which is the so-called "blocking effect". Introducing a site blocking factor C_t which denotes the fraction of the number of tetrahedral sites blocked by oxygen to the total number of tetrahedral sites, the partial configurational entropy term in eq. (3) may be rewritten as $kT \ln (C_H/(2-C_H-2C_t))$, or

$$\partial\bar{S}_H = k \ln (1 - C_t). \quad (11)$$

In the simple case, an oxygen atom on an octahedral site is presumed to prevent a hydrogen atom from occupying nearest tetrahedral sites. If the oxygen atom completely blocks adjacent six tetrahedral sites, the value of C_t is theoretically given by,

$$C_t = 1 - (1 - C_o)^3. \quad (12)$$

Substitution of eq. (12) into eq. (11) leads to the relation between $\partial\bar{S}_H$ and C_O shown by the dashed line in Fig. 9. The experimental $\partial\bar{S}_H$ agrees well with the

theoretical curve. Therefore, it can be concluded that an oxygen atom blocks six tetrahedral sites and that the blocking effect was hardly affected by the oxygen content.

For a αTi(O) solid solution, the negative change in the partial molar excess entropy is much larger than the corresponding change in the partial molar enthalpy. As a result, the hydrogen solubility at a fixed pressure decreases with increasing oxygen content in αTi(O) solid solution.

3.3. Deuterium solubility in the Ti-O solid solution

Measurements of deuterium solubility were made for pure titanium and αTi(O) solid solutions with oxygen contents of 0.111, 0.250 and 0.429 O/Ti. Figure 10 shows Sieverts' plots of deuterium solubility at 600°C. As shown in this figure, all the deuterium solubility data obtained for αTi(O) solutions were observed to obey Sieverts' law represented by eq. (1).

In Fig. 11, the temperature dependence of the Sieverts' constant K_D obtained for deuterium in αTi(O) solid solutions is indicated together with the results for pure titanium. It is apparent from this figure that for pure titanium and αTi(O) the linear relationships (i.e., eq. (2)) hold between the logarithm of Sieverts' constant and the reciprocal temperature. The values of A, B and ΔH obtained for deuterium solubility are listed in Table 1. The deuterium solubility decreased with the oxygen content in αTi(O). The enthalpy of solution obtained for αTi(O) was slightly lower than that for pure titanium and almost insensitive to the oxygen content. These trends were the same as those verified in hydrogen solubility.

Comparison of Fig. 11 with Fig. 5 reveals that Sieverts' constants of pure titanium and αTi(O) solid solutions are slightly smaller for deuterium than for hydrogen. As evidenced by Table 1, the enthalpy of solution for deuterium is larger than that for hydrogen. For pure titanium and αTi(O), solubility ratios between hydrogen and deuterium at a constant pressure were 1.09 to 1.23, which were consistent with the values of 1.0 - 1.2 derived from the literature data pertaining to dilute binary solutions of Ti-H and Ti-D listed in Table 2[13,14,16]. These results suggest that there exists a small isotope effect on solubility and enthalpy of solution for titanium with various oxygen contents.

The decrease in the deuterium solubility by oxygen dissolution is the same order as that in hydrogen solubility, which is attributable to repulsive interaction between deuterium and oxygen within titanium. Site occupancy of deuterium in titanium may be similar to hydrogen. The effect of oxygen on deuterium solubility can be analyzed by the dilute solution model proposed for hydrogen. The following solubility equation was applied to the deuterium data:

$$\ln (C_D\ T^{7/4}/2\ P_{D_2}{}^{1/2}\ A_{D_2}) = -\ (\bar{H}_D - E^d{}_{D_2})/kT + \bar{S}_D/k. \qquad (13)$$

Plots of $\ln (C_D\ T^{7/4}/2\ P_{D_2}{}^{1/2}\ A_{D_2})$ vs $1/T$ for deuterium in titanium and αTi(O) solid solutions are good straight lines with a slope given by $-(\bar{H}_D - E^d{}_{D_2})/k$ and with an intercept given by $\bar{S}_D/k$, as evidenced by Fig. 12. The values of the slope and the intercept yielded $\bar{H}_D - E^d{}_{D_2} = -28.5$ kJ/mol and $\bar{S}_D = 37.0$ J/mol K for pure titanium.

The changes in the deuterium solubility and the enthalpy of solution by incorporation of oxygen into titanium lattice were discussed on the basis of the differences in the partial molar enthalpy and excess entropy between pure titanium and αTi(O), defined as:

$$\partial\bar{H}_D = \bar{H}_D - \bar{H}_D{}^\circ \text{ and } \partial\bar{S}_D = \bar{S}_D - \bar{S}_D{}^\circ \qquad (14)$$

where $\bar{H}_D{}^\circ$ and $\bar{S}_D{}^\circ$ are the values for pure titanium. The changes in the $\partial\bar{H}_D$ and $\partial\bar{S}_D$ values with composition are shown in Figs. 13 and 14, together with the values for hydrogen.

As shown in Fig. 13, the partial molar enthalpy $\bar{H}_D$ for deuterium in titanium decreases with oxygen addition, which may be due to a lattice strain effect of solute oxygen. The change in $\partial\bar{H}$ value with oxygen content in αTi(O) scarcely differs from deuterium to hydrogen. On the assumption that the partial molar volume of deuterium in titanium is the same as that of hydrogen, the theoretical $\partial\bar{H}_D$ values were estimated, indicated by the dashed line in Fig. 13. There exists a large discrepancy between theoretical and experimental values at a high oxygen content.

As indicated in Fig. 14, $\partial\bar{S}_D$ appreciably decreases with oxygen content. The site blocking effect of oxygen is likely to cause the decrease in $\partial\bar{S}_D$. The dashed line in Fig. 14 reveals the theoretical $\partial\bar{S}_D$ value calculated from eqs. (11) and (12). The experimental data for both deuterium and hydrogen agree well with the theoretical curve.

The marked decrease in the partical molar excess entropy accounts for the reduction of deuterium solubility in αTi(O) solid solutions. There was no marked difference in $\partial\bar{H}$ and $\partial\bar{S}$ between hydrogen and deuterium. This may result from resemblance of the existing state in pure titanium and αTi(O) solid solutions. between hydrogen and deuterium

3.4. Isotope effect of hydrogen and deuterium solubilities

Comparison of the data for hydrogen with those for deuterium enables us to interpret the isotope effect on the solubilities in pure titanium and αTi(O) solid

solutions. The difference in the solubility between them can be written by

$$\ln [(C_H\ T^{7/4}/2\ P_{H_2}{}^{1/2}\ A_{H_2})/(C_D\ T^{7/4}/2\ P_{D_2}{}^{1/2}\ A_{D_2})]$$
$$= -[(\bar{H}_H - \bar{H}_D) - (E^d{}_{H_2} - E^d{}_{D_2})]/kT + (\bar{S}_H - \bar{S}_D)/k. \quad (15)$$

With the assumption that interstitial hydrogen and deuterium atoms in titanium behave as simple harmonic oscillators, the $\bar{H}_H - \bar{H}_D$ and the $\bar{S}_H - \bar{S}_D$ can be expressed in terms of vibrational frequencies of hydrogen and deuterium atoms (ν_H and ν_D) as follows:

$$\bar{H}_H - \bar{H}_D = 3\ (h\nu_H - h\nu_D)/2$$
$$+ 3\ [h\nu_H/(\exp(h\nu_H/kT) - 1) - h\nu_D/(\exp(h\nu_D/kT) - 1)] \quad (16)$$

$$\bar{S}_H - \bar{S}_D = -3k \ln [(1 - \exp(-h\nu_H/kT))/(1 - \exp(-h\nu_D/kT))]$$
$$+ 3\ [h\nu_H/(\exp(h\nu_H/kT) - 1)/T - h\nu_D/(\exp(h\nu_D/kT) - 1)/T]. \quad (17)$$

Setting $\nu_D = \nu_H/\sqrt{2}$, the right hand side of eq. (15) can be expressed as a function of the vibrational frequeny of hydrogen atom:

$$\ln [(C_H\ T^{7/4}/2\ P_{H_2}{}^{1/2}\ A_{H_2})/(C_D\ T^{7/4}/2\ P_{D_2}{}^{1/2}\ A_{D_2})]$$
$$= -3\ (1 - 1/\sqrt{2})(h\nu_H/kT)/2 + (E^d{}_{H_2} - E^d{}_{D_2})/kT$$
$$- 3 \ln [(1 - \exp(-h\nu_H/kT))/(1 - \exp(-h\nu_H/\sqrt{2}kT))]. \quad (18)$$

The $E^d{}_{H_2} - E^d{}_{D_2}$, A_{H_2} and A_{D_2} in eq. (18) can be evaluated from the published data[26,27].

In Fig. 15, the values of $\ln [(C_H\ T^{7/4}/2\ P_{H_2}{}^{1/2}\ A_{H_2})/(C_D\ T^{7/4}/2\ P_{D_2}{}^{1/2}\ A_{D_2})]$ obtained from the experimental data of hydrogen and deuterium solubilities were plotted against the reciprocal temperature 1/T. There appears little correlation between the experimental value and the oxygen content in titanium. Dashed curves in this figure were drawn from eq. (18) using vibrational frequencies ν_H of 800 - 1200 cm^{-1}. The experimental values distributed around the theoretical curve for ν_H = 1000 cm^{-1}, independent of the oxygen content in titanium.

Dantzer[19] has found from microcalorimetric studies at 733 K that the frequency of hydrogen atom is 970 cm^{-1} in αTi. Kohoda-Bakhsh et al.[23] have performed inelastic neutron scattering in αTiH_x at 588 K and reported a well defined peak at ν_H = 1135 cm^{-1}. The frequency of 1000 cm^{-1} estimated in the present study is fairly in accord with the reported values.

Consequently, the isotope effect on solubility is expected to arise mainly from different vibrational frequencies between hydrogen and deuterium atoms in titanium. The vibrational mode of hydrogen isotope atom may not be influenced by

coexisting oxygen atoms.

3.5. Estimation of tritium solubility

The tritium solubility in pure titanium and α Ti(O) solid solutions was estimated from the data for hydrogen and deuterium. The following relations analogous to eq. (15) hold between hydrogen, deuterium and tritium:

$$\ln [(C_T\ T^{7/4}/2\ P_{T_2}{}^{1/2}\ A_{T_2})/(C_H\ T^{7/4}/2\ P_{H_2}{}^{1/2}\ A_{H_2})] = -[(\bar{H}_T - \bar{H}_H) - (E^d{}_{T_2} - E^d{}_{H_2})]/kT + (\bar{S}_T - \bar{S}_H)/k. \quad (19)$$

and

$$\ln [(C_T\ T^{7/4}/2\ P_{T_2}{}^{1/2}\ A_{T_2})/(C_D\ T^{7/4}/2\ P_{D_2}{}^{1/2}\ A_{D_2})] = -[(\bar{H}_T - \bar{H}_D) - (E^d{}_{T_2} - E^d{}_{D_2})]/kT + (\bar{S}_T - \bar{S}_D)/k. \quad (20)$$

The isotope effect on the solubility is ascribed to the difference in vibrational frequency between hydrogen isotopes. Introducing the approximation that $\nu_T = \nu_H/\sqrt{3}$ and $\nu_D = \nu_H/\sqrt{2}$ provides the enthalpy terms of $\bar{H}_T - \bar{H}_H$ and $\bar{H}_T - \bar{H}_D$ and the entropy terms of $\bar{S}_T - \bar{S}_H$ and $\bar{S}_T - \bar{S}_D$, being a function of ν_H. The difference in dissociation energy of molecule in the gas (i.e., $E^d{}_{T_2} - E^d{}_{H_2}$ and $E^d{}_{T_2} - E^d{}_{D_2}$) and the value of A_{T_2} were calculated from universal constants and spectroscopic constants provided in the literature[26,27]. The value of 1000 cm^{-1} was used as the frequency of hydrogen atom in titanium. Thus, the value of ln ($C_T\ T^{7/4}/2\ P_{T_2}{}^{1/2}\ A_{T_2}$) for tritium was calculated by the use of solubility data for either hydrogen or deuterium. The estimated values are illustrated in Fig. 16. As indicated in this figure, the ln ($C_T\ T^{7/4}/2\ P_{T_2}{}^{1/2}\ A_{T_2}$) values calculated from the hydrogen data show agreement with those from the deuterium data. Sieverts' constants for tritium, K_T, were evaluated from the ln ($C_T\ T^{7/4}/2\ P_{T_2}{}^{1/2}\ A_{T_2}$) values thus obtained, and they conformed to eq. (2). The temperature dependence of the Sieverts' contant for tritium is shown in Fig. 17. The parameters A and B in eq. (2) and the enthalpy of solution of tritium are summarized in Table 1. The solubility in pure titanium and α Ti(O) solid solutions decreased in the order hydrogen, deuterium, tritium. Experimental measurements for solubility of tritium in titanium are needed to ascertain the validity of the estimated tritium solubility.

These results led to the quantitative expressions for the influence of oxygen contamination on solubility of hydrogen isotope in titanium. Since the solubilities of hydrogen isotopes in α phase, C_U (U/Ti, U = H, D and T), obey Sieverts' law, C_U is expressed by

$$C_U = (a + \exp(b/T)) \times P_{U2}^{1/2}. \quad (21)$$

Postulating that a and b in eq. (21) can be expressed as a function of oxygen content C_O (O/Ti) as follows:

$$a = a_0 (1 + a_1 C_O + a_2 C_O^2) \text{ and } b = b_0 (1 + b_1 C_O + b_2 C_O^2) \quad (22)$$

where a_0 and b_0 are the values for pure titanium, the best estimates of $a_{1,2}$ and $b_{1,2}$ were obtained by applying the method of least squares to the experimental and estimated solubility data, as listed in Table 3. These values and eqs. (21) and (22) allow us to predict the solubility of hydrogen isotope in titanium contaminated by oxygen.

4. Conclusions

The solubilities of hydrogen and deuterium in pure titanium and αTi(O) solid solutions (O/Ti atom ratio = 0.111 - 0.429) have been measured at temperatures of 600 - 850°C.

The isothermal section of the Ti-O-H system at 600°C was constructed from isothermal hydrogen pressure-hydrogen content relations. Oxygen slightly increased the terminal solubility in the α solution at the boundary between the α and $\alpha + \beta$ phases.

At pressures less than 10^2 Pa, all the solubility data for hydrogen and deuterium in pure titanium and αTi(O) solid solutions closely obeyed Sieverts' law. The solubility for hydrogen in titanium and αTi(O) solid solutions was larger than that for deuterium. Oxygen dissolved in titanium significantly reduced solubilities of hydrogen isotopes. The enthalpy of solution was slightly lower for αTi(O) than for pure titanium and scarcely varied with the oxygen content in titanium.

The simple model was proposed to estimate the partial thermodynamic functions of the dilute Ti-O-H and Ti-O-D ternary solid solutions. The decrease in the solubility was explained mainly by taking reduction in the partial molar excess entropy into account. There was no marked difference in the extent of the solute effect of oxygen between hydrogen and deuterium.

The isotope effect on the solubility was discussed on the assumption that interstitial hydrogen and deuterium atoms in the titanium matrix can be characterized only by vibrational motion. The vibrational frequency of hydrogen atom in titanium was obtained, which permitted to predict the solubility of tritium in pure titanium and αTi(O). The estimated tritium solubility was the

lowest among hydrogen isotopes.

When titanium is adopted as a tritium getter in the fuel cycle of fusion reactor, the adverse effect on sorption capacity and life time induced by oxygen contamination should be born in mind. The quantitative expressions for the influence of oxygen on solubilities of hydrogen isotopes will provide a foundation of design criteria for tritium processing with titanium bearing materials.

References

[1] P.E. Stott, C.C. Daughney and R.A. Ellis, Jr., Nucl. Fusion, 15(1975)431.
[2] R.J. Taylor, R.F. Bunshah and F. Schwirzke, J. Nucl. Mater., 93&94(1980)338.
[3] R.J. Taylor, J. Nucl. Mater., 145-147(1987)700.
[4] N.P. Kherani and W.T. Shmayda, Fusion Technology, 8(1985)2399.
[5] E. Willin, M. Sirch, R.D. Penzhorn and M. Devillers, Fusion Technology, 14(1988)756.
[6] F. Mannone and H. Dworschak, Fusion Engineering and Design, 5(1988)385.
[7] M. Nishikawa, H. Kido, K. Kotoh and M. Sugisaki, J. Nucl. Mater., 115(1983)101.
[8] R.I. Jaffee and I.E. Campbell, Trans. AIME, 185(1949)646.
[9] G.A. Lenning, C.M. Craighead and R.I. Jaffee, ibid., 200(1954)367.
[10] M. Nagasaka and T. Yamashina, Japan J. Appl. Phys. Suppl. 2, Pt. 1, (1974)61.
[11] J.W. Reichardt, J. Vac. Sci. Technol., 9(1971)548.
[12] A.D. McQuillan, Proc. Roy. Soc., 204(1950)309.
[13] T.A. Giorgi and F. Ricca, Nuovo Cimento, Suppl. 5, (1967)472.
[14] M. Nagasaka and T. Yamashina, J. Less-Common Metals, 45(1976)53.
[15] E. Veleckis and A.G. Rogers, ibid., 97(1984)79.
[16] K. Watanabe, J. Nucl. Mater., 136(1985)1.
[17] M. T. Hepworth and R. Schuhmann, Jr., Trans. Metall. Soc. AIME, 224(1962)928.
[18] A. Jostsons and A.E. Jenkins, ibid., 239(1967)1318.
[19] P. Dantzer, J. Phys. Chem. Solids, 44(1983)913.
[20] J.L. Murray, Phase Diagrams of Binary Titanium Alloys, (ASM, Ohio, 1987).
[21] M. Hirabayashi and S. Yamaguchi, Bull. Japan Inst. Metals, 10(1971)591.
[22] H. Pinto, C. Korn, S. Goren and M. Shaked, Solid State Commun., 32(1979)397.
[23] R. Khoda-Bakhsh and D.K. Ross, J. Phys. F, 12(1982)15.
[24] R.B. McLellan, Phase Stability in Metals and Alloys, (McGraw-Hill, New York, 1967).
[25] R.B. McLellan and M. Yoshihara, Acta Metall., 35(1987)197.
[26] G. Herzberg, Molecular Spectra and Molecular Structure, Vol. 1, (D. Van Nostrand Company, Inc., New York, 1950).
[27] M.W. Chase Jr., C.A. Davies, J.R. Downey Jr., D.J. Frurip, R.A. McDonald and A.N. Syverud, JANAF Thermochemical Tables, 3rd. Ed., (American Institute of Physics, Inc., New York, 1985).
[28] C. Wagner, Acta Metall., 19(1971)843.
[29] C.H.P. Lupis, ibid., 26(1978)211.

Table 1 Parameters of Sieverts' law A and B and enthalpy of solution ΔH.

Oxygen Content(O/Ti)	Isotope	A	B	ΔH(kJ/g-atom)
0	H_2	-11.6	5450	-45.3
	D_2	-11.5	5200	-43.2
	T_2*	-11.5	5190	-43.2
0.111	H_2	-11.9	5680	-47.2
	D_2	-11.9	5470	-45.5
	T_2*	-11.9	5430	-45.2
0.176	H_2	-12.1	5670	-47.1
0.250	H_2	-12.4	5590	-46.5
	D_2	-12.4	5510	-45.8
	T_2*	-12.3	5410	-45.0
0.333	H_2	-12.7	5620	-46.7
0.429	H_2	-13.2	5500	-45.7
	D_2	-13.1	5310	-44.2
	T_2*	-13.2	5330	-44.3

* Estimated value

Table 2 Parameters of Sieverts' law A and B and enthalpy of solution ΔH for pure titanium reported in the literature[12-16].

Isotope	Temperature range(°C)	A	B	ΔH(kJ/g-atom)	Ref.
H_2	600 - 850	-11.6	5450	-45.3	*
	480 - 900	-11.6	5640	-46.9	[12]
	350 - 800	-12.0	6090	-50.6	[13]
	500 - 800	-13.1	6340	-52.7	[14]
	370 - 850	-12.1	6090	-50.6	[15]
	420 - 840	-11.6	5350	-44.5	[16]
D_2	600 - 850	-11.5	5200	-43.2	*
	350 - 800	-11.5	6040	-50.2	[13]
	500 - 800	-13.1	6340	-52.7	[14]
	420 - 850	-11.6	5270	-43.8	[16]

* The present study

Table 3 Parameters $a_{0,1,2}$ and $b_{0,1,2}$ in eq. (22).

	H_2	D_2	T_2
$a_0 \times 10^5$	0.926	1.04	1.00
a_1	-2.66	-3.12	-2.80
a_2	1.90	2.89	2.13
$b_0 \times 10^{-3}$	5.45	5.20	5.19
b_1	0.352	0.551	0.405
b_2	-0.786	-1.18	-0.810

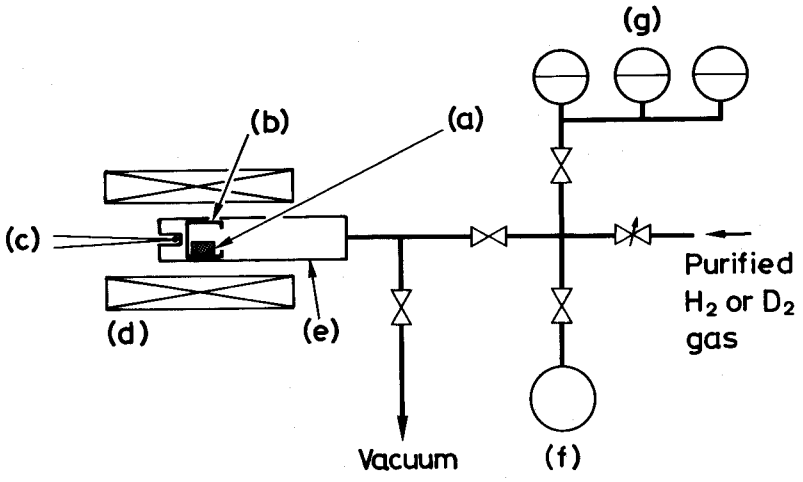

Fig. 1 Schematic diagram of experimental apparatus.
(a) specimen, (b) molybdenum crucible, (c) thermocouple, (d) furnace, (e) quartz tube, (f) standard volume, (g) capacitance manometer.

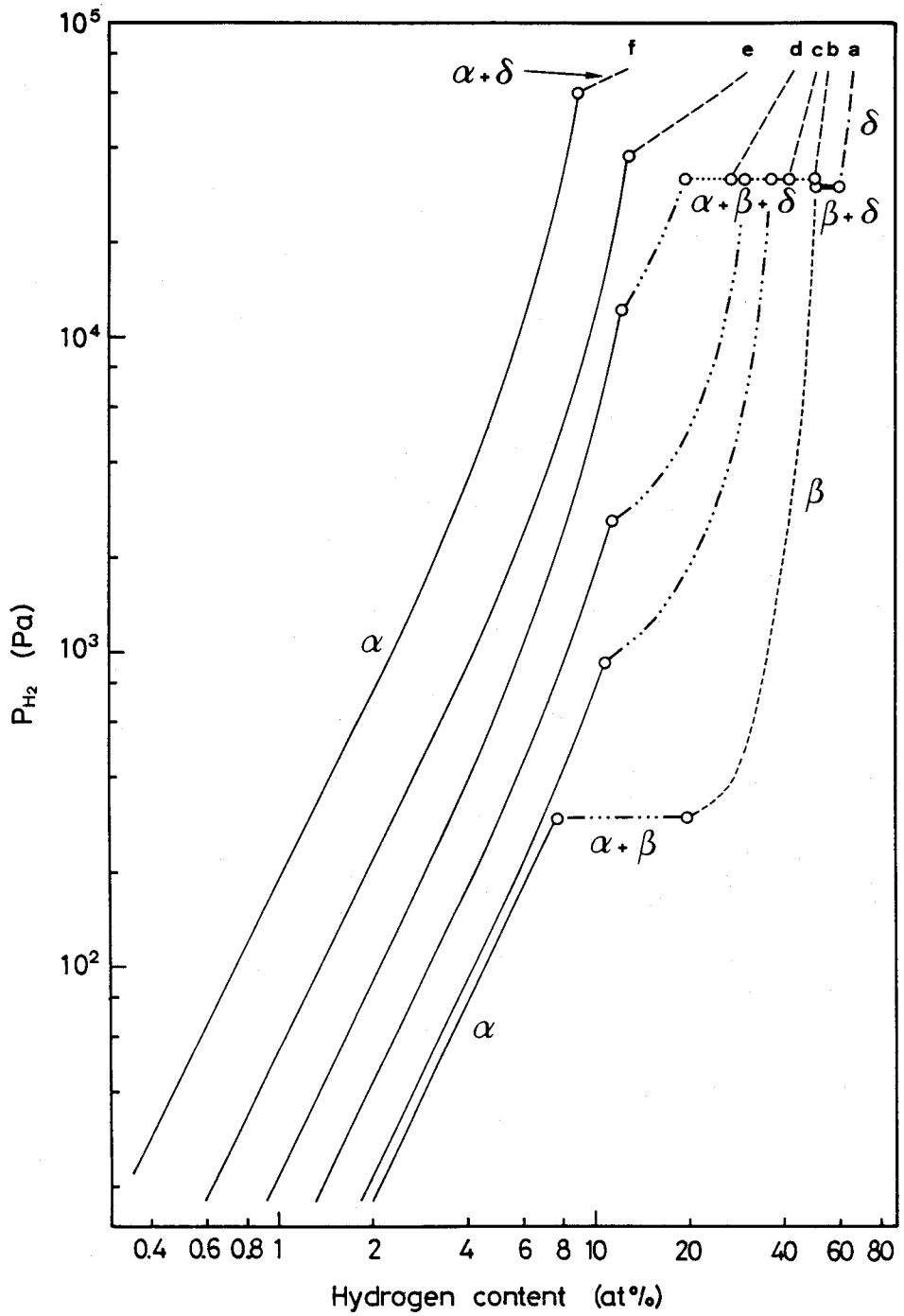

Fig. 2 Isothermal hydrogen pressure-hydrogen content curves for pure titanium and αTi(O) solid solutions at 600°C.
(a) pure titanium, (b) 0.111 O/Ti, (c) 0.176 O/Ti, (d) 0.250 O/Ti, (e) 0.333 O/Ti, (f) 0.429 O/Ti.

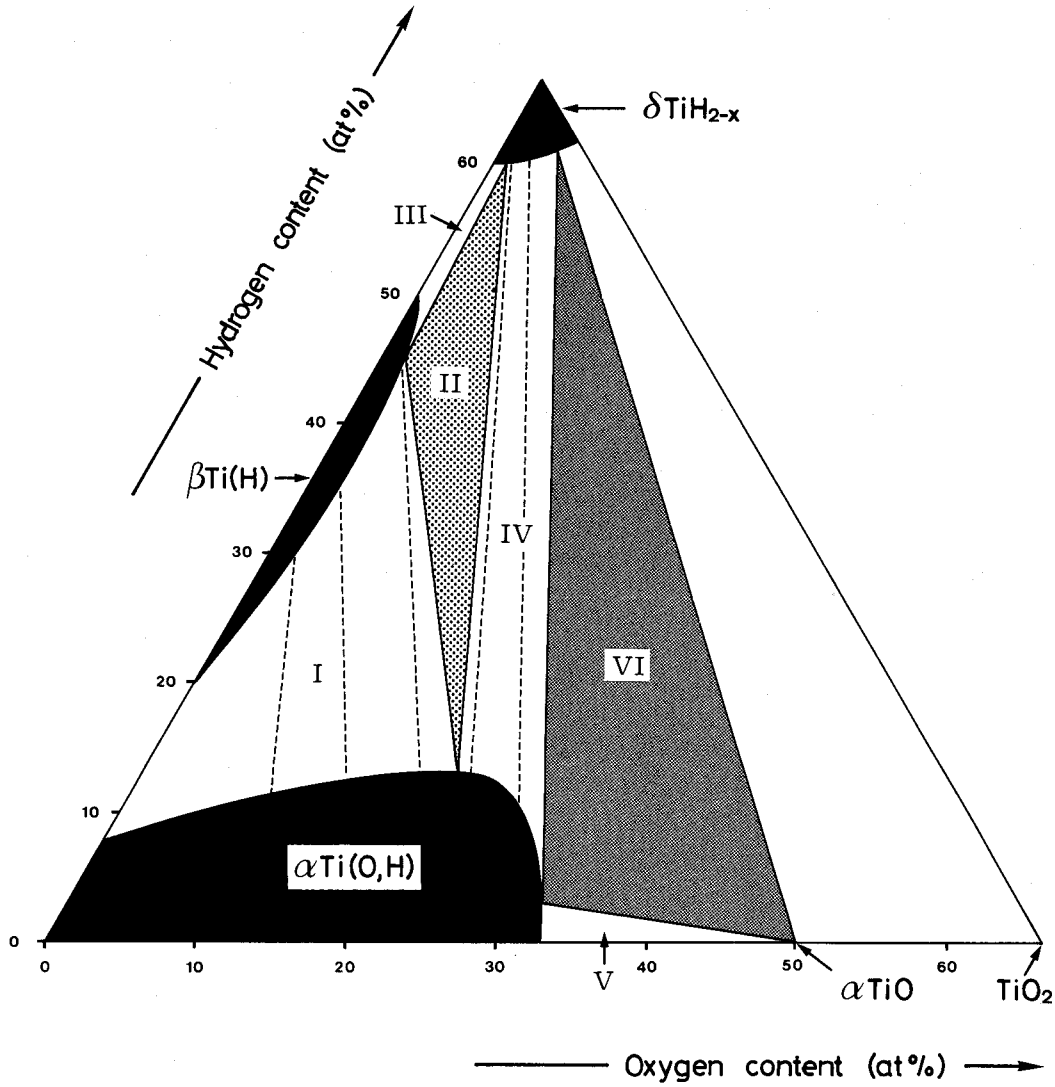

Fig. 3 Isothermal section of the Ti-O-H ternary system at 600°C.

Ⅰ αTi(O,H) + βTi(H), Ⅱ αTi(O,H) + βTi(H) + δTiH_{2-x},

Ⅲ βTi(H) + δTiH_{2-x}, Ⅳ αTi(O,H) + δTiH_{2-x},

Ⅴ αTi(O,H) + αTiO, Ⅵ αTi(O,H) + δTiH_{2-x} + αTiO.

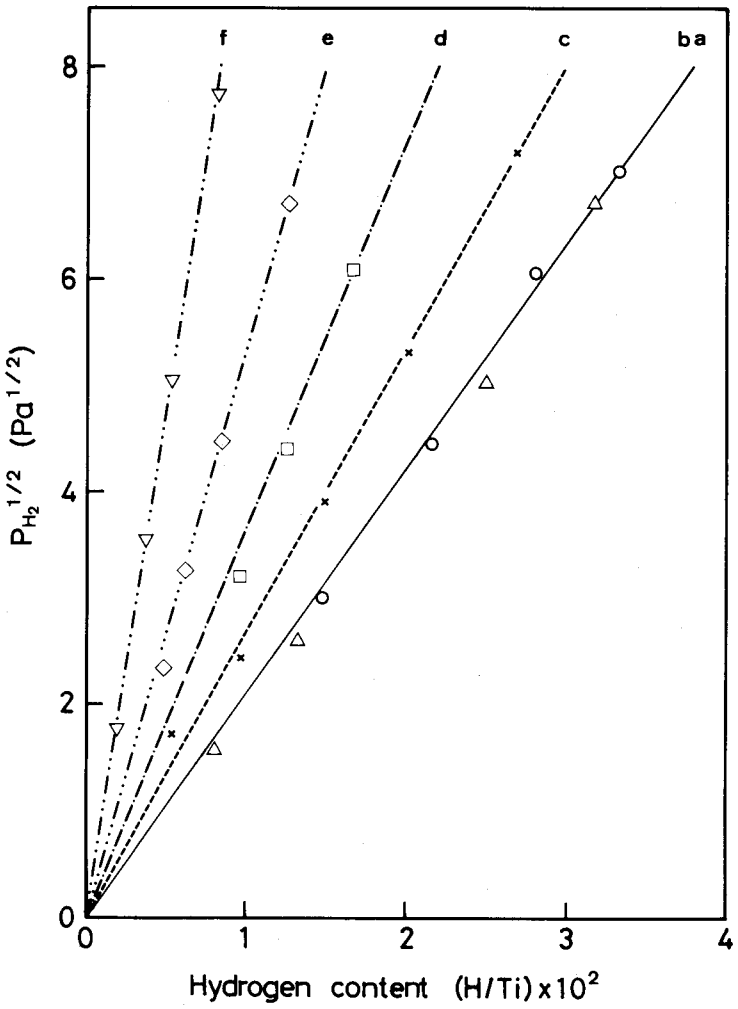

Fig. 4 Sieverts' plot for hydrogen in pure titanium and αTi(O) solid solutions at 600°C.
(a) pure titanium, (b) 0.111 O/Ti, (c) 0.176 O/Ti, (d) 0.250 O/Ti, (e) 0.333 O/Ti, (f) 0.429 O/Ti.

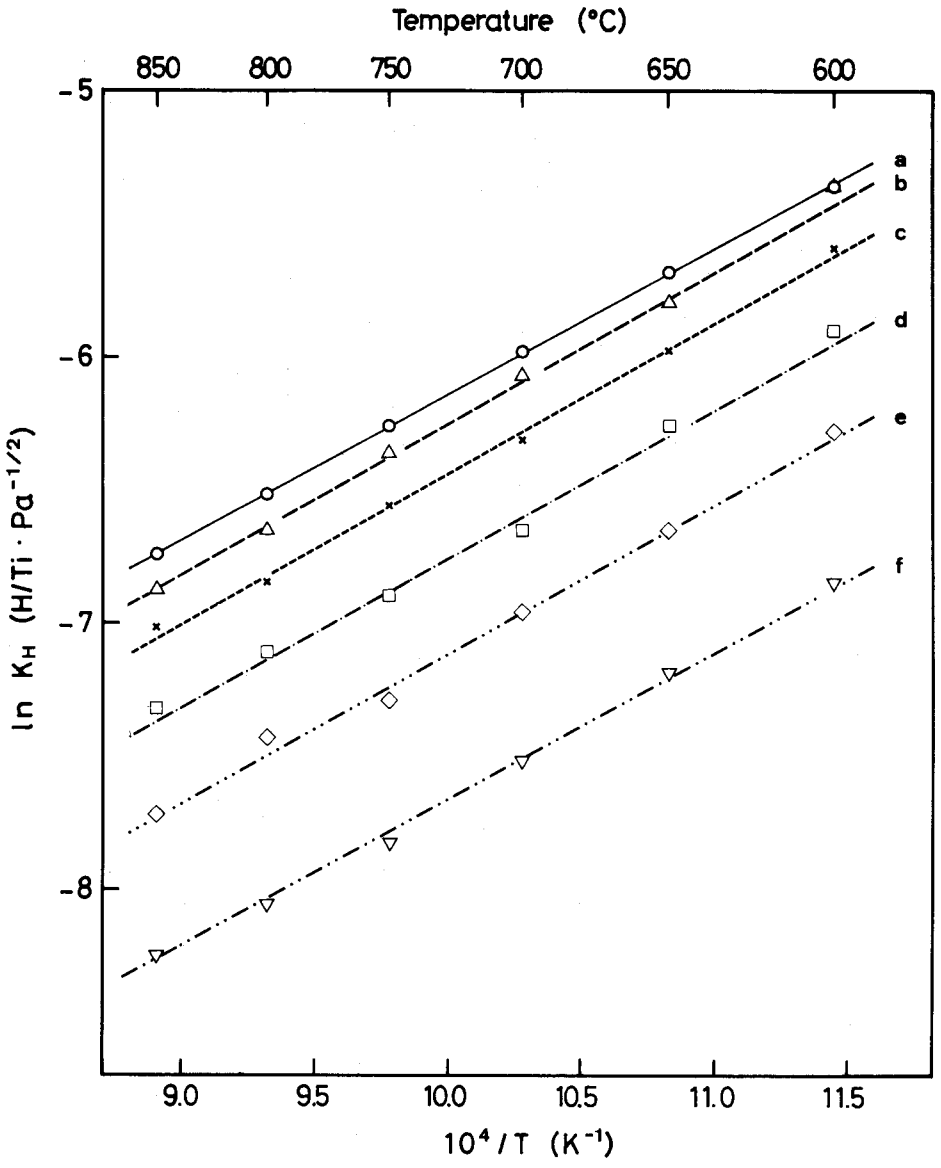

Fig. 5 Temperature dependence of Sieverts' constant K_H for hydrogen in pure titanium and αTi(O) solid solutions.
(a) pure titanium, (b) 0.111 O/Ti, (c) 0.176 O/Ti, (d) 0.250 O/Ti, (e) 0.333 O/Ti, (f) 0.429 O/Ti.

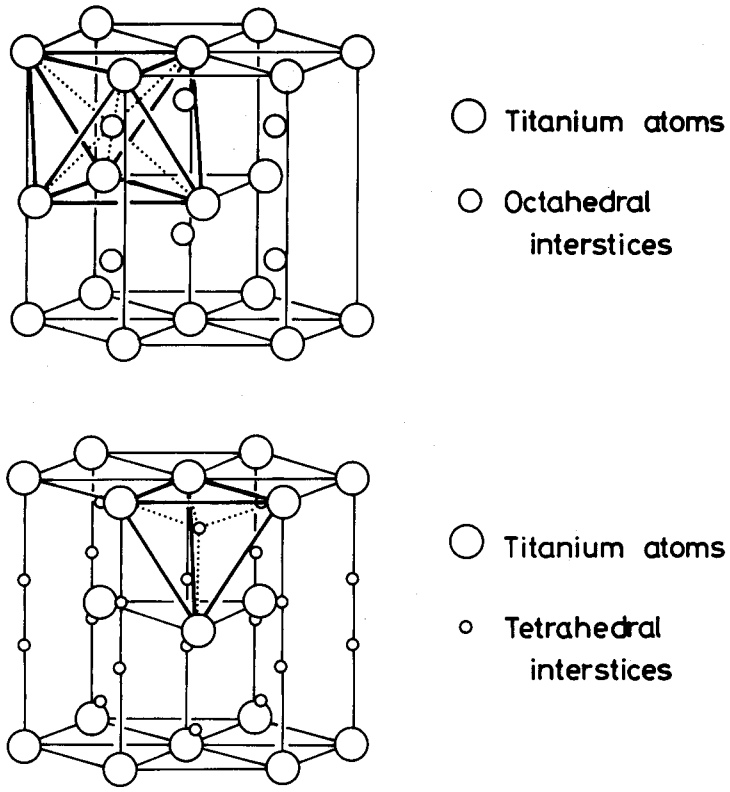

Fig. 6 Locations of interstitial sites in hexagonal titanium lattice.

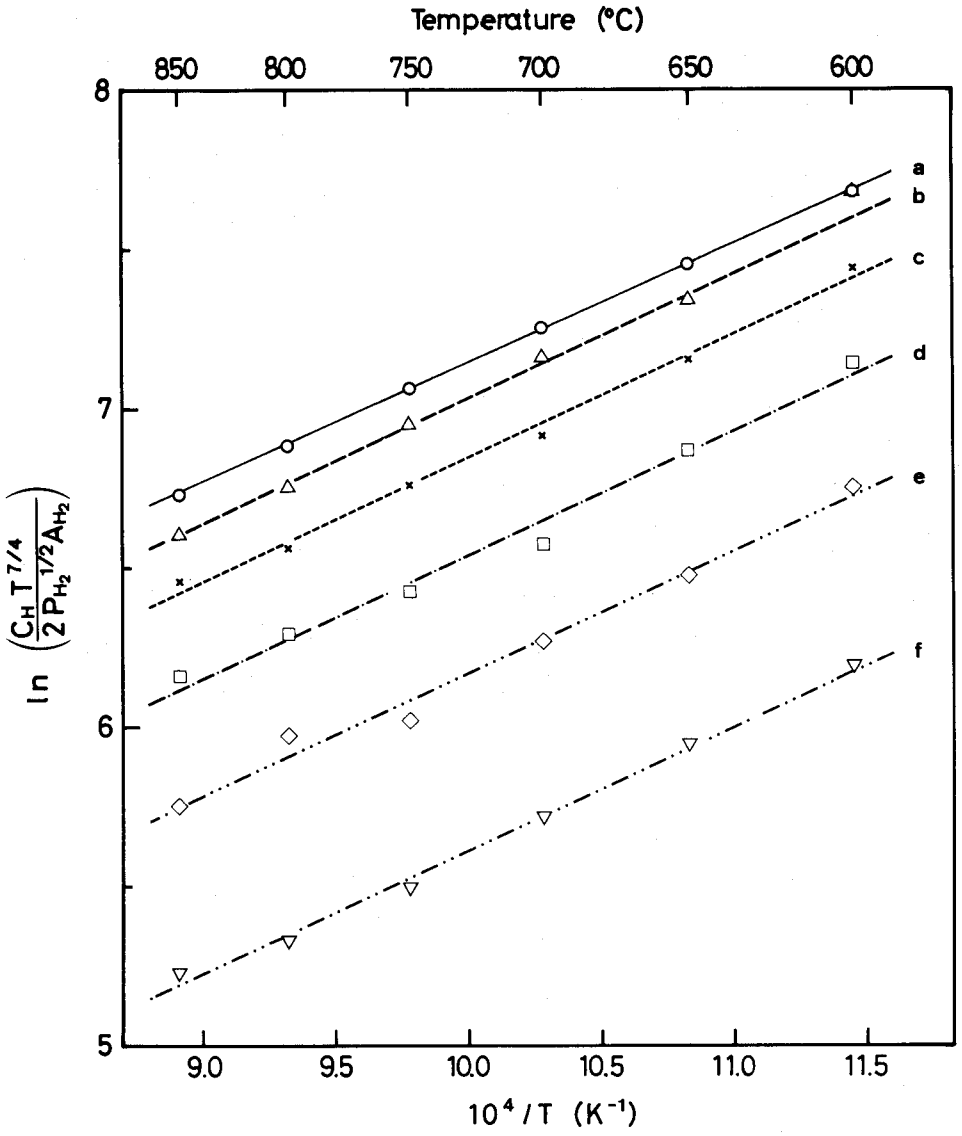

Fig. 7 Thermodynamic analysis of hydrogen solubility in αTi(O) solid solution.

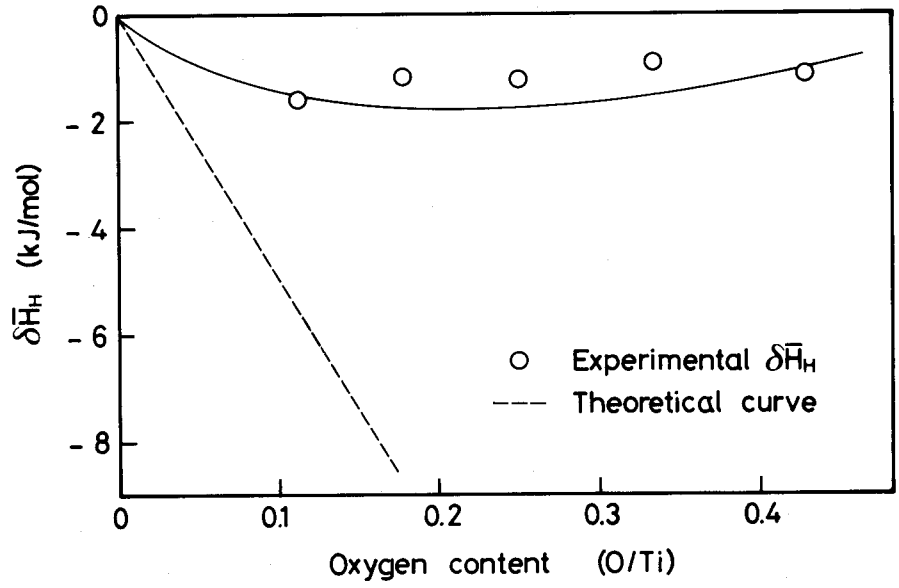

Fig. 8 Change in $\delta\bar{H}_H$ value with oxygen content in αTi(O) solid solution.

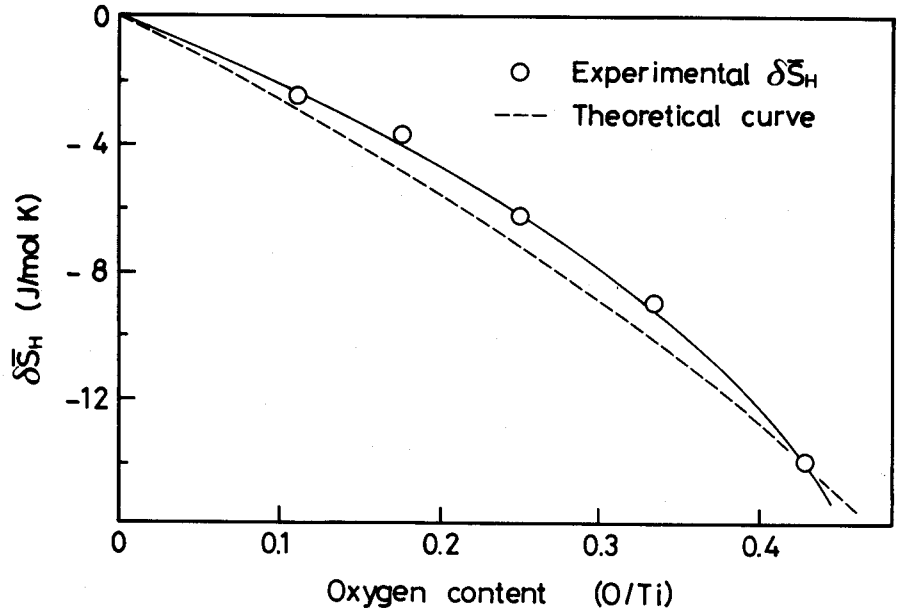

Fig. 9 Change in $\delta\bar{S}_H$ value with oxygen content in αTi(O) solid solution.

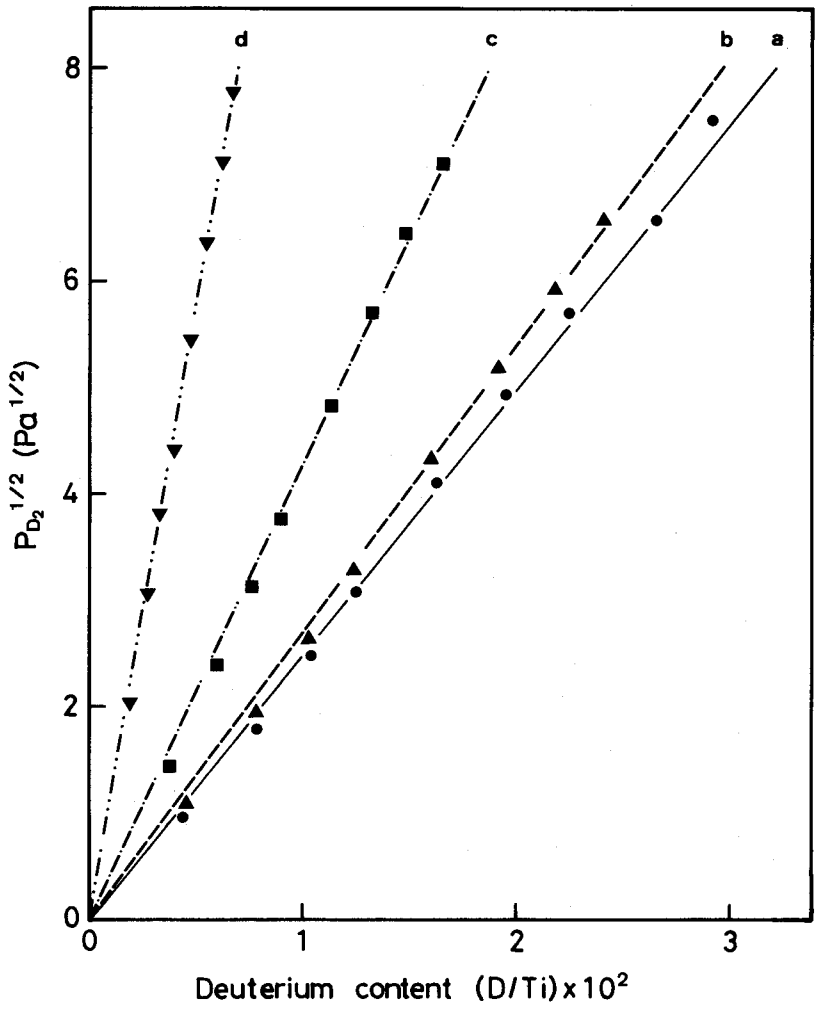

Fig. 10 Sieverts' plot for deuterium in pure titanium and αTi(O) solid solutions at 600°C.
(a) pure titanium, (b) 0.111 O/Ti, (c) 0.250 O/Ti, (d) 0.429 O/Ti.

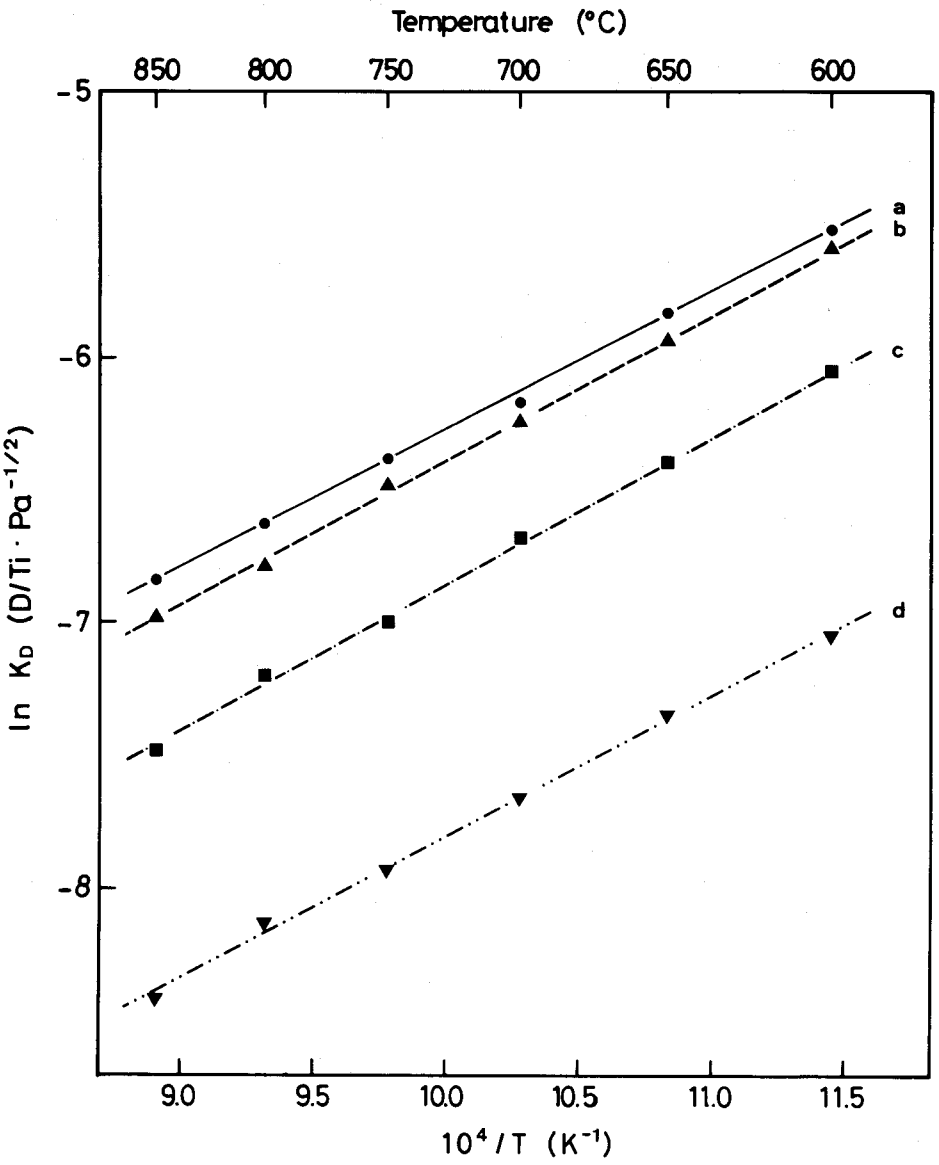

Fig. 11 Temperature dependence of Sieverts' constant K_D for deuterium in pure titanium and α Ti(O) solid solutions.
(a) pure titanium, (b) 0.111 O/Ti, (c) 0.250 O/Ti, (d) 0.429 O/Ti.

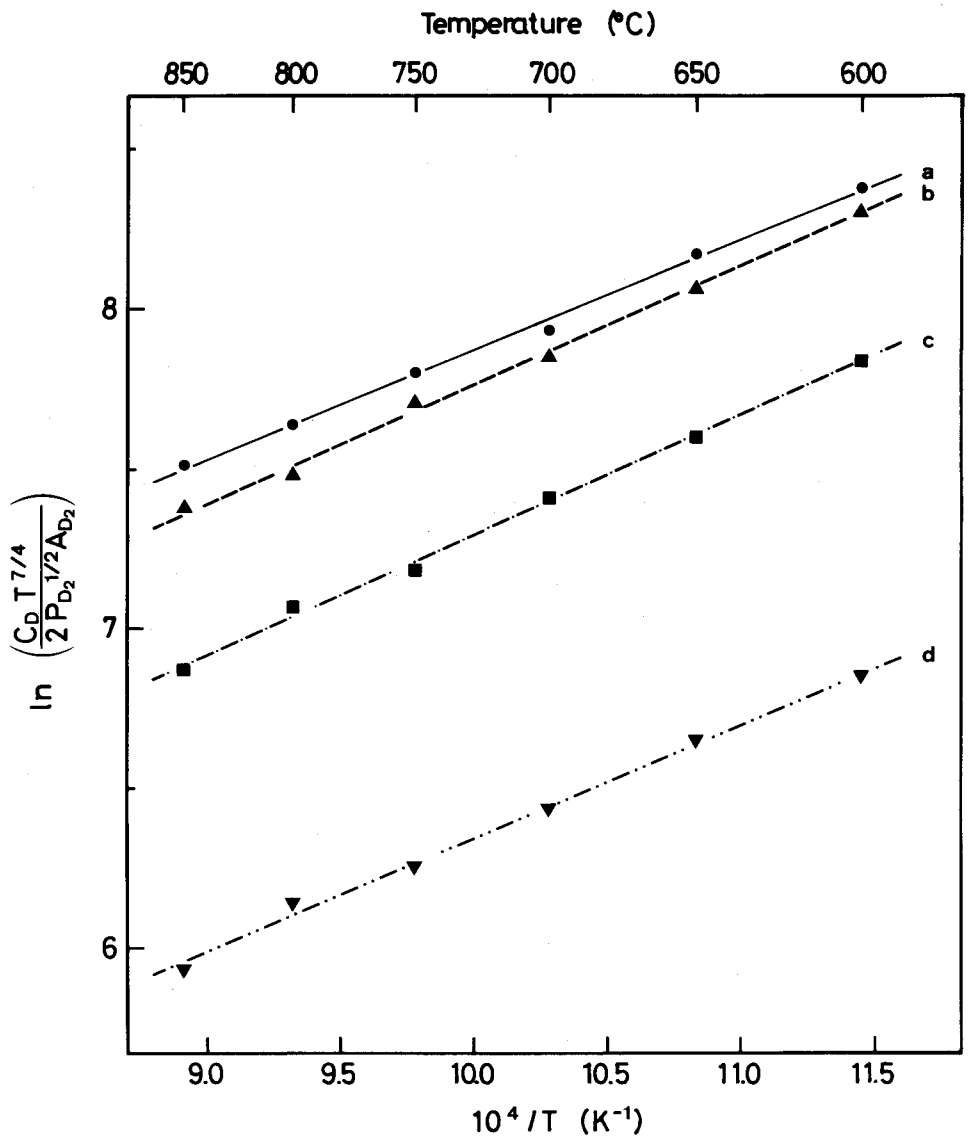

Fig. 12 Thermodynamic analysis of deuterium solubility in αTi(O) solid solution. (a) pure titanium, (b) 0.111 O/Ti, (c) 0.250 O/Ti, (d) 0.429 O/Ti.

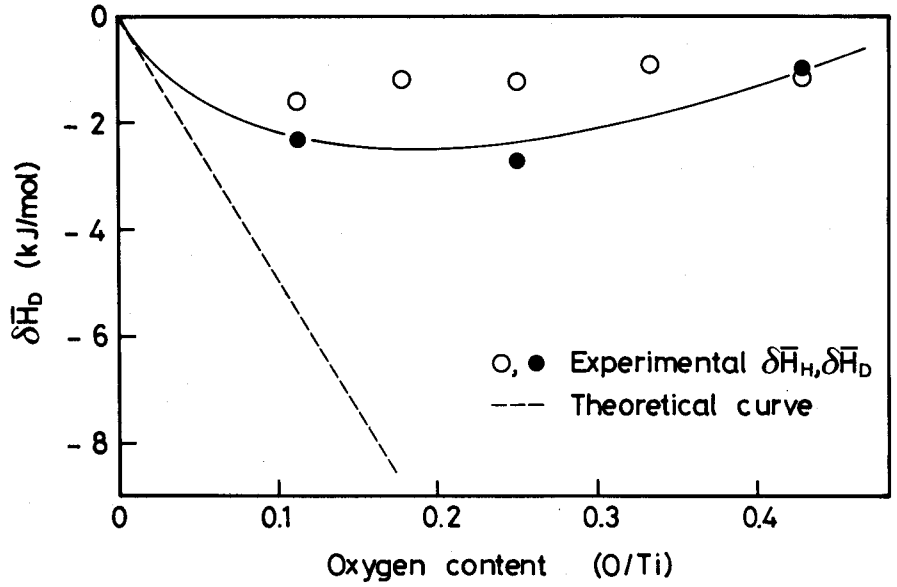

Fig. 13 Change in $\delta\bar{H}_D$ value with oxygen content in αTi(O) solid solution.

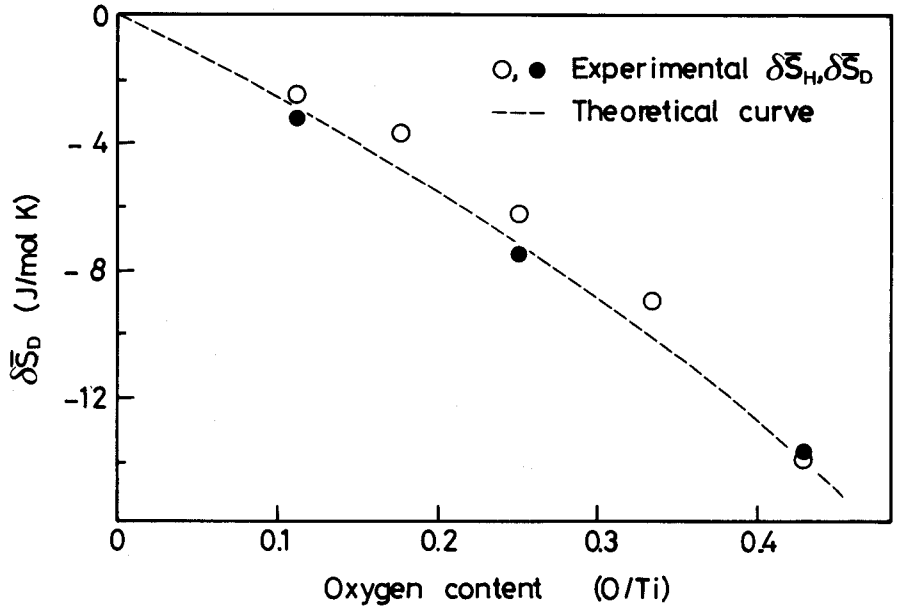

Fig. 14 Change in $\delta\bar{S}_D$ value with oxygen content in αTi(O) solid solution.

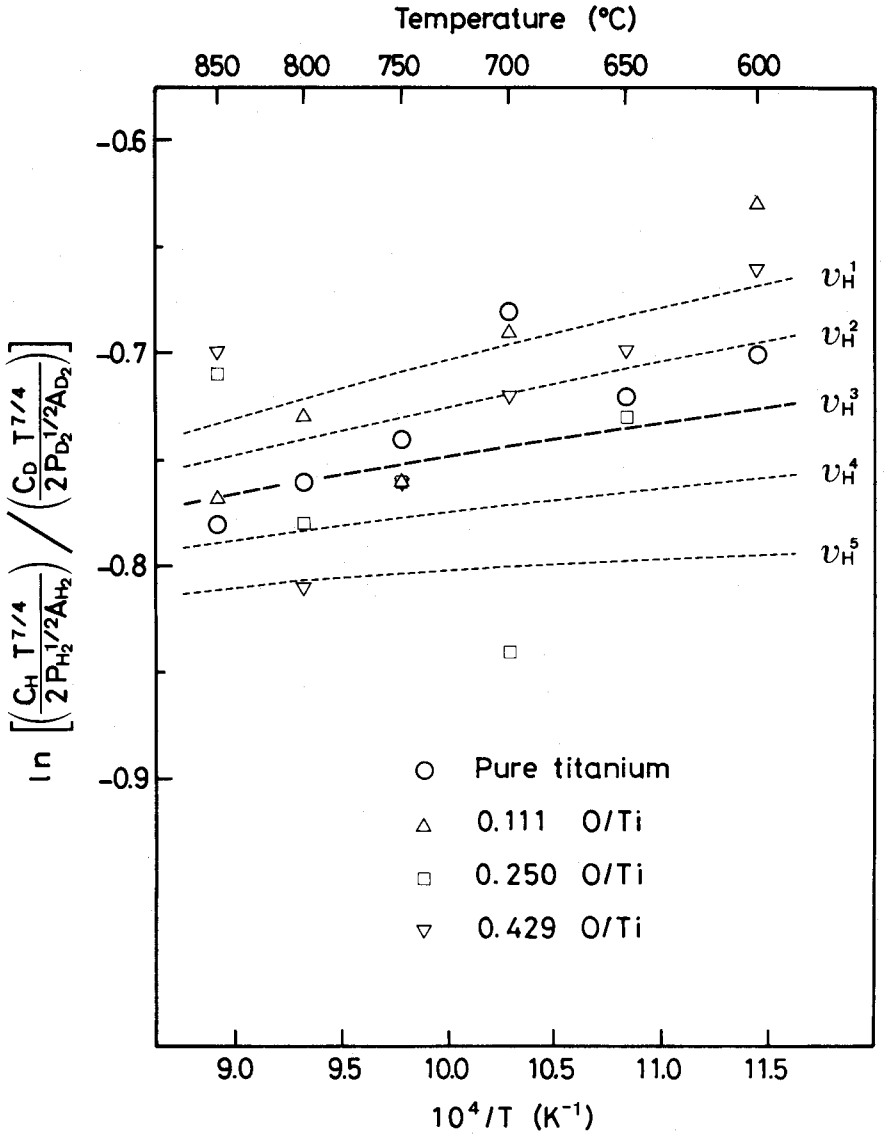

Fig. 15 Isotope effect on solubility in pure titanium and αTi(O) solid solutions.

ν_H^1 = 800 cm^{-1}, ν_H^2 = 900 cm^{-1}, ν_H^3 = 1000 cm^{-1}, ν_H^4 = 1100 cm^{-1}, ν_H^5 = 1200 cm^{-1}.

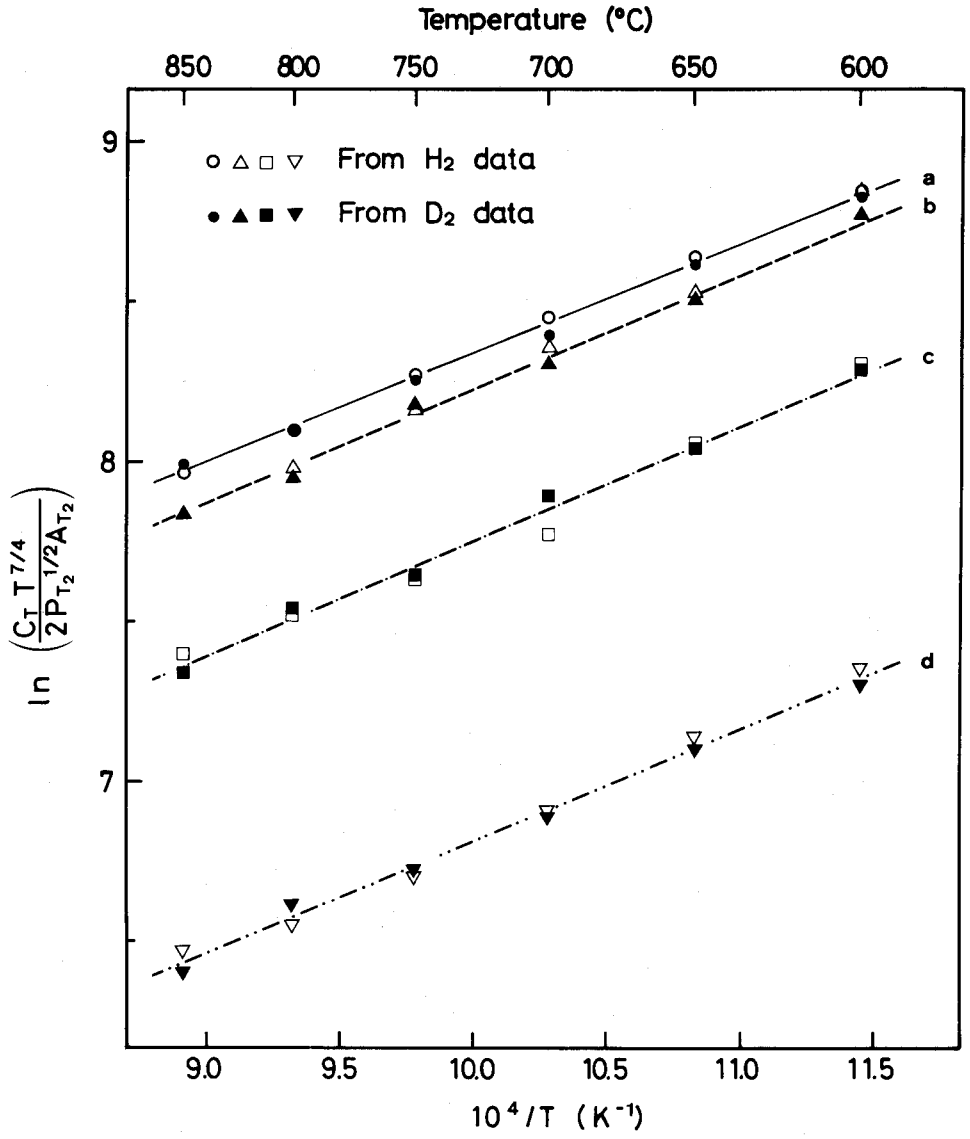

Fig. 16 Estimation of tritium solubility in pure titanium and αTi(O) solid solutions.
(a) pure titanium, (b) 0.111 O/Ti, (c) 0.250 O/Ti, (d) 0.429 O/Ti.

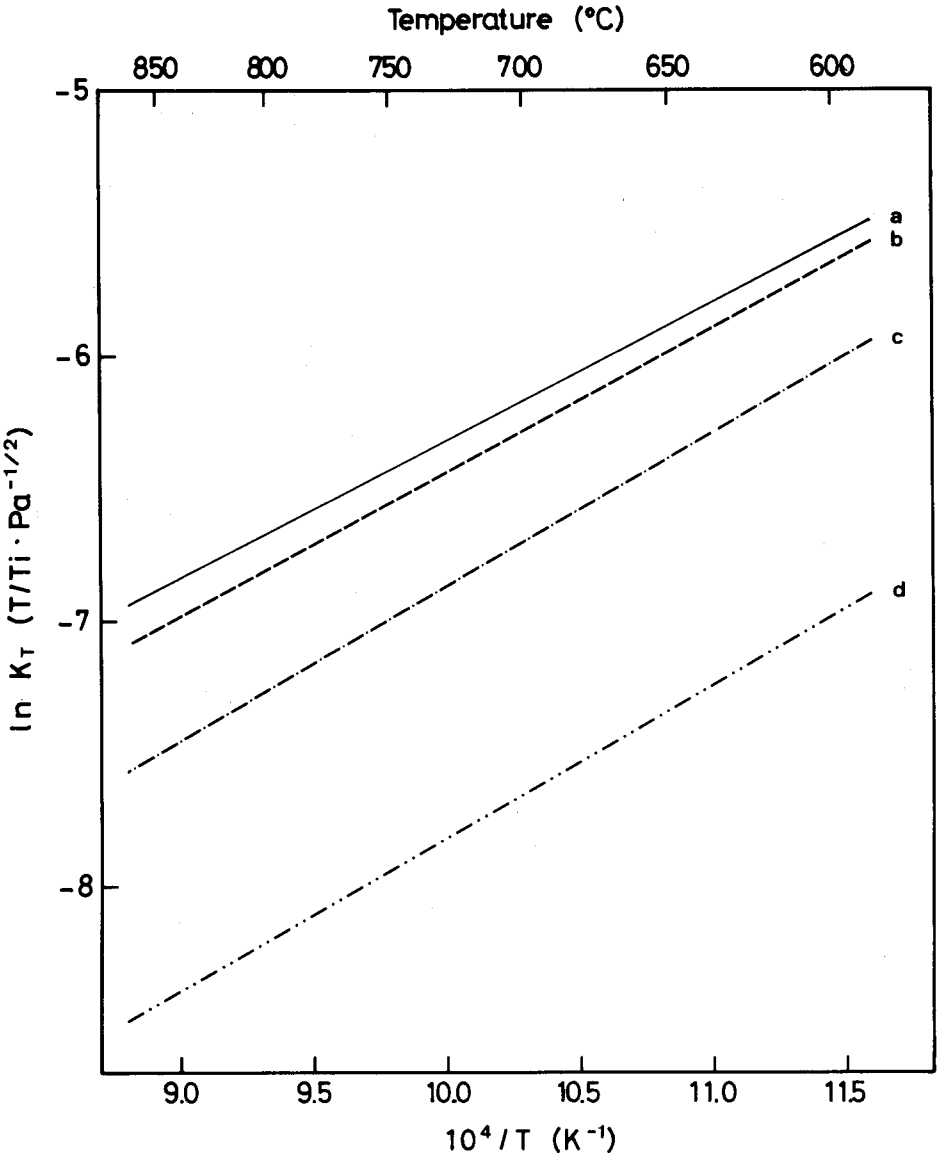

Fig. 17 Temperature dependence of Sieverts' constant K_T for tritium in pure titanium and αTi(O) solid solutions.
(a) pure titanium, (b) 0.111 O/Ti, (c) 0.250 O/Ti, (d) 0.429 O/Ti.

CHAPTER 7 SOLUBILITY OF HYDROGEN ISOTOPE IN ZIRCONIUM-OXYGEN SOLID SOLUTION

1. Introduction

It is well known that zirconium easily reacts with chemically active gases such as H_2, O_2, N_2, H_2O and CO_2. In the field of nuclear fusion engineering, zirconium and its bearing alloys have been proposed as tritium gettering and storage materials because of their great sorption ability for hydrogen isotope gas[1,2]. For the applications to tritium handling systems, the solubility of the hydrogen isotope in zirconium is one of the crucial factors, and the influence of impurity contamination on the solubility should be taken into account. Oxygen is the most important impurity interstitially dissolved in zirconium.

Problems in a fission reactor such as embrittlement of zircaloy cladding and treatment of zircaloy cladding hulls have also stirred interest in hydrogen behavior in zirconium-oxygen solid solution[3,4].

Information on the hydrogen and deuterium solubilities in pure zirconium and the phase diagram of Zr-H binary system is available in the literature[5-12]. However, there are insufficient data for the Zr-O-H ternary system[7,8,13,14]. Hall et al.[13] and Edward et al.[14] have studied phase equilibria in the Zr-O-H ternary system at hydrogen pressures above 10^2 Pa and found reduction in the solubility of hydrogen with addition of oxygen into zirconium. On the contrary, Mallet and Albrecht[8] have reported that the hydrogen solubility increases with oxygen content in zirconium.

The present study aims to reexamine the phase equilibria in the Zr-O-H ternary system and to elucidate the effect of solute oxygen on the solubilities of hydrogen and deuterium in zirconium. Solubility measurements have been performed, and thermodynamic properties of hydrogen and deuterium in zirconium-oxygen solid solutions were derived on the basis of a dilute solution model. The isotope effect of hydrogen and deuterium on the solubility was discussed, and tritium solubility was estimated from hydrogen and deuterium data.

2. Experimental

Pure zirconium and zirconium-oxygen solid solutions, αZr(O), were used in the present study. High purity zirconium crystal bar was cut into sheets (1 mm x 10 mm x 10 mm), mechanically polished and degreased in acetone. The principal impurities of pure zirconium specimen were 74 wtppm Fe, 43 wtppm Hf, < 50 wtppm O,

< 30 wtppm C, < 5 wtppm N and 8 wtppm H. The αZr(O) solid solutions were in the form of pellets (8 mmϕ x 3 - 4 mmh), the oxygen contents of which were 0.026, 0.053, 0.111, 0.176, 0.250, 0.333 and 0.389 O/Zr atom ratios. These pellets of αZr(O) were prepared by vacuum annealing of Zr (purity, 99.9 wt%) and ZrO_2 (purity, 99.99 wt%) mixed powders. Phase identification by X-ray diffraction technique indicated that the pellets thus prepared were α solid solutions with a hcp structure. The homogeneity of the pellets was also checked by a microhardness tester and a microscope. The compositions were chemically analyzed before and after solubility measurements. Hydrogen gas (purity, 99.999 vol%) and deuterium gas (99.5 vol%) were used with purification by hot titanium sponges.

Solubilities of hydrogen and deuterium in pure zirconium and αZr(O) solid solutions were examined by a modified Sieverts' apparatus. The measurements of phase relationships in the Zr-O-H system were performed only at a temperature of 700°C at pressures up to 10^4 Pa, and the solubility at low pressures was measured in the temperature range of 600 to 775°C at pressures below 10^2 Pa. Details of the apparatus and the procedure were similar to those described in the preceding chapter.

3. Results and Discussion

3.1. Phase equilibria in the Zr-O-H ternary system

The results of measurements of the phase relationships in the Zr-O-H ternary system at 700°C are shown in Fig. 1, in which the equilibrium hydrogen pressure is given as a function of hydrogen content for each αZr(O) solid solution.

At low hydrogen contents, the isothermal hydrogen pressure-hydrogen content (P-C) curve indicates a linear relation for each αZr(O) solution. This suggests that in the dilute ternary solution Zr(O,H) with α phase the solubility data follow Sieverts' law. However, deviations become apparent in O-rich solid solutions as hydrogen pressure increases above 10^2 Pa.

On the P-C curves, discontinuities in slope appear at a higher hydrogen content, as indicated by open circles in Fig. 1. This change in slope signals the appearance of a different phase, which is βZr(H) (bcc solid solution), δZrH_{2-x} (fcc hydride) or εZrH_2 (fct hydride). For pure zirconium, plateau pressure regions were observed, where two solid phases, αZr(H) + βZr(H) or βZr(H) + δZrH_{2-x}, are in equilibrium. The phase boundaries obtained in the present study were consistent with the reported values of the Zr-H binary system at 700°C[15].

The P-C curves for the αZr(O) solutions show some curvature in the two-phase region. A single pressure arrest is found for the αZr(O) solutions containing

0.111, 0.176 and 0.250 O/Zr. In this region, three solid phases which consist of αZr(O,H), βZr(H) and δZrH_{2-x} coexist. At higher pressures, the P-C curve for the αZr(O) (0.053 - 0.333 O/Zr) corresponds to the two-phase region of βZr(H) + δZrH_{2-x} or αZr(O,H) + δZrH_{2-x}. If the δZrH_{2-x} phase dissolved only a limited amount of oxygen, the P-C curve for αZr(O) of 0.389 O/Zr would represent αZr(O,H) + εZrH_2 two-phase region.

The isothermal section of the Zr-O-H ternary system at 700°C constructed from these results is shown together with tie lines in Fig. 2. The phase boundary of the Zr-O binary system at 700°C was taken from the literature[15]. In the isothermal section at 700°C, there exists a characteristic triangle representing the αZr(O,H) + βZr(H) + δZrH_{2-x} three-phase region (region Ⅱ in Fig. 2). Compositions of the solid phases and hydrogen pressure are thermodynamically fixed in this three-phase region. The experimental data are in agreement with the phase rule. This three-phase region is adjacent to two-phase regions (region Ⅰ, Ⅲ and Ⅳ) of αZr(O,H) + βZr(H), βZr(H) + δZrH_{2-x} and αZr(O,H) + δZrH_{2-x}. The tie lines in the isothermal section connect the conjugate phases in the two-phase regions.

The terminal solubility of hydrogen in the α phase is slightly increased by the presence of solute oxygen, and oxygen has a lower solubility in the β and δ phases than in the α phase. These features are qualitatively consistent with previous results at a higher temperature[7,14]. Ells et al.[7] have proposed that at 750°C the solute oxygen in zirconium stabilizes the α phase up to 30 at%H. However, the present data show a smaller stabilizing effect of oxygen on α phase. Although the εZrH_2 phase region could not be experimentally determined in the present study, the phase regions Ⅴ - Ⅱ including the εZrH_2 phase appear to exist at 700°C, as shown in Fig. 2. Further studies are required to establish a complete phase diagram of the Zr-O-H ternary system.

3.2. Hydrogen solubility in the Zr-O solid solution

At low pressures less than 10^2 Pa, all the solubility data for hydrogen in pure zirconium and αZr(O) solid solutions with an oxygen content of 0.026 to 0.389 O/Zr closely obeyed Sieverts' law,

$$C_H = K_H \times P_{H_2}^{1/2} \qquad (1)$$

where C_H is the hydrogen content in atom ratio (H/Zr), P_{H_2} the equilibrium hydrogen pressure in Pa and K_H the Sieverts' constant. An example of the linear relation between the square root of the equilibrium pressure and the hydrogen content is shown in Fig. 3, in which the data for αZr(O) with 0.026 O/Zr are excluded for the sake of clarity. Since Sieverts' law applied in all the αZr(O)

solid solutions, hydrogen-hydrogen interaction in the ternary solution appears to be insignificant at a low hydrogen pressure.

The temperature dependence of the Sieverts' constant K_H is illustrated in Fig. 4, indicating the following relationship holds,

$$\ln K_H = A + B/T \qquad (2)$$

where A and B are constants and T is the temperature in K. The enthalpy of solution of hydrogen ΔH (kJ/g-atom) can be obtained from the B value. In Table 1, the values of A, B and ΔH are summarized.

There exist large discrepancies in previously reported data[7-12] for hydrogen solubility in pure zirconium, as given in Table 2. The A value distributes from 9.3 to 12.5 and the B value from 3900 to 7000. The present values of A = -11.8 and B = 6440 for pure zirconium agree with the data recently reported by Watanabe[12].

It is obvious from Fig. 4 that the αZr(O) solid solutions of 0.026 - 0.176 O/Zr have larger solubility of hydrogen at a fixed pressure than pure zirconium. The hydrogen solubility in the αZr(O) goes through a maximum at 0.111 O/Zr, and above 0.176 O/Zr it decreases with increasing oxygen content in zirconium. As can be seen in Table 1, the enthalpy of solution first decreases with oxygen content and then passes through a minimum at 0.111 O/Zr.

Thus, the variations in the solubility and the enthalpy of solution with oxygen content in zirconium are complicated. An increase in hydrogen solubility can be ascribed to an attractive interaction between hydrogen and oxygen in zirconium, but this situation may be reversed at a higher oxygen content.

The hydrogen solubility in a metal is closely associated with the state and location of hydrogen in the metal lattice. It is evident from previous experiments of Zr-O binary solution[16-18] that octahedral interstitial sites in a hexagonal lattice of zirconium are highly favored to receive oxygen atoms. Hydrogen atoms in zirconium are located on the tetrahedral sites[19,20]. Mukawa et al.[21] have found from elastic and inelastic neutron scattering measurements for the hexagonal $ZrO_{0.4}H_{0.1}$ solid solution that hydrogen atoms occupy tetrahedral sites in the ternary solution. They also confirmed the octahedral occupation of oxygen atoms and the tetrahedral occupation of deuterium atoms by means of single crystal neutron diffraction. The presence of oxygen in an octahedral site appears to affect the state and configuration of hydrogen atoms in adjacent tetrahedral sites. This is likely to change the hydrogen solubility in zirconium.

The effect of oxygen on the hydrogen solubility in zirconium was analyzed by the dilute solution model based on statistical thermodynamics, and it can be explained in terms of the following solubility equation:

$$\ln (C_H\ T^{7/4}/2\ P_{H_2}{}^{1/2}\ A_{H_2}) = -(\bar{H}_H - E^d{}_{H_2})/kT + \bar{S}_H/k. \quad (3)$$

On the assumption that hydrogen randomly distributes on the tetrahedral interstitial site in zirconium and the solution is sufficiently dilute to neglect hydrogen-hydrogen interaction, this equation was developed in the same way as the solubility equation for hydrogen in titanium. In eq. (3), the A_{H_2} refers to partition functions of hydrogen gas, $-2\ E^d{}_{H_2}$ the dissociation energy of hydrogen molecule at 0 K, and k the Boltzmann constant, the values of which were calculated from universal constants and spectroscopic data[22,23]. The $\bar{H}_H$ is the enthalpy difference between a hydrogen atom at rest in the gas and in the solution, and $\bar{S}_H$ the partial molar excess entropy of the solute hydrogen atoms.

Figure 5 demonstrates linear relationships between $\ln (C_H\ T^{7/4}/\ 2\ P_{H_2}{}^{1/2}\ A_{H_2})$ and 1/T for hydrogen in pure zirconium and αZr(O) solid solutions. The slope of the straight line is for $-(\bar{H}_H - E^d{}_{H_2})/k$ and the intercept for $\bar{S}_H/k$. For pure zirconium, the enthalpy term of $\bar{H}_H - E^d{}_{H_2}$ and the entropy term of $\bar{S}_H$ were estimated to be -39.5 kJ/mol and 26.5 J/mol K, respectively. Complex changes in the values of the two terms with oxygen content were observed for αZr(O) solid solutions.

The variations in the hydrogen solubility and the enthalpy of solution with oxygen addition into zirconium can be discussed in terms of differences in the partial molar enthalpy and the partial molar excess entropy between pure zirconium and αZr(O), which are defined as,

$$\partial\bar{H}_H = \bar{H}_H - \bar{H}_H^\circ \text{ and } \partial\bar{S}_H = \bar{S}_H - \bar{S}_H^\circ \quad (4)$$

where $\bar{H}_H^\circ$ and $\bar{S}_H^\circ$ are the values for pure zirconium.

Figure 6 reveals the change in the $\partial\bar{H}_H$ value with oxygen content C_O (O/Zr). The $\partial\bar{H}_H$-C_O curve exhibits a pronounced minimum. Oxygen in zirconium distorts the hexagonal lattice[24-26]. The lattice strain resulting from solute oxygen strongly influences the $\partial\bar{H}_H$ value. As discussed in the preceding chapter, the partial molar enthalpy of hydrogen in αZr(O) solid solution $\bar{H}_H$ is approximately:

$$\bar{H}_H = \tilde{E}_H - (\bar{V}_H\bar{V}_O/V_{Zr}K_{Zr}) \times C_O$$
$$\tilde{E}_H = (\partial E/\partial n)_{V,T} \quad (5)$$

where $\tilde{E}_H$ is the partial molar energy of hydrogen at constant volume. The $\bar{V}_H$ and $\bar{V}_O$ are the partial molar volumes of hydrogen and oxygen in zirconium, and V_{Zr} (1.40×10^{-5} m^3/mol) and K_{Zr} (1.20×10^{-11} m^2/N) are the molar volume and the compressibility for pure zirconium. If $\tilde{E}_H$ is independent of oxygen content in zirconium, the change in the partial molar enthalpy $\partial\bar{H}_H$ due to the lattice strain

contribution is expressed as

$$\delta\bar{H}_H = -(\bar{V}_H\bar{V}_O/V_{Zr}K_{Zr}) \times C_O. \quad (6)$$

The partial molar volume of oxygen in zirconium was estimated from the data sets of lattice spacing of αZr(O)[24-26], the obtained value of $\bar{V}_O$ was from 2×10^{-6} to 3×10^{-6} cm^3/mol. Using $\bar{V}_H = 2\times10^{-6}$ m^3/mol and $\bar{V}_O = 3\times10^{-6}$ m^3/mol, the volume contribution to $\delta\bar{H}_H$ was calculated. The theoretical value of $\delta\bar{H}_H$ is given by the dashed line in Fig. 6. It should be noted that at a low oxygen content there appears no marked difference between the calculated and experimental $\delta\bar{H}_H$ values. At higher oxygen contents, the calculated values are in wide disagreement with the experimental findings. Other physical effects such as a repulsive interaction of oxygen with hydrogen and an electronic contribution of oxygen could give rise to the discrepancy.

In Fig. 7, the change in the $\delta\bar{S}_H$ value with oxygen content in zirconium is shown. The value of $\delta\bar{S}_H$ continuously decreases with oxygen content. This trend quite differs from $\delta\bar{H}_H$. When non-configurational contributions to the partial molar excess entropy $\bar{S}_H$ such as vibrational and electronic excess entropy are independent of oxygen content, $\delta\bar{S}_H$ would be ascribed mainly to deviation from complete randomness in the distribution of hydrogen. In a zirconium lattice, oxygen atoms on octahedral sites are inferred to interact repulsively with hydrogen atoms on tetrahedral sites. This results in "blocking effect" on the hydrogen solubility. One octahedral interstice possesses six nearest tetrahedral neighbors. If an oxygen atom on an octahedral site completely blocks adjacent tetrahedral sites, the change in the partial configurational entropy $\delta\bar{S}_H$ is offered by the equation (7).

$$\delta\bar{S}_H = k \ln (1 - C_O)^3. \quad (7)$$

The relation between $\delta\bar{S}_H$ and C_O is shown by the dashed line in Fig. 7. The experimental $\delta\bar{S}_H$ is consistent with the theoretical curve at a low oxygen content. However, the theoretical $\delta\bar{S}_H$ deviates from the exerimental value for the αZr(O) with a higher oxygen content. This implies that oxygen in zirconium may have a smaller blocking effect than expected or other effects may dominate $\delta\bar{S}_H$ at a high oxygen content.

For a αZr(O) solid solution with a low oxygen content, the negative change in the partial molar enthalpy is larger than the corresponding change in the partial molar excess entropy. As a result, the hydrogen solubility at a fixed pressure increases. Above an oxygen content of about 0.25 O/Zr, the partial molar enthalpy increases, whereas the partial molar excess entropy decreases appreciably,

consequently, the solubility in the αZr(O) solid solution with a higher oxygen content falls below that in pure zirconium.

3.3. Deuterium solubility in the Zr-O solid solution

The deuterium solubility was measured for pure zirconium and αZr(O) solid solutions with oxygen contents of 0.053, 0.111, 0.176, 0.250 and 0.389 O/Zr. All the deuterium solubility data below 10^2 Pa almost obeyed Sieverts' law, as shown in Fig. 8.

Figure 9 indicates the change in the Sieverts' constant K_D for deuterium with temperature. As can be seen in this figure, ln K_D is proportional to the reciprocal temperature. This implies the same relation as hydrogen (eq. (2)) holds for the deuterium solubility in pure zirconium and αZr(O) solid solutions. The parameters of Sieverts' law A and B and the enthalpy of solution ΔH are listed in Table 1.

The deuterium solubility and the enthalpy of solution obtained for pure zirconium is found from Table 2 to be close to the data obtained by Watanabe[12].

It is clear from Fig. 9 that the solubility of deuterium at a fixed pressure first increased with oxygen content in zirconium, then decreased above 0.176 O/Zr. The enthalpy of solution showed a pronounced minimum at 0.176 O/Zr, as indicated in Table 1. Similar dependence of solubility on oxygen content in zirconium was observed for hydrogen and deuterium. For each αZr(O) solid solution, the deuterium solubility was however lower and the enthaply of solution of deuterium was larger, with respect to hydrogen.

The following equation, which is analogous to the analysis of hydrogen solubility, was applied to the deuterium data:

$$\ln (C_D\, T^{7/4}/2\, P_{D_2}{}^{1/2}\, A_{D_2}) = -(\bar{H}_D - E^d{}_{D_2})/kT + \bar{S}_D/k. \qquad (8)$$

Figure 10 shows the thermodynamic analysis of the deuterium solubility data by eq. (8). Linear relationships held between ln $(C_D\, T^{7/4}/2\, P_{D_2}{}^{1/2}\, A_{D_2})$ and 1/T, irrespective of the oxygen content in zirconium. The values of $-(\bar{H}_D - E^d{}_{D_2})/k$ and $\bar{S}_D/k$ were derived from the slope and the intercept of the straight line. $\bar{H}_D - E^d{}_{D_2} = -38.2$ kJ/mol and $\bar{S}_D = 34.1$ J/mol K were evaluated for pure zirconium.

Differences in the partial molar quantities between pure zirconium and αZr(O) difined as:

$$\delta\bar{H}_D = \bar{H}_D - \bar{H}_D{}^\circ \text{ and } \delta\bar{S}_D = \bar{S}_D - \bar{S}_D{}^\circ \qquad (9)$$

were employed for discussion of the changes in the deuterium solubility and the

enthalpy of solution with oxygen content in zirconium. Figures 11 and 12 reveal the changes in the $\delta\bar{H}_D$ and $\delta\bar{S}_D$ values with the oxygen content.

As shown in Fig. 11, the partial molar enthalpy $\bar{H}_D$ for deuterium in zirconium once decreases with oxygen addition, which may be due to a lattice strain effect of solute oxygen. Above an oxygen content of 0.176 O/Zr, $\bar{H}_D$ value increases, resulting chiefly from a strong interaction of deuterium with oxygen in zirconium. The change in $\delta\bar{H}$ value with oxygen content in zirconium is hardly different from deuterium to hydrogen. If the partial molar volume of deuterium in titanium is the same as hydrogen, the theoretical $\delta\bar{H}_D$ values can be estimated by the same manner as hydrogen. The volume contribution is indicated by the dashed line in Fig. 11. There is no definite discrepancy between the theoretical and experimental $\delta\bar{H}_D$ values at a low oxygen content.

It is found from Fig. 12 that the $\delta\bar{S}_D$ value monotonically decreases with oxygen content. No significant isotope effect on the $\delta\bar{S}$ value is observed. The blocking effect of oxygen appears to be a main reason for the decrease in $\delta\bar{S}_D$. The dashed line in Fig. 12 is the theoretical $\delta\bar{S}_D$ value calculated from the same equation as eq. (7). At a low oxygen content, the experimental data for both deuterium and hydrogen are in accordance with the theoretical curve. Oxygen in zirconium might have a smaller blocking effect on hydrogen and deuterium than expected.

The complicated changes in the deuterium solubility and the enthalpy of solution with oxygen content are attributable to a net result of $\delta\bar{H}_D$ and $\delta\bar{S}_D$ variations. It should be noted that there exists no marked difference in $\delta\bar{H}$ and $\delta\bar{S}$ between hydrogen and deuterium. This appears to come from similarity of the existing state of hydrogen and deuterium in pure zirconium and αZr(O) solid solutions.

3.4. Isotope effect of hydrogen and deuterium solubilities

The influence of temperature and oxygen content on the value of $\ln [(C_H T^{7/4}/2 P_{H_2}{}^{1/2} A_{H_2})/(C_D T^{7/4}/2 P_{D_2}{}^{1/2} A_{D_2})]$ must be examined to interpret the isotope effect on solubilities of hydrogen and deuterium in pure zirconium and αZr(O) solid solution. In Fig. 13, the values of $\ln [(C_H T^{7/4}/2 P_{H_2}{}^{1/2} A_{H_2})/(C_D T^{7/4}/2 P_{D_2}{}^{1/2} A_{D_2})]$ obtained from experimental data are plotted against 1/T. There exists little correlation between $\ln [(C_H T^{7/4}/2 P_{H_2}{}^{1/2} A_{H_2})/(C_D T^{7/4}/2 P_{D_2}{}^{1/2} A_{D_2})]$ and the oxygen content in zirconium.

On the assumption that interstitial hydrogen atoms in zirconium behave simple harmonic oscillators having vibrational frequencies ν_H in the range of 800 - 1200 cm^{-1}, the dashed curves in Fig. 13 were theoretically drawn by use of eq. (10).

$$\ln [(C_H T^{7/4}/2 P_{H_2}^{1/2} A_{H_2})/(C_D T^{7/4}/2 P_{D_2}^{1/2} A_{D_2})]$$
$$= -3(1 - 1/\sqrt{2})(h\nu_H/kT)/2 + (E^d_{H_2} - E^d_{D_2})/kT$$
$$- 3 \ln [(1 - \exp(-h\nu_H/kT))/(1 - \exp(-h\nu_H/\sqrt{2}kT))]. \quad (10)$$

The experimental $\ln [(C_H T^{7/4}/2 P_{H_2}^{1/2} A_{H_2})/(C_D T^{7/4}/2 P_{D_2}^{1/2} A_{D_2})]$ values are found from this figure to scatter around the theoretical curve for the vibrational frequency ν_H = 1000 cm^{-1}.

Kohoda-Bakhsh et al.[20] have carried out inelastic neutron scattering in $\alpha ZrH_{0.05}$ at 600°C and reported that the vibrational frequency of hydrogen on a tetrahedral hole, ν_H, is 1161 cm^{-1}. Mukawa and his coworkers[21] have performed time-of-flight measurements of elastic and inelestic neutron scattering for the ternary solution of $ZrO_{0.4}H_{0.1}$ and observed the primary harmonic peak at ν_H = 1090cm^{-1}. The frequency of 1000 cm^{-1} estimated from the solubility data fairly agrees with the reported values.

These results mean that the difference in the solubility between hydrogen and deuterium is practically unaffected by the coexsitence of oxygen. In other words, the isotope effect on solubilities of hydrogen and deuterium in a $\alpha Zr(O)$ solid solution can be explained only by different vibrational frequencies between the two isotopes. The vibrational mode of hydrogen isotope atom may not be influenced by coexisting oxygen atoms.

3.5. Estimation of tritium solubility

The relationship between hydrogen and deuterium solubilities in pure zirconium and $\alpha Zr(O)$ solid solutions was shown as a function of vibrational frequency of hydrogen in eq. (10). The isotope effect on the solubility is attributed to the difference in vibrational frequency among hydrogen isotopes. Consequently, assuming that the vibrational frequency of tritium $\nu_T = \nu_H/\sqrt{3}$, similar equations to eq. (10) hold between hydrogen, deuterium and tritium solubilities. Alternatively, $\ln [(C_T T^{7/4}/2 P_{T_2}^{1/2} A_{T_2})/(C_H T^{7/4}/2 P_{H_2}^{1/2} A_{H_2})]$ and $\ln [(C_T T^{7/4}/2 P_{T_2}^{1/2} A_{T_2})/(C_D T^{7/4}/2 P_{D_2}^{1/2} A_{D_2})]$ are functions of ν_H. For calculation of $\ln [(C_T T^{7/4}/2 P_{T_2}^{1/2} A_{T_2})/(C_H T^{7/4}/2 P_{H_2}^{1/2} A_{H_2})]$ and $\ln [(C_T T^{7/4}/2 P_{T_2}^{1/2} A_{T_2})/(C_D T^{7/4}/2 P_{D_2}^{1/2} A_{D_2})]$, the dissociation energy of tritium gas, $-2 E^d_{T_2}$, and the value of A_{T_2} related to partition functions of tritium molecule are necessary, but they can be easily evaluated from universal constants and spectroscopic constants provided in the literature[22]. As mentioned in the preceding chapter, these solubility ratios permit us to estimate the tritium solubility in $\alpha Zr(O)$ solid solutions as well as pure zirconium.

Using ν_H = 1000 cm^{-1}, the value of $\ln (C_T T^{7/4}/2 P_{T_2}^{1/2} A_{T_2})$ for tritium was estimated from the solubility data of hydrogen or deuterium. Figure 14 indicates

the relations of the ln ($C_T\ T^{7/4}/2\ P_{T_2}{}^{1/2}\ A_{T_2}$) values with temperature. It is apparent from this figure that the agreement of the ln ($C_T\ T^{7/4}/2\ P_{T_2}{}^{1/2}\ A_{T_2}$) values calculated from the hydrogen data with those from the deuterium data is fairly good. Sieverts' constants for tritium, K_T, were evaluated from the ln ($C_T\ T^{7/4}/2\ P_{T_2}{}^{1/2}\ A_{T_2}$) values thus obtained and followed eq. (2), as shown in Fig. 15. The parameters A and B and the enthalpy of solution for tritium are listed in Table 1. The estimated solubility of tritium in pure zirconium and αZr(O) solid solutions was smallest, followed by deuterium and hydrogen. Although the solubility for tritium could not be compared with the literature data because of the lack of information, the estimated values appear to be close to the real values.

Quantitative expressions for the poisoning effect of oxygen on the solubilities of hydrogen isotopes were derived from the experimental and estimated data. The solubilities of hydrogen isotopes C_U in U/Zr atom ratio where U = H, D and T can be represented as follows:

$$C_U = (a + \exp(b/T)) \times P_{U_2}{}^{1/2}. \tag{11}$$

On the assumption that the parameters a and b are written in the form:

$$a = a_0\ (1 + a_1\ C_O + a_2\ C_O{}^2) \text{ and } b = b_0\ (1 + b_1\ C_O + b_2\ C_O{}^2) \tag{12}$$

where C_O is the oxygen content in zirconium and a_0 and b_0 the values for pure zirconium, fitting the solubility data to the eqs. (12), the $a_{1,2}$ and $b_{1,2}$ were obtained as given in Table 3. From a practical standpoint, these expressions are useful for predicting the influence of oxygen poisoning effect on solubilities of hydrogen isotopes in zirconium.

4. Conclusions

The solubilities of hydrogen and deuterium in pure zirconium and αZr(O) solid solutions with O/Zr atom ratio ranging from 0.026 to 0.389 have been measured at temperatures of 700 - 775°C.

The isothermal section of the Zr-O-H ternary system at 700°C was constructed on the basis of the results for isothermal hydrogen pressure-hydrogen content curves. The terminal solubility in the α solution at the boundary between the α and $\alpha + \beta$ phases was increased by the presence of oxygen.

All the solubility data for hydrogen and deuterium in pure zirconium and αZr(O) solutions at pressures below 10^2 Pa closely followed Sieverts' law. Both

hydrogen and deuterium solubilities at a fixed pressure first increased with oxygen content in zirconium, then passed through a maximum. For the αZr(O) above 0.250 O/Zr, the solubility was lower than that for pure zirconium. The change in enthalpy of solution with oxygen content showed a pronounced minimum. The solubility in αZr(O) was lower for deuterium than for hydrogen, and the enthalpy of solution slightly differed from hydrogen to deuterium.

The solubility data were analyzed by the dilute solution model, and the partial thermodynamic functions of hydrogen and deuterium in the Zr-O-H and Zr-O-D ternary solutions were estimated. The change in the solubility of hydrogen isotope with oxygen content was explained in terms of the differences in the partial molar enthalpy and the partial molar excess entropy between pure zirconium and αZr(O). The complicated change in the solubility due to incorporation of oxygen atoms into zirconium lattice was attributed to the combined effect of $\delta\bar{H}$ and $\delta\bar{S}$. However, there was no marked difference in $\delta\bar{H}$ and $\delta\bar{S}$ values between the two isotopes.

The isotope effect of hydrogen and deuterium on the solubility in pure zirconium and αZr(O) solid solutions was analyzed on the assumption that an interstitial hydrogen isotope atom behaves as a simple harmonic oscillator in the zirconium matrix. The vibrational frequency of hydrogen atom in zirconium was obtained, which allowed prediction of tritium solubility. The solubilities decreased in the order hydrogen, deuterium, tritium.

The quantitative expressions for the influence of oxygen contamination on solubilities of hydrogen isotopes were obtained, which will offer a foundation of design criteria for tritium processing with zirconium and its alloys.

References

[1] L.S. Krochmalnek, J.P. Krasznai and M. Carney, Fusion and Engineering and Design, 5(1988)337.
[2] A. Uritani and K. Akaishi, ibid., 4(1987)405.
[3] W.H. Erikson and D. Hardie, J. Nucl. Mater., 13(1964)254.
[4] R. Tegman and M. Burstrom, SKB Technical Report 84-14, (1984).
[5] M. Someno, J. Jpn. Soc. Met., 24(1955)136.
[6] E.A. Gulbransen and K.F. Andrew, J. Metals, 7(1955)136.
[7] C.E. Ells and A.D. McQuillan, J. Inst. Metals, 85(1956)89.
[8] M.W. Mallet and W.M. Albrecht, J. Elechrochem. Soc., 104(1957)142.
[9] F. Rica and T.A. Giorgi, J. Phys. Chem., 71(1967)3627.
[10] M. Tada and Yen C. Haung, Titanium-Zirconium, 19(1971)260.
[11] M. Nagasaka and T. Yamashina, J. Less-Common Metals, 45(1976)53.
[12] K. Watanabe, J. Nucl. Mater., 136(1985)1.
[13] M.M.A. Hall, S.L.H. Martin and A.L.G. Rees, Trans. Faraday Soc., 41(1945)306.
[14] R.K. Edwards and P. Levesque, J. American Chem. Soc., 77(1955)1312.
[15] T.B. Massalski, Binary Alloy Phase Diagrams, (ASM, Ohio, 1986).
[16] S. Yamaguchi, J. Phys. Soc. Japan, 24(1968)855.

[17] T. Arai and M. Hirabayashi, J. Less-Common Metals, 44(1976)291.
[18] J.P. Abriata, J. Garces and R. Versaci, Bulletin of Alloy Phase Diagrams, 7(1986)116.
[19] P.P. Narang, G.L. Paul and K.N.R. Taylor, J. Less-Common Metals, 56(1977)125.
[20] B. Khoda-Bakhsh and D.K. Ross, J. Phys. F. Met. Phys., 12(1982)15.
[21] S. Mukawa, T. Kajitani and M. Hirabayashi, J. Less-Common Metals, 103(1984)19.
[22] G. Herzberg, Molecular Spectra and Molecular Structure, Vol 1, (D. Van Nostrand Company, Inc., New York, 1950).
[23] M.W. Chase Jr., C.A. Davies, J.R. Downey Jr., D.J. Frurip, R.A. McDonald and A.N. Syverud, JANAF Thermochemical Tables, 3rd. Ed., (American Institute of Physics, Inc., New York, 1985).
[24] R.F. Domagala and D.J. McPherson, J. Metals, 6(1954)238.
[25] B. Holmberg and T. Dagerhamn, Acta Chemica Scand., 15(1961)919.
[26] P. Boisot and G. Beranger, C. R. Acad. Sc. Paris, C 269(1969)587.

Table 1 Parameters of Sieverts' law A and B and enthalpy of solution ΔH.

Oxygen Content(O/Zr)	Isotope	A	B	ΔH(kJ/g-atom)
0	H_2	-11.8	6440	-53.5
	D_2	-11.8	6300	-52.3
	T_2*	-11.8	6250	-52.0
0.026	H_2	-11.8	6600	-54.9
0.053	H_2	-12.0	6780	-56.4
	D_2	-12.0	6640	-55.2
	T_2*	-12.0	6500	-54.1
0.111	H_2	-12.1	6920	-57.6
	D_2	-12.1	6760	-56.2
	T_2*	-12.1	6710	-55.8
0.176	H_2	-12.2	6900	-57.4
	D_2	-12.2	6770	-56.3
	T_2*	-12.2	6720	-55.9
0.250	H_2	-12.2	6700	-55.7
	D_2	-12.3	6660	-55.4
	T_2*	-12.3	6580	-54.7
0.333	H_2	-12.3	6490	-54.0
0.389	H_2	-12.6	6420	-53.4
	D_2	-12.6	6330	-52.6
	T_2*	-12.5	6240	-51.9

* Estimated value

Table 2 Parameters of Sieverts' law A and B and enthalpy of solution ΔH for pure zirconium reported in the literature[9-12].

Isotope	Temperature range(°C)	A	B	ΔH(kJ/g-atom)	Ref.
H_2	600 - 775	-11.8	6440	-53.5	*
	500 - 900	-12.5	6980	-58.0	[5]
	450 - 600	-12.4	7110	-59.2	[6]
	480 - 950	-10.7	5450	-45.3	[7]
	700 - 1000	-9.34	3910	-32.5	[8]
	450 - 750	-11.6	6260	-52.1	[9]
	400 - 900	-11.0	6240	-51.9	[10]
	500 - 800	-11.8	7700	-64.0	[11]
	480 - 760	-12.1	6570	-54.6	[12]
D_2	600 - 775	-11.8	6300	-52.3	*
	450 - 750	-11.2	6190	-51.5	[9]
	500 - 800	-11.8	7700	-64.0	[11]
	490 - 750	-12.1	6540	-54.4	[12]

* The present study

Table 3 Parameters $a_{0,1,2}$ and $b_{0,1,2}$ in eq. (12).

	H_2	D_2	T_2
$a_0 \times 10^6$	7.73	7.89	7.81
a_1	-2.43	-2.78	-2.47
a_2	3.01	3.68	2.92
$b_0 \times 10^{-3}$	6.44	6.30	6.25
b_1	0.761	0.712	0.782
b_2	-2.09	-1.87	-2.05

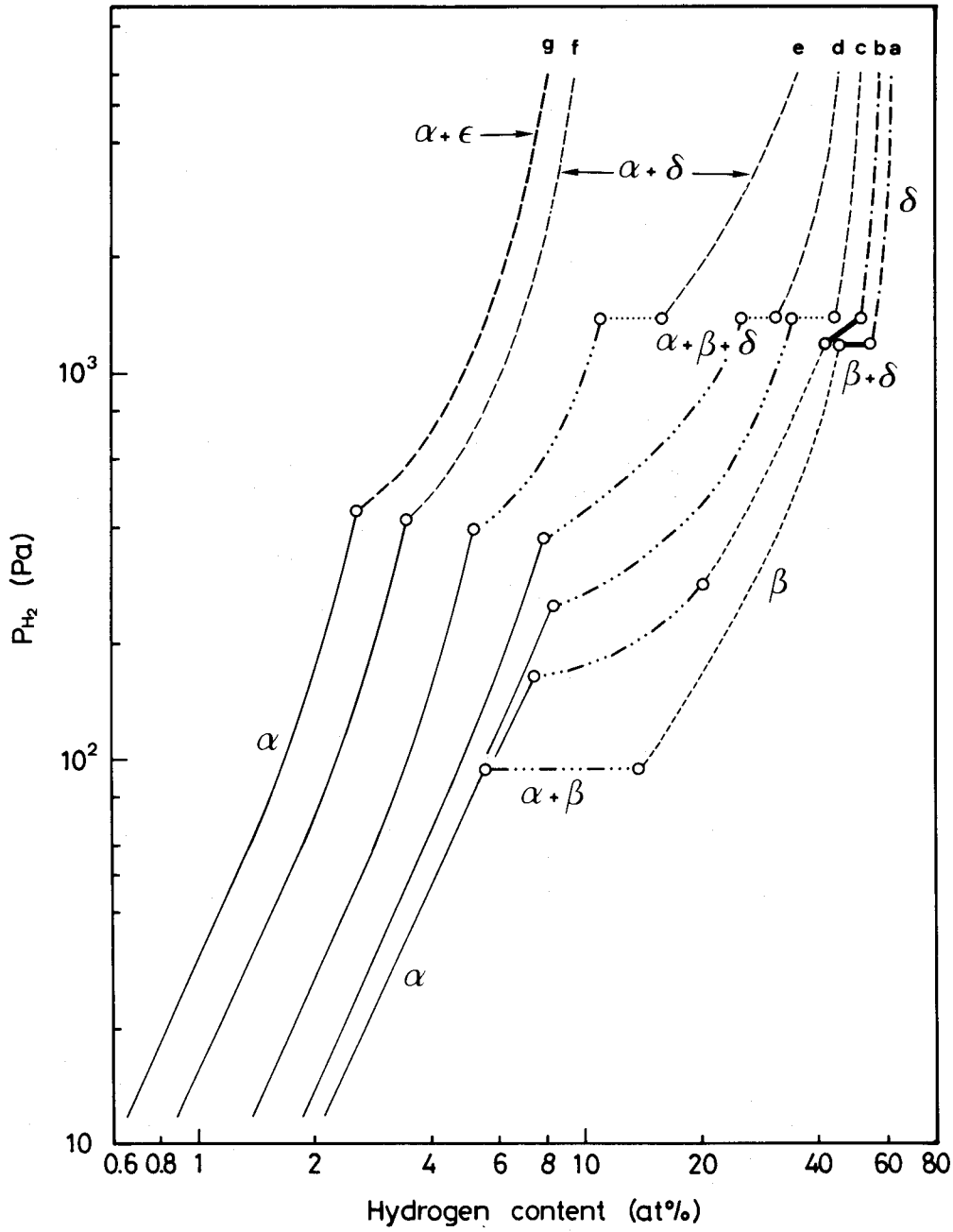

Fig. 1 Isothermal hydrogen pressure-hydrogen content curves for pure zirconium and αZr(O) solid solutions at 700°C.
(a) pure zirconium, (b) 0.053 O/Zr, (c) 0.111 O/Zr, (d) 0.176 O/Zr, (e) 0.250 O/Zr, (f) 0.333 O/Zr, (g) 0.389 O/Zr.

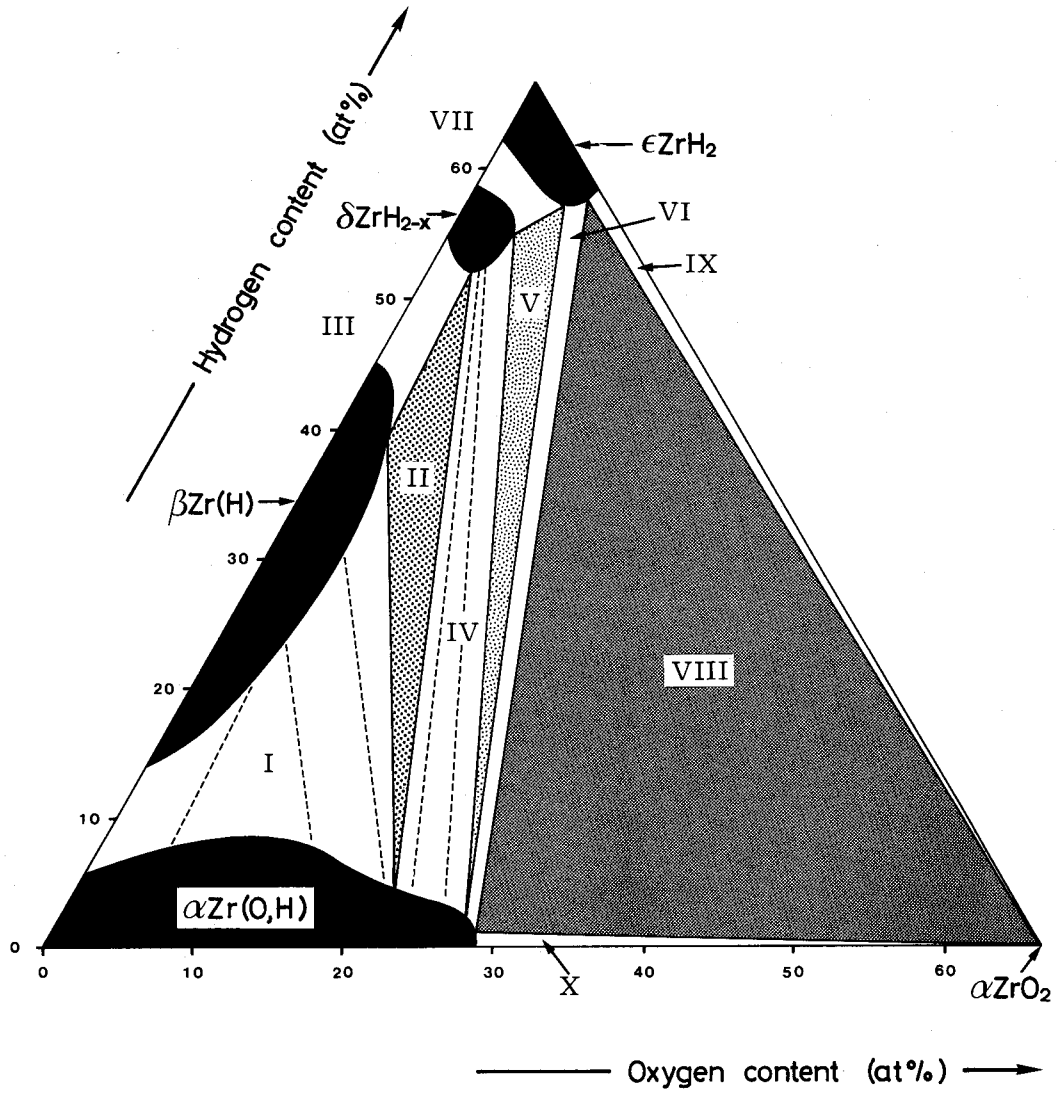

Fig. 2 Isothermal section of the Zr-O-H system at 700°C.

Ⅰ $\alpha Zr(O,H) + \beta Zr(H)$,
Ⅱ $\alpha Zr(O,H) + \beta Zr(H) + \delta ZrH_{2-x}$,
Ⅲ $\beta Zr(H) + \delta ZrH_{2-x}$,
Ⅳ $\alpha Zr(O,H) + \delta ZrH_{2-x}$,
Ⅴ $\alpha Zr(O,H) + \delta ZrH_{2-x} + \varepsilon ZrH_2$,
Ⅵ $\alpha Zr(O,H) + \varepsilon ZrH_2$,
Ⅶ $\delta ZrH_{2-x} + \varepsilon ZrH_2$,
Ⅷ $\alpha Zr(O,H) + \varepsilon ZrH_2 + \alpha ZrO_2$,
Ⅸ $\varepsilon ZrH_2 + \alpha ZrO_2$,
Ⅹ $\alpha Zr(O,H) + \alpha ZrO_2$.

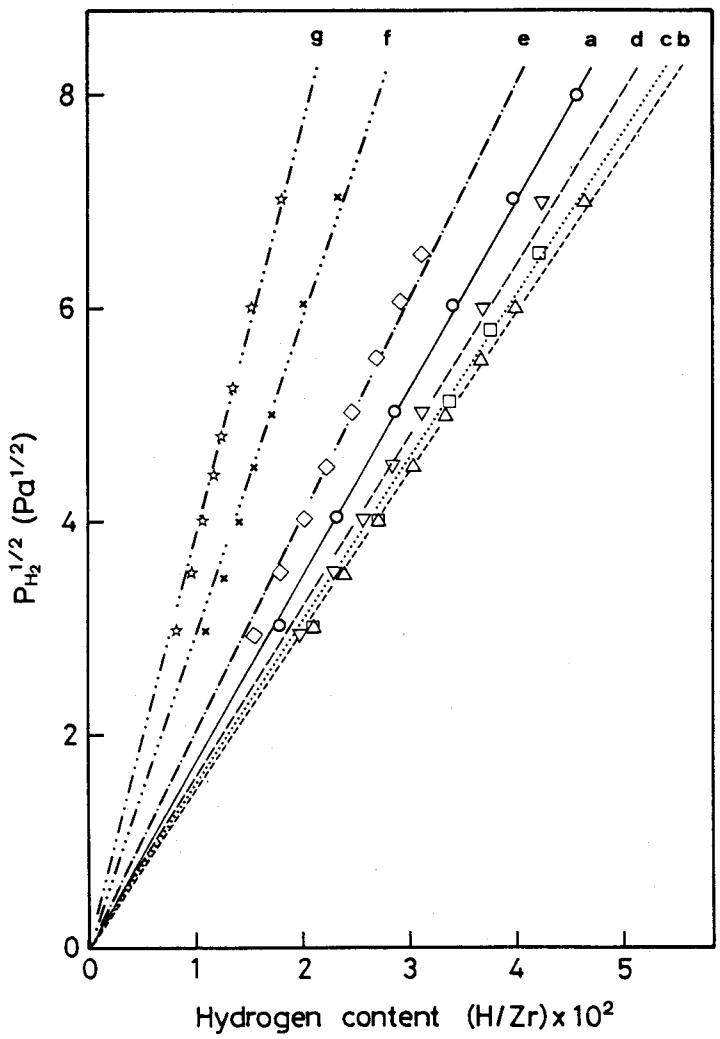

Fig. 3 Sieverts' plot for hydrogen in pure zirconium and αZr(O) solid solutions at 700°C.

(a) pure zirconium, (b) 0.053 O/Zr, (c) 0.111 O/Zr, (d) 0.176 O/Zr, (e) 0.250 O/Zr, (f) 0.333 O/Zr, (g) 0.389 O/Zr.

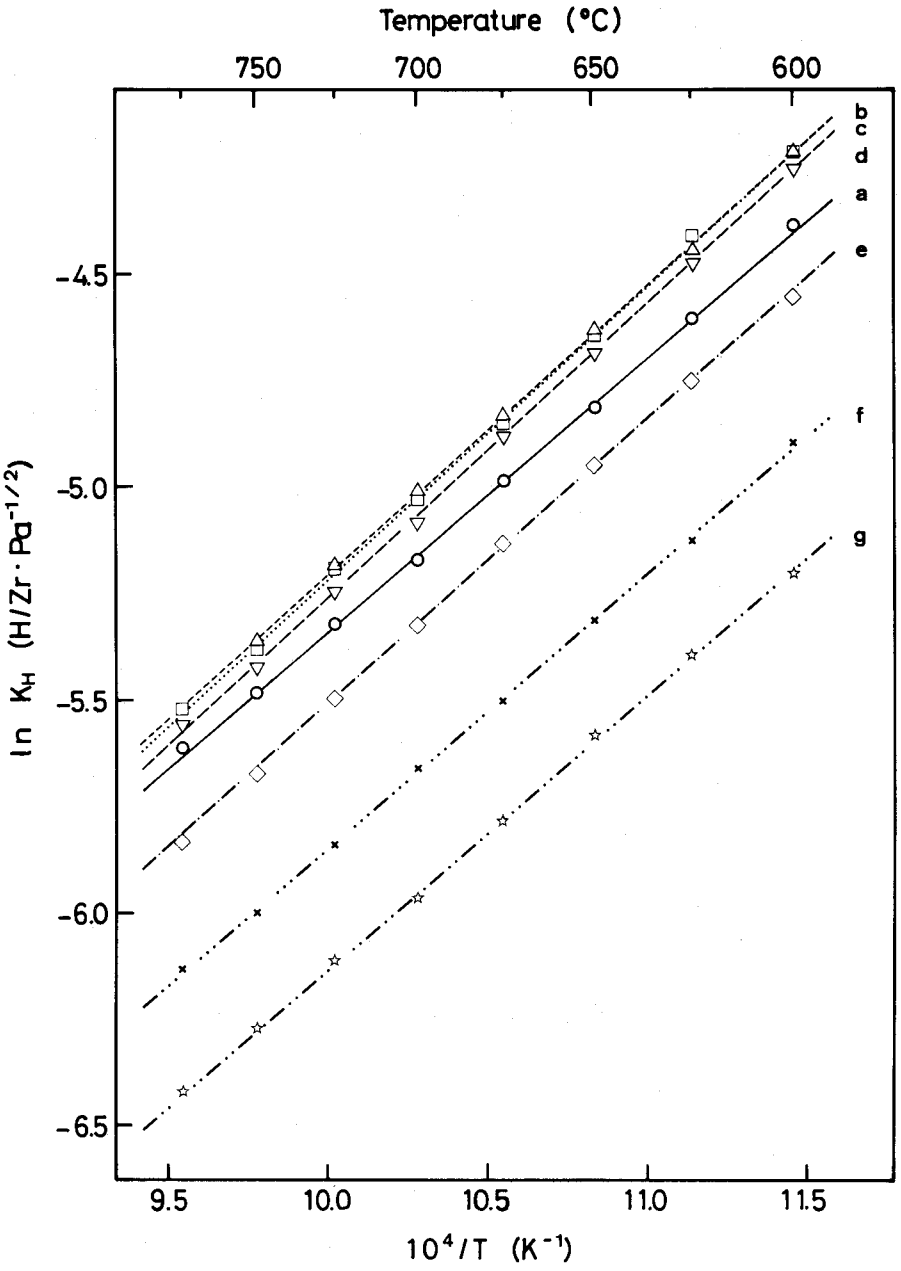

Fig. 4 Temperature dependence of Sieverts' constant K_H for hydrogen in pure zirconium and αZr(O) solid solutions.
(a) pure zirconium, (b) 0.053 O/Zr, (c) 0.111 O/Zr, (d) 0.176 O/Zr, (e) 0.250 O/Zr, (f) 0.333 O/Zr, (g) 0.389 O/Zr.

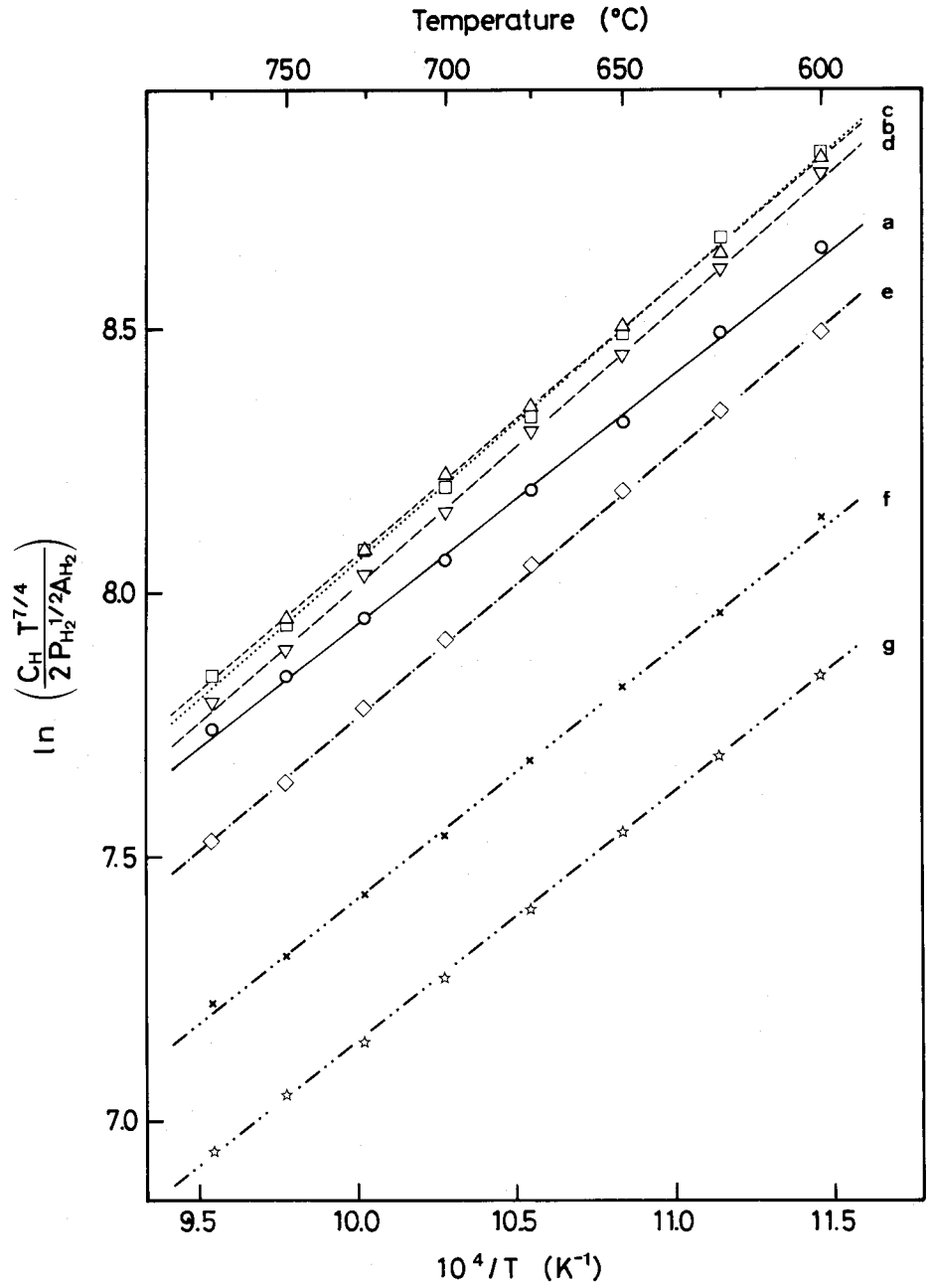

Fig. 5 Thermodynamic analysis of hydrogen solubility in αZr(O) solid solution. (a) pure zirconium, (b) 0.053 O/Zr, (c) 0.111 O/Zr, (d) 0.176 O/Zr, (e) 0.250 O/Zr, (f) 0.333 O/Zr, (g) 0.389 O/Zr.

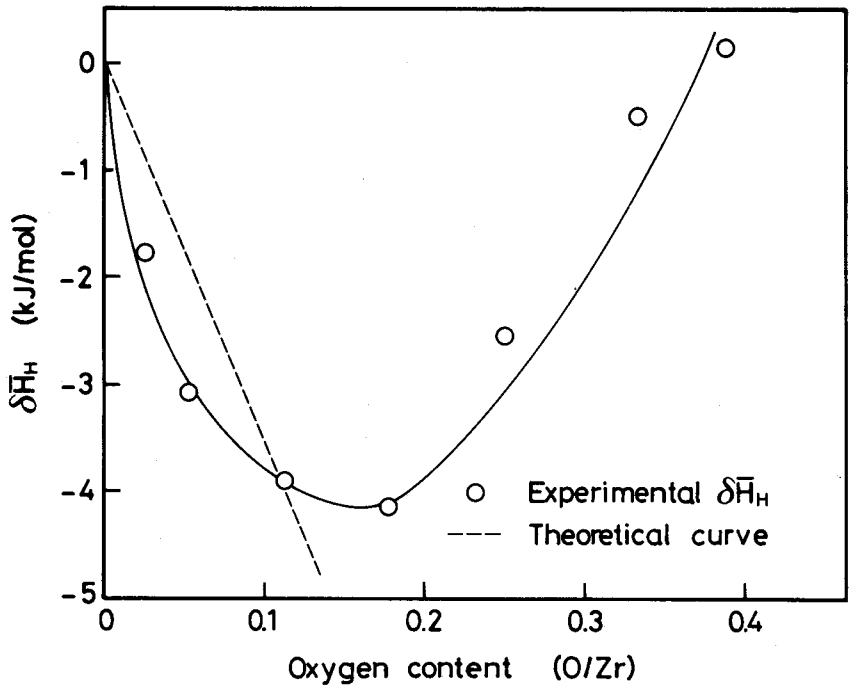

Fig. 6 Change in $\delta\bar{H}_H$ value with oxygen content in αZr(O) solid solution.

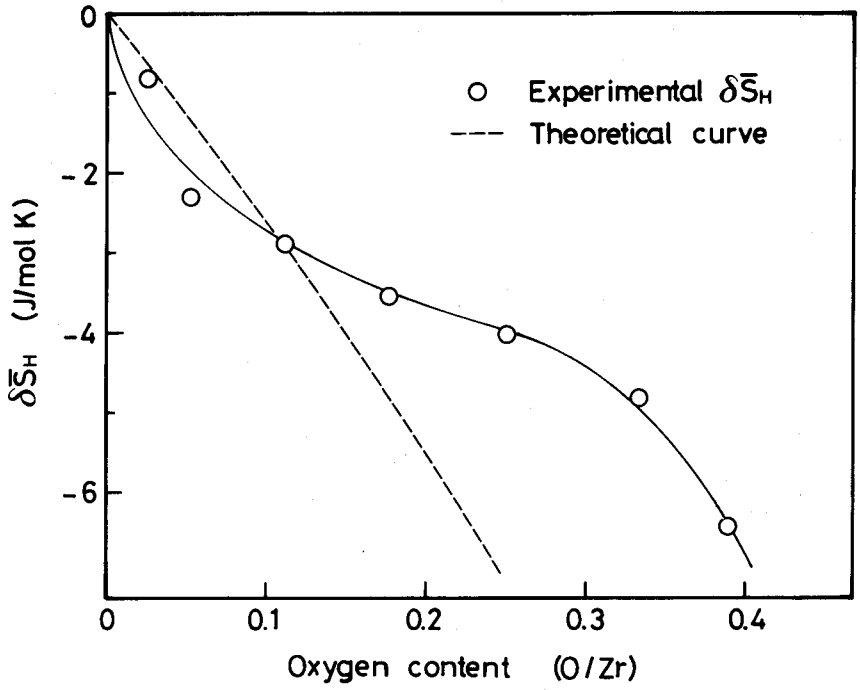

Fig. 7 Change in $\delta\bar{S}_H$ value with oxygen content in αZr(O) solid solution.

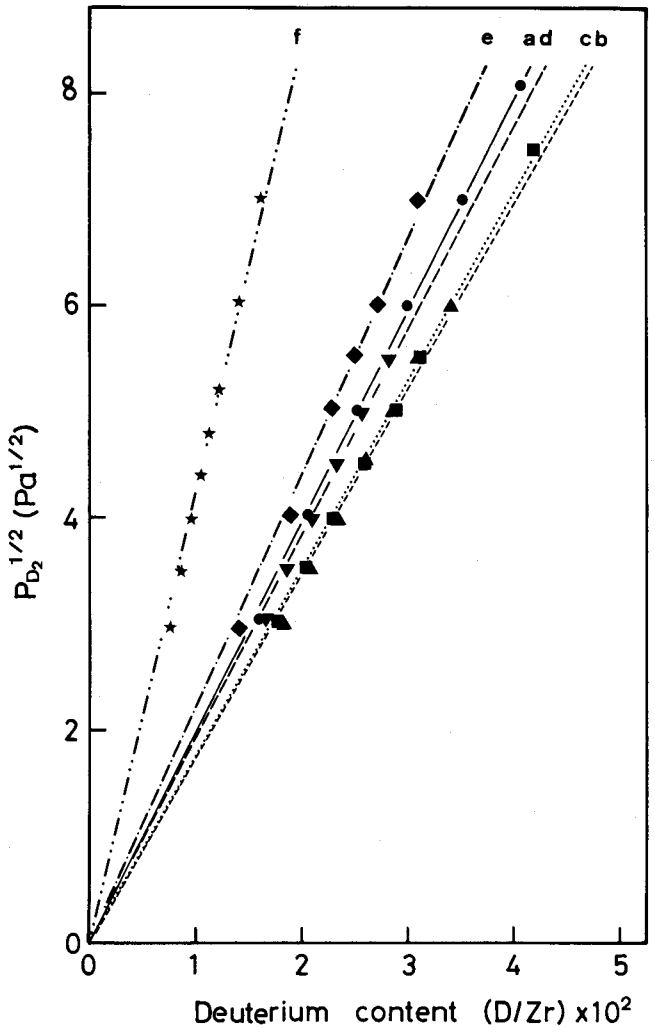

Fig. 8 Sieverts' plot for deuterium in pure zirconium and αZr(O) solid solutions at 700°C.

(a) pure zirconium, (b) 0.053 O/Zr, (c) 0.111 O/Zr, (d) 0.176 O/Zr, (e) 0.250 O/Zr, (f) 0.389 O/Zr.

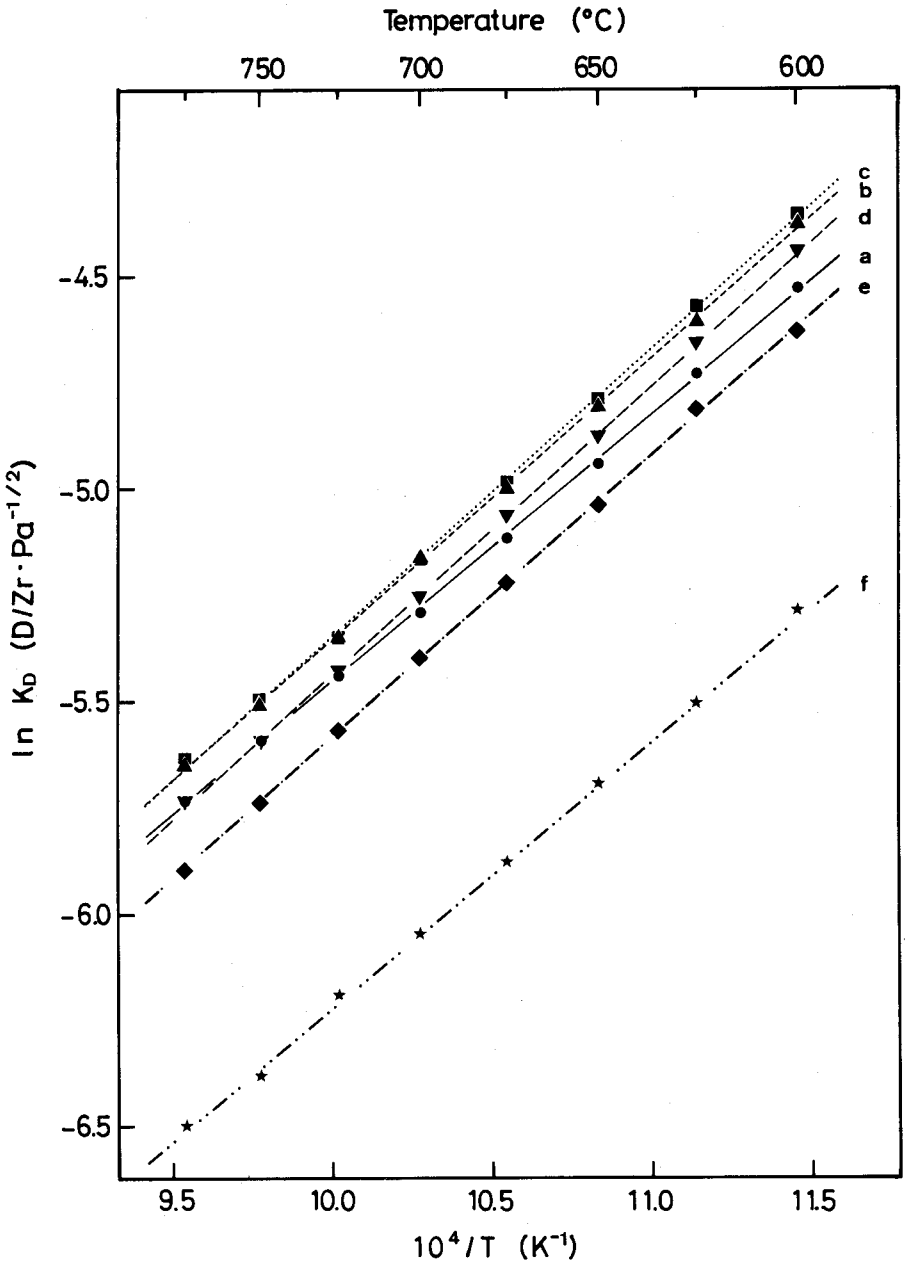

Fig. 9 Temperature dependence of Sieverts' constant K_D for deuterium in pure zirconium and αZr(O) solid solutions.
(a) pure zirconium, (b) 0.053 O/Zr, (c) 0.111 O/Zr, (d) 0.176 O/Zr, (e) 0.250 O/Zr, (f) 0.389 O/Zr.

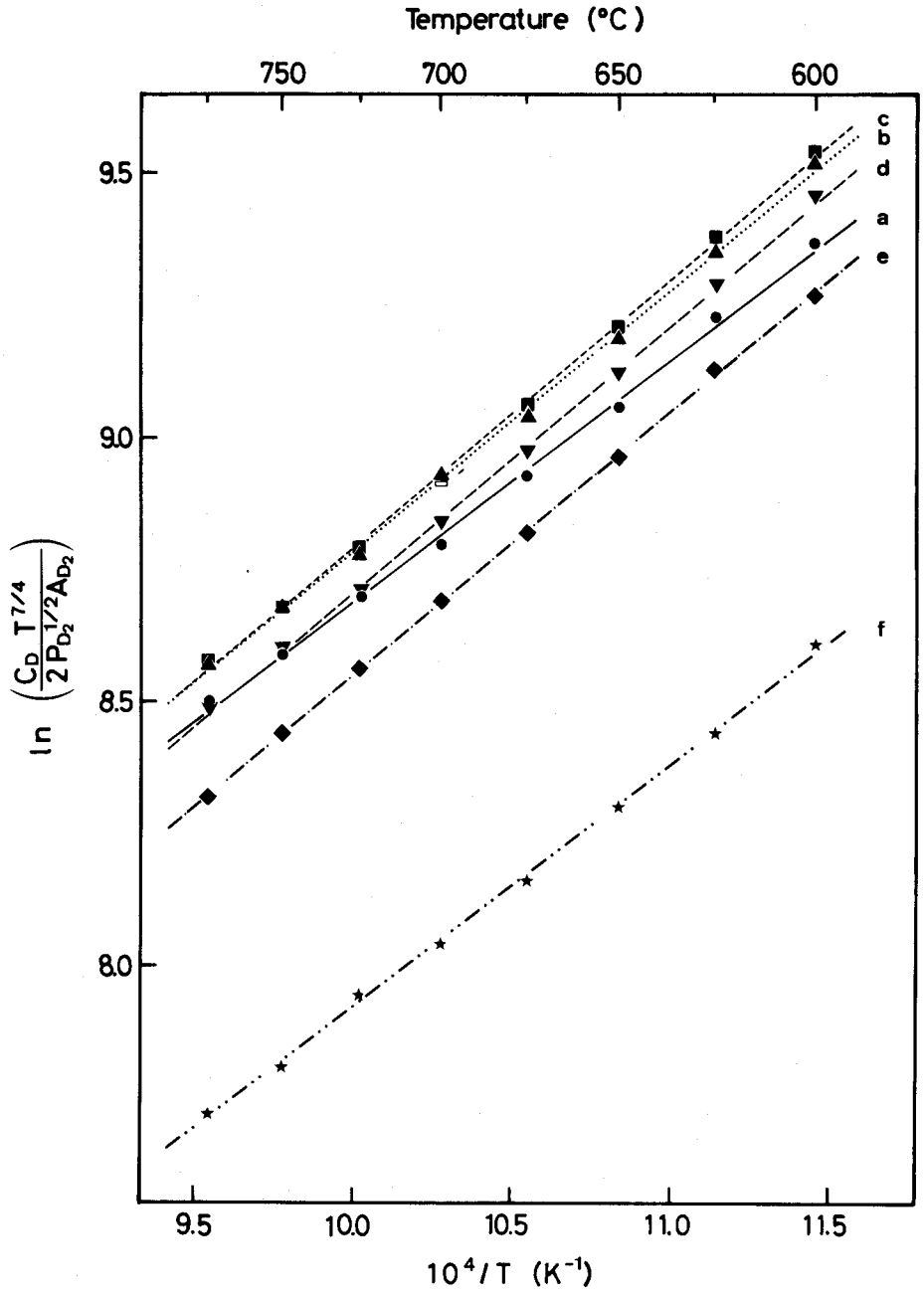

Fig. 10 Thermodynamic analysis of deuterium solubility in αZr(O) solid solution. (a) pure zirconium, (b) 0.053 O/Zr, (c) 0.111 O/Zr, (d) 0.176 O/Zr, (e) 0.250 O/Zr, (f) 0.389 O/Zr.

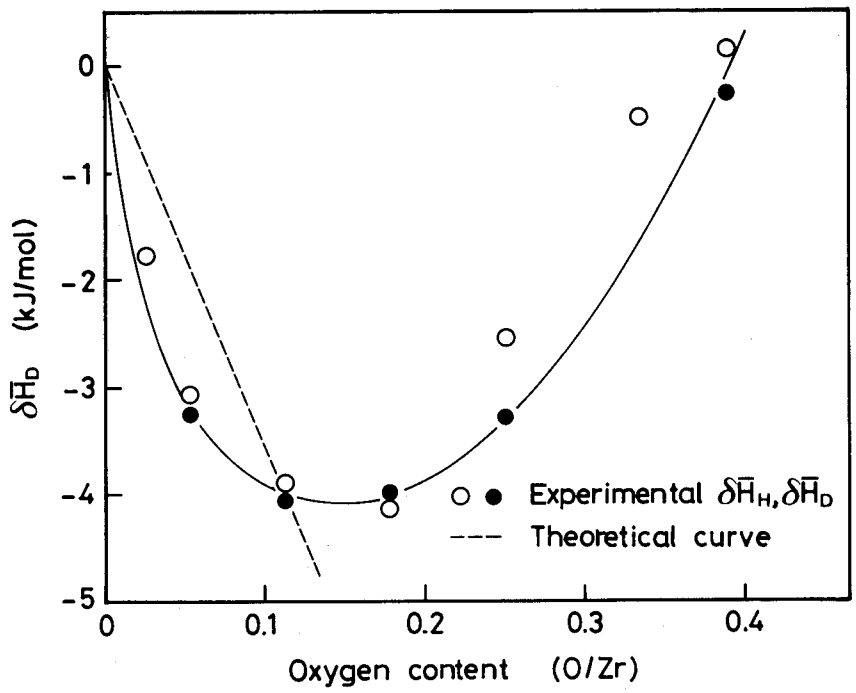

Fig. 11 Change in $\delta\bar{H}_D$ value with oxygen content in αZr(O) solid solution.

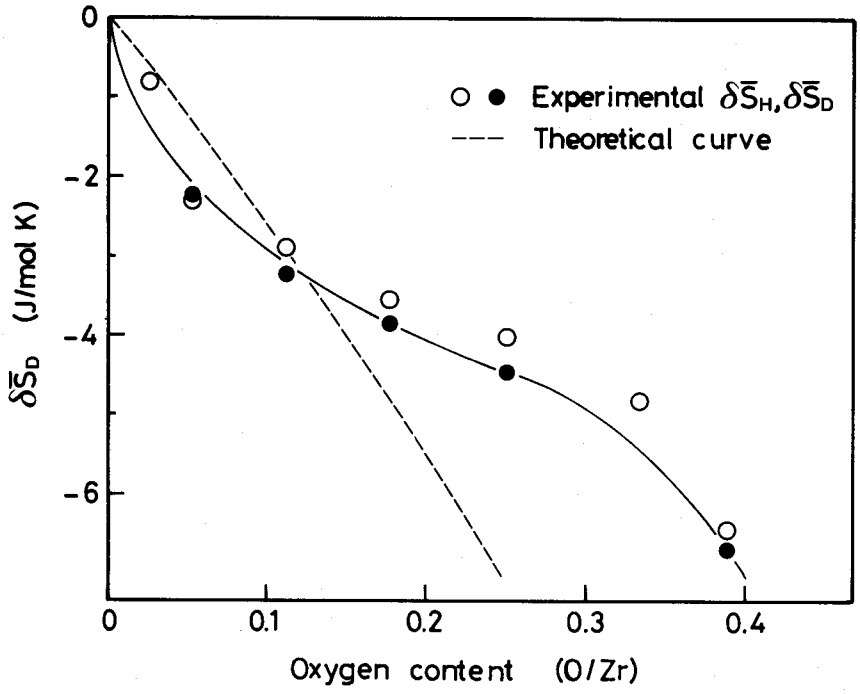

Fig. 12 Change in $\delta\bar{S}_D$ value with oxygen content in αZr(O) solid solution.

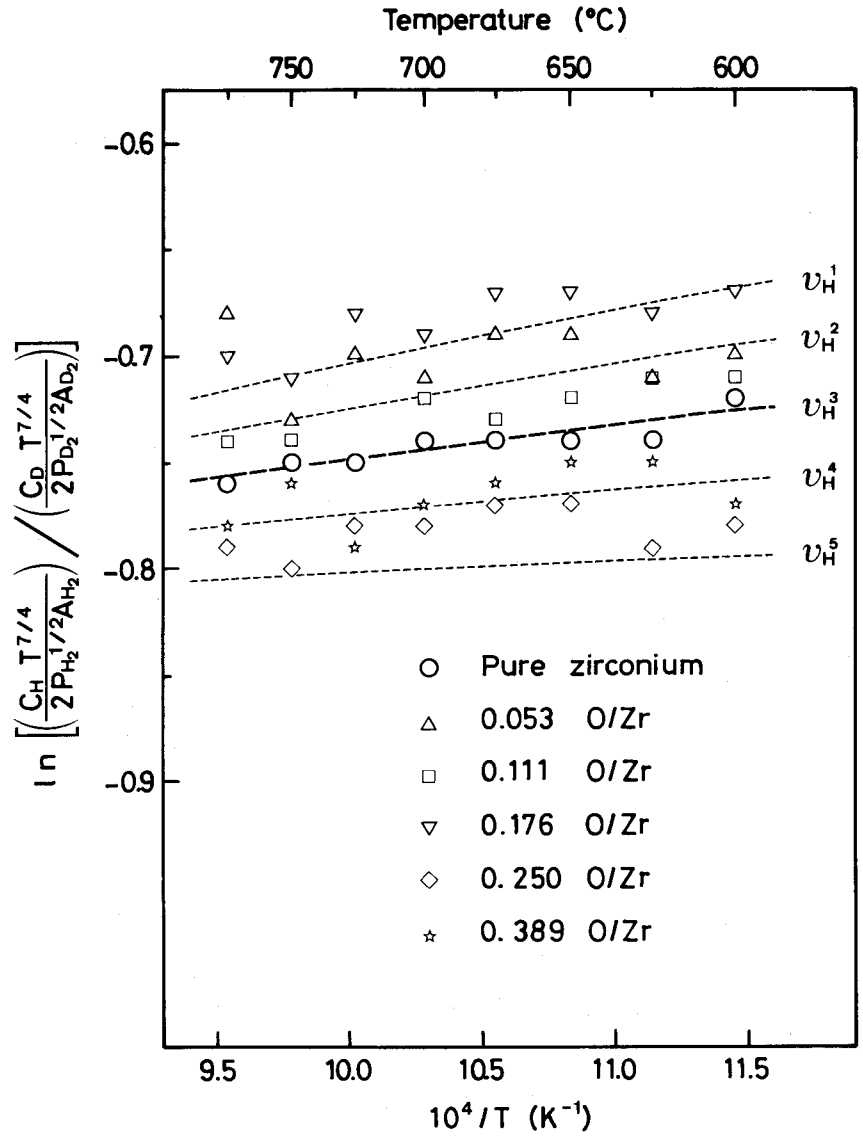

Fig. 13 Isotope effect on solubility in pure zirconium and αZr(O) solid solutions.

ν_H^1 = 800 cm^{-1}, ν_H^2 = 900 cm^{-1}, ν_H^3 = 1000 cm^{-1}, ν_H^4 = 1100 cm^{-1}, ν_H^5 = 1200 cm^{-1}.

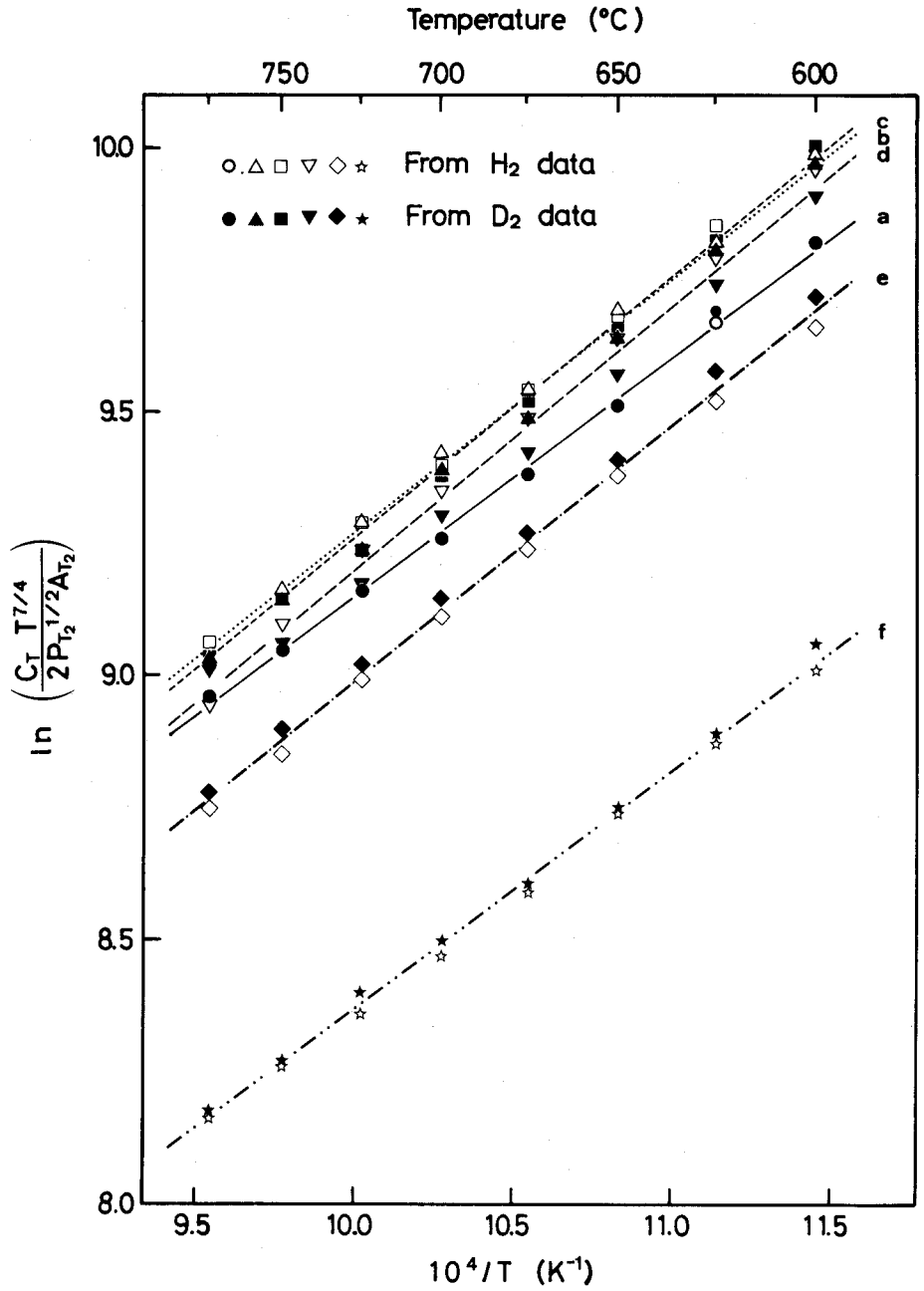

Fig. 14 Estimation of tritium solubility in pure zirconium and αZr(O) solid solutions.

(a) pure zirconium, (b) 0.053 O/Zr, (c) 0.111 O/Zr, (d) 0.176 O/Zr, (e) 0.250 O/Zr, (f) 0.389 O/Zr.

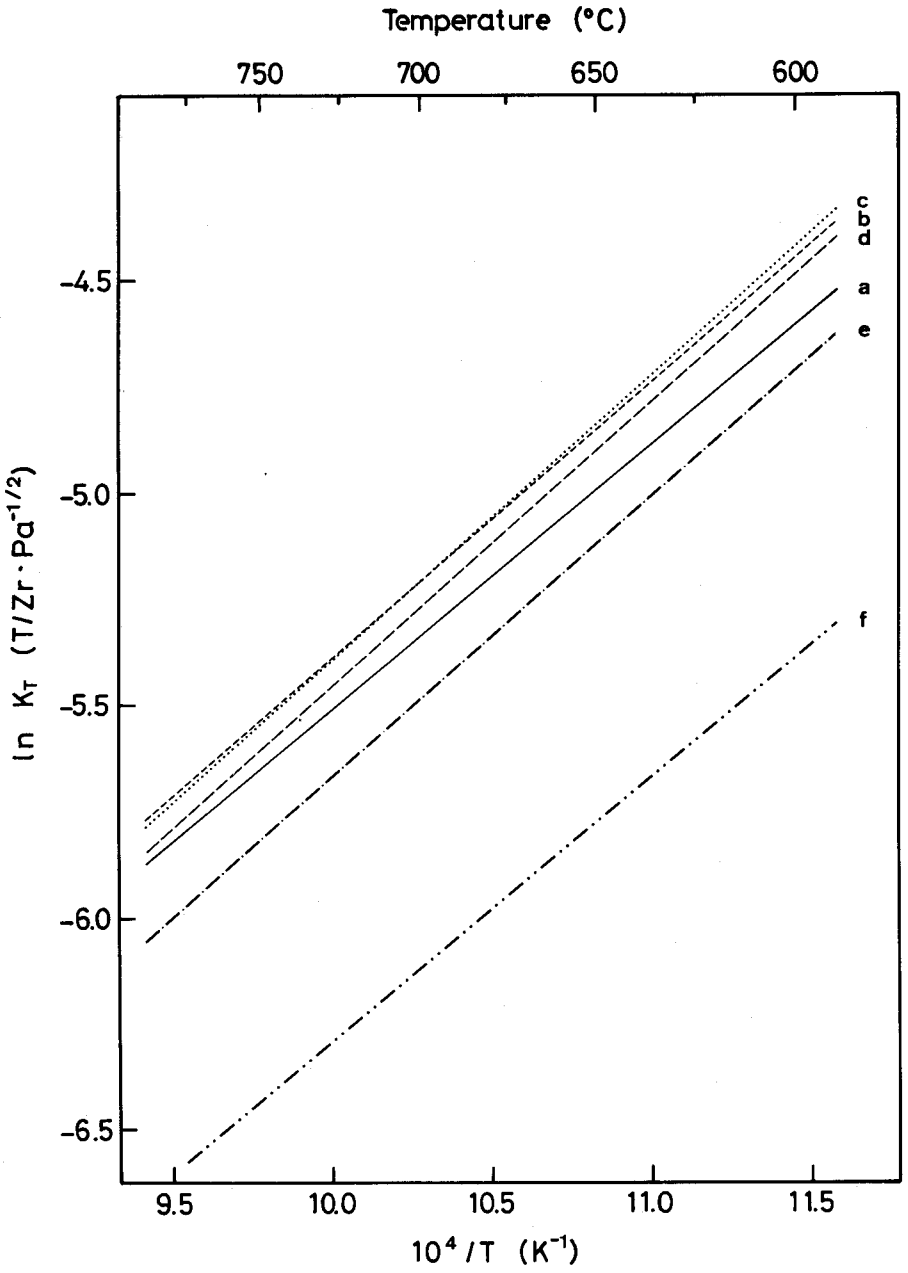

Fig. 15 Temperature dependence of Sieverts' constant K_T for tritium in pure zirconium and αZr(O) solid solutions.
(a) pure zirconium, (b) 0.053 O/Zr, (c) 0.111 O/Zr, (d) 0.176 O/Zr, (e) 0.250 O/Zr, (f) 0.389 O/Zr.

CHAPTER 8 SUMMARY

The author's attention has been focused on the ternary phase equilibria of interest in applying titanium and zirconium to nuclear engineering. The elements chosen in the present study were oxygen, uranium, tellurium and hydrogen, which are directly associated with the substances of nuclear fission and fusion reactors. The conclusions drawn from the present study are summarized as follows:

The present study established the phase relationships of the U-Ti-O ternary system at 1000°C on the basis of X-ray diffraction analysis. From the proposed isothermal section at 1000°C, the αTi(O) solid solution in equilibrium with UO_2 appears to have an oxygen content ranging from 22 to 33 at%. The formation of the (γU,βTi) solid solution phase was found to take place owing to the reduction of UO_2 by titanium. The oxygen potential over the αTi(O) solid solution was estimated from the results for the U-Ti-O ternary equilibria.

The phase relationships of the U-Zr-O ternary system at 1000 and 1400°C were accomplished, based on the results for X-ray diffractometry and metallography. From the isothermal sections at 1000 and 1400°C proposed in the present study, the αZr(O) in equilibrium with UO_2 appears to possess an oxygen content above 25 at%. At 1400°C, the formation of the liquid phase due to the reduction of UO_2 by zirconium was confirmed to take place. The partial thermodynamic properties of the αZr(O) solid solution were derived from the equilibrium data for the U-Zr-O ternary system.

The phase equilibria in the Ti-Te-O ternary system at 700°C were studied by X-ray diffraction technique. In the isothermal section proposed in the present study, the $TiTe_3O_8$ double oxide existed. Three tellurides, Ti_5Te_4, monoclinic $Ti_{2-x}Te_2$ and hexagonal $Ti_{2-x}Te_2$ were found to be stable in the ternary system. The titanium tellurides can equilibrate with αTiO and Ti_2O_3. The stability diagram for the Ti-Te-O system at 700°C was established using the known and estimated thermodynamic data for the relevant species. The phase relations experimentally obtained were consistent with the thermodynamic constraints imposed by the stability diagram. Oxygen is inferred from these results to reduce the chemical stability of titanium tellurides, and titanium oxides appear to be stable compounds over a wide range of Te_2 and O_2 pressures. At a high oxygen potential, $TiTe_3O_8$ may become more stable with respect to the simple oxides.

The constitutional studies on the Zr-Te-O ternary system at 700°C were performed by X-ray diffraction technique. In the isothermal section, the ternary compound $ZrTe_3O_8$ existed. Three tellurides, Zr_5Te_4, $Zr_{1+x}Te_2$ and $ZrTe_3$ were confirmed to be stable in the ternary system. All the phases other than TeO_2 were found to be in equilibrium with αZrO_2. The phase stability diagrams for the Zr-

Te-O system at 300 and 700°C were constructed using the known and estimated thermodynamic data for the relevant species. The phase relationships experimentally observed satisfied the thermodynamic restrictions derived from the stability diagram. Oxygen is considered to reduce the chemical stability of zirconium tellurides, and ZrO_2 appears to be a more stable compound over a wide range of Te_2 and O_2 pressures. At a high oxygen potential, $ZrTe_3O_8$ may be formed instead of ZrO_2.

The solubility measurements of hydrogen and deuterium gases in pure titanium and αTi(O) solid solutions with 0.111 - 0.429 O/Ti were made at temperatures of 600 - 850°C at pressures below 10^5 Pa by a constant volume method. The isothermal section of the Ti-O-H ternary system at 600°C was proposed. All the solubility data below 10^2 Pa obeyed Sieverts' law. The solubility of hydrogen isotope decreased with increasing oxygen content in titanium, while the enthalpy of solution was almost constant, irrespective of the oxygen content. The reduction in the solubility by solute oxygen was explained by the dilute solution model. The solubility of hydrogen was larger than that of deuterium. The isotope effect on the solubility was discussed, and the vibrational frequency of hydrogen atom in titanium was obtained, which allowed prediction of tritium solubility. The estimated solubility of tritium in pure titanium and αTi(O) solid solutions was smallest, followed by deuterium and hydrogen.

The hydrogen and deuterium solubilities were measured for pure zirconium and αZr(O) solid solutions with 0.026 - 0.389 O/Zr in the range of 600 - 775°C. The isothermal section of the Zr-O-H ternary system at 700°C was constructed from P-C curves. All the solubility data below 10^2 Pa obeyed Sieverts' law. The solubility of hydrogen first increased with oxygen content in zirconium, then decreased above 0.176 O/Zr. The enthalpy of solution of hydrogen showed a pronounced minimum at 0.111 O/Zr. The partial thermodynamic functions for the Zr-O-H ternary solution were derived by applying the dilute solution model to the solubility data. These trends in the deuterium solubility were similar to those verified in the hydrogen solubility. The isotope effect on the solubility in pure zirconium and αZr(O) solid solutions was discussed, and the tritium solubility was estimated.

The results for the phase equilibria obtained in the present study can contribute to the understanding of the chemical stability of titanium and zirconium under various environments encountered in nuclear fission and fusion reactors. It is the author's hope that the present study may provide some insight and guidance for future applications of titanium and zirconium in nuclear industries.

ACKNOWLEDGMENTS

The author would like to thank Prof. Dr. M. Miyake for drawing his attention to this problem and providing support, guidance and especially inexhaustible patience throughout this research.

The author is also grateful to Prof. Dr. T. Sekiya, Prof. Dr. K. Ogino, Prof. Dr. K. Sumita, Prof. Dr. T. Okada, Prof. Dr. T. Yamamoto and Prof. Dr. K. Miyazaki for their critical reading of this thesis and valuable advice.

His deep gratitude is expressed here to Prof. Emeritus T. Sano and Prof. Emeritus S. Imoto, both of the Osaka University, who first awoke his interest in the subject of chemical thermodynamics.

The author would like to acknowledge his great debt to Assoc. Prof. Dr. M. Katsura from whom in altogether fifteen years' happy association at the Osaka University the author learnt how to think about statistical thermodynamics.

The author is deeply indebted to Dr. P. Son for encouraging advice and constructive criticism. Thanks are due Dr. T. Tanabe for stimulating discussion and providing information about hydrogen behavior in metal.

Many colleagues and friends offered helpful comments and suggestions. Although the author cannot cite them all, he wishes to acknowledge the contributions of Mr. T. Yamamoto, Mr. Y. Murakami, Mr. S. Tsuboi, Mr. N. Takatsuka and Mr. T. Tanaka.

The graduate students of the Nuclear Material Division of the Osaka University are acknowledged for their hospitality and encouragement. Moreover, their considerable assistance during the preparation of this thesis is sincerely appreciated.

Finally, the author wishes to express his appreciation and love to his family who helped him to prepare this thesis whenever needed. Without their support and sacrifices, this thesis would not be accomplished.

LIST OF ACADEMIC PUBLICATIONS

1) Study on the reaction between UO_2 and Zr,
M. Katsura, S. Yamanaka, S. Imoto and M. Miyake,
Proceedings of the 8th NSRR Technical Review Meeting, (1984)173.

2) On the Reaction between UO_2 and Zr,
S. Yamanaka, M. Katsura, M. Miyake, S. Imoto and S. Kawasaki,
J. Nucl. Mater., 130(1985)524.

3) Study of the U-Zr-O Ternary System,
S. Yamanaka, M. Katsura, S. Imoto and M. Miyake,
Inorg. Chimica Acta, 140(1987)127.

4) A Study of the Reaction between UO_2 and Zr,
M. Miyake, M. Katsura and S. Yamanaka,
J. Nucl. Mater., 154(1988)123.

5) An Estimation of Thermodynamic Stability of Zirconium Tellurides,
S. Yamanaka, M. Katsura and M. Miyake,
Technology Reports of the Osaka University, 38(1988)59.

6) Effect of Interstitial Impurities on Hydrogen Solubility in Titanium,
S. Yamanaka, T. Tanaka, Y. Sato and M. Miyake,
Proceedings of the First International Conference on the Metallurgy and Materials Science of Tungsten, Titanium, Rare Earths and Antimony, Vol. 2, (1988)1018.

7) Study of the U-Ti-O Ternary System,
S. Yamanaka and M. Miyake,
J. Nucl. Mater., 161(1989)204.

8) Study of the Zr-Te-O Ternary System,
S. Yamanaka, N. Takatsuka, M. Katsura and M. Miyake,
J. Nucl. Mater., 161(1989)210.

9) Hydrogen Solubility in Titanium and Solute Nonmetallic Element,
M. Miyake and S. Yamanaka,
Metals & Technology KINZOKU, 5(1989)22.

10) Influence of Impurity Contamination on Solubility of Hydrogen Isotope in Titanium,
S. Yamanaka, Y. Sato, T. Tanaka and M. Miyake,
Fusion Technology 1988, Vol 2, (1989)1249.

11) Effect of Oxygen on Solubility of Hydrogen Isotopes in Titanium,
S. Yamanaka, T. Tanaka, S. Tsuboi and M. Miyake,
Fusion Engineering and Design, 10(1989)303.

12) Effect of Oxygen on Hydrogen Solubility in Zirconium,
S. Yamanaka, T. Tanaka and M. Miyake,
J. Nucl. Mater., 166(1989), in press.
13) Hydrogen Solubility in Titanium-Oxygen Solid Solution,
S. Yamanaka, S. Tsuboi, T. Tanaka and M. Miyake
Technology Reports of the Osaka University, 39(1989), in press.
14) Study of the Uranium-Transition Metal-Oxygen Ternary System,
S. Yamanaka and M. Miyake,
Proceedings of ACTINIDE '89, to be published.
15) Study of the Ti-Te-O Ternary System,
S. Yamanaka and M. Miyake,
J. Less-Common Metals, to be published.
16) Phase Equilibria in the U-Zr-O Ternary System,
S. Yamanaka, M. Katsura, M. Kawano and M. Miyake,
J. Nucl. Mater, to be submitted.
17) Influence of Interstitial Impurities on Hydrogen Solubility in Zirconium,
S. Yamanaka, H. Ogawa, Y. Sato, T. Tanaka and M. Miyake,
J. Nucl. Sci. Eng., to be submitted.